

**SECTOR ANTENNA FOR CELLULAR BASE STATION
USING SLOT ARRAY AND EBG**

Paowphattra Kamphikul

**A Thesis Submitted in Partial Fulfillment of the Requirements for the
Degree of Doctor of Philosophy in Telecommunication Engineering**

Suranaree University of Technology

Academic Year 2014

สายอากาศแบบเชิงเตอร้สำหรับสถานีฐานระบบเซลลูลาร์โดยใช้
แวลลุ่มร่ร่งร่วร่กับโพรงช่องว่างแวลแม่เหล็กไฟฟ้า

นางสาวภาภัทร่า ค่ำพิกุล

วิทยานิพนธ์นี้เป็นส่วนหนึ่งของการศึกษาตามหลักสูตรปริญญาวิศวกรรมศาสตรดุษฎีบัณฑิต
สาขาวิชาวิศวกรรมโทรคมนาคม
มหาวิทยาลัยเทคโนโลยีสุรนารี
ปีการศึกษา 2557

**SECTOR ANTENNA FOR CELLULAR BASE STATION
USING SLOT ARRAY AND EBG**

Suranaree University of Technology has approved this thesis submitted in partial fulfillment of the requirements for the Degree of Doctor of Philosophy.

Thesis Examining Committee

(Asst. Prof. Dr. Chutima Prommak)

Chairperson

(Assoc. Prof. Dr. Rangsak Wongsak)

Member (Thesis Advisor)

(Asst. Prof. Dr. Piyaporn Mesawat)

Member

(Prof. Dr. Prayoot Akkarakhalin)

Member

(Assoc. Prof. Dr. Chuwong Pongcharoenpanich)

Member

(Prof. Dr. Sukit Limpijumong)

Vice Rector for Academic Affairs
and Innovation

(Assoc. Prof. Ft. Dr. Kontorn Chamniprasart)

Dean of Institute of Engineering

เกาภัทธา คำพิกุล : สายอากาศแบบเซ็กเตอร์สำหรับสถานีฐานระบบเซลลูลาร์โดยใช้
แถวลำดับร่องร่วมกับโพรงช่องว่างแถบแม่เหล็กไฟฟ้า (SECTOR ANTENNA FOR
CELLULAR BASE STATION USING SLOT ARRAY AND EBG)

อาจารย์ที่ปรึกษา : รองศาสตราจารย์ ดร.รังสรรค์ วงศ์สรรค์, 183 หน้า.

ระบบโทรศัพท์เซลลูลาร์ (cellular phone system) ได้มีการปรับปรุงและพัฒนาให้เหมาะสม
กับการใช้งานในระบบโทรศัพท์เคลื่อนที่ที่สามารถให้บริการมัลติมีเดียในลักษณะที่สามารถโต้ตอบ
ได้ มีความกว้างแถบที่กว้างเพียงพอให้สามารถรับ-ส่งข้อมูลด้วยอัตราความเร็วที่สูง และสามารถใช้
งานได้ทั่วโลก ปัจจุบันระบบโทรศัพท์เซลลูลาร์กำลังมุ่งเน้นพัฒนาเทคโนโลยีไปสู่ยุค 3.9G
และสูงกว่า ดังนั้นงานวิจัยนี้จึงได้ออกแบบระบบสายอากาศแบบเซ็กเตอร์สำหรับรองรับ
เทคโนโลยีดังกล่าว สำหรับการประยุกต์ใช้งานกับสถานีฐาน (base station) ให้เป็นไปตาม
มาตรฐาน IEEE802.16e mobile WiMAX ที่ความถี่ 2.1 GHz โดยใช้เทคโนโลยีใหม่ในการเพิ่ม
อัตราขยายของสายอากาศแถวลำดับร่อง (slot antenna array) ให้สูงขึ้น ด้วยการนำโพรงช่องว่าง
แถบแม่เหล็กไฟฟ้า (Electromagnetic Band Gap หรือ EBG) มาทำการวิจัยและออกแบบให้ใช้งาน
ร่วมกับสายอากาศดังกล่าว โดยระบบสายอากาศจะประกอบด้วยสามองค์ประกอบหลักดังนี้
(1) สายอากาศแถวลำดับร่องที่มีการปรับปรุงความกว้างแถบให้เหมาะสมกับการใช้งานในระบบ
3.9G (2) โครงสร้าง EBG ที่ได้ทำการวิจัยและออกแบบ และ (3) ระบบป้อนกำลังงาน (feed
system) โดยใช้โปรแกรมสำเร็จรูป CST (Computer Simulation Technology) ในการออกแบบและ
ใช้ระเบียบวิธีของวิธีผลต่างสืบเนื่องเชิงเวลา (Finite Difference Time Domain method หรือ FDTD)
ในการคำนวณผลเฉลยของสนามแม่ไฟฟ้า (E-field) และสนามแม่เหล็ก (H-field) จากการวิจัย
พบว่าโครงสร้าง EBG ที่มีความเหมาะสมสามารถเพิ่มอัตราขยายให้กับสายอากาศได้เช่นเดียวกัน
กับการเพิ่มวงจรเรโซแนนซ์ (resonant circuit) ที่ความถี่ 2.1 GHz เมื่อนำมาวางด้านหน้าสายอากาศ
แถวลำดับ สดุดท้ายจะสร้างระบบสายอากาศต้นแบบที่ได้จากการคำนวณในลักษณะของเซ็กเตอร์
เพื่อนำมาวัดทดสอบเปรียบเทียบผลที่ได้จากการวัดทดสอบ และจากระเบียบวิธีของ FDTD

PAOWPHATTRA KAMPHIKUL : SECTOR ANTENNA FOR CELLULAR
BASE STATION USING SLOT ARRAY AND EBG.

THESIS ADVISOR : ASSOC. PROF. RANGSAN WONGSAN, D.Eng.,

183 PP.

SECTOR ANTENNA/CELLULAR BASE STATION/ELECTROMAGNETIC
BAND GAP/FINITE DIFFERENCE TIME DOMAIN

The cellular phone system is suitably improved and developed for mobile phone communication system for supporting the real time interactive multimedia services, and providing enough bandwidth for high bit rate receiving and transmitting data for global mobility. Nowadays, the cellular phone system has been innovated into 3.9G technology and beyond. Therefore, this research aims to design a sector antenna system for the age of Third Generation (3.9G) applying for the cellular base station, following IEEE802.16e Mobile WiMAX Standards at 2.1GHz. The Electromagnetic Band Gap (EBG), a new technology for increasing the gain of slot array antenna, is investigated and designed to cooperate with such antenna. The antenna system comprises of three main parts as follow: (1) slot array antenna that provides the wide-bandwidth covered frequency ranges for 3.9G system, (2) the appropriate EBG structures, and (3) feed system by using the CST (Computer Simulation Technology) to investigate and design all of them. While Finite Difference Time Domain method (FDTD) is conducted to carry out the E- and H-fields.

From the research, it found that the proper structure of EBG is capable to enhance the gain of antenna as the additional resonant circuit, exhibit bandgap characteristics at 2.1 GHz, which installed at front of the array panel. Finally, the prototype of this sector antenna system is fabricated from the calculated results and then has been validated with the measured results and compared to some parameters from the FDTD calculation.

School of Telecommunication Engineering Student's Signature _____

Academic Year 2014

Advisor's Signature _____

ACKNOWLEDGEMENTS

I would like to thank the office of the National Research Council of Thailand (NRCT) for supporting by grant under the program strategic scholarships for the joint Ph.D. program Thai doctoral degree.

I am so grateful to my advisor, Assoc. Prof. Dr. Rangsana Wongsan for consistent thesis supervision and thoughtfully comment on several drafts and advice towards the completion of this study.

I would like to express my gratitude to the thesis examination committees, Asst. Prof. Dr. Chutima Prommak, Assoc. Prof. Dr. Rangsana Wongsan, Asst. Prof. Dr. Piyaporn Mesawad, Prof. Dr. Prayoot Akkaraekthalin, and Assoc. Prof. Dr. Chuwong Pongcharoenpanich, for their invaluable advices and kind supports.

I would like to thank for the fellow members of the Wireless Communication Research and Laboratory, Suranaree University of Technology, for providing a pleasant and inspiring environment to work in.

Finally, I am greatly indebted to all of my teachers in the past and my family, who love me and give encouragement.

Paowphattra Kamphikul

TABLE OF CONTENTS

	Page
ABSTRACT (THAI).....	I
ABSTRACT (ENGLISH)	II
ACKNOWLEDGMENTS.....	IV
TABLE OF CONTENTS	V
LIST OF TABLES.....	IX
LIST OF FIGURES	X
CHAPTER	
I INTRODUCTION.....	1
1.1 Background of Problems and Significance of the Study	1
1.2 Research Objectives	4
1.3 Scope of the Study.....	5
1.4 Expected Benefits.....	5
1.5 Thesis Organization.....	5
II LITERATURE REVIEW	6
2.1 Introduction.....	6
2.2 Antenna for Wireless Communications.....	6
2.3 Electromagnetic Band Gap	11

TABLE OF CONTENTS (Continued)

	Page
2.3.1 MSA Surrounded by EBG Structures	12
2.3.2 MSA on Top of EBG Structures.....	15
2.3.3 Mutual Coupling Reduction by the EBG Structures.....	15
2.3.4 Gain Enhancement of Resonator Antenna by Woodpile EBG Structures	17
2.4 The Origin of Finite Difference Time Domain	18
2.5 Chapter Summary.....	27
III BACKGROUND THEORY.....	29
3.1 Introduction.....	29
3.2 Microstrip Antenna.....	29
3.2.1 Microstrip Slot Antenna	31
3.2.3 Microstrip Slot Antenna Array	34
3.3 Electromagnetic Band Gap Structures.....	34
3.3.1 EBG Definition.....	34
3.3.2 EBG and Metamaterials	38
3.3.3 Analysis Methods for EBG Structures.....	40
3.3.4 Woodpile EBG Structures.....	46
3.4 The Finite Difference Time Domain Method	51
3.4.1 The Yee Algorithm	55

TABLE OF CONTENTS (Continued)

	Page
3.5 Artificial Neural Network.....	60
3.5.1 The Levenberg–Marquardt algorithm.....	61
3.6 Chapter Summary.....	64
IV ANTENNA ANALYSIS AND DESIGN.....	65
4.1 Introduction.....	65
4.2 Microstrip Slot Antenna Configuration.....	65
4.2.1 A Microstrip Slot Antenna	65
4.2.2 A 1×8 Array of Microstrip Slot Antennas.....	66
4.3 Electromagnetic Band Gap Configuration.....	75
4.4 Design of Antenna System by CST Software.....	75
4.5 Parameter Computation by FDTD and ANN Methods	87
4.6 Chapter Summary.....	96
V MEASUREMENT AND DISCUSSION.....	97
5.1 Introduction.....	97
5.2 The Antenna Prototype	97
5.2.1 A 1×8 Array of Microstrip Slot Antennas and U-shaped Reflector.....	97
5.2.2 The Curved Woodpile EBG Structures.....	100

TABLE OF CONTENTS (Continued)

	Page
5.3 Antenna Measurement.....	102
5.3.1 Radiation Patterns.....	105
5.3.2 Gain.....	108
5.3.3 Bandwidth.....	109
5.3.4 Input Impedance, Standing Wave Ratio and Reflected Power.....	110
5.4 Experimental Results.....	110
5.5 Chapter Summary.....	119
VI CONCLUSIONS	120
6.1 Thesis Concluding Remarks.....	120
6.2 Remark for Future Studies.....	121
REFERENCES.....	122
APPENDICES	
APPENDIX A. THE FDTD CODE.....	131
APPENDIX B. LIST OF PUBLICATIONS.....	146
APPENDIX C. COMPARISON OF 3G BASE STATION DIRECTIONAL ANTENNAS.....	180
BIOGRAPHY.....	183

TABLE OF CONTENTS

	Page
ABSTRACT (THAI).....	I
ABSTRACT (ENGLISH)	II
ACKNOWLEDGMENTS.....	IV
TABLE OF CONTENTS	V
LIST OF TABLES.....	IX
LIST OF FIGURES	X
CHAPTER	
I INTRODUCTION.....	1
1.1 Background of Problems and Significance of the Study	1
1.2 Research Objectives	4
1.3 Scope of the Study.....	5
1.4 Expected Benefits.....	5
1.5 Thesis Organization.....	5
II LITERATURE REVIEW	6
2.1 Introduction.....	6
2.2 Antenna for Wireless Communications.....	6
2.3 Electromagnetic Band Gap	11

TABLE OF CONTENTS (Continued)

	Page
2.3.1 MSA Surrounded by EBG Structures	12
2.3.2 MSA on Top of EBG Structures.....	15
2.3.3 Mutual Coupling Reduction by the EBG Structures.....	15
2.3.4 Gain Enhancement of Resonator Antenna by Woodpile EBG Structures	17
2.4 The Origin of Finite Difference Time Domain	18
2.5 Chapter Summary.....	27
III BACKGROUND THEORY.....	29
3.1 Introduction.....	29
3.2 Microstrip Antenna.....	29
3.2.1 Microstrip Slot Antenna	31
3.2.3 Microstrip Slot Antenna Array	34
3.3 Electromagnetic Band Gap Structures.....	34
3.3.1 EBG Definition.....	34
3.3.2 EBG and Metamaterials	38
3.3.3 Analysis Methods for EBG Structures.....	40
3.3.4 Woodpile EBG Structures.....	46
3.4 The Finite Difference Time Domain Method	51
3.4.1 The Yee Algorithm	55

TABLE OF CONTENTS (Continued)

	Page
3.5 Artificial Neural Network.....	60
3.5.1 The Levenberg–Marquardt algorithm.....	61
3.6 Chapter Summary.....	64
IV ANTENNA ANALYSIS AND DESIGN.....	65
4.1 Introduction.....	65
4.2 Microstrip Slot Antenna Configuration.....	65
4.2.1 A Microstrip Slot Antenna	65
4.2.2 A 1×8 Array of Microstrip Slot Antennas.....	66
4.3 Electromagnetic Band Gap Configuration.....	75
4.4 Design of Antenna System by CST Software.....	75
4.5 Parameter Computation by FDTD and ANN Methods	87
4.6 Chapter Summary.....	96
V MEASUREMENT AND DISCUSSION.....	97
5.1 Introduction.....	97
5.2 The Antenna Prototype	97
5.2.1 A 1×8 Array of Microstrip Slot Antennas and U-shaped Reflector.....	97
5.2.2 The Curved Woodpile EBG Structures.....	100

TABLE OF CONTENTS (Continued)

	Page
5.3 Antenna Measurement.....	102
5.3.1 Radiation Patterns.....	105
5.3.2 Gain.....	108
5.3.3 Bandwidth.....	109
5.3.4 Input Impedance, Standing Wave Ratio and Reflected Power.....	110
5.4 Experimental Results.....	110
5.5 Chapter Summary.....	119
VI CONCLUSIONS	120
6.1 Thesis Concluding Remarks.....	120
6.2 Remark for Future Studies.....	121
REFERENCES.....	122
APPENDICES	
APPENDIX A. THE FDTD CODE.....	131
APPENDIX B. LIST OF PUBLICATIONS.....	146
APPENDIX C. COMPARISON OF 3G BASE STATION DIRECTIONAL ANTENNAS.....	180
BIOGRAPHY.....	183

LIST OF TABLES

Table	Page
2.1 Partial chronology of FDTD techniques and applications	20
4.1 Results of simulation.....	82
5.1 Dimensions of the microstrip slot antenna.....	98
5.2 Dimensions of the curved woodpile EBG structures.....	100
5.3 Comparison of simulated, calculated, and measured results.....	119

LIST OF FIGURES

Figure	Page
2.1 A triangular array of dipoles.....	9
2.2 (a) Sleeve antenna with ground wires (b) Sleeve antenna (c) Monopole antenna with ground wires $l_1 = 0.25\lambda$, $\rho_1 = \rho_3 = 1.7 \times 10^{-3}\lambda$, $\rho_2 = 6.8 \times 10^{-3}\lambda$ (Taguchi, Egashira, and Tanaka, 1991).....	10
2.3 The geometry of rectangular MSA	10
2.4 An ultra-wideband circular MSA fed by microstrip line above wide-slot ground plane (Chawanonphithak and Phongcharoenpanich, 2007).	11
2.5 Patch antenna on a step-like substrate (Yang and Rahmat-Samii, 2001)	13
2.6 Patch antenna surrounded by mushroom-like EBG structures (Yang and Rahmat-Samii, 2001)	13
2.7 Prototype of two patch antenna designs with enhanced performance (Yang and Rahmat-Samii, 2001)	14
2.8 Geometry of MSA on top of EBG structures (Shafai, and Foroozesh, 2006).....	16
2.9 MSA separated by the mushroom-like EBG structures (Yang and Rahmat-Samii, 2003)	17

LIST OF FIGURES (Continued)

Figure	Page
2.10 A high gain antenna design using the woodpile EBG structures (Weilyet al., 2005).....	18
2.11 An estimated FDTD-related publications (http://upload.wikimedia.org/wikipedia/en/a/a3/Yearly_FDTD_publications.png)	25
3.1 The shapes of microstrip patch elements	32
3.2 Center-fed microstrip slot antenna configurations (Yoshimura, 1972)	33
3.3 The 1D EBG transmission lines.....	36
3.4 The 2D EBG planar surfaces	37
3.5 The 3D EBG volumetric structures.....	38
3.6 The geometry of a mushroom-like EBG structures (Sievenpiper et al., 1999).....	42
3.7 The lumped element model for the mushroom-like EBG structures.....	43
3.8 The transmission line model of EBG structures (Rahman and Stuchly, 2001)	45
3.9 The full wave FDTD model for the EBG analysis (Kim, Yang, and Elsherbeni, 2007)	46

LIST OF FIGURES (Continued)

Figure	Page
3.10 A unit cell of the planar woodpile EBG structure (Weily et al., 2005).....	48
3.11 The geometry of the cylindrical woodpile EBG structures (Lee et al., 2010).....	49
3.12 The geometry of the curved woodpile EBG structures.....	50
3.13 The Yee cell with labeled field components	56
3.14 2D FDTD calculation grid for TE mode	58
3.15 An ANN with three layers.....	61
3.16 The flowchart of the training process using Levenberg–Marquardt algorithm (Hao, 2011)	63
4.1 A 1×8 array of microstrip slot antennas (antenna type <i>A</i>).....	67
4.2 Simulated results of reflected power of antenna type <i>A</i>	67
4.3 Simulated normalized radiation patterns of antenna type <i>A</i>	68
4.4 Simulated results of reflected power against variation of d_r	70
4.5 Simulated gain against w_r	70
4.6 Simulated gain against h_r	71
4.7 A 1×8 array of microstrip slot antennas and U-shaped reflector (antenna type <i>B</i>).....	72
4.8 Simulated results of reflected power of antenna type <i>B</i>	73

LIST OF FIGURES (Continued)

Figure	Page
4.9 Simulated normalized radiation patterns of antenna type <i>B</i>	74
4.10 A 1×8 array of microstrip slot antennas and U-shaped reflector improved gain with curved woodpile EBG structures (antenna type <i>C</i>)	77
4.11 Simulated gain against <i>R</i>	78
4.12 Simulated gain against <i>d</i>	78
4.13 Simulated gain against <i>h</i>	79
4.14 Simulated radiated power of variation of N_c	79
4.15 Simulated results of reflected power of antenna type <i>C</i>	80
4.16 Simulated normalized radiation patterns of antenna type <i>C</i>	81
4.17 Simulated results of reflected power of three type antennas	83
4.18 Simulated normalized radiation patterns of three type antennas	84
4.19 The lumped <i>LC</i> model	85
4.20 The cavity model of the unit cell of curved woodpile EBG	86
4.21 The bandgap characteristics of the unit cell of curved woodpile EBG	86
4.22 The model to calculate S_{11} , E-, and H-fields	88
4.23 Training model of S_{11}	89
4.24 Training model of E-field	89
4.25 Training model of H-field	90

LIST OF FIGURES (Continued)

Figure	Page
4.26 The feature of the program on MATLAB	91
4.27 The running program on MATLAB.....	92
4.28 Computed reflected power.....	94
4.29 Computed normalized radiation patterns	95
5.1 The prototype of a 1×8 array of microstrip slot antennas and U-shaped reflector (antenna type <i>B</i>).....	99
5.2 The prototype of the curved woodpile EBG structures.....	101
5.3 The prototype of the antenna system	103
5.4 The three regions of an antenna (Balanis, 2005)	104
5.5 Measurement set up for the E-plane radiation pattern	106
5.6 Measurement set up for the H-plane radiation pattern.....	107
5.7 Measured reflected power	111
5.8 Measured bandwidth	110
5.9 Measured standing wave ratio	113
5.10 Measured impedance.....	114
5.11 Measured radiation patterns.....	115
5.12 The reflected power.....	116
5.13 The radiation patterns.....	117

CHAPTER I

INTRODUCTION

1.1 Background of Problems and Significance of the Study

Nowadays, wireless communication is used increasingly because users can connect to the network system from any area within the signal coverage range, so the users can conveniently connect to the system. The mobile networks or cellular networks, the wireless communication, are the radio networks distributed over land areas called cells, each cell served by at least one fixed-location transceiver, known as a cell site or base station. In the cellular network, each cell uses a different set of frequencies from neighboring cells, to avoid interference and provide guaranteed bandwidth within each cell. When they joined together, these cells will provide radio coverage over a wide geographic area. This enables a large number of the portable transceivers (mobile phones or cell phone) to communicate with each other and with fixed transceivers and telephones anywhere in the network via base stations, even some of the transceivers are moving pass more than one cell during transmission. Currently, the mobile phone or cell phone has a great influence in our live and is very convenient to keep with us. Cell phone is a faster route and yields more effectiveness to transfer information and is a resource that gives the great advantages for users that can be used almost everywhere without cables. Besides this, if there is an emergency situation, cell phone can be also useful for showing the location of users. Furthermore, we can also access to the internet by using a cell phone. Nowadays, the world's most common means of communication is Short Message Service (SMS),

which is included this cell phone system. Therefore, in this way, we can communicate with someone cheaper cost than by normal calling. According to these advantages, the development of the cellular phone system is advanced, especially in Thailand operating with Third Generation (3.9G) and beyond following Universal Mobile Telecommunication Systems (UMTS).

The development of antennas with high performances becomes currently imperatively essential for the new services and networks of telecommunication. Microstrip antenna (MSA) is an attractive choice for many modern communication systems due to its light weight, low profile with conformability, and low cost (Bahl and Bhartia, 1980; Bhartia et al., 2000). In principle, the MSA is a resonant-type antenna, where the antenna size is determined by the operating wavelength while the bandwidth is determined by the Q factor of the resonance. Two of the major disadvantages are the low gain and very narrow impedance bandwidth due to the resonant nature of the conventional MSA. Parasitic patches are used to form a multi-resonant circuit so that the operating bandwidth can be improved (Kumar and Gupta, 1985). From the research of Pozar (1985), a multi-layer MSA is investigated with parasitic patches stacked on the top of the main patch. The multi-resonant behavior can also be realized by incorporating slots into the metal patch. Furthermore, several single-layer single-patch MSAs have been reported, such as the U-slot MSA (Huynh and Lee, 1995) and the E-shaped patch antenna (Yang et al., 2001). Another important topic in MSA designs is to miniaturize the patch antenna size. Increasing the dielectric constant of the substrate is also a simple and effective way for reducing the antenna size (Lo et al., 1997). However, there are several drawbacks with the use of high dielectric constant substrate, narrow bandwidth, low radiation efficiency, and

poor radiation patterns, which results from strong surface waves excited in the substrate. The narrow bandwidth can be expanded by increasing the substrate thickness, but, will launch stronger surface waves. As a result, the radiation efficiency and patterns of the antenna will be further degraded. Chawanonphithak and Phongcharoenpanich (2007) presented an ultra-wideband circular MSA fed by microstrip line above wide-slot ground plane, a microstrip slot antenna that is developed from MSA by adding slot on ground plane, which can be expanded the bandwidth of antenna.

Many new technologies have emerged in the modern antenna design arena and one exciting breakthrough is the development of Electromagnetic Band Gap (EBG) structure. The applications of EBG structures in antenna designs have become a thrilling topic for antenna engineering (Yang and Rahmat-Samii, 2009). It's a matter of the technology of EBG structure, a new technology for the improvement of the performances of antenna, applicable on a frequential spectrum extremely wide covered from the acoustic until to the optical frequencies (Elayachi, Brachat, and Ratajczak, 2006). Besides, EBG structure, also known as photonic crystals (Joannopoulos, Meade, and Winn, 1995), is also used to improve the antenna performance (Gonzalo, Maagt, and Sorolla, 1999; Yang and Rahmat-Samii, 2003; Llombart et al., 2005). This structure has the ability to open a bandgap, which is a frequency range for which the propagation of electromagnetic waves is forbidden. By employing, EBG structures are capable to enhance the performance of slot antenna in terms of gain, side and back lobe levels, and also mutual coupling. This is due to EBG exhibits frequency band-pass and band-stop that can block the surface wave excitation in the operational frequency range of antennas (Illuz, Shavit, and

Bauer, 2004). The objectives in using EBG were basically either to increase the gain, to reduce the side and back lobe levels, and to reduce the mutual coupling (S_{21}) or to produce dual band to operate at different frequencies (Tan, Rahman, and Rahim, 2010).

Therefore, this research aims to design a sector antenna system for the age of Third Generation (3.9G) applying for the cellular base station, following IEEE802.16e Mobile WiMAX Standards at 2.1 GHz. The antenna system comprises of three main parts as follow: (1) microstrip slot antenna, an attractive choice for many modern communication systems due to its light weight, low profile with conformability, low cost, and wide-bandwidth, that provides the enough bandwidth covered frequency ranges for 3.9G system, (2) Electromagnetic Band Gap (EBG) structure, a new technology for the improvement of the performances of slot antenna in terms of gain, side and back lobe levels, and also mutual coupling, and (3) feed system.

1.2 Research Objectives

The objectives of this research are as follows:

1.2.1 To study the information for designing and developing the slot antenna and the EBG structures applying for the cellular phone system.

1.2.2 To study the proposed concept, the slot array covered with EBG structures will be designed and simulated based on the Computer Simulation Technology (CST) software.

1.2.3 To compare the simulated results from the CST software and the Finite Difference Time Domain (FDTD) method for validating of these results.

1.2.4 To implement and experiment an antenna model to validate the developing analysis tool at 2.1 GHz.

1.3 Scope of the Study

The design of a sector antenna for base station of mobile phone using slot array covered with woodpile EBG structures is presented. The licensed CST is utilized to investigate and design all of them, while the FDTD is conducted to carry out the E- and H-fields. To verify the performances of the antenna, a prototype has been fabricated at operating frequency of 2.1 GHz. This proposed antenna is experimentally tested to validate the developing analysis tool.

1.4 Expected Benefits

1.4.1 To obtain a sector antenna for base station of mobile phone.

1.4.2 To obtain the simulation program developed from the FDTD which can be applied to use with the realized problem of slot array covered with EBG structures.

1.4.3 To obtain an antenna prototype at 2.1 GHz.

1.5 Thesis Organization

The remainder of this thesis is organized as follows. In chapter 2, we present a several types of the antenna for applying to wireless communication system a for Wireless Local Area Network (WLAN) and cellular phone system. In addition, the EBG types and applications are presented. Furthermore, an introduction of original of the FDTD is presented in this chapter. The conclusion of this chapter is mentioned in last section.

In chapter 3, we present the theory and principle of analysis and design a sector antenna applying for the cellular base station. The theory and principle are composed of the microstrip slot antenna and EBG structures and the FDTD method. In the last section of this chapter, summary will be presented.

In chapter 4, the procedure to investigate and design the microstrip slot array covered with EBG structures by using the CST software is introduced. In addition, we will explain the step by step of the FDTD method to carry out the E- and H-fields. The last section of this chapter will be summarized.

To verify the performances of the proposed antenna discussed, a prototype has been designed and developed, which is given in chapter 5 and the fabrication process is described. Furthermore, the experimental process was carried out, followed by a completed description of the results obtained in the outdoors. Performance comparison between the simulated and measured results is also conducted.

The last chapter, chapter 6 provides conclusions of the research work and suggestion for future studies.

CHAPTER II

LITERATURE REVIEW

2.1 Introduction

This research aims to design and fabricate a sector antenna system for the age of Third Generation (3.9G) applying for the cellular base station, following IEEE802.16e Mobile WiMAX Standards at 2.1 GHz. The antenna system is developed from slot array and EBG structures, so that we are necessary to review and study the literature and information of microstrip slot antenna and EBG to indicate the method and suggestion.

In this chapter, we will present several types of the antenna for applying to wireless communications. In addition, the EBG types and applications are presented. Furthermore, an introduction of original of the FDTD method is also presented in this chapter and the conclusion has been mentioned in the last section.

2.2 Antenna for Wireless Communications

The dipole, monopole, sleeve, and microstrip are the most widely used as antennas for wireless communication systems (Fujimoto and James, 1994; Katsibas, 1996; Katsibas et al., 1998). A dipole antenna is widely used as a base station antenna for mobile communication, a triangular array of dipoles, as shown in Figure 2.1. It is a triangular array configuration consisting of twelve dipoles, with four dipoles on each side of the triangle. Each four-element array, on each side of the triangle, is used to cover an angular sector of 120° of user area. An array of dipole

elements is extensively used as an antenna at the base station of a land mobile system. While the monopole (Chen, Peng, and Liang, 2005), its broadband characteristics and simple construction, is the most common antenna element for portable equipment such as cellular telephones, cordless telephones, and automobiles. The dipole and monopole antennas, if they are designed correctly, they will provide the excellent performance. However, there are significant disadvantages: susceptibility to damage, additional manufacturing cost, and potential performance degradation due to the user's interaction with the exposed antenna. The sleeve antenna (Taguchi, Egashira, and Tanaka, 1991) has a straight metal element, often a rod or wire, placed and centered inside a straight metal tube, which acts as a sleeve over the center element as shown in Figure 2.2. It gets the most use in high-frequency band applications such as citizens band (CB) radio base station, maritime ship-to-ship, and ship-to-shore radio antennas. Because the sleeve antenna has not the ground plane, when it is installed with a path of metal, its gain is decreased. Microstrip antenna (MSA) (Richards, 1988; James and Hall, 1989), the most common of which is the microstrip patch antenna or patch antenna, consists of a thin sheet of low-loss insulating material called the dielectric substrate, which is completely covered with a metal on one side, called the ground plane, and partly metalized on other side, called the patch, where the antenna patch is printed on such substrate. Figure 2.3 shows the geometry of rectangular patch which is the most commonly employed MSA. This antenna is low profile, conformable to planar and nonplanar surfaces, and inexpensive to manufacture using modern printed-circuit technology, they are very versatile in terms of resonant frequency, polarization, pattern, and impedance. It can be used in high-performance aircraft, spacecraft, satellite, and missile applications, where size,

weight, cost, performance, ease of installation, and aerodynamic profile are constraints, low-profile antennas may be required (Richards, Lo, and Harrison, 1981). However, MSA also has an important limitation compared to the conventional microwave antennas that is narrow bandwidth and associated tolerance problems. Consequently, an ultra-wideband circular MSA fed by microstrip line above wide-slot ground plane (Chawanonphithak and Phongcharoenpanich, 2007), a microstrip slot antenna that is developed from MSA by adding slot on ground plane to expand the bandwidth of antenna, is applied for a sector antenna for mobile base station in this research as shown in Figure 2.4.

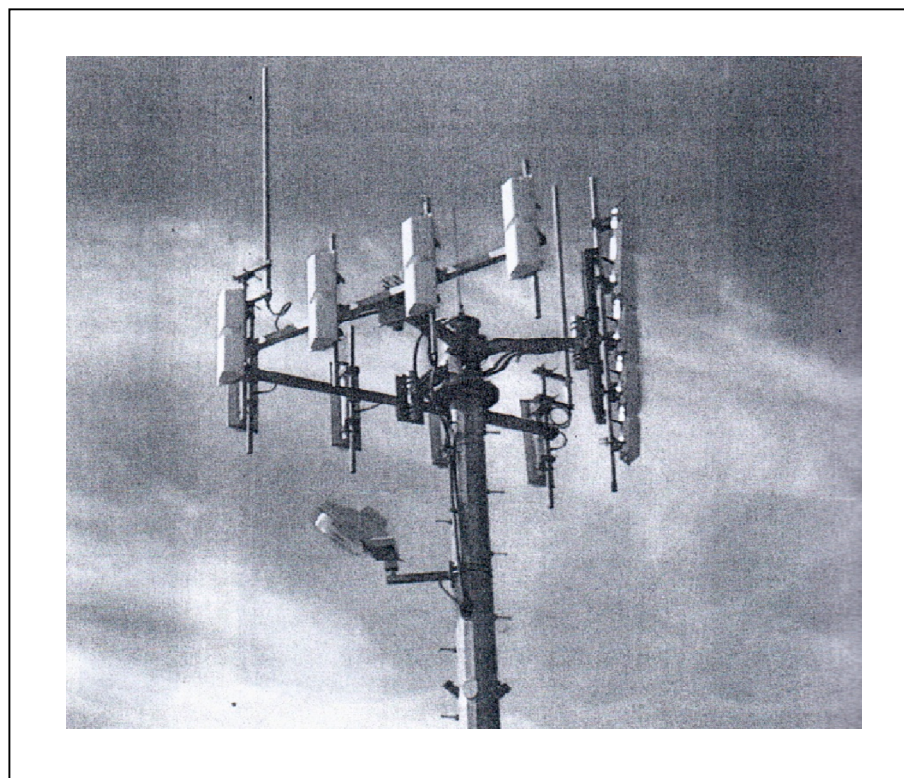


Figure 2.1 A triangular array of dipoles.

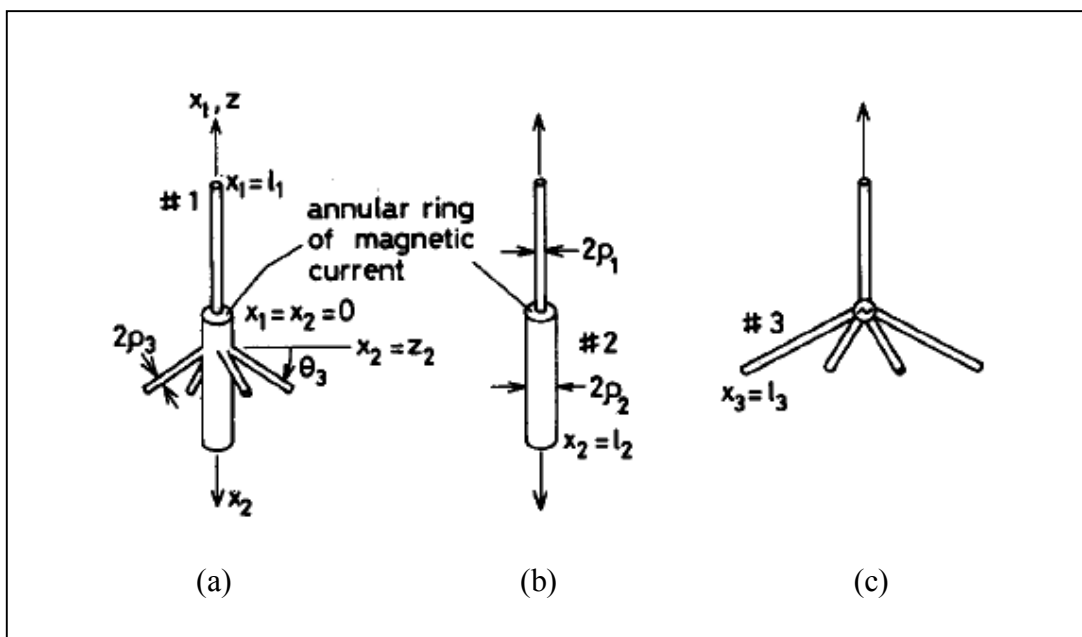


Figure 2.2 (a) Sleeve antenna with ground wires. (b) Sleeve antenna. (c) Monopole antenna with ground wires. $l_1 = 0.25\lambda$, $\rho_1 = \rho_3 = 1.7 \times 10^{-3}\lambda$, $\rho_2 = 6.8 \times 10^{-3}\lambda$

(Taguchi, Egashira, and Tanaka, 1991).

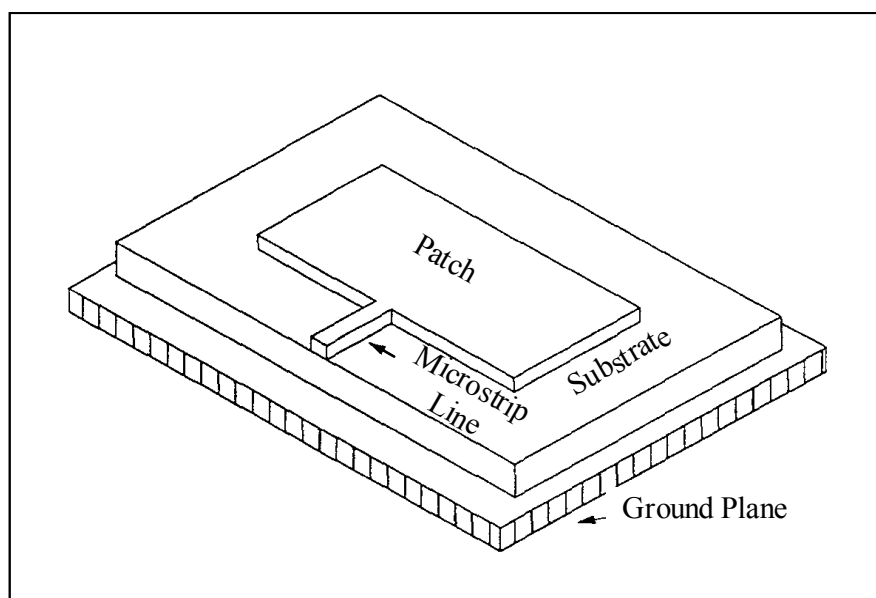


Figure 2.3 The geometry of rectangular MSA.

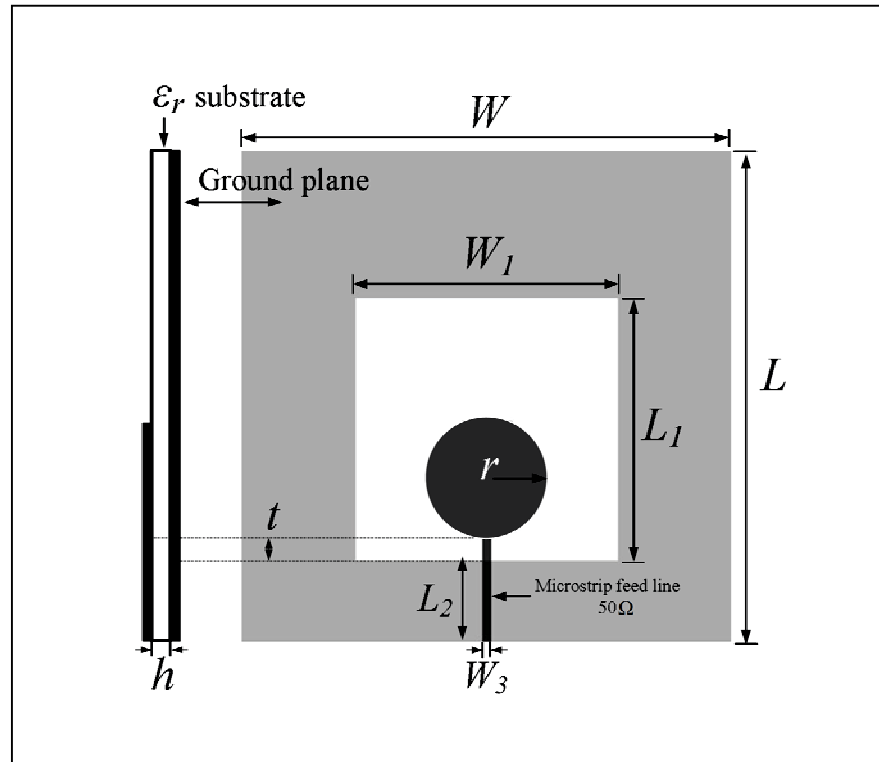


Figure 2.4 An ultra-wideband circular MSA fed by microstrip line above wide-slot ground plane (Chawanonphithak and Phongcharoenpanich, 2007).

2.3 Electromagnetic Band Gap

In the recent years, EBG structures have attracted increasing interests because of their desirable electromagnetic properties that cannot be observed in natural material. In this respect, EBG structures are a subset of metamaterials. Diverse research activities on EBG structures are on the rise in the electromagnetic and antenna community such as low profile antennas, active phased array, TEM waveguides, and microwave filters. The unique electromagnetic properties of EBG structures have led to a wide range of applications in MSA engineering because the EBG structures can be integrated into MSA designs and their surface wave band gap

property helps to increase the antenna gain, minimize the side and back lobes, and reduce mutual coupling in array elements (Yang and Rahmat-Samii, 2009).

2.3.1 MSA Surrounded by EBG Structures

Yang and Rahmat-Samii (2001) presented the comparison of the step-like substrate and EBG structures to be applied to the patch antennas separately to overcome the undesirable features of the high dielectric constant substrate without sacrificing any of desirable features, namely, small size and wide bandwidth. The first approach, a step-like substrate is used as shown in Figure 2.5. The idea is to use a thick substrate under the patch which helps to remain the compact size and bandwidth and use a thin substrate around the patch which is beneficial to reduce the surface wave. This structure looks as a step. The distance between patch and the step will be carefully chosen. If the distance is too small, the resonance feature of the patch will change and the bandwidth will decrease. If the distance is too large, it cannot reduce the surface waves. The second approach, the patch surrounded by EBG structures is considered as shown in Figure 2.6. The EBG structures are designed for providing the surface wave band gap covers the antenna resonant frequency. As a result, the surface waves excited by the patch antenna are inhibited from propagation by the EBG structures. To effectively suppress the surface waves, four rows of EBG cells are used in the design. Figure 2.7 shows the photos of the patch antennas on step-like substrate and surrounded by EBG structure prototype. From above comparisons, Yang and Rahmat-Samii (2001) summarized that the EBG structures can improve the radiation performances of patch antenna while maintaining its compact size and adequate bandwidth.

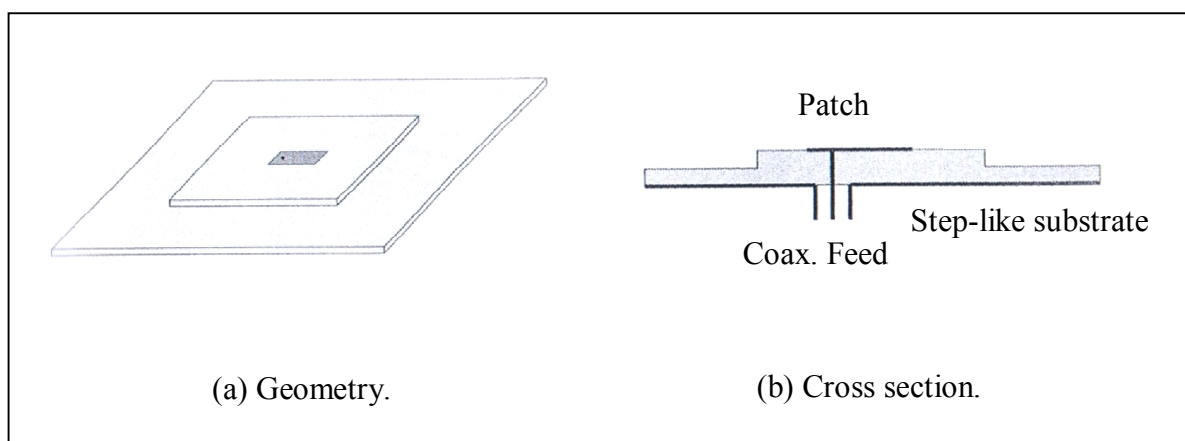


Figure 2.5 Patch antenna on a step-like substrate (Yang and Rahmat-Samii, 2001).

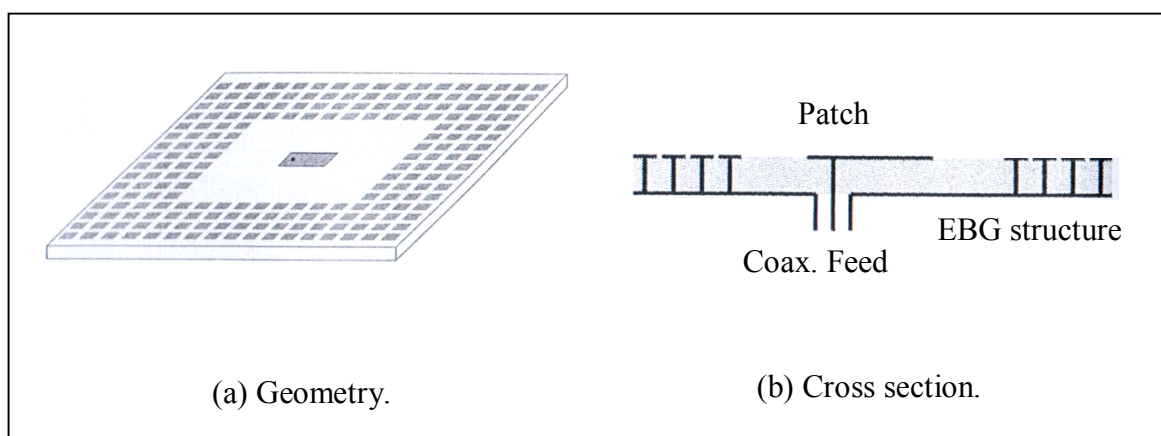
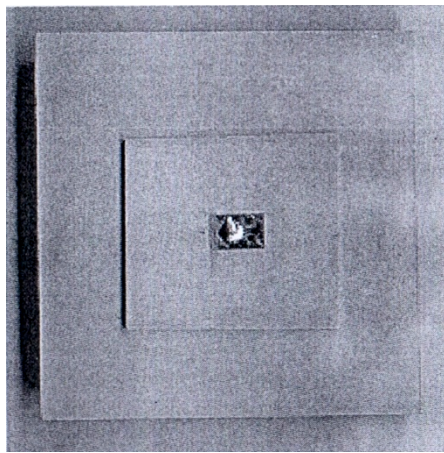
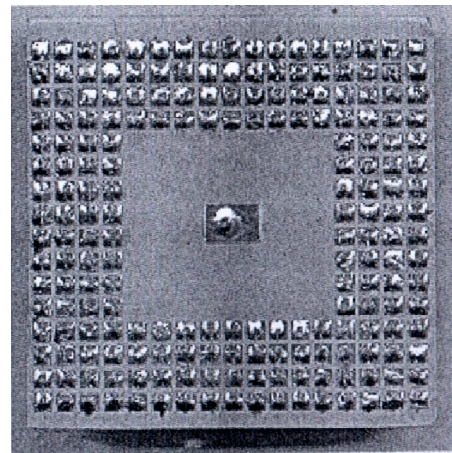


Figure 2.6 Patch antenna surrounded by mushroom-like EBG structures
(Yang and Rahmat-Samii, 2001).



(a) Patch antenna on a step-like substrate.



(b) Patch antenna surrounded by mushroom-like EBG structures.

Figure 2.7 Prototype of two patch antenna designs with enhanced performance
(Yang and Rahmat-Samii, 2001).

2.3.2 MSA on Top of EBG Structures

In this section, the MSA performance on top of EBG substrates (Fan et al., 2003; Qu, Shafai, and Foroozesh, 2006) is discussed, the near field of the antenna is also significantly altered by the existence of the EBG structures. The conducting ground plane of MSA is replaced by a high impedance EBG layer (Shafai, and Foroozesh, 2006) as shown in Figure 2.8. Parametric studies are conducted to maximize their impedance bandwidths and gains. It is found that very wide bandwidths, of around 25%, can be obtained by variation of the original antenna and EBG parameters such as the feed location, patch width, ground plane size, and EBG spacing. As a result, the MSA over the EBG ground plane has a significantly improved performance in its impedance bandwidth, gain, and cross polarization.

2.3.3 Mutual Coupling Reduction by the EBG Structures

As an important parameter in array design, the mutual coupling between array elements is investigated both numerically and experimentally. Because the strong mutual coupling could reduce the array efficiency and cause the scan blindness in phased array systems. To reduce the strong mutual coupling of the E-plane coupled MSA on a thick and high permittivity substrate, the mushroom-like EBG structures are inserted between antenna elements (Yang and Rahmat-Samii, 2003), as shown in Figure 2.9. When the EBG parameters are properly designed, the pronounced surface waves are suppressed, resulting in a low mutual coupling.

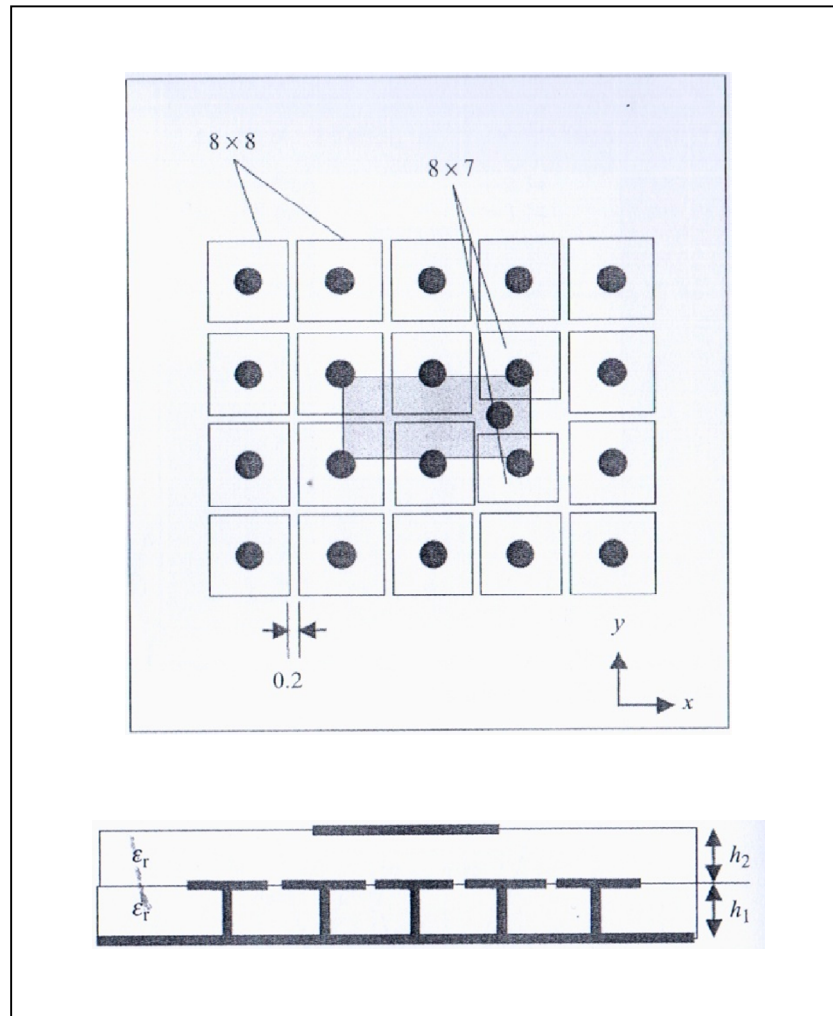


Figure 2.8 Geometry of MSA on top of EBG structures
(Shafai, and Foroozesh, 2006).

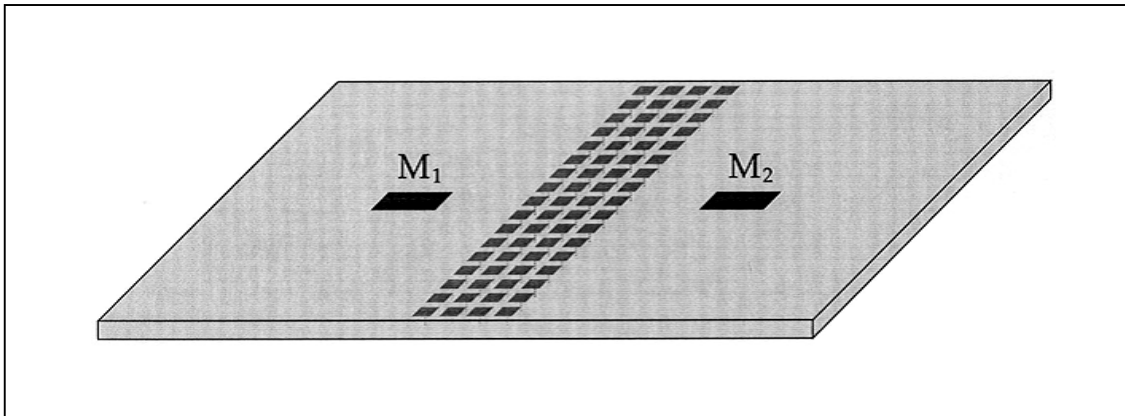


Figure 2.9 MSA separated by the mushroom-like EBG structures

(Yang and Rahmat-Samii, 2003).

2.3.4 Gain Enhancement of Resonator Antenna by Woodpile EBG Structures

Traditionally, high gain antennas are realized using either parabolic antennas or large antenna arrays. However, the curved surface of parabolic antennas makes it difficult to be conformal with mobile platforms, while large antenna arrays always suffer from loss in the feeding network. A new resonator antenna has been developed from the woodpile EBG structures and a metallic ground plane (Weily et al., 2005). This device exploits the bandgap of the EBG structures to create highly directional radiation by virtue of the resonator's angle-dependent transmission properties. The configuration of the EBG resonator antenna with a MSA feed is shown in Figure 2.10. The patch antenna is fed from below by a coaxial probe, and mounted on an aluminum ground plane. After optimizing parameters of this woodpile EBG design, a 19 dBi antenna gain is obtained.

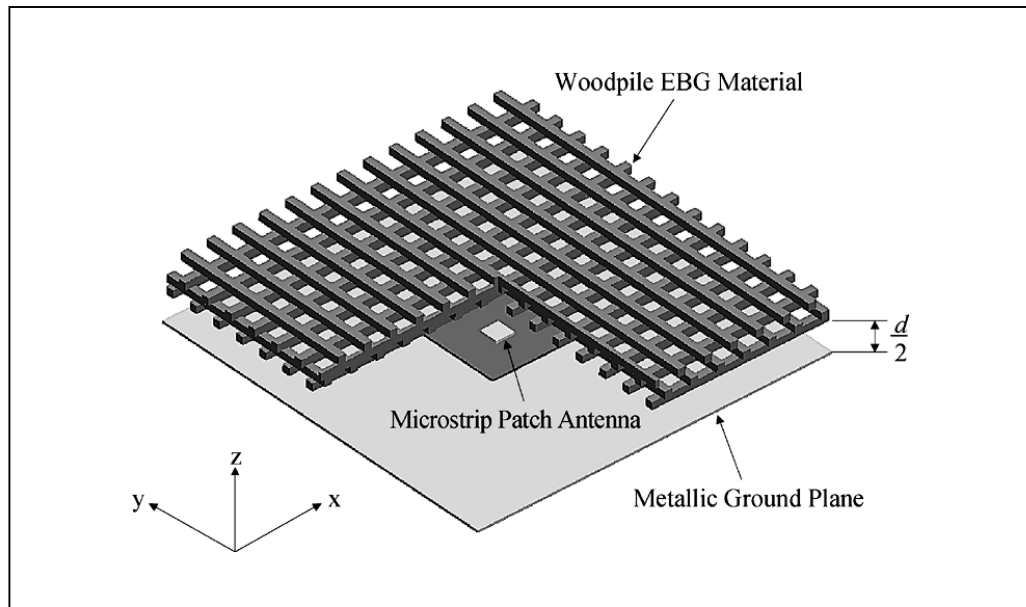


Figure 2.10 A high gain antenna design using the woodpile EBG structures

(Weily et al., 2005).

From this concept, the research presents an array antenna using slots covered with woodpile EBG structures providing the high gain and proper beamwidth suitable for mobile phone base station as following IEEE802.16e mobile WiMAX.

2.4 The Origin of Finite Difference Time Domain

The FDTD method is a numerical analysis technique used for modeling computational electrodynamics (finding approximate solutions to the associated system of differential equations). While many electromagnetic simulation techniques are applied in the frequency-domain but FDTD solves Maxwell's equations in the time domain. This means that the calculation of the electromagnetic field values progress at discrete steps in time. One benefit of the time domain approach is to give broadband output from a single execution of the program. However, the main reason

for using the FDTD approach is the excellent scaling performance of the method as the problem size grows. As the number of unknowns increases, the FDTD approach quickly outpaces other methods in efficiency.

The basic FDTD space grid and time-stepping algorithm trace back to a seminal paper in 1966 by Yee. However, the Yee scheme can be rewritten as a finite difference scheme to solve the electromagnetic wave equation and this basic finite difference scheme for the wave equation goes back to Courant, Friedrichs, and Lewy's seminal paper from 1928. The description "Finite-difference time-domain" and its corresponding "FDTD" acronym were originated by Taflove in 1980. Since about 1990, FDTD techniques have emerged as primary means to computationally model many scientific and engineering problems dealing with electromagnetic wave interactions with material structures. The current FDTD modeling applications range from near-DC (ultralow-frequency geophysics involving the entire Earth-ionosphere waveguide) through microwaves (radar signature technology, antennas, wireless communications devices, digital interconnects, and biomedical imaging/treatment) to visible light (photonic crystals, nanoplasmonics, solitons, and biophotonics) (Taflove and Hagness, 2005). In 2006, an estimated 2,000 FDTD-related publication appeared in the science and engineering literatures. In 2008, there are at least 27 commercial/proprietary FDTD software vendors; 8 free-software/open-source-software FDTD projects; and 2 freeware/closed-source FDTD projects. Table 2.1 shows partial chronology of FDTD techniques and applications for Maxwell's equations (http://en.wikipedia.org/wiki/Finite-difference_time-domain_method).

Table 2.1 Partial chronology of FDTD techniques and applications.

Authors	Event	Year
Courant, Friedrichs, and Lewy	Courant, Freidrichs, and Lewy published seminal paper with finite difference scheme for solving second-order wave equation in 1D and 2D.	1928
Yee	Yee described the basis of the FDTD numerical technique for solving Maxwell's curl equations directly in the time domain on a space grid.	1966
Taflove and Brodwin	Taflove and Brodwin reported the correct numerical stability criterion for Yee's algorithm; the first sinusoidal steady-state FDTD solutions of 2D and 3D electromagnetic wave interactions with material structures; and the first bioelectromagnetics models.	1975
Holland (1977) and Kunz and Lee (1978)	Holland and Kunz and Lee applied Yee's algorithm to EMP problems.	1977-1978
Taflove	Taflove coined the FDTD acronym and published the first validated FDTD models of sinusoidal steady-state electromagnetic wave penetration into a 3D metal cavity.	1980
Mur	Mur published the first numerically stable, second-order accurate, absorbing boundary condition (ABC) for Yee's grid.	1981
Taflove and Umashankar	Taflove and Umashankar developed the first FDTD electromagnetic wave scattering models computing sinusoidal steady state near fields, far fields, and radar cross section for 2D and 3D structures.	1982-1983
Liao et al.	Liao et al. reported an improved ABC based upon space-time extrapolation of the field adjacent to the outer grid boundary.	1984

Authors	Event	Year
Gwarek	Gwarek introduced the lumped equivalent circuit formulation of FDTD.	1985
Choi and Hoefler	Choi and Hoefler published the first FDTD simulation of waveguide structures.	1986
Kriegsmann et al. (1987) and Moore et al. (1988)	Kriegsmann et al. and Moore et al. published the first articles on ABC theory in <i>IEEE Transactions on Antennas and Propagation</i> .	1987-1988
Umashankar et al. (1987), Taflove et al. (1988), and Jurgens et al. (1992)	Contour-path sub cell techniques were introduced by Umashankar et al. to permit FDTD modeling of thin wires and wire bundles, by Taflove et al. to model penetration through cracks in conducting screens, and by Jurgens et al. to conformally model the surface of a smoothly curved scatterer.	1987-1988, 1992
Sullivan et al.	Sullivan et al. published the first 3D FDTD model of sinusoidal steady-state electromagnetic wave absorption by a complete human body.	1988
Zhang et al.	FDTD modeling of microstrips was introduced by Zhang et al.	1988
Kashiwa and Fukai (1990), Luebbers et al. (1990), and Joseph et al. (1991)	FDTD modeling of frequency-dependent dielectric permittivity was introduced by Kashiwa and Fukai, Luebbers et al., and Joseph et al.	1990-1991
Maloney et al. (1990), Katz et al. (1991), and Tirkas and Balanis (1991)	FDTD modeling of antennas was introduced by Maloney et al., Katz et al., and Tirkas and Balanis.	1990-1991
Sano and Shibata, and El-Ghazaly et al.	FDTD modeling of picosecond optoelectronic switches was introduced by Sano and Shibata, and El-Ghazaly et al.	1990

Authors	Event	Year
Goorjian and Taflove (1992), Ziolkowski and Judkins (1993), Joseph et al. (1993), and Joseph and Taflove (1994)	FDTD modeling of the propagation of optical pulses in nonlinear dispersive media was introduced, including the first temporal solitons in 1D by Goorjian and Taflove; beam self-focusing by Ziolkowski and Judkins; the first temporal solitons in 2D by Joseph et al.; and the first spatial solitons in 2D by Joseph and Taflove.	1992-1994
Sui et al.	FDTD modeling of lumped electronic circuit elements was introduced by Sui et al.	1992
Toland et al.	Toland et al. published the first FDTD models of gain devices (tunnel diodes and Gunn diodes) exciting cavities and antennas.	1993
Aoyagi et al.	Aoyagi et al. presented a hybrid Yee algorithm/scalar-wave equation and demonstrate equivalence of Yee scheme to finite difference scheme for electromagnetic wave equation.	1993
Thomas et al.	Thomas et al. introduced a Norton's equivalent circuit for the FDTD space lattice, which permits the SPICE circuit analysis tool to implement accurate subgrid models of nonlinear electronic components or complete circuits embedded within the lattice	1994
Berenger, Katz et al., and Reuter et al.	Berenger introduced the highly effective, perfectly matched layer (PML) ABC for 2D FDTD grids, which was extended to 3D by Katz et al., and to dispersive waveguide terminations by Reuter et al.	1994
Chew and Weedon	Chew and Weedon introduced the coordinate stretching PML that is easily extended to 3D, other coordinate systems and other physical equations.	1994

Authors	Event	Year
Sacks et al. (1995) and Gedney (1996)	Sacks et al. and Gedney introduced a physically realizable, uniaxial perfectly matched layer (UPML) ABC.	1995-1996
Liu	Liu introduced the pseudospectral time-domain (PSTD) method, which permits extremely coarse spatial sampling of the electromagnetic field at the Nyquist limit.	1997
Ramahi	Ramahi introduced the complementary operators method (COM) to implement highly effective analytical ABCs.	1997
Maloney and Kesler	Maloney and Kesler introduced several novel means to analyze periodic structures in the FDTD space lattice.	1998
Nagra and York	Nagra and York introduced a hybrid FDTD-quantum mechanics model of electromagnetic wave interactions with materials having electrons transitioning between multiple energy levels.	1998
Hagness et al.	Hagness et al. introduced FDTD modeling of the detection of breast cancer using ultrawideband radar techniques.	1998
Schneider and Wagner	Schneider and Wagner introduced a comprehensive analysis of FDTD grid dispersion based upon complex wave numbers.	1999
Zheng, Chen, and Zhang	Zheng, Chen, and Zhang introduced the first 3D alternating-direction implicit (ADI) FDTD algorithm with provable unconditional numerical stability.	2000-2001
Roden and Gedney	Roden and Gedney introduced the advanced convolutional PML (CPML) ABC.	2000

Authors	Event	Year
Rylander and Bondeson	Rylander and Bondeson introduced a provably stable FDTD finite-element time-domain hybrid technique.	2000
Hayakawa et al. and Simpson and Taflove	Hayakawa et al. and Simpson and Taflove independently introduced FDTD modeling of the global Earth-ionosphere waveguide for extremely low-frequency geophysical phenomena.	2002
DeRaedt	DeRaedt introduced the unconditionally stable, “one-step” FDTD technique.	2003
Ahmed et al.	Ahmed et al. introduced the 3D locally 1D (LOD) FDTD method and proved unconditional numerical stability.	2008
Chaudhury and Boeuf	Chaudhury and Boeuf demonstrated the numerical procedure to couple FDTD and Plasma fluid model for studying Microwave Plasma Interaction.	2010
Moxley et al.	Moxley et al. developed a generalized FDTD quantum method for the N-body interacting Hamiltonian.	2012
Moxley et al.	Moxley et al. developed a generalized FDTD scheme for solving nonlinear Schrodinger equations.	2013
Moxley et al.	Moxley et al. developed an implicit generalized FDTD scheme for solving nonlinear Schrodinger equations.	2014

The interest in FDTD Maxwell’s equations solvers has increased nearly exponentially over the past 20 years. Increasingly, engineers and scientists in nontraditional electromagnetics-related areas such as photonics and nanotechnology have become aware of the power of FDTD techniques. As shown in Figure 2.11,

an estimated 2,000 FDTD-related publication appeared in the science and engineering literatures in 2006, as opposed to fewer than 10 as recently as 1985. The current rate of growth (based upon a study of ISI Web of Science data) is approximately 5:1 over the period 1995 to 2006. Furthermore, the descriptor FDTD has become widely used, having appeared in this exact form in 43,900 articles as of August 7, 2011, according to Google Scholar.

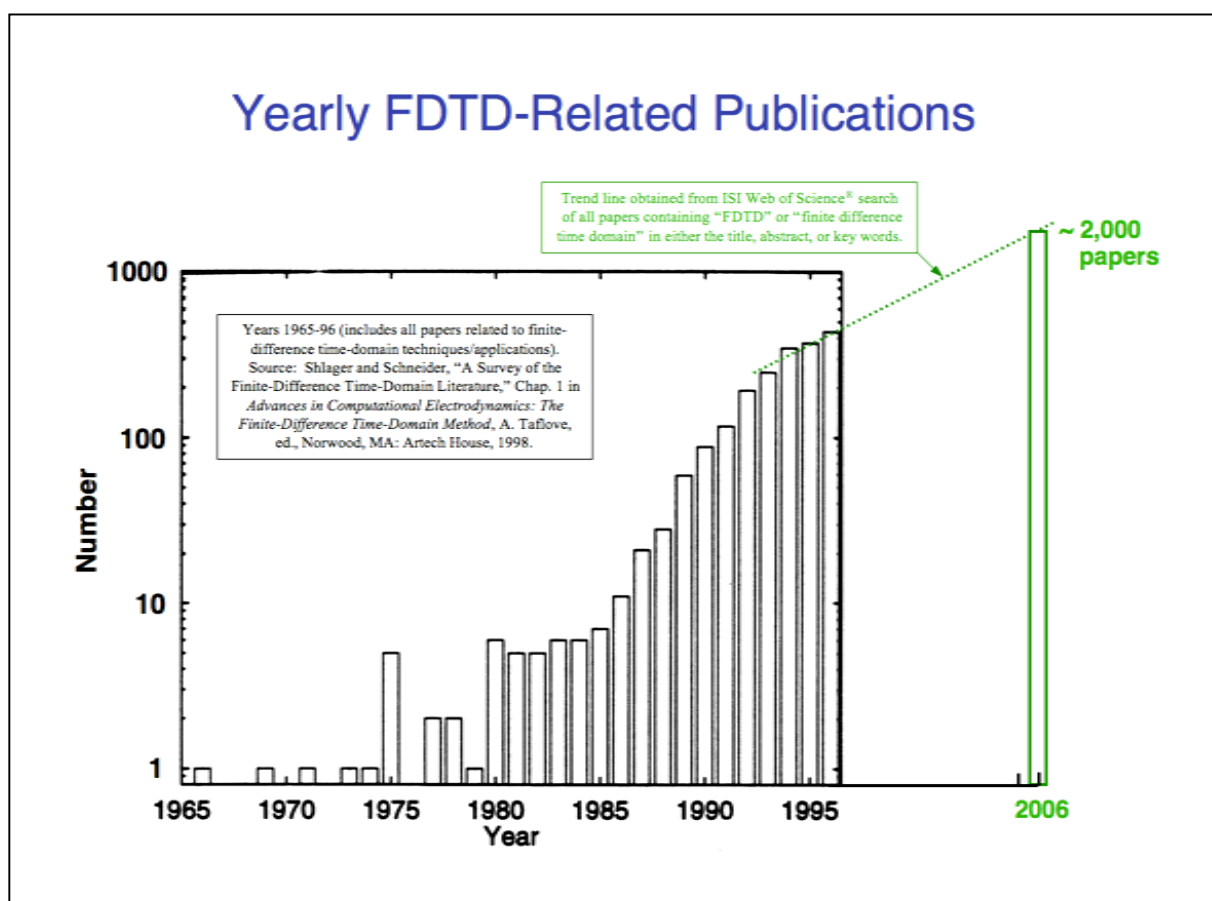


Figure 2.11 An estimated FDTD-related publications

(http://upload.wikimedia.org/wikipedia/en/a/a3/Yearly_FDTD_publications.png).

On the other hand, both the general increase in academic publication throughput during the same period and the overall expansion of interest in all computational electromagnetics (CEM) techniques, there are seven primary reasons for the tremendous expansion of interest in FDTD computational solution approaches for Maxwell's equations (Taflove and Hagness, 2005):

(1). FDTD uses no linear algebra. Being a fully explicit computation, FDTD avoids the difficulties with linear algebra that limits the size of frequency-domain integral-equation and finite-element electromagnetics models to generally fewer than 10^9 electromagnetic field unknowns. FDTD models with as many as 10^9 field unknowns have been run; there is no intrinsic upper bound to this number.

(2). FDTD is accurate and robust. The sources of error in FDTD calculations are well understood, and can be bounded to permit accurate models for a very large variety of electromagnetic wave interaction problems.

(3). FDTD treats impulsive behavior naturally. Being a time-domain technique, FDTD directly calculates the impulse response of an electromagnetic system. Therefore, a single FDTD simulation can provide either ultrawideband temporal waveforms or the sinusoidal steady-state response at any frequency within the excitation spectrum.

(4). FDTD treats nonlinear behavior naturally. Being a time-domain technique, FDTD directly calculates the nonlinear response of an electromagnetic system. This allows natural hybridizing of FDTD with sets of auxiliary differential equations that describe nonlinearities from either the classical or semi-classical standpoint. One research frontier is the development of hybrid algorithms which join FDTD classical electrodynamics models with phenomena arising from

quantum electrodynamics, especially vacuum fluctuations, such as the Casimir effect (Johnson, 2011).

(5). FDTD is a systematic approach. With FDTD, specifying a new structure to be modeled is reduced to a problem of mesh generation rather than the potentially complex reformulation of an integral equation. For example, FDTD requires no calculation of structure-dependent Green functions.

(6). Parallel-processing computer architectures have come to dominate supercomputing. FDTD scales with high efficiency on parallel-processing CPU-based computers, and extremely well on recently developed GPU-based accelerator technology.

(7). Computer visualization capabilities are increasing rapidly. While this trend positively influences all numerical techniques, it is of particular advantage to FDTD methods, which generate time-marched arrays of field quantities suitable for use in color videos to illustrate the field dynamics.

Taflove and Hagness (2005) have argued that these factors combine to suggest that FDTD will remain one of the dominant computational electrodynamics techniques (as well as potentially other multiphysics problems).

2.5 Chapter Summary

This chapter gives a detail and literature surveys of the antenna applying for wireless communications. It was found that an array of dipole elements is extensively used as an antenna at the base station of a land mobile system while a monopole, its broadband characteristics and simple construction, is perhaps to the most common antenna element for portable equipment such as cellular telephones, cordless

telephones, and automobiles. However, there are significant disadvantages: susceptibility to damage, additional manufacturing cost, and potential performance degradation. The sleeve antenna gets the most use in high-frequency band applications. Because it has not the ground plane, when it is installed with a path of metal, its gain is decreased. The MSA is low profile, conformable to planar and nonplanar surfaces, simple and inexpensive to manufacture using modern printed-circuit technology, it is very versatile in terms of resonant frequency, polarization, pattern, and impedance. Nevertheless, the narrow bandwidth is an important limitation of MSA. By adding slot on ground plane can be expanded the bandwidth of antenna which is property of slot antenna. Therefore, the slot antenna is an alternative choice for wireless communications. In order to improve efficiency of the antenna, the EBG can help to increase the antenna gain, minimize the side and back lobes, and reduce mutual coupling in array elements. In addition, the literature surveys of the FDTD method was presented in the last section. This thesis focuses on the 2D FDTD technique, the formulations and the numerical example of antenna analysis will be detailed in following chapter.

CHAPTER III

BACKGROUND THEORY

3.1 Introduction

The purpose of this chapter is to describe the theory and principle of microstrip slot antenna and EBG structures. Moreover, the FDTD method is presented with a focus on 2D FDTD, which is used as efficient computation engine for the analysis of dielectric material. The fundamentals of the FDTD method are reviewed and the artificial neural network (ANN) are discussed to model the computational method. In the last section of this chapter, the conclusion will be presented.

3.2 Microstrip Antenna

The MSAs (Garg et al., 2001) have several advantages compared to the conventional microwave antennas and many applications cover the broad frequency range from 100 MHz to 100 GHz. Some of the principle advantages of MSAs compared to the conventional microwave antennas are:

- Light weight, low volume, and low profile configurations, which can be made conformal;
- Low fabrication cost; readily amenable to mass production;
- Linear and circular polarizations are possible with simple feed;
- Conformable to planar and nonplanar surfaces;
- Simple and inexpensive to manufacture using modern printed-circuit technology;

- Mechanically robust when mounted on rigid surfaces;
- Compatible with Monolithic Microwave Integrated Circuit (MMIC) designs;
- Dual-frequency and dual-polarization antennas can be easily made;
- No cavity backing is required;
- Can be easily integrated with microwave integrated circuits;
- Feed lines and matching networks can be fabricated simultaneously with the antenna structure;
- Adaptive elements with variable resonant frequency, impedance, polarization, and pattern can be designed.

However, MSAs also have some limitations compared to the conventional microwave antennas:

- Narrow bandwidth and associated tolerance problems;
- Somewhat lower gain (about 6 dB);
- Large ohmic loss in the feed structure of arrays;
- Most MSAs radiate into half-space;
- Complex feed structure required for high-performance arrays;
- Polarization purity is difficult to achieve;
- Poor end-fire radiator, except tapered slot antenna;
- Extraneous radiation from feeds and junctions;
- Lower power handling capability (about 100 W);
- Reduced gain and efficiency as well as unacceptably high levels of cross-polarization and mutual coupling within an array environment at high frequencies;

- Excitation of surface waves;
- MSAs fabricated on substrate with a high dielectric constant are strongly preferred for easy integration with MMIC RF front-end circuitry. However, using high dielectric constant substrate leads to poor efficiency and narrow bandwidth.

There are procedures to minimize the effect of some of these limitations of MSAs. For instance, the bandwidth can be increased to more than 60 percent by using special techniques such as using stacked elements (Long and Walton, 1978), using coplanar parasitic elements (Wood, 1980), using a nearly square patch that excited two modes with orthogonal polarizations (Yano and Ishimaru, 1981), and adding slot on ground plane (Chawanonphithak and Phongcharoenpanich, 2007). Lower gain and lower power handling limitations can be overcome through an array configuration. Surface wave-associated limitations such as poor efficiency, increased mutual coupling, reduced gain and radiation pattern degradations can be overcome by using the Photonic Band Gap (PBG) or EBG structures (Qian et al., 1999).

3.2.1 Microstrip Slot Antenna

The concept of microstrip slot antenna has evolved from slot antennas excited by a strip line (Garg et al., 2001). It comprises a slot cut on the ground plane of a grounded substrate. The slot can have practically any shape which most of the microstrip patch shapes as shown in Figure 3.1 can be realized in the form of a microstrip slot antenna.

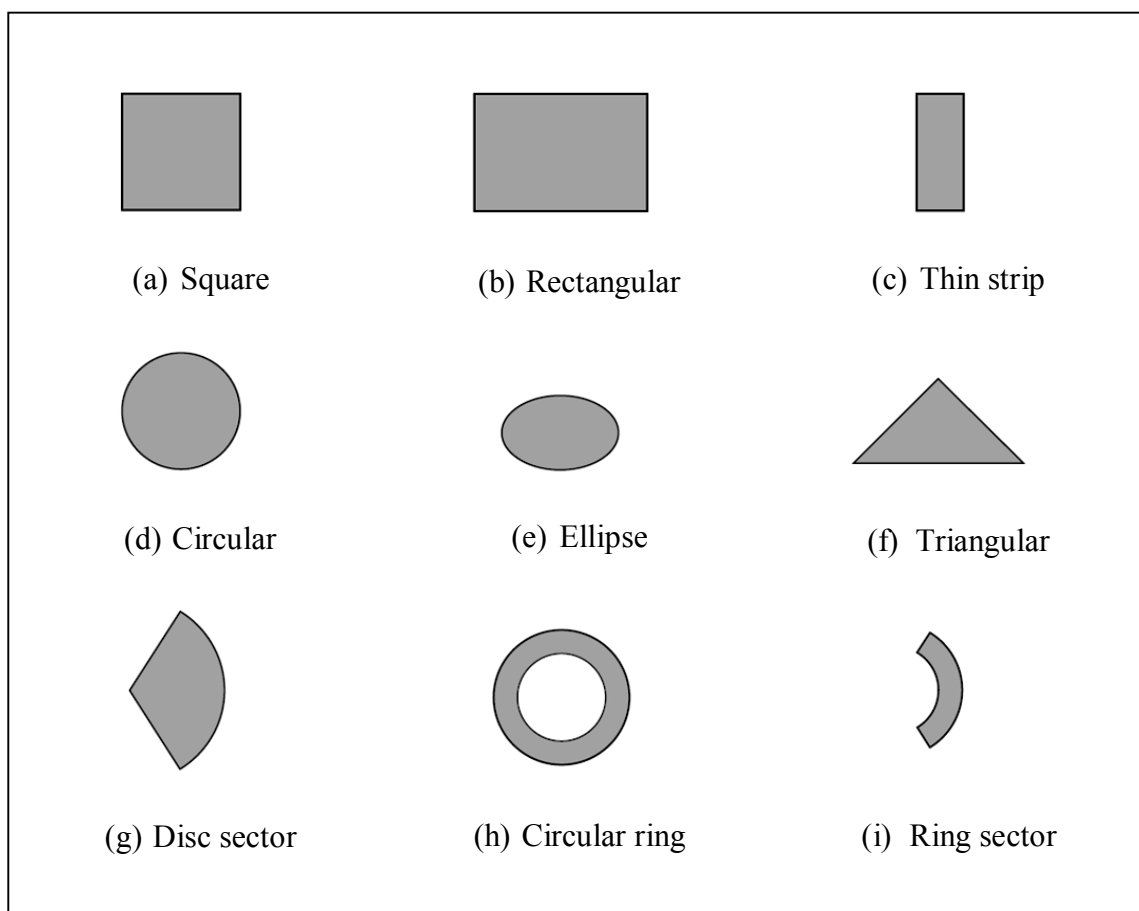


Figure 3.1 The shapes of microstrip patch elements.

Microstrip slot antenna has the advantage of being able to produce bidirectional radiation with larger bandwidth which is radiated on both sides of the slot. Moreover, unidirectional radiation is obtained by using a reflector plate on one side of the slot. Like microstrip patch antennas, the microstrip slot antennas can be fed either by a microstrip-line or a coplanar waveguide. The microstrip-line feed is the simplest method to feed a microstrip slot antenna. The fields of the microstrip-line excite the slot. To increase efficiency excitation of the slot, the strip conductor is either short-circuited through the dielectric substrate to the edge of the slot as shown in Figure 3.2(a), or the strip conductor is terminated in an open-circuited stub beyond

the edge of the slot as shown in Figure 3.2(b) (Yoshimura, 1972). The length L_m of the open-circuited microstrip stub is approximately a quarter-wave long, therefore, an effective short circuit is realized at the outer edge of the slot. The most advantage of this method is very low cross-polarization (typically -35 dB) when compared to the microstrip patch antennas (Axelrod, Kisliuk, and Maoz, 1989). In addition, it is easy to fabricate, simple to match by controlling the outer edge of the slot and rather simple to model.

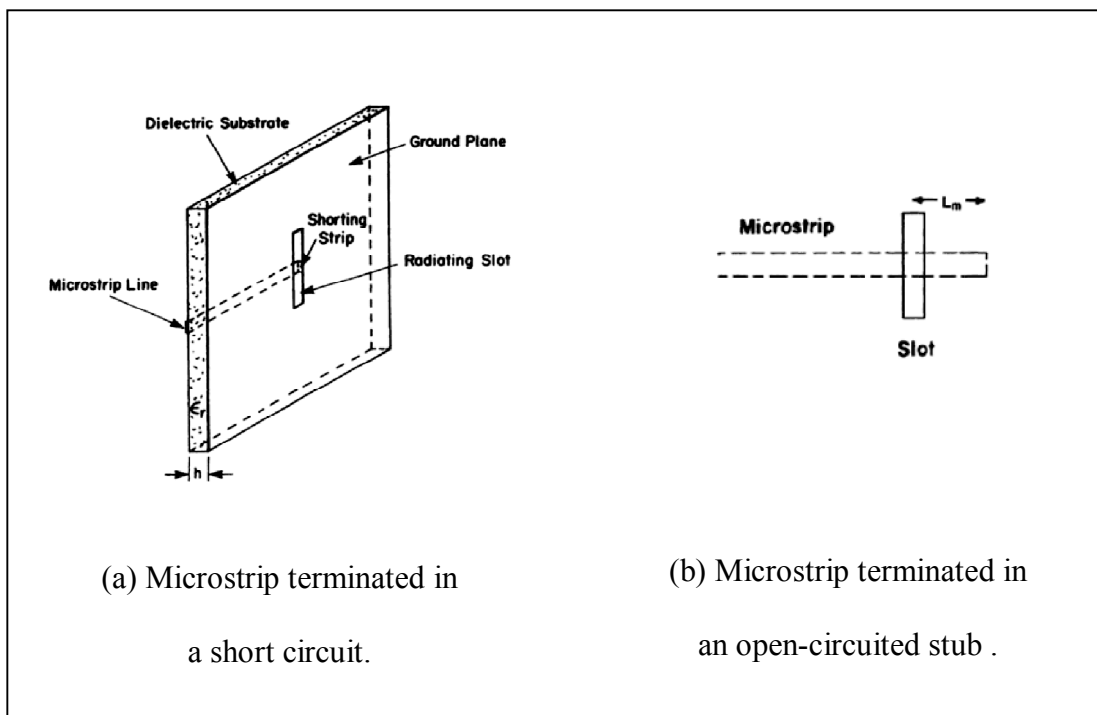


Figure 3.2 Center-fed microstrip slot antenna configurations

(Yoshimura, 1972).

3.2.2 Microstrip Slot Antenna Array

Microstrip slot antennas are used not only as single elements but are also very popular in arrays. In many applications, it is necessary to design antennas with very directive characteristics (very high gains) to meet the demands of long distance communication. This can only be accomplished by increasing the electrical size of the antenna. To enlarge the dimensions of the antenna, without necessarily increasing the size of the individual elements, is to form an assembly of radiating elements in an electrical and geometrical configuration. This new antenna, formed by multielements, is referred to as an array. The importance parameters of antenna array are the spacing between the elements and the difference in amplitude and phase fed to each element which would cause the radiating field of element to combine constructively in the intended direction and cancel out each other at other undesired directions in the far field (Balanis, 1997). Thus higher gain and more flexibility in controlling the shape of the beamwidth and side lobe levels can be achieved from this method.

3.3 Electromagnetic Band Gap Structures

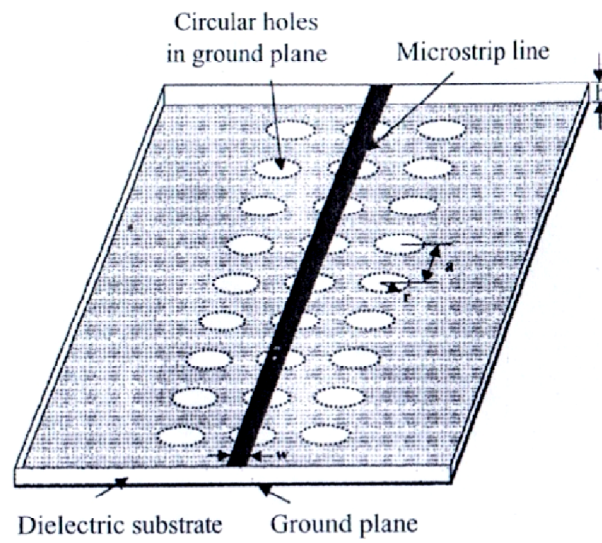
This section addresses the definition of EBG structures, the relation between EBG and metamaterials, and the analysis methods for EBG structures. Moreover, the woodpile EBG structures are investigated in this.

3.3.1 EBG Definition

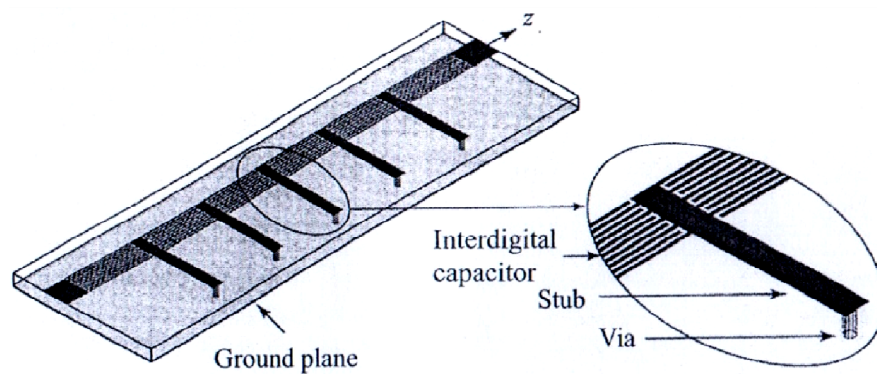
The EBG structures, also known as Photonic Crystals (Joannopoulos, Meade, and Finn, 1995) or Photonic Band Gap (PBG) Materials (Yablonovitch, 1987) are periodic structures which do not allow the propagation of electromagnetic waves

with in certain frequency ranges. Generally speaking, the EBG structures are defined as “*artificial periodic (or sometimes non-periodic) objects that prevent/assist the propagation of electromagnetic waves in a specified band of frequency for all incident angles and all polarization states*” (Yang and Rahmat-Samii, 2009). The EBG structures are usually realized by periodic arrangement of dielectric material and metallic conductors. In general, they can be categorized into three groups according to their geometric configuration such as (1) one-dimensional (1D) transmission lines, (2) two-dimensional (2D) planar surfaces, and (3) three-dimensional (3D) volumetric structures.

Figure 3.3 shows the 1D EBG transmission lines design, a microstrip line with periodic holes on the ground plane (Radisic et al., 1998) and a composite right- and left-handed transmission line (Caloz and Itoh, 2005). The 2D planar surfaces, a mushroom-like surface (Sievenpiper et al., 1999) and a uni-planar design without vertical vias (Yang et al., 1999), are shown in Figure 3.4. In Figure 3.5, the 3D volumetric structures are shown in two representative structures such as a woodpile structure consisting of square dielectric bars (Ozbay et al., 1994) and a multi-layer metallic tripod array (Barlevy and Rahmat-Samii, 2001).



(a) A microstrip line with periodic holes on the ground plane (Radisic et al., 1998).



(b) A composite right- and left-handed transmission line (Caloz and Itoh, 2005).

Figure 3.3 The 1D EBG transmission lines.

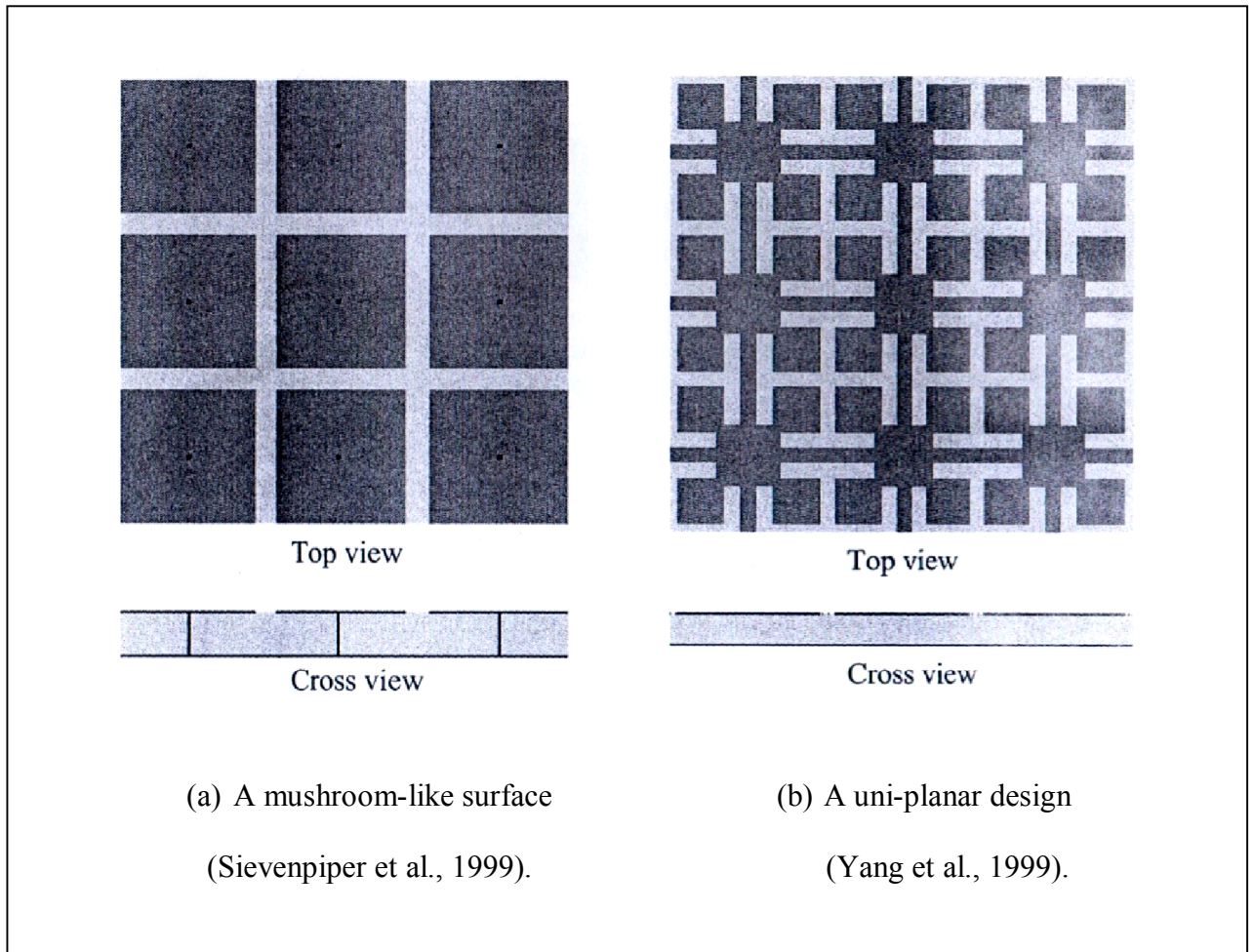


Figure 3.4 The 2D EBG planar surfaces.

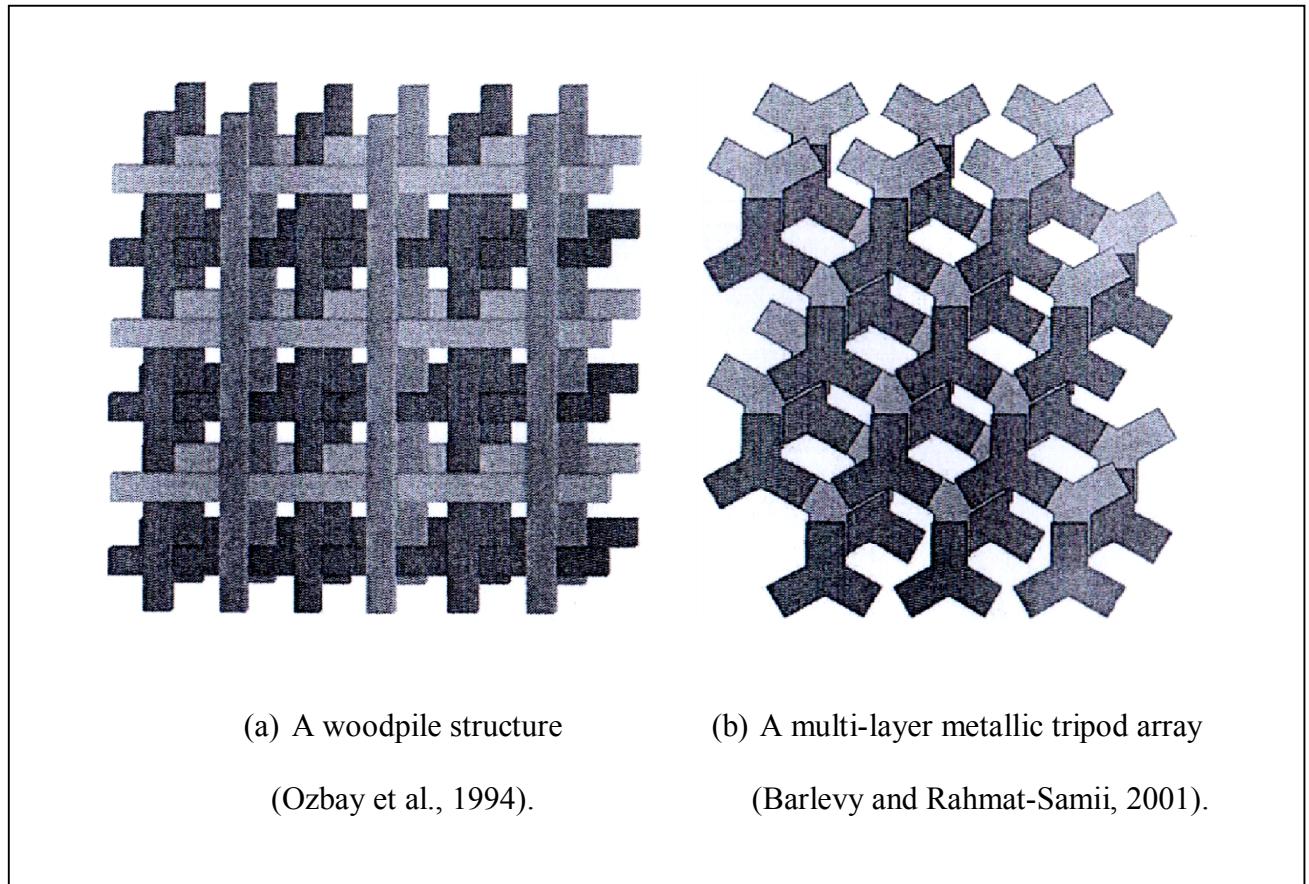


Figure 3.5 The 3D EBG volumetric structures.

3.3.2 EBG and Metamaterials

Metamaterials, materials of interest exhibit properties not found in nature such as negative index of refraction, are artificial media structure on a size scale smaller than the wavelength of external stimuli. Its research is interdisciplinary and involves fields including electrical engineering, electromagnetic, solid state physics, microwave and antenna engineering, optoelectronics, classic optics, material sciences, semiconductor engineering, and nanoscience (Zouhdi et al., 2008). The electromagnetic metamaterials affect electromagnetic waves by having structural features smaller than the wavelength of the respective electromagnetic waves.

To behave as a homogeneous material accurately described by an effective refractive index, its features must be much smaller than the wavelength. Depending on the exhibited electromagnetic properties, various names have been introduced in the literature, including (Yang and Rahmat-Samii, 2009):

- Double negative (DNG) materials with both negative permittivity and permeability;
- Left-handed (LH) materials inside which the electric field (E-field) direction, magnetic field (H-field) direction, and propagation direction satisfy a left-hand relation;
- Negative refractive index (NRI) materials that have a negative refractive index;
- Magneto materials with artificially controlled high permeability;
- Soft and hard surfaces that stop or support the propagation of waves;
- High impedance surfaces with relatively large surface impedances for both TE and TM waves;
- Artificial magnetic conductors (AMC) that exhibit the same properties as a perfect magnetic conductor.

Due to their unique band gap features, EBG structures can be regarded as a special type of metamaterials. The EBG structures have the goal of creating high quality, low loss, periodic, and dielectric structures. An EBG affects photons in the same way semiconductor materials affect electrons. The EBG structures are designed to prevent the propagation of an allocated bandwidth of frequencies, for certain arrival

angles and polarizations. The various geometries and structures have been proposed to fabricate EBG special properties (Engheta et al, 2006; Zouhdi et al, 2008). The EBG structures have been manufactured for frequencies ranging from a few gigahertz (GHz) up to a few terahertz (THz), radio, microwave and mid-infrared frequency regions. Besides the band gap feature, EBG also possesses some other exciting properties such as high impedance and AMC. For example, a mushroom-like EBG surface exhibits high surface impedances for both TE and TM polarizations. In addition, soft and hard operations of an EBG surface have also been identified in the frequency-wave number plane. These interesting features have led to a wide range of applications in antenna engineering, from wire antennas to MSAs, from linearly polarized antennas to circularly polarized antennas, and from the conventional antenna structures to novel surface wave antenna concepts and reconfigurable antenna designs (Yang and Rahmat-Samii, 2009).

3.3.3 Analysis Methods for EBG Structures

To analyze unique features of EBG structures, three categories have been implemented: (1) lumped element model, (2) periodic transmission line method, and (3) full wave numerical methods.

The lumped element model is the simplest one that describes the EBG structures as an LC resonant circuit (Sievenpiper, 1999). The values of the inductance L and capacitance C are determined by the EBG geometry and its resonance behavior is used to explain the band gap feature of EBG structures. This model is simple to understand, but the results are not very accurate because of the simplified approximation of L and C . A simple 2D planar EBG structures, the geometry is similar to the shape of a mushroom, consists of four parts: a metal ground plane,

a dielectric substrate, periodic metal patches on top of the substrate, and vertical vias connecting the patches to the ground plane (Sievenpiper et al., 1999) as shown in Figure 3.6. The parameters of the EBG structure are the patch width (W), the gap width (g), the substrate thickness (h), the dielectric constant (ϵ_r), and the vias radius (r). When the periodicity ($W + g$) is small compared to the operating wavelength, the operation mechanism of this EBG structure can be explained using an effective medium model with equivalent lumped LC elements, as shown in Figure 3.7. The capacitor results from the gap between the patches and the inductor results from the current a long adjacent patches. The impedance of parallel resonant LC circuit is given by:

$$Z = \frac{j\omega L}{1 - \omega^2 LC} \quad (3.1)$$

The resonance frequency of the circuit is calculated as following:

$$\omega_0 = \frac{1}{\sqrt{LC}} \quad (3.2)$$

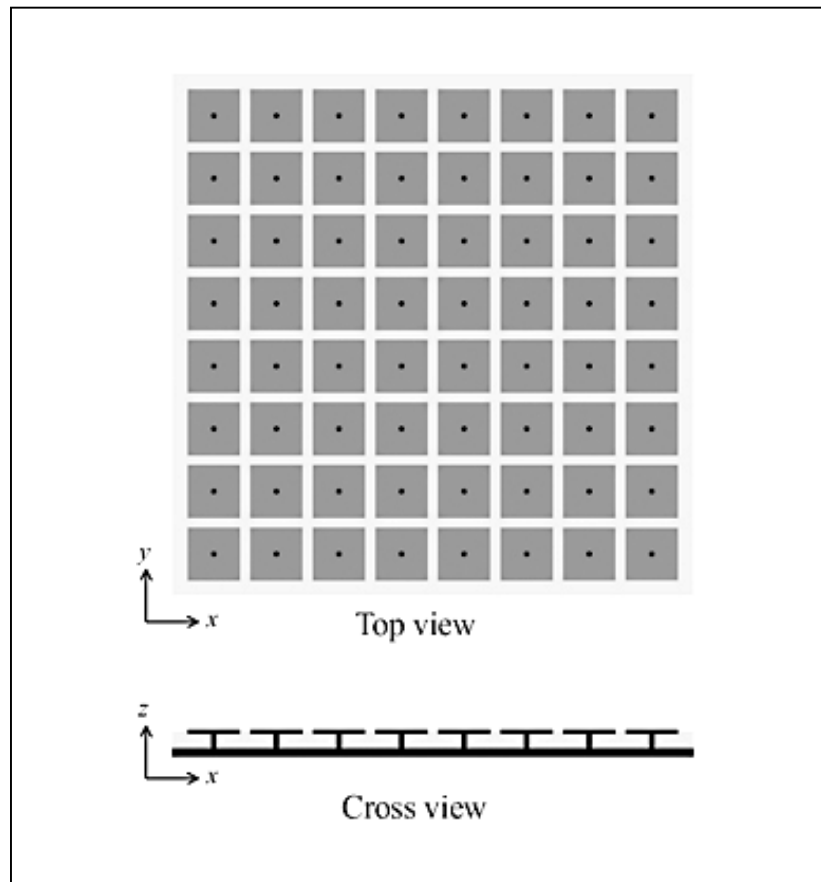


Figure 3.6 The geometry of a mushroom-like EBG structures
(Sievenpiper et al., 1999).

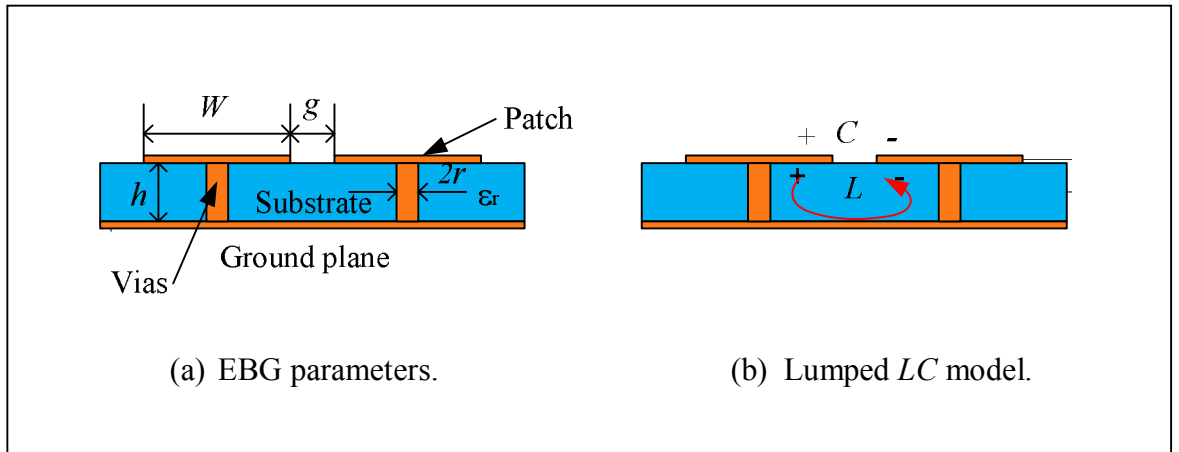


Figure 3.7 The lumped element model for the mushroom-like EBG structures.

At low frequencies, the impedance is inductive and will support TM surface waves. Inversely, it becomes capacitive at high frequencies and TE surface waves are supported. At near the resonance frequency ω_0 , high impedance is obtained and the EBG does not support any surface waves, resulting in frequency band gap. The high surface impedance also ensures that a plane wave will be reflected without the phase reversal that occurs on a perfect electric conductor (PEC).

The value of the capacitor is given by the fringing capacitance between neighboring co-planar metal sheets. This can be derived using conformal mapping, a common technique for determining 2D electrostatic field distributions. The edge capacitance for narrow gap situation is given by the following equation (Sievenpiper, 1999):

$$C = \frac{W \epsilon_0 (1 + \epsilon_r)}{\pi} \cosh^{-1} \left(\frac{W + g}{g} \right). \quad (3.3)$$

The value of the inductor is derived from the current loop in Figure 3.7(b), consisting of the vias and metal sheets. The equivalent inductor is then computed from the stored H-field energy and the excitation current. The inductance is expressed as below (Sievenpiper, 1999), which depends only on the thickness of the structure and the permeability:

$$L = \mu h . \quad (3.4)$$

The periodic transmission line method is another analytical model proposed to characterize EBG structures (Rahman and Stuchly, 2001). A mushroom-like EBG structure as shown in Figure 3.6, the impedance of each section is calculated using transmission line theory, and the whole structure is then cascaded together using the theory of periodic circuit. Figure 3.8 depicts a transmission line model of EBG structures. Between two nodes of the periodic structure, there are two contributions (Z_P and X_C) to the total impedance, which Z_P is the impedance for each periodic element and X_C is the coupling capacitor. After analyzing the cascaded transmission line, the dispersion curve can be readily obtained, which provides more information than the lumped element method. A challenge in this method is how to accurately obtain the equivalent Z_P and X_C values for general EBG structures with arbitrary geometries. In addition, the surface wave modes, the leaky wave modes, the left- and right-hand regions, and the band gaps can be easily identified from the dispersion curve. However, it is not applicable for plane wave incidences.

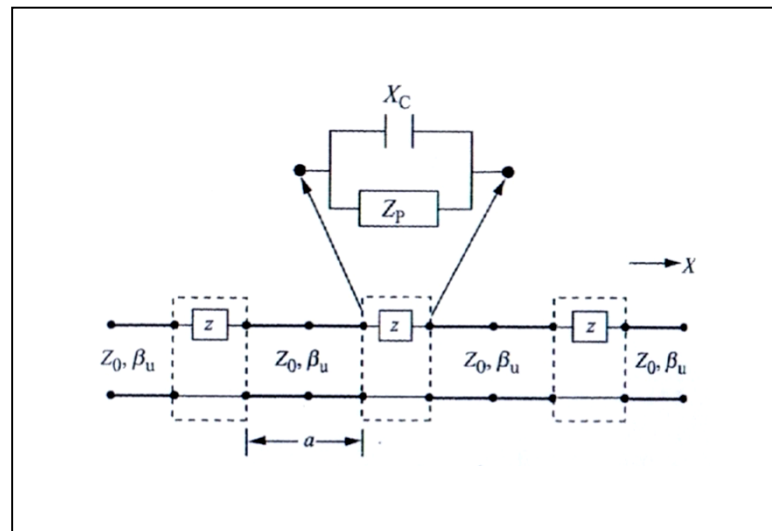


Figure 3.8 The transmission line model of EBG structures
(Rahman and Stuchly, 2001).

The full wave numerical methods, both the frequency domain methods such as the Method of Moments (MoM) and the Finite Element Method (FEM) and the time domain method like the FDTD method have been utilized by different research groups to characterize EBG structures. For instance, Figure 3.9 shows an FDTD model for the mushroom-like EBG analysis (Kim, Yang, and Elsherbeni, 2007). The computational code is based on a Cartesian grid cell with the absorbing boundary conditions (Jensen, 1994). The important advantages of the full wave numerical methods are the versatility and accuracy in analyzing different EBG geometries and the capability to the various EBG characteristics, such as the surface impedance, reflection phase, dispersion curve, and band gap.

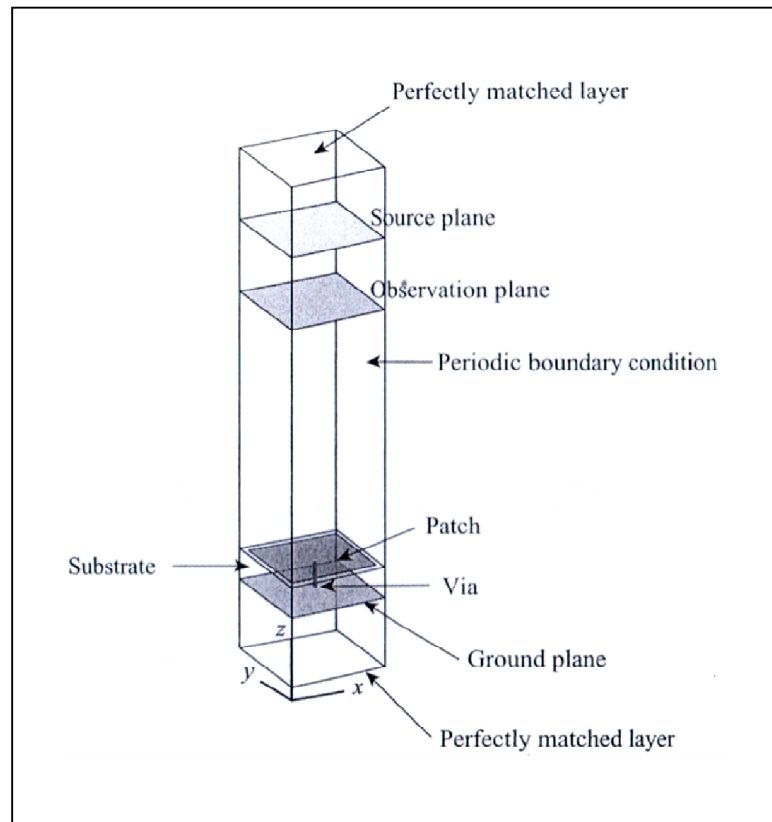


Figure 3.9 The full wave FDTD model for the EBG analysis
(Kim, Yang, and Elsherbeni, 2007).

In this research, the FDTD method is used to clearly visualize the frequency band gap feature of this proposed antenna system. A detailed discussion on the FDTD method will be presented in Chapter 4.

3.3.4 Woodpile EBG Structures

In this section provides some background information of the planar, the cylindrical ,and the sector of curved woodpile EBG structures. The woodpile is also referred to as a layer-by-layer photonic crystal in the physics literature. A unit cell of the planar woodpile EBG structure is defined by the lattice constant or repeat distance in the horizontal plane (a), the rod width (w), the rod height (h), and the total

height of the unit cell (b) as shown in Figure 3.10. These consecutive layers are orthogonal to each other, and the parallel rods are offset from the rods two layers below by half of a lattice constant, to obtain a four layer stacking sequence. The lattice symmetry of this material is face-centered tetragonal (FCT) from solid state physics theory. The cross section of the rods may be circular or square shape, and the inverse structure made of air rods in dielectric background also has a completed bandgap (Weily et al., 2005).

Unlike the planar woodpile EBG structures, the horizontal filaments are not interleaved in the cylindrical woodpile, but aligned at the same horizontal location. For TM mode resonances in the cylindrical cavity, the structure does not require a 3D bandgap but only needs a bandgap along the radial direction. As the constructed cylindrical cavity will be excited by vertical (axis of the cylinder) E-fields, vertically aligned gratings are essential, which are implemented by stacked horizontal filaments crossing at the same location. Figure 3.11 shows the geometry of the cylindrical woodpile EBG structures with two filament rings with different diameters and 16 radial filaments layered together (Lee et al., 2010). The design parameters for the cylindrical woodpile EBG structures are the filament thickness or diameter (w), the height or length (h), the number of radial filaments (N_{rad}), the number of rings (N_{ring}) of the cylinder and the radii of each ring (R_1, R_2, \dots, R_n), where $n = N_{ring}$.

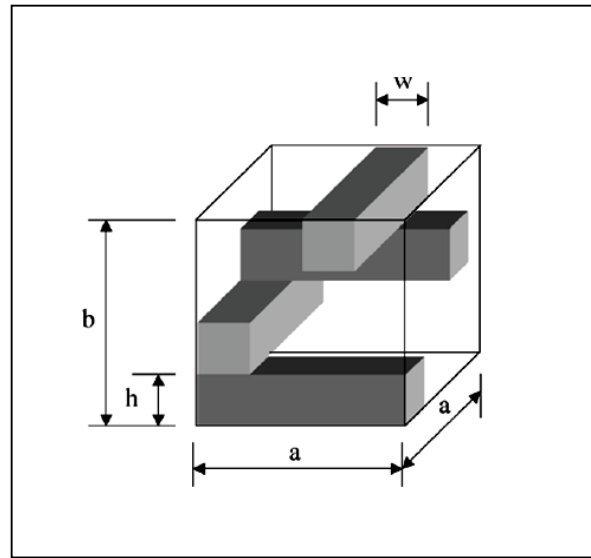


Figure 3.10 A unit cell of the planar woodpile EBG structure (Weily et al., 2005).

This research has applied the similar geometry of the planar (Weily et al., 2005; Lee et al., 2009) and the cylindrical (Lee et al., 2010) to be the sector of curved woodpile EBG structures. Figure 3.12 shows the geometry of the curved woodpile EBG structures with two filament rings with different diameters and three radial filaments layered together. The parameters for these structures are similar to the cylindrical woodpile EBG structures.

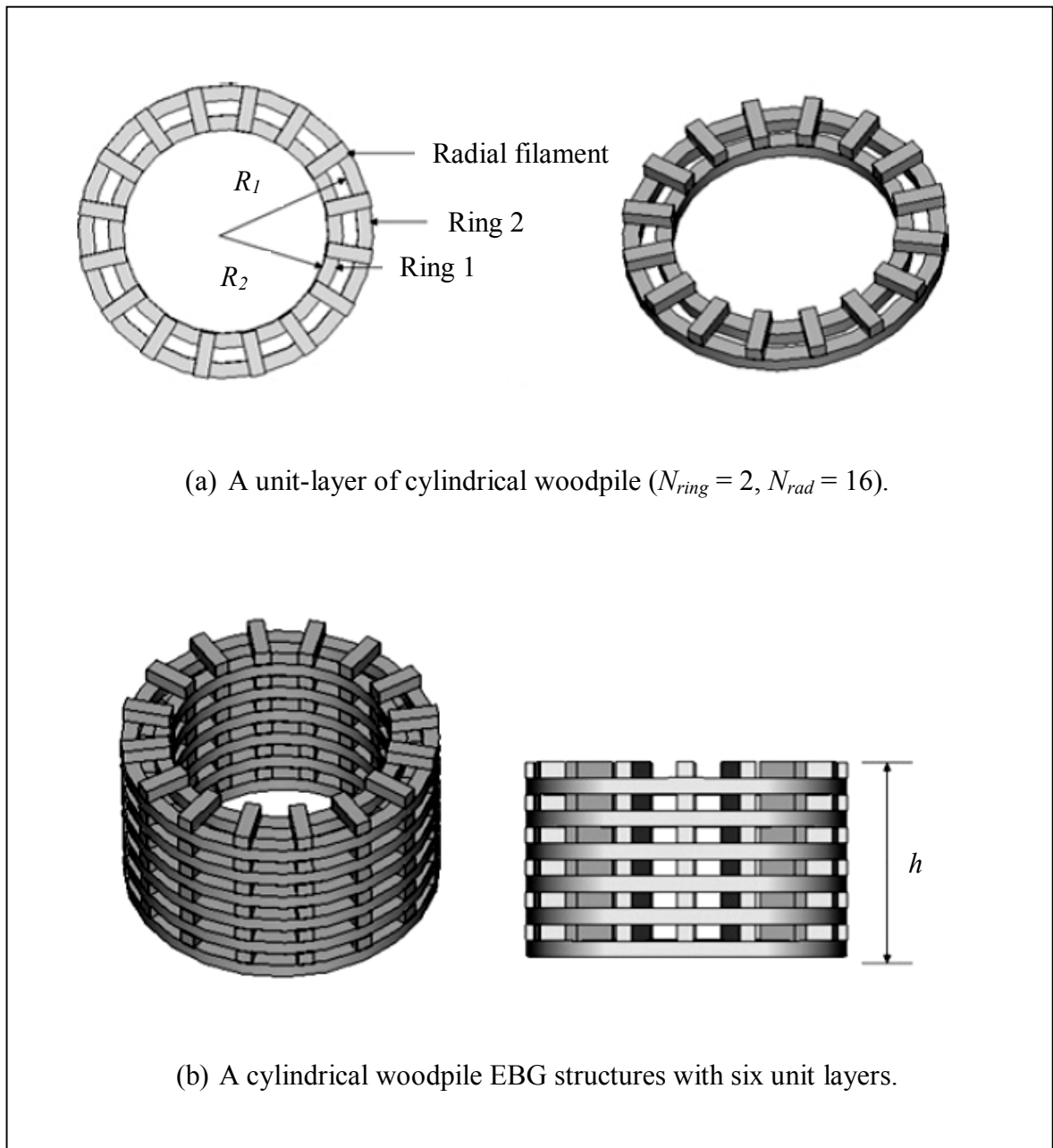
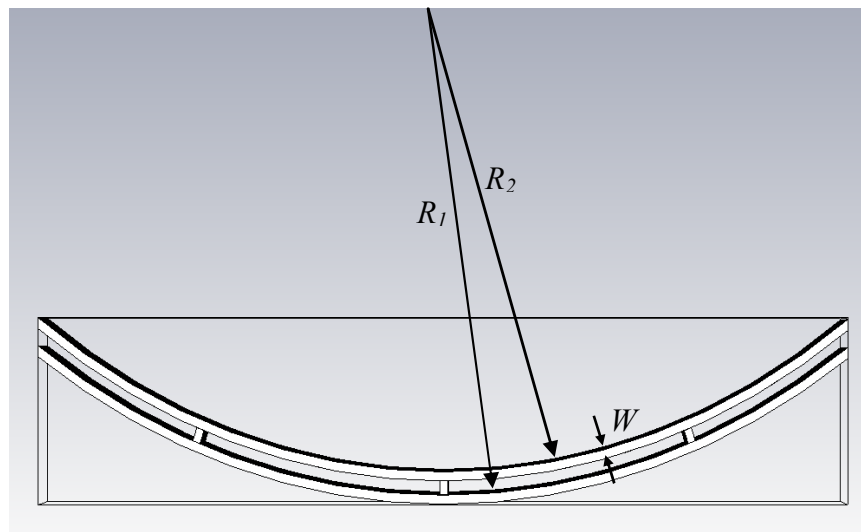
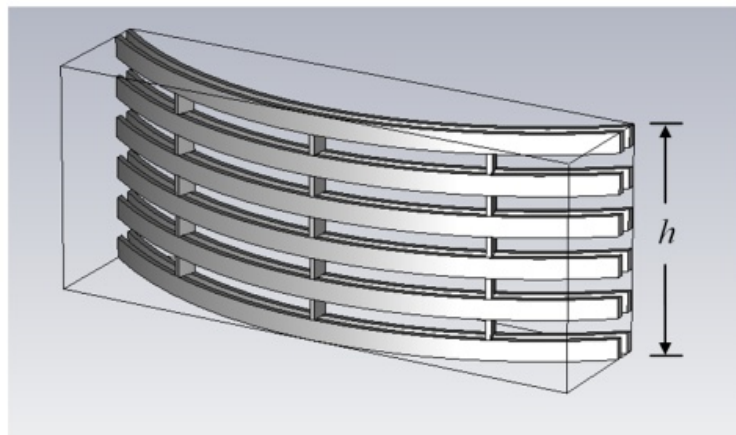


Figure 3.11 The geometry of the cylindrical woodpile EBG structures

(Lee et al., 2010).



(a) A unit-layer of curved woodpile ($N_{ring} = 2, N_{rad} = 3$).



(b) A curved woodpile EBG structures with six unit layers.

Figure 3.12 The geometry of the curved woodpile EBG structures.

3.4 The Finite Difference Time Domain Method

The FDTD method is the simplest, both conceptually and in terms of implementation, of the full-wave techniques is used to solve problems in electromagnetic. It can accurately tackle a wide range of problems. However, as with all numerical methods, it does have its share of artifacts and the accuracy is contingent upon the implementation. The FDTD method solves Maxwell's equations in the time domain. It means that the calculation of the electromagnetic field values progresses at discrete steps in time. One benefit of the time domain approach is that it gives broadband output from a single execution of the program; however, the main reason for using the FDTD approach is the excellent scaling performance of the method as the problem size grows. As the number of unknowns increases, the FDTD approach quickly outpaces other methods in efficiency.

To implement the FDTD solution of Maxwell's equations, a computational domain must firstly be established. The computational domain is simply the physical region over which the simulation will be performed. The E- and H-fields are determined at every point in space within the computational domain while the material of each cell within the computational domain must be specified. Typically, the materials are free-space or air (1D FDTD), metal or dielectric material (2D FDTD), and lossy dielectric material or frequency-dependent material (3D FDTD).

The FDTD method uses Maxwell's equations to define the propagation of an electromagnetic wave and the relationship between the E- and H-fields, these are:

$$\nabla \times \bar{E} = -\bar{M} - \frac{\partial \bar{B}}{\partial t}, \quad (3.5a)$$

$$\nabla \times \bar{H} = \bar{J} + \frac{\partial \bar{D}}{\partial t}, \quad (3.5b)$$

$$\nabla \cdot \bar{D} = \rho_e, \quad (3.5c)$$

$$\nabla \cdot \bar{B} = \rho_m = 0. \quad (3.5d)$$

All these field quantities: \bar{E} , \bar{H} , \bar{D} , \bar{B} , \bar{J} , \bar{M} and ρ_e , ρ_m are assumed to be time-varying, and each quantity is function of the space coordinates and time, that is

$\bar{E} = \bar{E}(x, y, z; t)$. The definitions and unit of the quantities are

\bar{E} = electric field intensity (volts/meter),

\bar{H} = magnetic field intensity (amperes / meter),

\bar{D} = electric flux density (coulombs / square meter),

\bar{B} = magnetic flux density (webers / square meter),

\bar{J} = electric current density (amperes / square meter),

\bar{M} = magnetic current density (volts / square meter),

ρ_e = electric charge density (coulombs / cubic meter),

ρ_m = magnetic charge density (webers / cubic meter).

One of the constitutive relations relates in the time domain the electric flux density to the electric field intensity by

$$\bar{D} = \varepsilon \bar{E}, \quad (3.6)$$

where ε is the time-varying permittivity of the medium (farads / meter) and indicates convolution. Another relation equates in the time domain the magnetic flux density to the magnetic field intensity by

$$\bar{B} = \mu \bar{H}, \quad (3.7)$$

where μ is the time-varying permeability of the medium (henries / meter). Finally, the currents density, the electric conduction current density is related in the time domain to the electric field intensity by

$$\bar{J}_c = \sigma \bar{E}, \quad (3.8)$$

where σ is the time-varying electric conductivity of the medium (siemens / meter) and the magnetic current density is related in the time domain to the magnetic field intensity by

$$\bar{M} = \chi \bar{H}, \quad (3.9)$$

where χ is the time-varying magnetic susceptibility of the medium (henrys / meter).

For a uniform, isotropic and homogeneous medium Maxwell's curl equations then become:

$$\mu \frac{\partial \bar{H}}{\partial t} + \chi \bar{H} = -\nabla \times \bar{E}, \quad (3.10a)$$

$$\mu \frac{\partial \bar{E}}{\partial t} + \sigma \bar{E} = \nabla \times \bar{H}, \quad (3.10b)$$

or

$$\frac{\partial \bar{H}}{\partial t} = -\frac{1}{\mu} \nabla \times \bar{E} - \frac{\chi}{\mu} \bar{H}, \quad (3.11a)$$

$$\frac{\partial \bar{E}}{\partial t} = \frac{1}{\varepsilon} \nabla \times \bar{H} - \frac{\sigma}{\varepsilon} \bar{E}. \quad (3.11b)$$

By using the vector identity,

$$\nabla \times \bar{A} = \hat{a}_x \left[\frac{\partial A_z}{\partial y} - \frac{\partial A_y}{\partial z} \right] + \hat{a}_y \left[\frac{\partial A_x}{\partial z} - \frac{\partial A_z}{\partial x} \right] + \hat{a}_z \left[\frac{\partial A_y}{\partial x} - \frac{\partial A_x}{\partial y} \right], \quad (3.12)$$

can rewrite (3.11a) and (3.11b) in a rectangular coordinate system as

$$\mu \frac{\partial H_x}{\partial t} + \chi H_x = \frac{\partial E_y}{\partial z} - \frac{\partial E_z}{\partial y}, \quad (3.13a)$$

$$\mu \frac{\partial H_y}{\partial t} + \chi H_y = \frac{\partial E_z}{\partial x} - \frac{\partial E_x}{\partial z}, \quad (3.13b)$$

$$\mu \frac{\partial H_z}{\partial t} + \chi H_z = \frac{\partial E_x}{\partial y} - \frac{\partial E_y}{\partial x}, \quad (3.13c)$$

$$\varepsilon \frac{\partial E_x}{\partial t} + \sigma E_x = \frac{\partial H_z}{\partial y} - \frac{\partial H_y}{\partial z}, \quad (3.13d)$$

$$\varepsilon \frac{\partial E_y}{\partial t} + \sigma E_y = \frac{\partial H_x}{\partial z} - \frac{\partial H_z}{\partial x}, \quad (3.13e)$$

$$\varepsilon \frac{\partial E_z}{\partial t} + \sigma E_z = \frac{\partial H_y}{\partial x} - \frac{\partial H_x}{\partial y}. \quad (3.13f)$$

3.4.1 The Yee Algorithm

In the FDTD approach, both space and time are divided into discrete segments. Space is segmented into box-shaped cells, which are small compared to the wavelength. The E-fields are located on the edges of the box and the H-fields are positioned on the faces as shown in Figure 3.13. This orientation of the fields is known as the Yee cell (Yee, 1966), which E- and H-fields vector components are distributed. It is visualized as a cubic volume element, the E-field components form the edges of the cube, and the H-field components form the normal to the faces of the cube. A 3D space lattice consists of a multiplicity of such Yee cells. An electromagnetic wave interaction structure is mapped into the space lattice by assigning appropriate values of permittivity to each E-field component, and permeability to each H-field component.

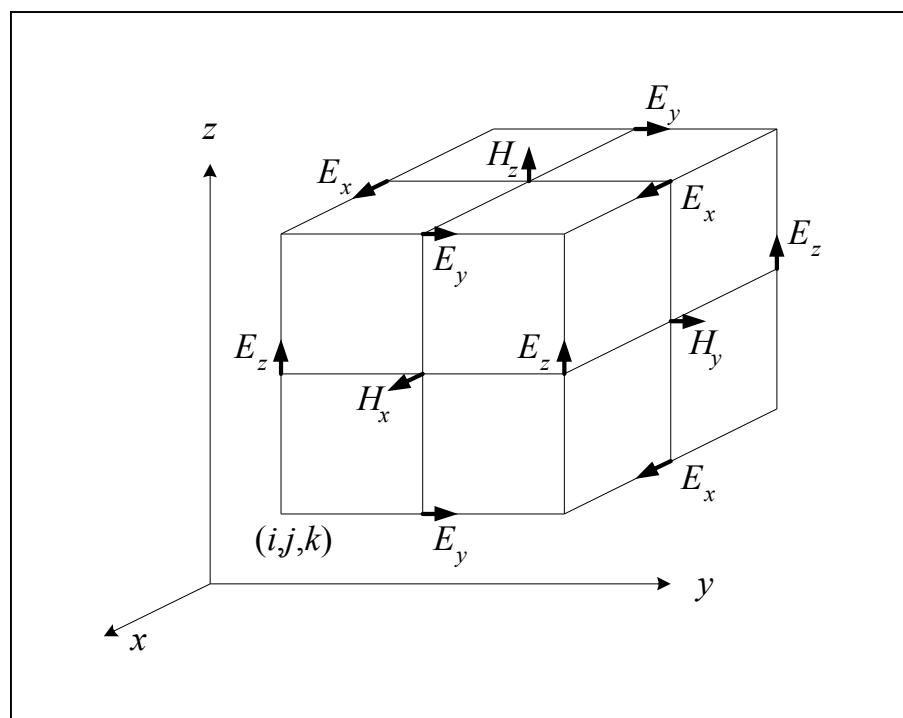


Figure 3.13 The Yee cell with labeled field components.

This description holds true for 1D, 2D, and 3D FDTD techniques. When multiple dimensions are considered, calculating the numerical curl can become complication. Kane Yee's seminal 1966 paper proposed spatially staggering the vector components of the E- and H-fields about rectangular unit cells of a Cartesian computational grid so that each E-field vector component is located midway between a pair of H-field vector components, and conversely. A Yee cell has proven to be very robust, and remains at the core of many current FDTD software constructs. Furthermore, Yee proposed a leapfrog scheme for marching in time wherein the E- and H-fields updates are staggered so that E-field updates are conducted midway during each time-step between successive H-field updates, and conversely (Yee, 1966). On the plus side, this explicit time-stepping scheme avoids the need to solve

simultaneous equations, and furthermore yields dissipation-free numerical wave propagation. On the minus side, this scheme mandates an upper bound on the time-step to ensure numerical stability (Taflove and Brodwin, 1975). As a result, certain classes of simulations can require many thousands of time-steps for completion.

3.4.2 Two Dimensional Finite Difference Time Domain Method

The 2D FDTD is utilized for analyzing of this research because the microstrip slot antennas array are constructed by the dielectric material of FR4. In doing 2D FDTD simulation, we choose between one of two groups of three vectors each: (1) the transverse magnetic (TM^z) mode, which is composed of E_z , H_x , and H_y or (2) the transverse electric (TE^z) mode, which is composed of E_x , E_y , and H_z . We will work with the TE^z mode. In TE^z mode, the E-field is transverse to the z direction. The fields may vary in the x and y directions but are invariant in z . The governing equations are:

$$\sigma E_x + \varepsilon \frac{\partial E_x}{\partial t} = \frac{\partial H_z}{\partial y}, \quad (3.14a)$$

$$\sigma E_y + \varepsilon \frac{\partial E_y}{\partial t} = \frac{\partial H_z}{\partial x}, \quad (3.14b)$$

$$-\chi H_z - \mu \frac{\partial H_z}{\partial t} = \frac{\partial E_y}{\partial x} + \frac{\partial E_x}{\partial y}. \quad (3.14c)$$

This is illustrated in the 2D FDTD for TE mode (electric field in the plane of calculation) as shown Figure 3.14 (http://www.silvaco.com/tech_lib_TCAD/simulationstandard/2010/apr_may_jun/a1/a1.html). The half step sizes have been introduced for obtaining accurate approximations of the derivatives; the algorithm proceeds with full step size.

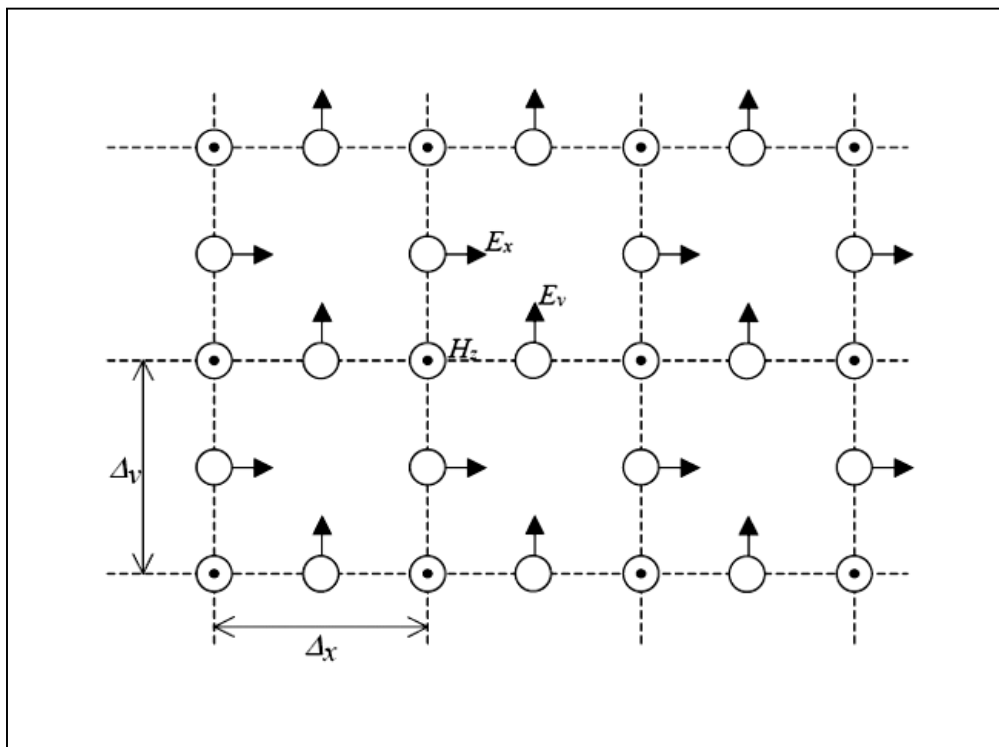


Figure 3.14 2D FDTD calculation grid for TE mode.

Putting the equations (3.14a) to (3.14c) into the finite differencing scheme results in the following difference equations:

$$E_x^n(i, k) = E_x^{n-1}(i, k) + \frac{\Delta t}{\varepsilon \Delta z} \left[H_y^{n-1/2}(i, k+1/2) - H_y^{n-1/2}(i, k-1/2) \right] - \frac{\Delta t}{\varepsilon \Delta y} \left[H_z^{n-1/2}(i+1/2, k) - H_z^{n-1/2}(i-1/2, k) \right], \quad (3.15a)$$

$$E_y^n(i, k) = E_y^{n-1}(i, k) + \frac{\Delta t}{\varepsilon \Delta z} \left[H_x^{n-1/2}(i, k+1/2) - H_x^{n-1/2}(i, k-1/2) \right] - \frac{\Delta t}{\varepsilon \Delta x} \left[H_z^{n-1/2}(i+1/2, k) - H_z^{n-1/2}(i-1/2, k) \right], \quad (3.15b)$$

$$H_z^{n+1/2}(i+1/2, k) = H_z^{n-1/2}(i+1/2, k) - \frac{\Delta t}{\mu_0 \Delta x} \left[E_y^n(i+1, k) - E_y^n(i, k) \right]. \quad (3.15c)$$

The superscript n labels the time steps while the indices i and k label the space steps and Δx and Δz along the x and z directions, respectively. This is the Yee's numerical scheme which is applied to the 2D FDTD for TE mode. It uses central difference approximations for the numerical derivatives in space and time, both having second order accuracy. The sampling in space is on a sub-wavelength scale. Typically, 10 to 20 steps per wavelength are needed. The sampling in time is selected to ensure numerical stability of the algorithm. The time step is determined by the Courant limit (<http://optiwave.com/optifdtd-manuals/fdtd-fdtd-basics/>):

$$\Delta t \leq 1 / \left(c \sqrt{1 / (\Delta x)^2 + 1 / (\Delta z)^2} \right). \quad (3.16)$$

3.5 Artificial Neural Network

An Artificial Neural Network (ANN) is computational models inspired by the way biological nervous systems, such as the brain, process information. The key element of this paradigm is the novel structure of the information processing system. It is composed of a large number of highly interconnected processing elements (neurons) working in unison to solve specific problems (http://en.wikipedia.org/wiki/Artificial_neural_network; http://www.doc.ic.ac.uk/~nd/surprise_96/journal/vol4/cs11/report.html#Introduction to neural networks). An ANN refers to the interconnections between the neurons in the different layers of each system. Figure 3.15 shows the example system of an ANN which has three layers. The first layer has input neurons (input nodes) which send data via synapses to the second layer of neurons (hidden nodes), and then via more synapses to the third layer of output neurons (output node). Here, each node represents an artificial neuron and an arrow represents a connection from the output of one neuron to the input of another. More complex systems will have more layers of neurons with some having increased layers of input neurons and output neurons. The synapses store parameters called weights that manipulate the data in the calculations. An ANN is typically defined by three types of parameters such as (1) the interconnection pattern between the different layers of neurons, (2) the learning process for updating the weights of the interconnections, and (3) the activation function that converts a neuron's weighted input to its output activation.

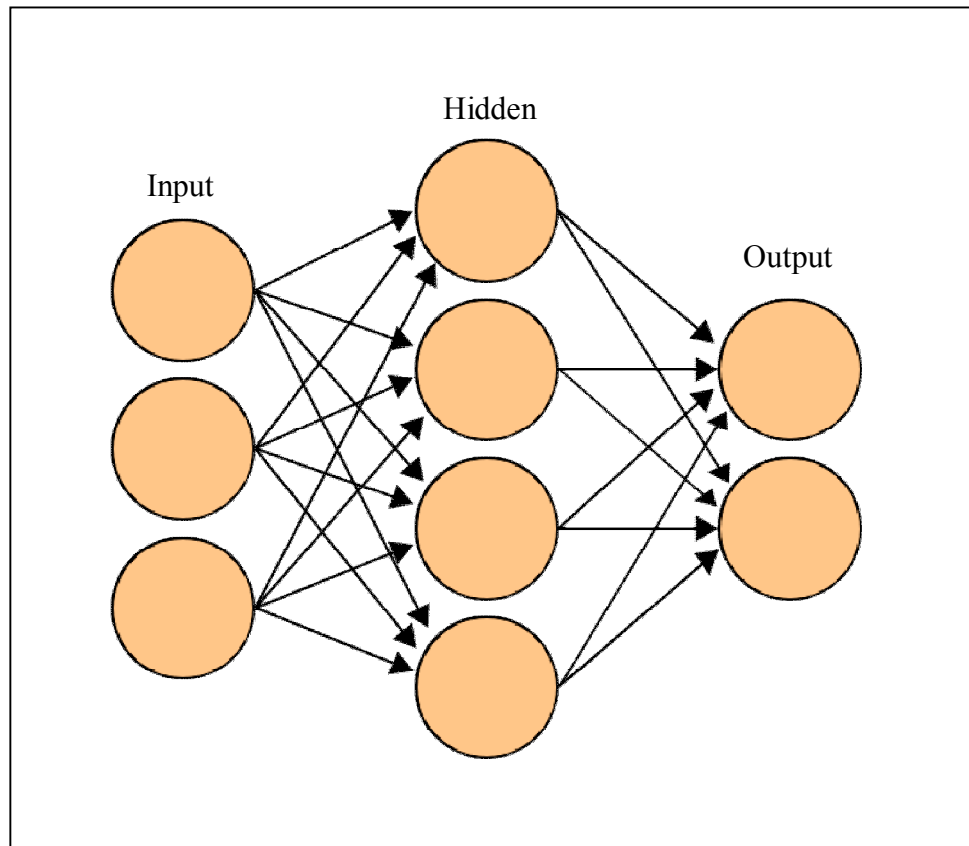


Figure 3.15 An ANN with three layers.

3.5.1 The Levenberg–Marquardt algorithm

The Levenberg–Marquardt algorithm (Levenberg, 1944; Marquardt, 1963), which was independently developed by Kenneth Levenberg and Donald Marquardt, provides a numerical solution to the problem of minimizing a nonlinear function. It is fast and has stable convergence. In the ANN field, this algorithm is suitable for training small- and medium-sized problems. The implementation of training with the Levenberg–Marquardt algorithm will achieve in two parts: (1) calculation of Jacobian matrix and (2) training process design.

In order to assure that the approximated Hessian matrix $J^T J$ is invertible, Levenberg–Marquardt algorithm introduces another approximation to Hessian matrix:

$$H \approx J^T J + \mu I, \quad (3.17)$$

where μ is always positive, called combination coefficient and I is the identity matrix. The update rule of Levenberg–Marquardt algorithm can be presented as:

$$w_{k+1} = w_k - (J_k^T J_k + \mu I)^{-1} J_k e_k, \quad (3.18)$$

where w_k is the current weight and w_{k+1} is the next weight.

Figure 3.16 shows the flowchart of the training process using Levenberg–Marquardt algorithm, where E_{k+1} is the current total error and E_k is the last total error. This training process could be designed as follows (Hao, 2011):

- (1) with the initial weights (randomly generated), evaluate the total error (SSE),
- (2) do an update as directed by Equation (3.18) to adjust weights,
- (3) with the new weights, evaluate the total error,
- (4) if the current total error is increased as a result of the update, then retract the step (such as reset the weight vector to the precious value) and increase combination coefficient μ by a factor of 10 or by some other factors. Then go to step ii and try an update again,

(5) if the current total error is decreased as a result of the update, then accept the step (such as keep the new weight vector as the current one) and decrease the combination coefficient μ by a factor of 10 or by the same factor as step (4),

(6) go to step (2) with the new weights until the current total error is smaller than the required value.

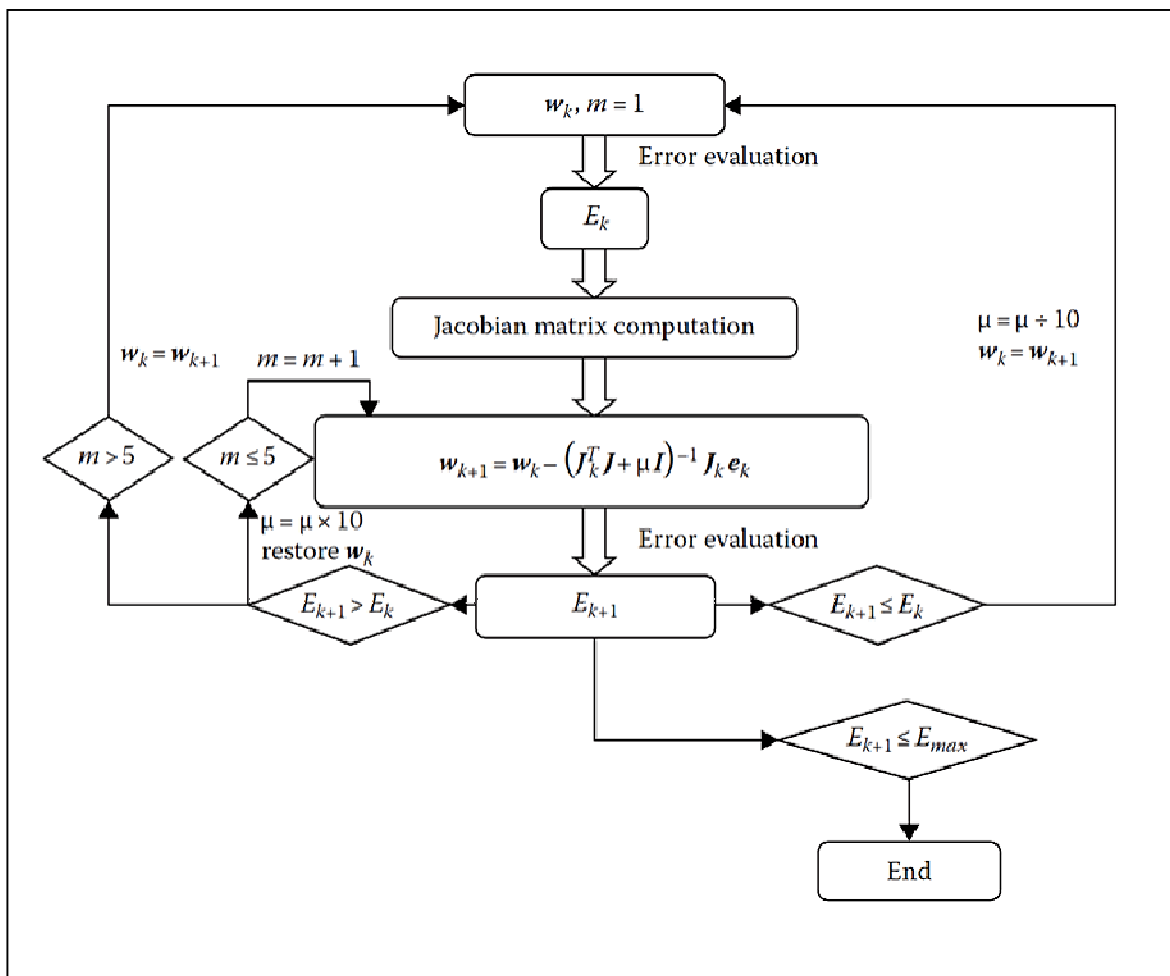


Figure 3.16 The flowchart of the training process using Levenberg–Marquardt algorithm (Hao, 2011).

3.6 Chapter Summary

The theory and principle of microstrip slot antenna and EBG structures are presented in this chapter. Microstrip slot antenna is relatively inexpensive to manufacture and design because of the simple 2D physical geometry. Moreover, microstrip slot antennas array can provide much higher gains than a single element at little additional cost. While the matching method and phase adjustment can be performed with printed microstrip-line feed structures above slot, again in the same operations that form the radiating slots. The ability to create high gain arrays in a low-profile antenna is one reason that microstrip slot antennas array are widely used in many modern communication systems. The applications of EBG structures in antenna designs have become a thrilling topic for antenna engineering since these EBG structures are capable to enhance the performance of MSA in terms of gain, side and back lobes level and also mutual coupling. In addition, the concept of FDTD method is presented which belongs in the general class of grid-based differential time-domain numerical modeling methods (finite difference methods). The time-dependent Maxwell's equations are discrete by using central-difference approximations to the space and time partial derivatives. Besides, an ANN method is introduced to be a computational model inspired in the natural neurons. These basically consist of inputs, which are multiplied by weights, and then computed by a mathematical function which determines the activation of the neuron. Another function computes the output of the artificial neuron.

CHAPTER IV

ANTENNA ANALYSIS AND DESIGN

4.1 Introduction

This chapter presents analysis and design of microstrip slot antenna array covered with curved woodpile EBG structures. The antenna system consists of three main parts as follow: (1) microstrip slot antenna array (2) curved woodpile EBG structures, and (3) feed system. The general approach will be presented including the configurations of microstrip slot antenna and EBG structures as shown in sections 4.2 and 4.3, respectively. Next section gives the details of design of antenna system by utilizing CST software. Then the FDTD and ANN methods are conducted to carry out S_{11} , E- and H-fields of this proposed antenna. The last section of this chapter will be a summary.

4.2 Microstrip Slot Antenna Configuration

4.2.1 A Microstrip Slot Antenna

An ultra-wideband circular MSA fed by microstrip line above wide-slot ground plane (Chawanonphithak and Phongcharoenpanich, 2007), is shown in Figure 2.4, designed for working as a microstrip slot antenna in the UMTS band of 2.1 GHz frequency is utilized be the prototype for this proposed antenna. The antenna is printed on FR4 substrate ($\epsilon_r = 4.5$, $\tan\delta = 0.02$) with the size of 60 mm \times 60 mm and the thickness of 1.6 mm. A microstrip slot antenna structure consists of the circular patch of the radius (a). This gap of distance (t) between the microstrip line

length (L_2) is used for adjusting the impedance matching. The substrate is located on the ground plane of the width (W) and the length (L). This ground plane is cut to form the wide-slot ground plane (Size $W_1 \times L_1$). The design of a microstrip slot antenna is based on the conventional transmission line model at 2.1 GHz. The desired bandwidth is 1.920 – 2.170 GHz. The tuning stub is used to improve the level of reflection coefficient, while the microstrip-line is designed to provide 50Ω at the operating frequency of 2.1 GHz. The dimension of the wide-slot ground plane is varied to enhance the bandwidth as illustrated in Chawanonphithak and Phongcharoenpanich, 2007. The simulated result with CST software shows that the gain at 2.1 GHz is 5 dB.

4.2.2 A 1×8 Array of Microstrip Slot Antennas

To enhance gain characteristic, a microstrip slot antenna will be arrayed with element spacing of $3\lambda/4$ (antenna type A) as shown in Figure 4.1. The simulated results with CST software show that the reflected power or S_{11} (-10 dB) and the normalized radiation patterns of the antenna type A at 2.1 GHz with the gain of 14 dB as shown in Figure 4.2 and 4.3, respectively. The Half-Power Beamwidth (HPBW) in the E- and H-Planes, which shown as the ratio of azimuth pattern to elevation pattern (AZ:EL), of the antenna type A is $97.4^\circ:8.4^\circ$.

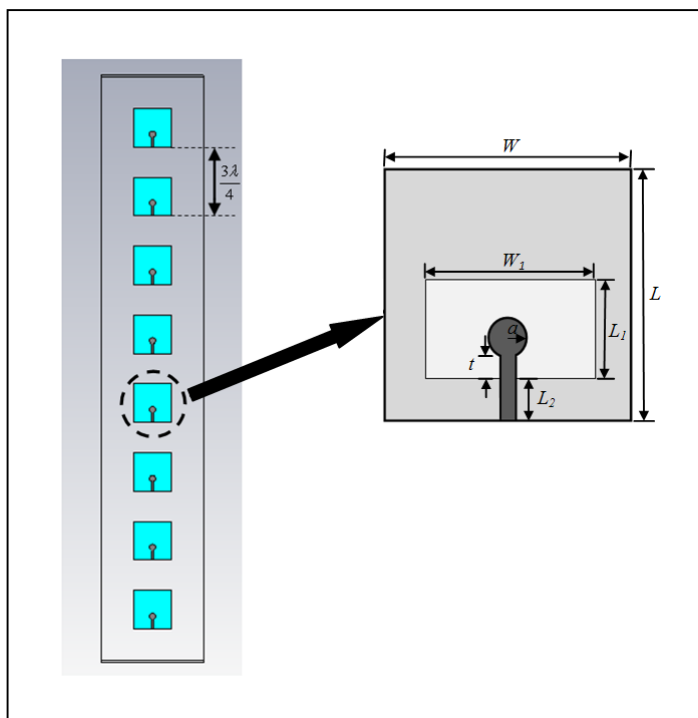


Figure 4.1 A 1×8 array of microstrip slot antennas (antenna type *A*).

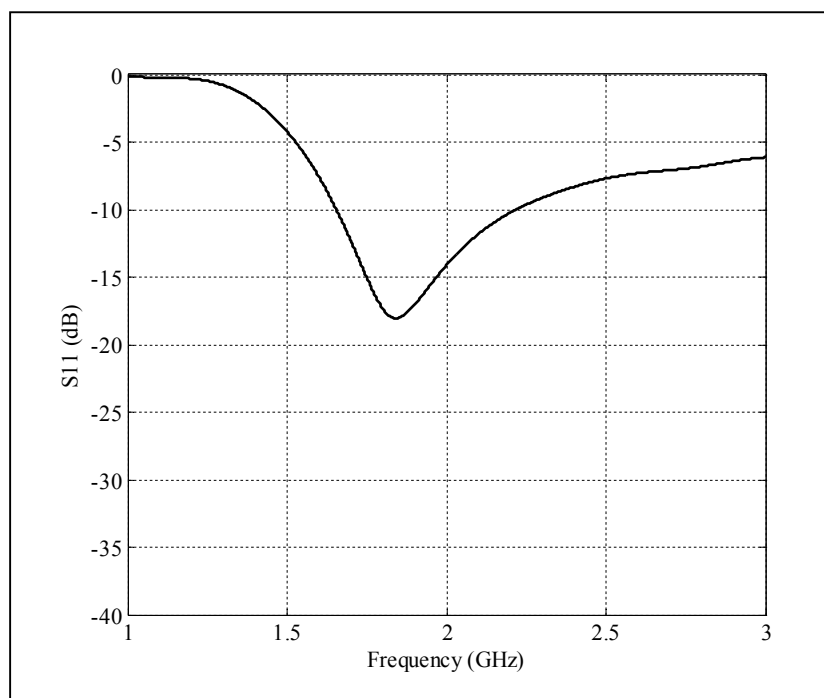


Figure 4.2 Simulated results of reflected power of antenna type *A*.

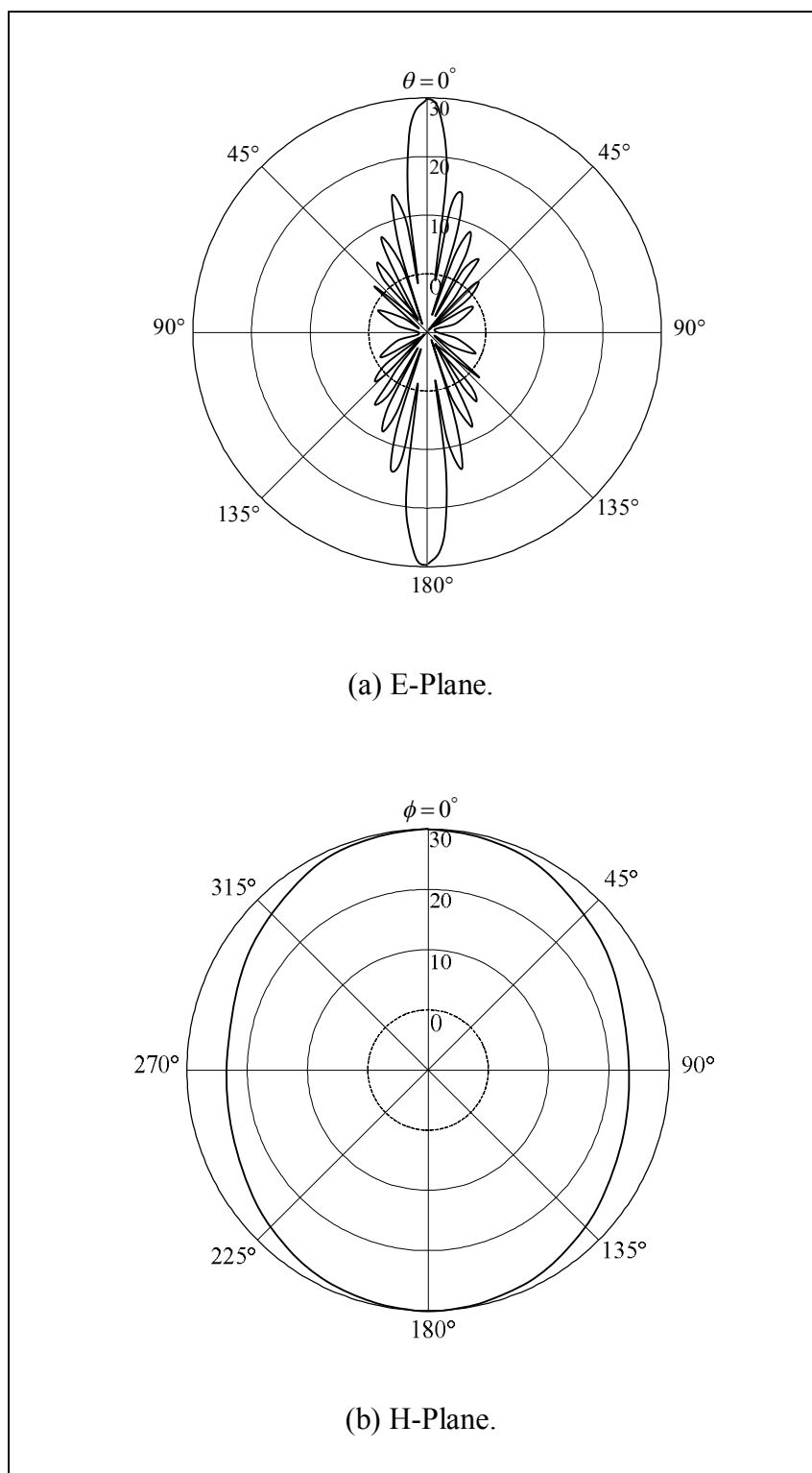


Figure 4.3 Simulated normalized radiation patterns of antenna type A.

Furthermore, the proposed antenna in this research has added a U-shaped reflector behind the panel of microstrip slot antennas array to control the radiation pattern to be the directional pattern. The design parameters of a U-shaped reflector are the distance between a U-shaped reflector and microstrip slot antennas array (d_r), the width of U-shaped reflector (w_r), and the height of U-shaped reflector (h_r). Firstly, we look at the effect of the variation of d_r , w_r and h_r are fixed at 400 mm and 1,000 mm, respectively. We found that, this property can be used to control the resonant frequency of microstrip slot antennas array because its resonant frequency will change when d_r is changed as shown in Figure 4.4, therefore, $d_r = \lambda/4$ is utilized. Secondly, we have studied the effect of the width w_r , while d_r and h_r are fixed at $\lambda/4$ and 1,000 mm, respectively. It notes that the highest gain of 17.83 dB is achieved when $w_r = 400$ mm as shown in Figure 4.5. Next, we have investigated the effect of the height h_r variation versus the gain, d_r and w_r are fixed at $\lambda/4$ and 400 mm, respectively, thus its result is shown in Figure 4.6. It finds that the highest gain of 17.83 dB is achieved when $h_r = 1,000$ mm. Therefore, the highest gain of 17.83 dB is optimized with $d_r = \lambda/4$, $w_r = 400$ mm, and $h_r = 1,000$ mm.

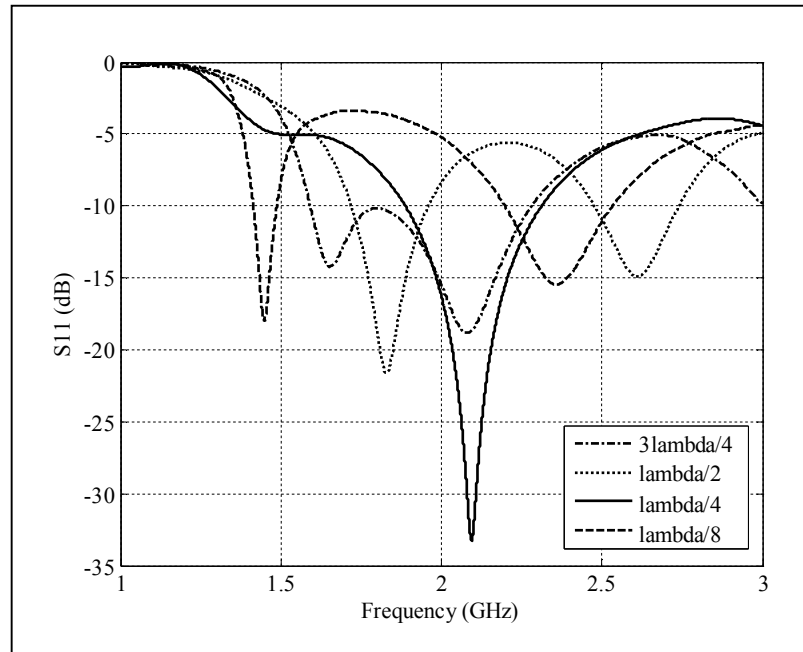


Figure 4.4 Simulated results of reflected power against variation of d_r .

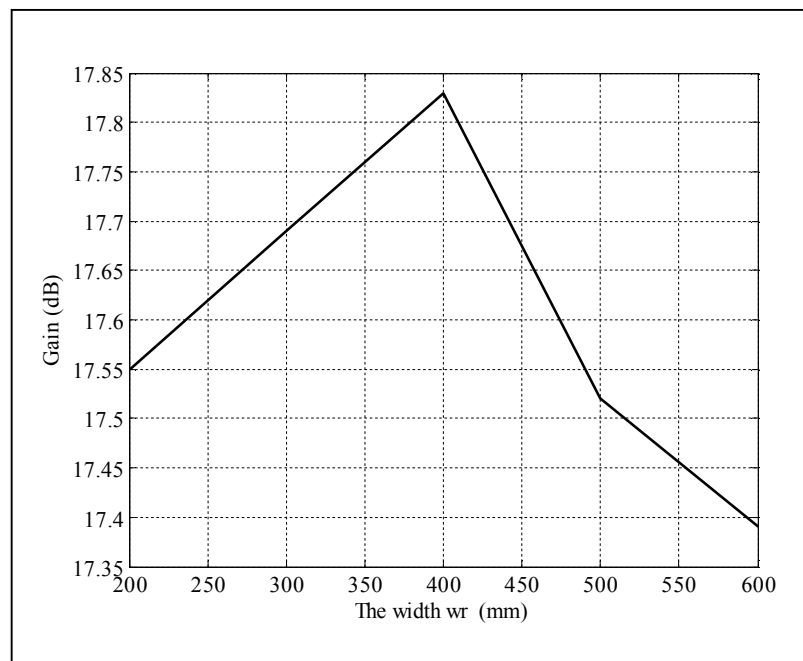


Figure 4.5 Simulated gain against w_r .

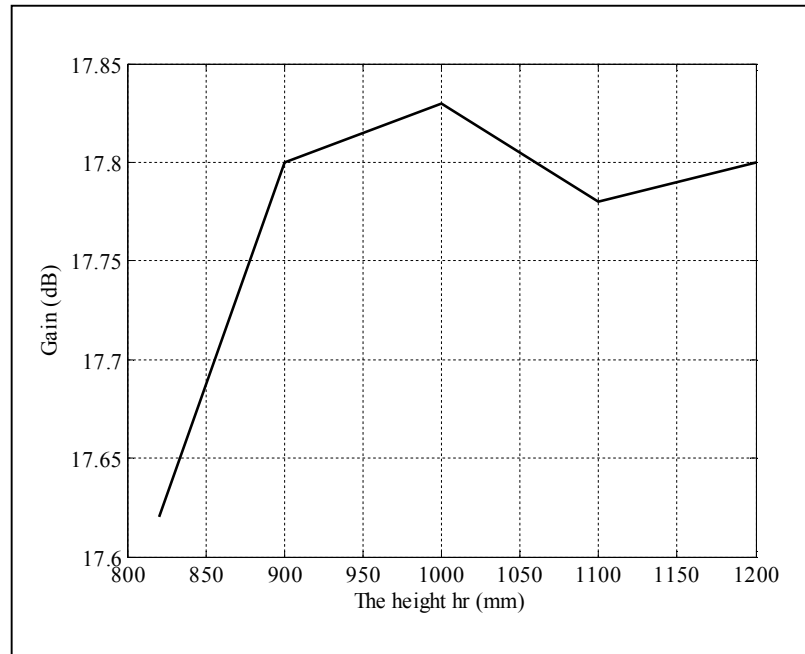


Figure 4.6 Simulated gain against h_r .

Figure 4.7 shows a 1×8 array of microstrip slot antennas and U-shaped reflector with the size of $400 \text{ mm} \times 1,000 \text{ mm}$ (antenna type *B*). The simulated results with CST software show that the S_{11} and the normalized radiation patterns of the antenna type *B* at 2.1 GHz with the gain of 17.83 dB as shown in Figure 4.8 and 4.9, respectively. The HPBW in the E- and H-Plane of the antenna type *B* is $89.4^\circ:8.3^\circ$.

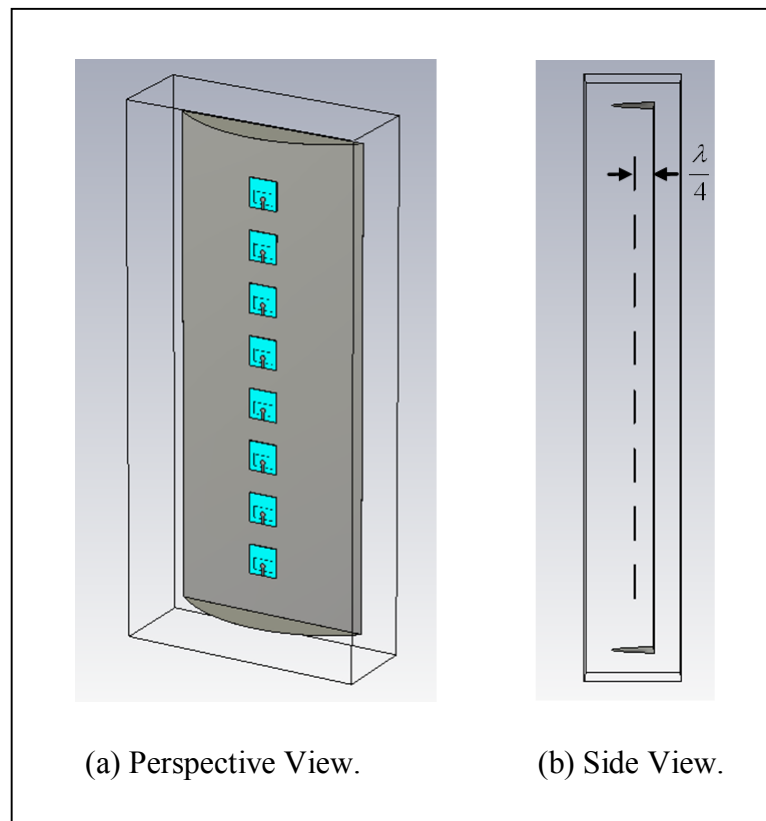


Figure 4.7 A 1×8 array of microstrip slot antennas and U-shaped reflector (antenna type *B*).

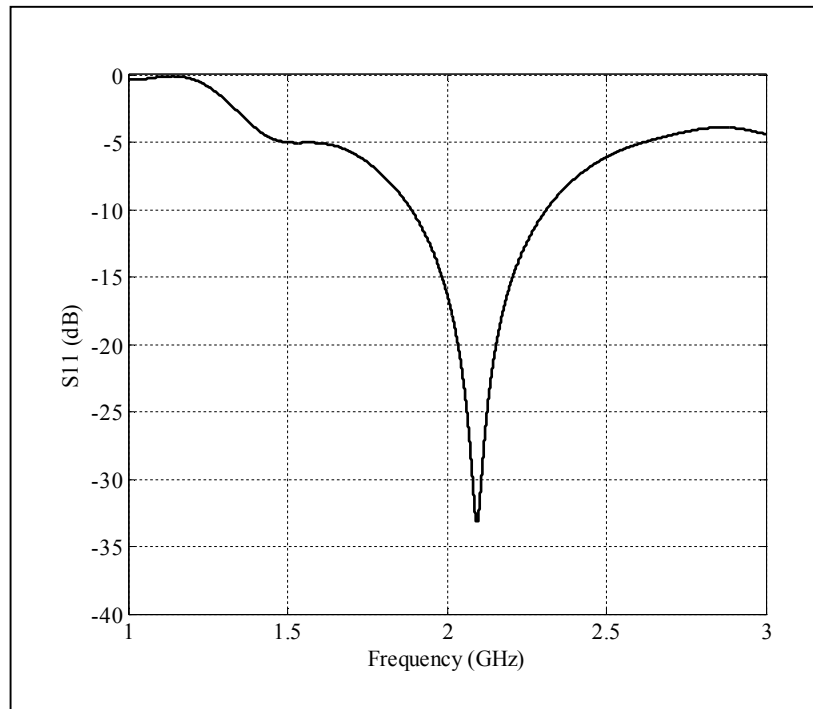


Figure 4.8 Simulated results of reflected power of antenna type *B*.

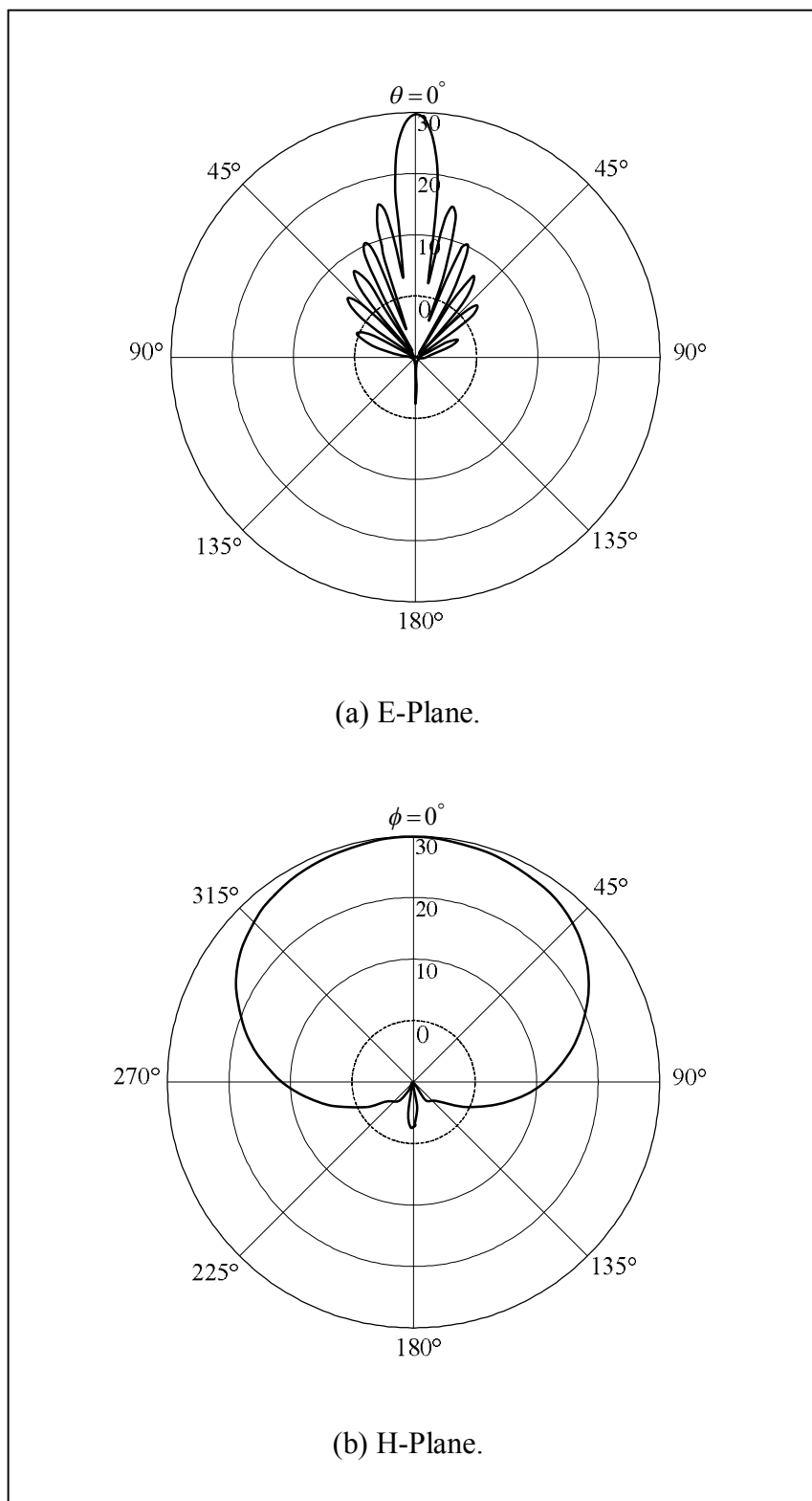


Figure 4.9 Simulated normalized radiation patterns of antenna type *B*.

4.3 Electromagnetic Band Gap Configuration

In this section, the modified antenna type *B* has increased the gain by using new technique of EBG structures instead. The conventional method for gain increment, a lot of elements will be added in the array, which causes the dimension of antenna too long and its weight too heavy. Moreover, the great number of electromagnetic energy will be lost inside the phasing line. From our study, we found that the proper structure of EBG is capable to enhance the gain of antenna as the additional resonant circuit which installed at front of the array panel. Furthermore, the EBG structures can be appropriately shaped for reducing the side and back lobes of the directional antenna too (Weily et al., 2005; Lee et al., 2009). From investigation, the sector of cylindrical woodpile EBG structures (Lee et al., 2010) is more suitable for the antenna type *B*. Figure 3.12 in Chapter 3 shows the geometry of the curved woodpile EBG structures with two layers of the different diameters. To implement the curved woodpile EBG, we have used alumina rods (rectangular cross section) with parameters $\epsilon_r = 8.4$ and $\tan\delta = 0.002$.

4.4 Design of Antenna System by CST Software

The gain improvement of a 1×8 array of microstrip slot antennas and U-shaped reflector with curved woodpile EBG structures (antenna type *C*) was simulated by CST software as shown in Figure 4.10.

The design parameters of the gain improvement for an antenna type *C* are the radius (R), the distance between a 1×8 array of microstrip slot antennas and curved woodpile EBG structures (d), and the height of curved woodpile EBG (h) or the number of curved filaments/ring (N_c). Firstly, we look at the effect of the variation of

R , d and h are fixed at 0λ and 1.23λ ($N_c = 6$ curved filaments/ring), respectively. Figure 4.11 shows the gain against the R at operating frequency of 2.1 GHz. The highest gain of 18.72 dB is provided at R is around at 3.34λ . Also, the appropriate HPBW in the H-plane appears at same radius of R of curved woodpile EBG structures, while its HPBW will be enlarged when the dimension of R increased. Secondly, we have investigated the effect of the distance d , while R and h are fixed at 3.34λ and 1.23λ , respectively. It notes that the highest gain of 18.72 dB is achieved when $d = 0\lambda$ as shown in Figure 4.12. This property can be used to control the resonant frequency of curved woodpile EBG structures because its resonant frequency will change when d is changed, while the bandwidth is constant. Next, we have studied the effect of the h variation versus the gain, R and d are fixed at 3.34λ and 0λ , respectively, thus its result is improved as shown in Figure 4.13. It finds that the gain is increased from 18.72 dB to 20.84 dB at h equals to 3.91λ approximately ($N_c = 18$ curved filaments/ring). Although the gain increases when h also increases, while h is higher than 5.25λ ($N_c = 24$ curved filaments/ring), the operating frequency of bandwidth will be shifted to the undesired frequency and the bandwidth will be not wide enough for utilizing for 3G base station as shown in Figure 4.14.

Finally, the highest gain of an antenna type C is optimized with $R = 3.34\lambda$, $d = 0\lambda$, and $h = 3.91\lambda$ ($N_c = 18$ curved filaments/ring). The simulated results with CST software show that the S_{11} and the normalized radiation patterns of the antenna type C at 2.1 GHz with the gain of 20.84 dB as shown in Figure 4.15 and 4.16, respectively. The HPBW in the E- and H-Planes of the antenna type C is $37.2^\circ:8.7^\circ$.

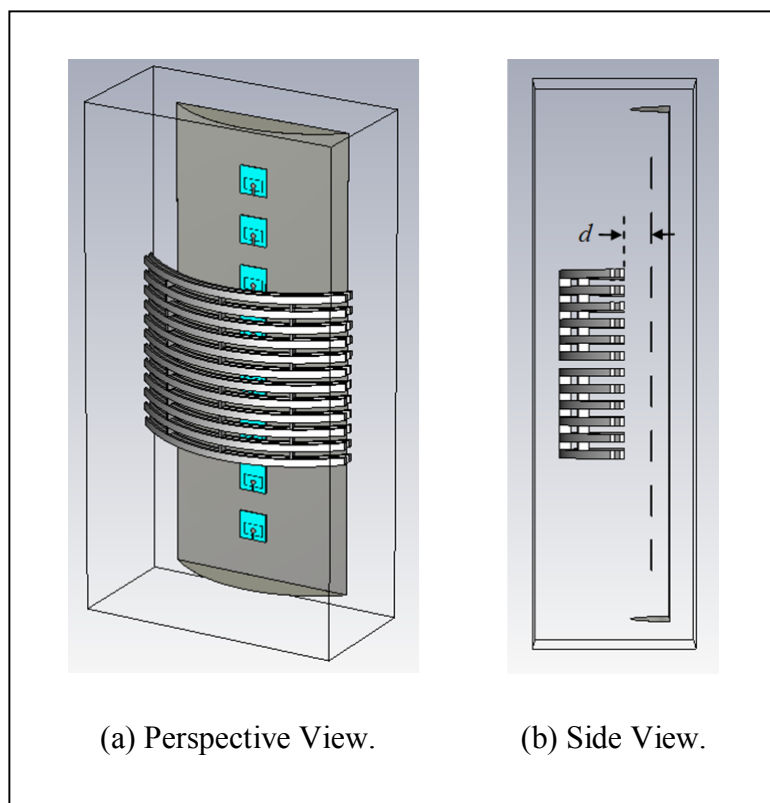


Figure 4.10 A 1×8 array of microstrip slot antennas and U-shaped reflector improved gain with curved woodpile EBG structures (antenna type C).

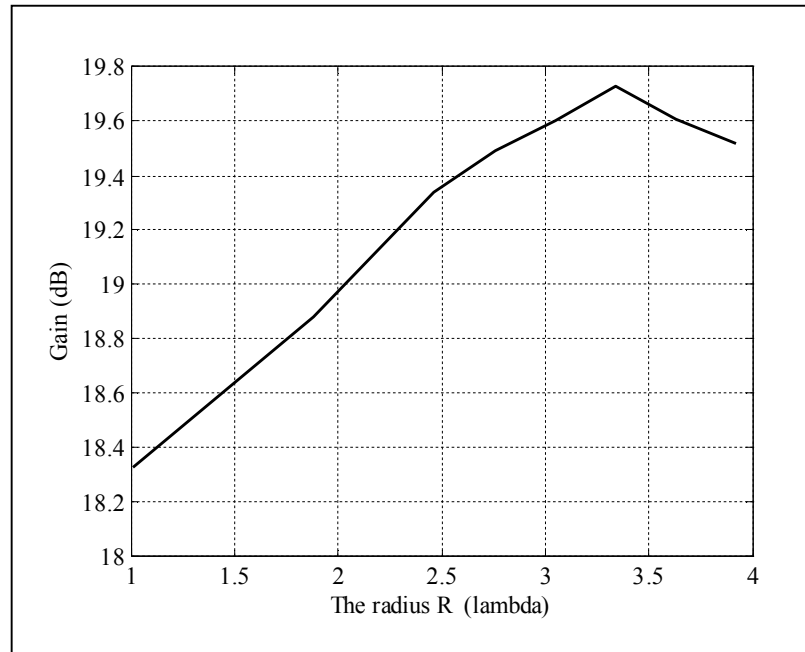


Figure 4.11 Simulated gain against R .

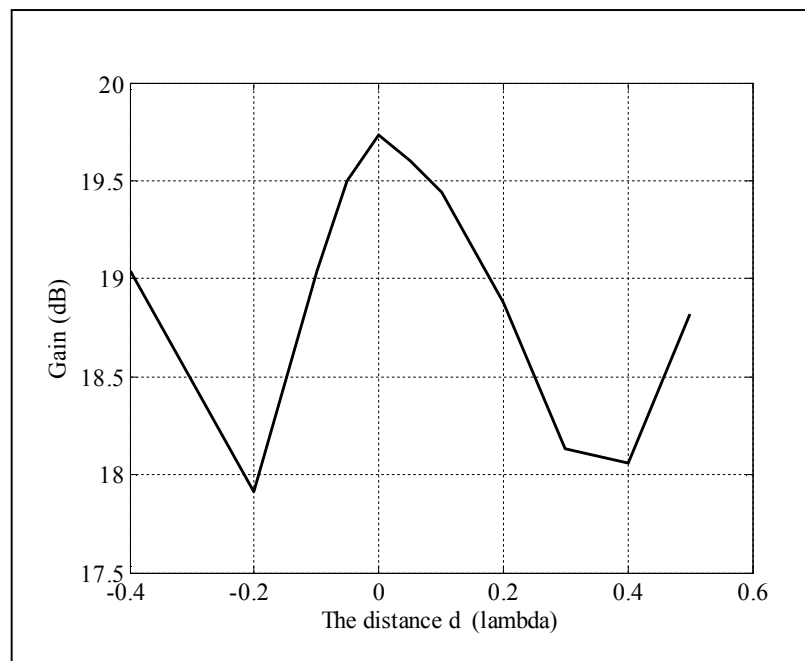


Figure 4.12 Simulated gain against d .

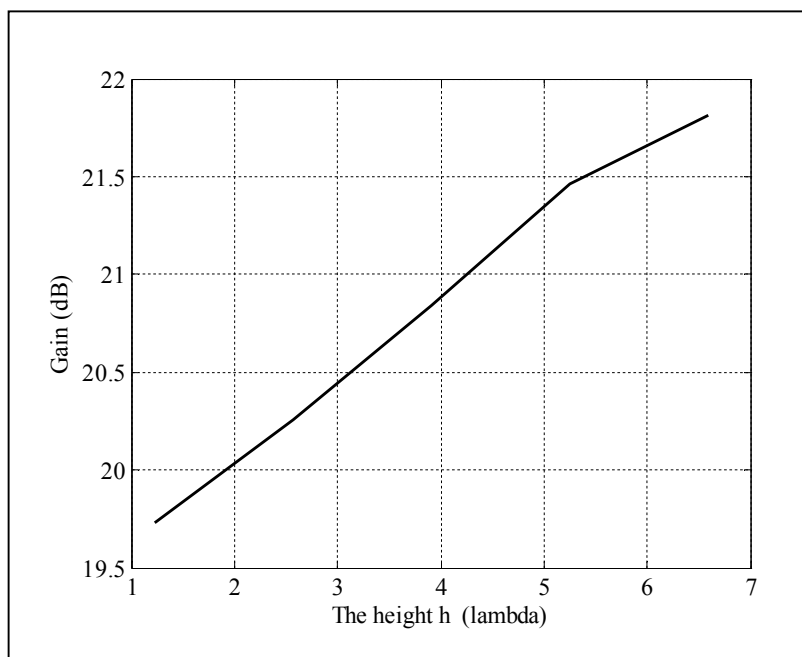


Figure 4.13 Simulated gain against h .

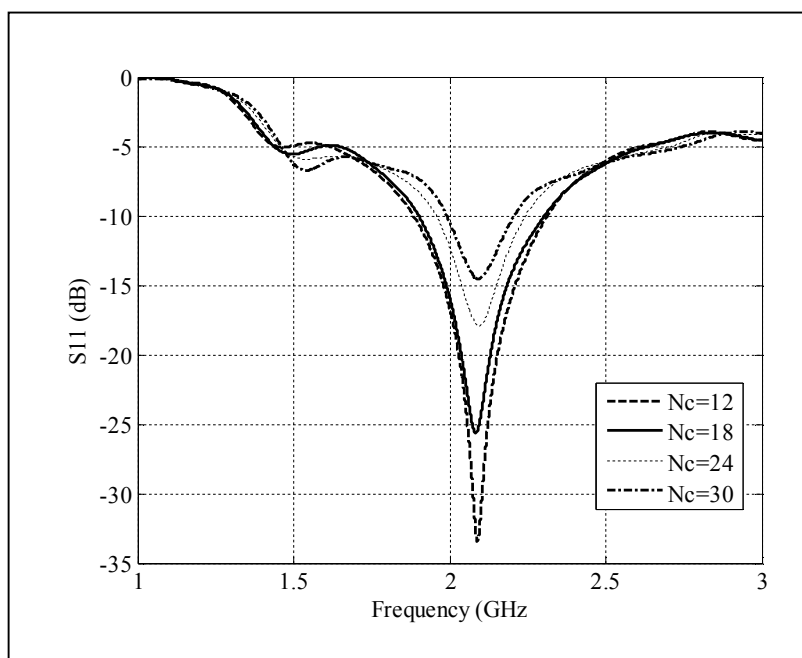


Figure 4.14 Simulated radiated power of variation of N_c .

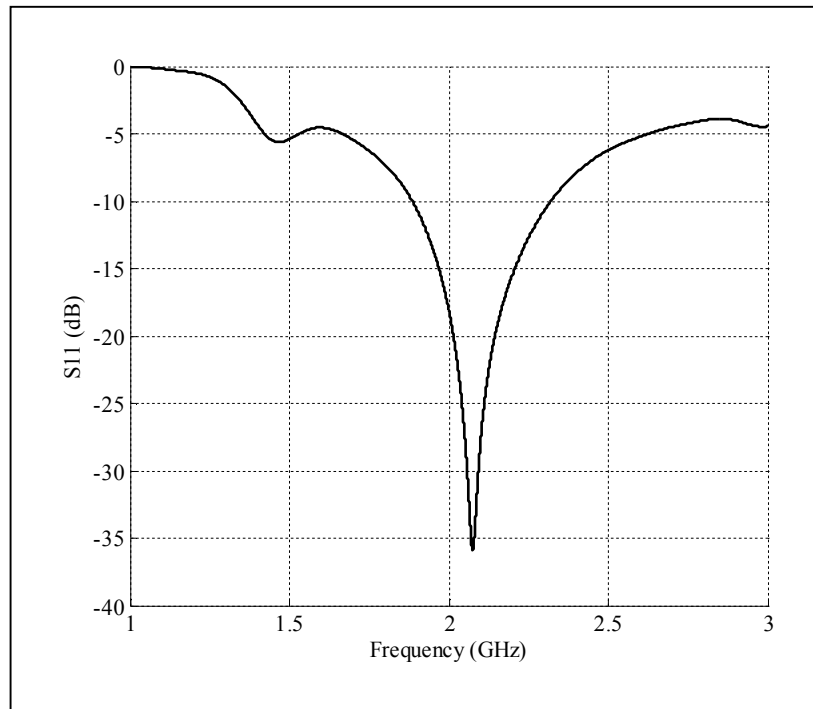


Figure 4.15 Simulated results of reflected power of antenna type *C*.

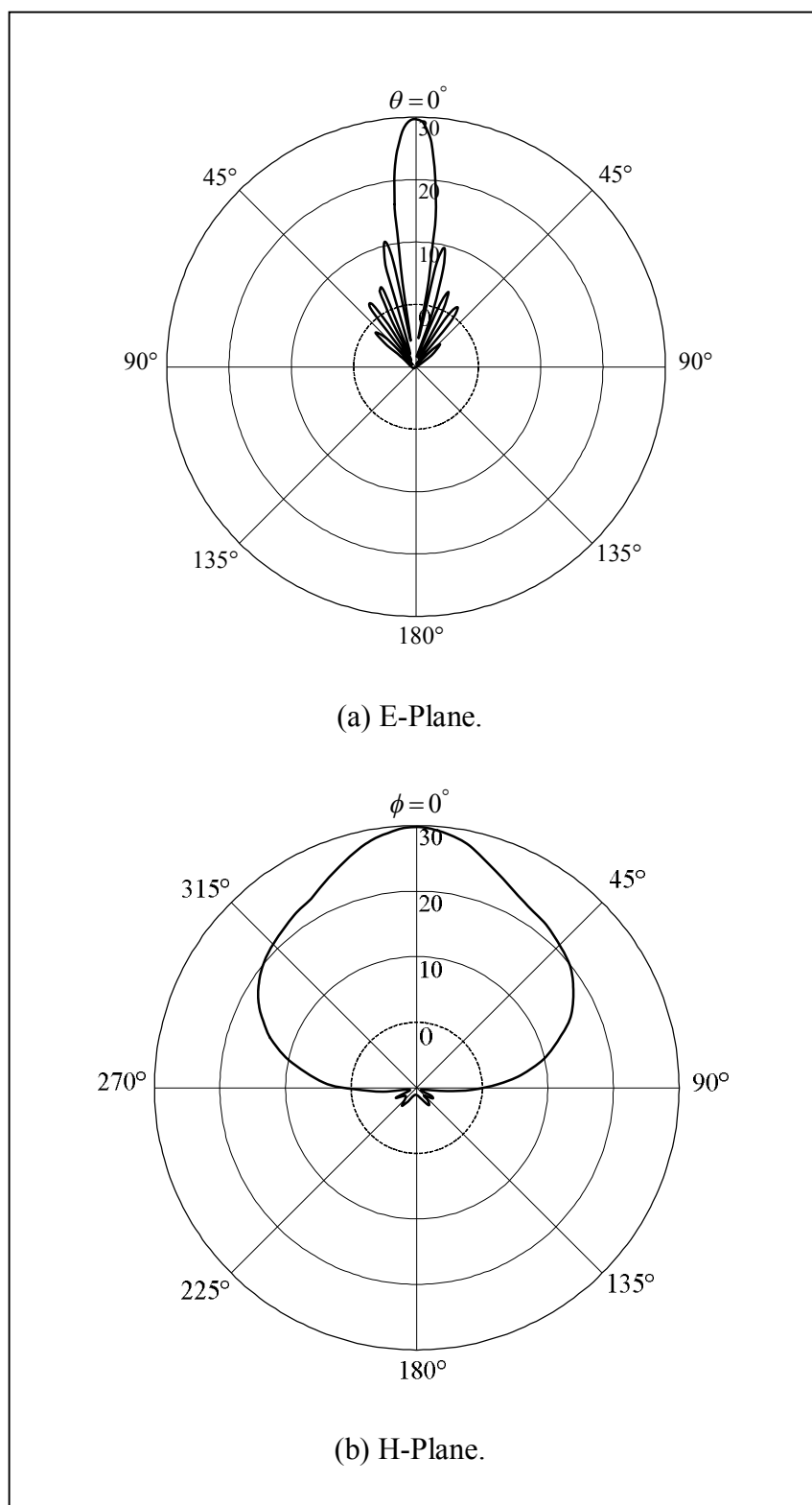


Figure 4.16 Simulated normalized radiation patterns of antenna type C.

The S_{11} of the antenna type *A*, *B*, and *C*, covered 1.920 to 2.170 GHz, which are wide enough and can be well utilized for 3G base station as shown in Figure 4.17. Figure 4.18 shows the normalized radiation patterns at 2.1 GHz of the antenna type *A*, *B*, and *C*. Although its HPBW of the antenna type *C* will narrow, but it can cover the desired service area of base station for mobile phone and still provides the highest gain. Also, the HPBW, the Side Lobe Level (SLL), and the gain of the antenna type *A*, *B*, and *C* are shown in Table 4.1.

Table 4.1 Results of simulation.

Parameters	Antenna type <i>A</i>	Antenna type <i>B</i>	Antenna type <i>C</i>
The HPBW (AZ:EL)	97.4°:8.4° 11.6:1	89.4°:8.3° 10.8:1	37.2°:8.7° 4.3:1
The E-plane SLL	-12.9 dB	-13.2 dB	-14.4 dB
The H-plane SLL	-	-30.6 dB	-27.3 dB
The Gain	14 dB	17.83 dB	20.84 dB

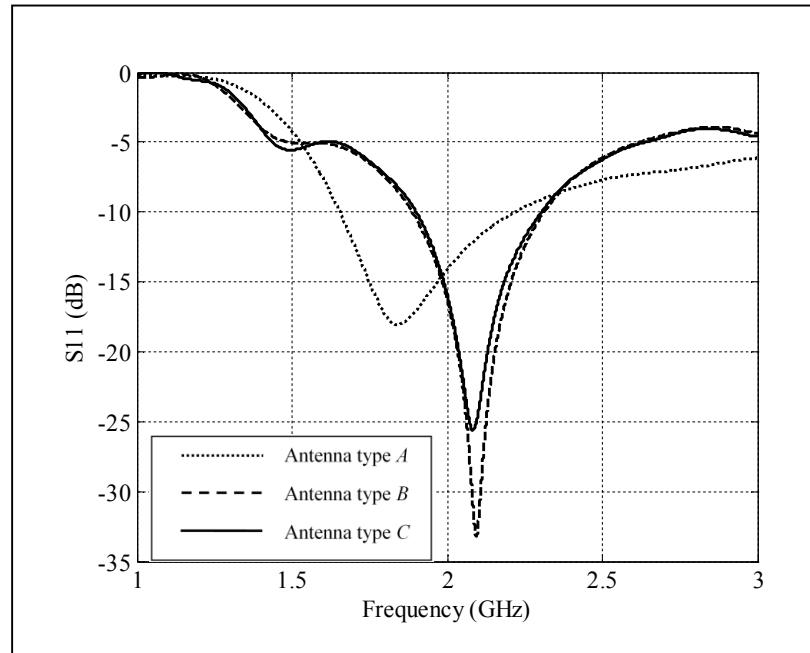


Figure 4.17 Simulated results of reflected power of three type antennas.

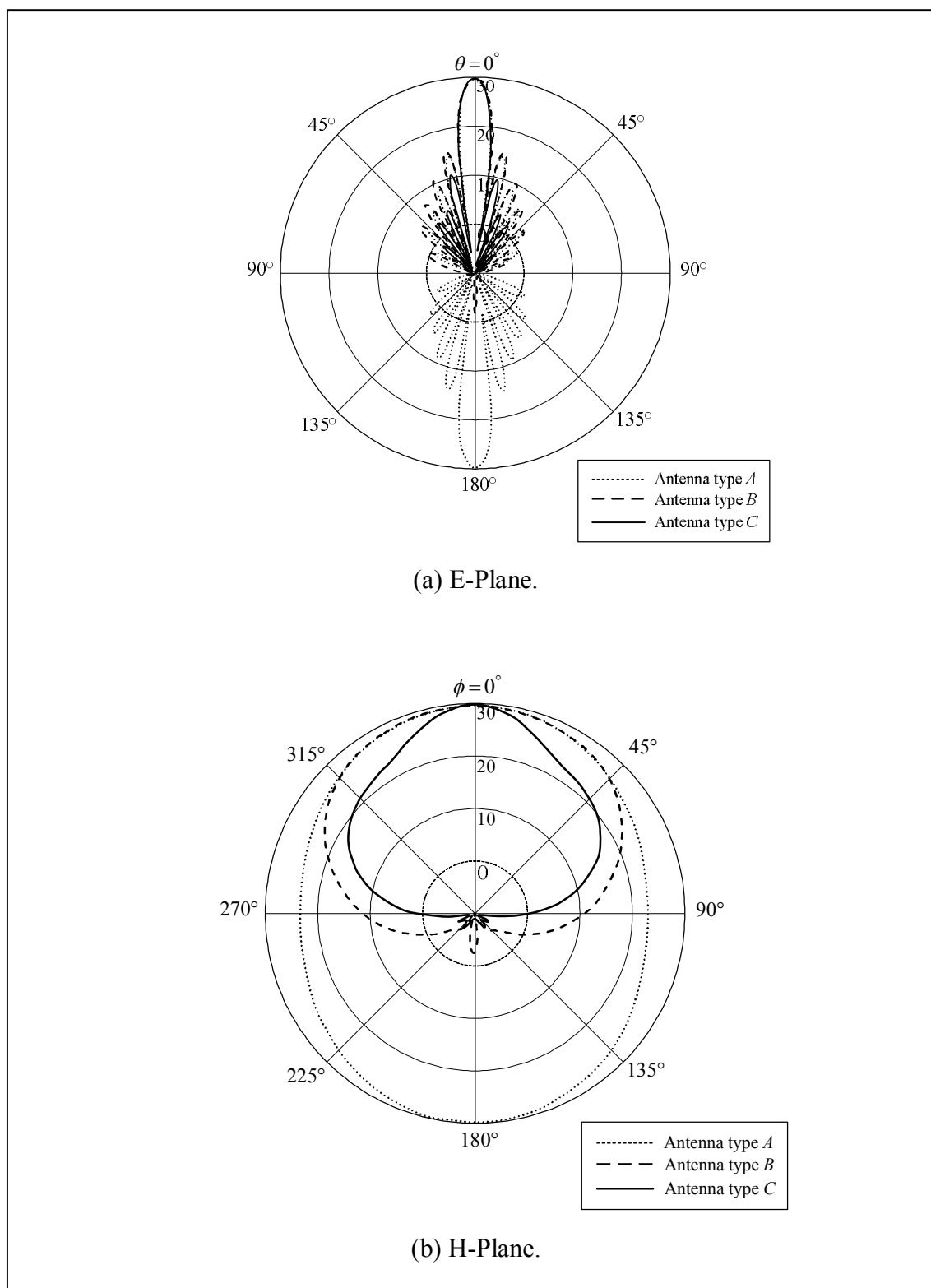


Figure 4.18 Simulated normalized radiation patterns of three type antennas.

To analyze unique features of curved woodpile EBG structures, the lumped element model has been implemented as shown in Figure 4.19. From the results of the design parameters of the gain improvement, we found that the capacitance C can be used to adjust the HPBW and the inductance L can be used to control the resonant frequency and the bandwidth of the antenna. Furthermore, the unit cell of curved woodpile EBG is analyzed by using the cavity model with CST software to be certain the exhibition bandgap characteristics at 2.1 GHz. Figure 4.20 and 4.21 show the unit cell of curved woodpile EBG in form of the cavity model and the bandgap characteristics of this the unit cell.

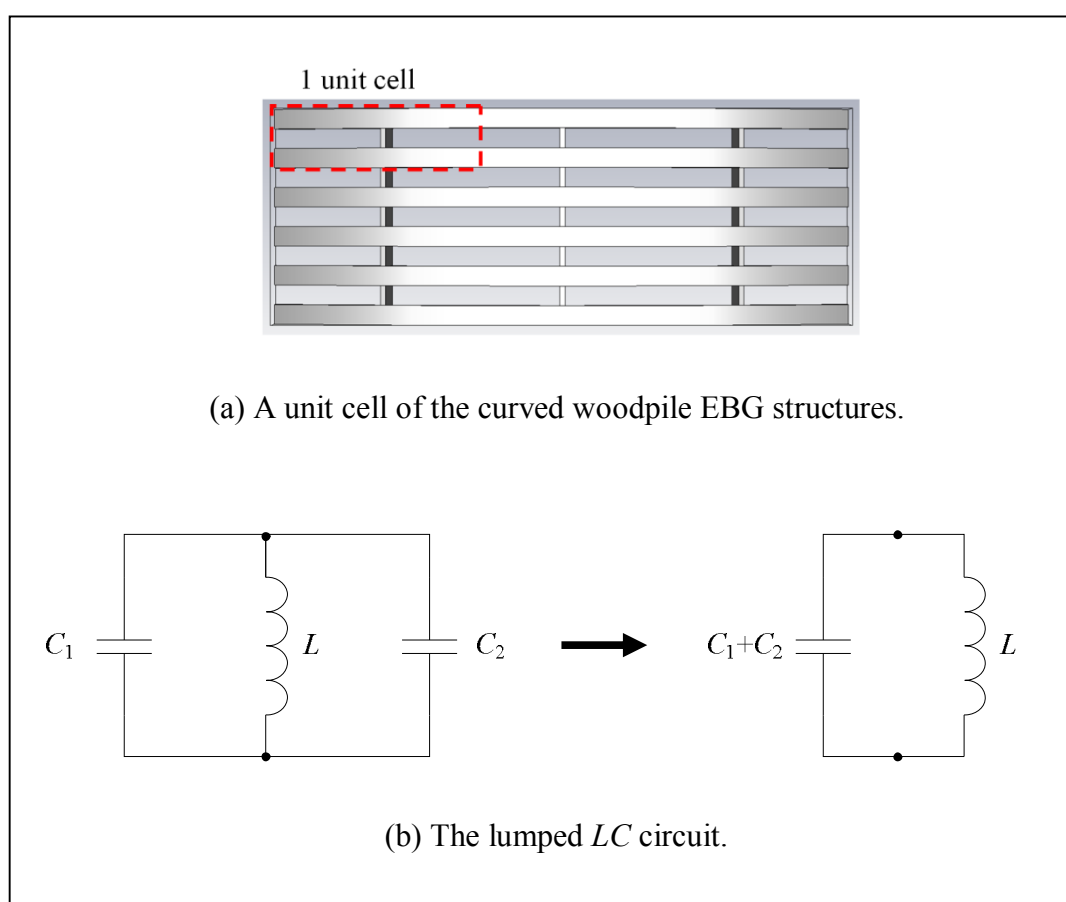


Figure 4.19 The lumped LC model.

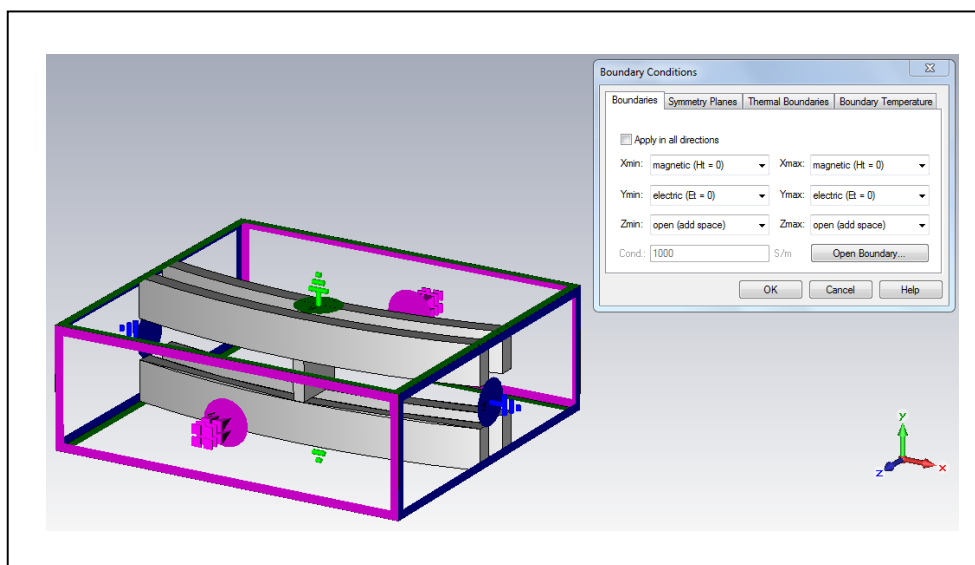


Figure 4.20 The cavity model of the unit cell of curved woodpile EBG.

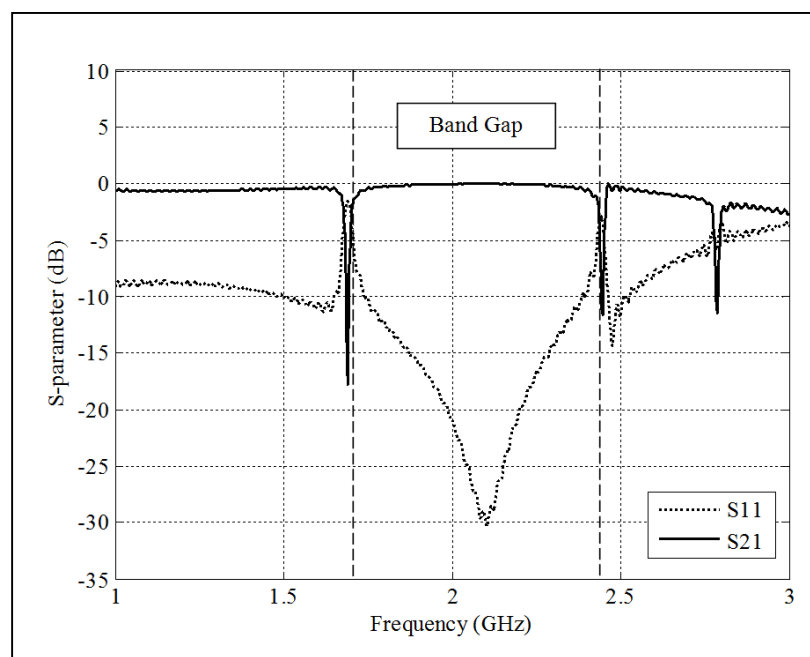


Figure 4.21 The bandgap characteristics of the unit cell of curved woodpile EBG.

4.5 Parameter Computation by FDTD and ANN Methods

To design the processing model to compute the parameters of the proposed antenna, the FDTD and ANN methods are utilized to calculate this model. The 2D FDTD in TE mode is utilized for analyzing of a 1×8 array of microstrip slot antennas and U-shaped reflector. While the ANN is utilized for analyzing of grid cells of the antenna system and training model to obtain the results. We construct the model to calculate the parameters of the proposed antenna by using the activate function of Levenberg-Marquardt algorithm as shown in Figure 4.22. Moreover, the backpropagation algorithm, an abbreviation for backward propagation of errors, is applied for looking the minimum of the error function in weight space by using the method of gradient descent. Figure 4.23 to 4.25 show the process of training models of the S_{11} , E-, and H-fields, respectively. These models can be accepted when the root mean square error (RMSE), a frequently used measure of the difference between values predicted by a model and the values actually observed from the environment that is being modeled, is less than 1. The RMSE of a model prediction with respect to the estimated variable X_{model} is defined as the square root of the mean squared error:

$$RMSE = \sqrt{\frac{\sum_{i=1}^n (X_{obs,i} - X_{model,i})^2}{n}}, \quad (4.1)$$

where X_{obs} is observed values and X_{model} is modeled values at time/place i .

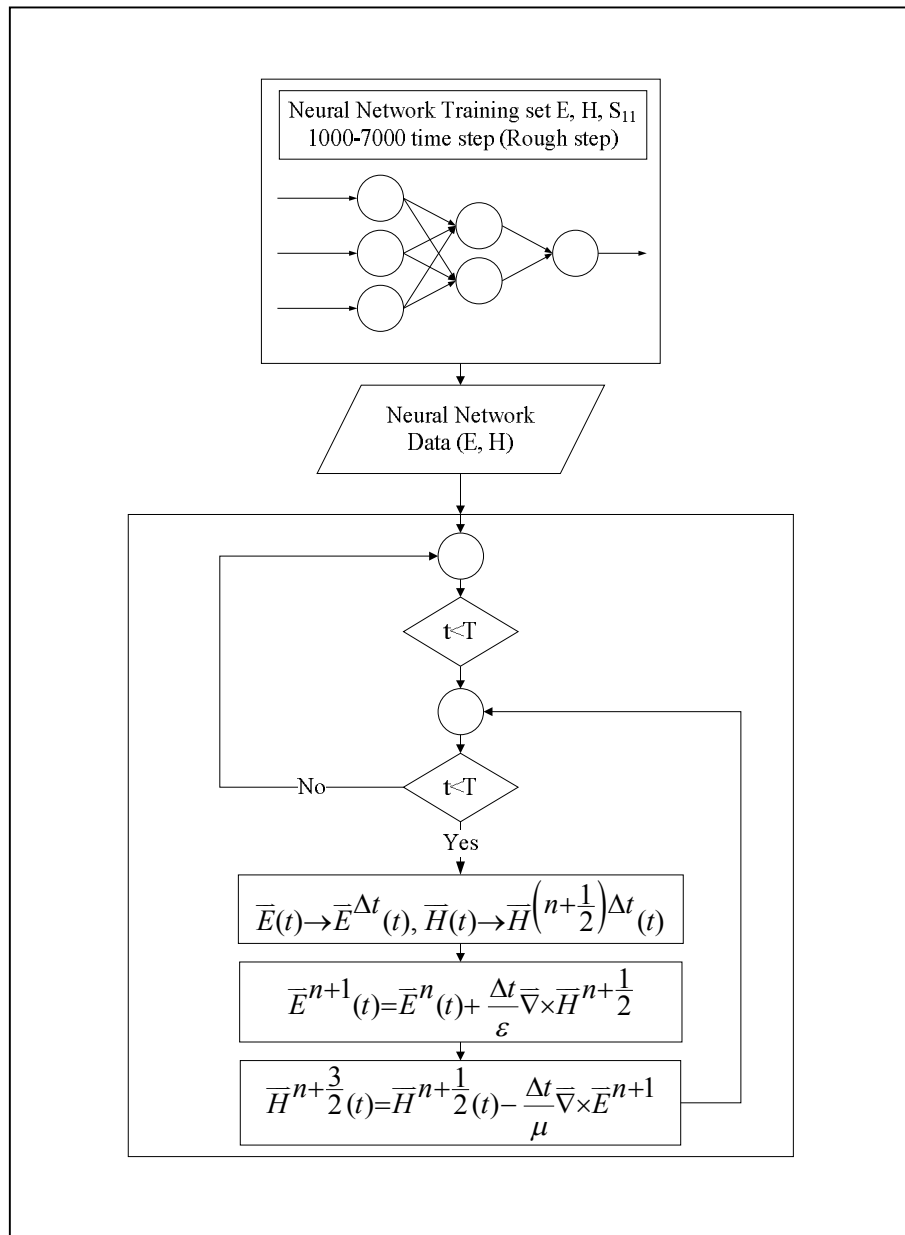


Figure 4.22 The model to calculate S_{11} , E -, and H -fields.

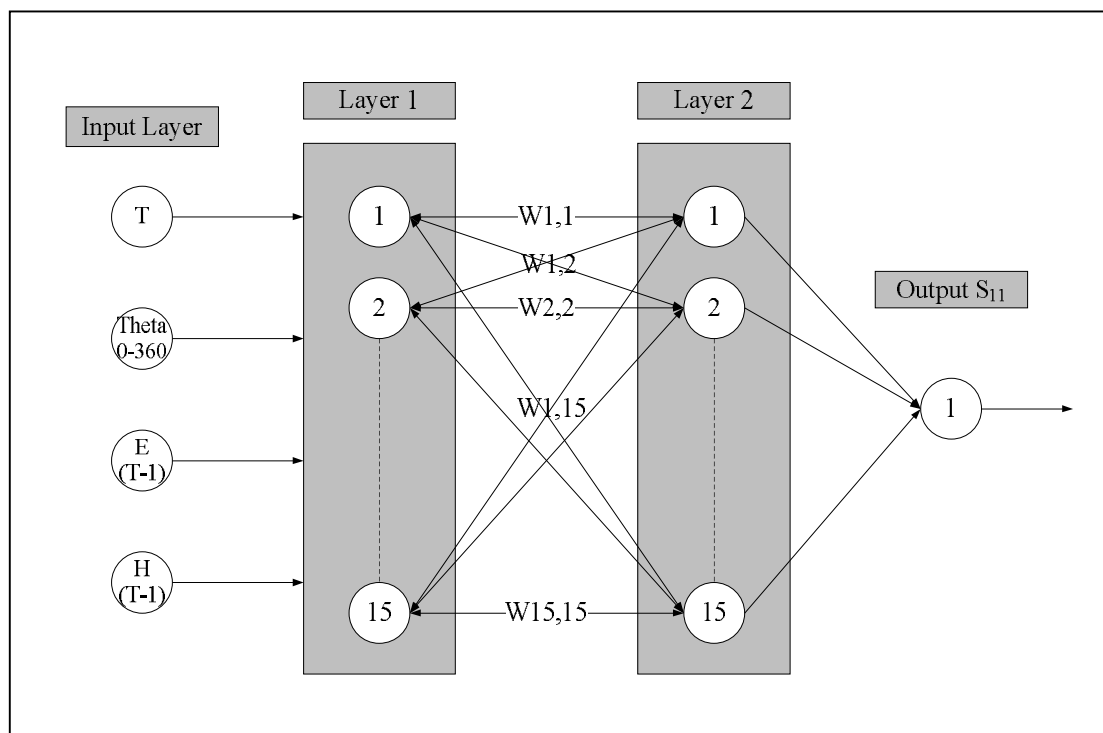


Figure 4.23 Training model of S_{11} .

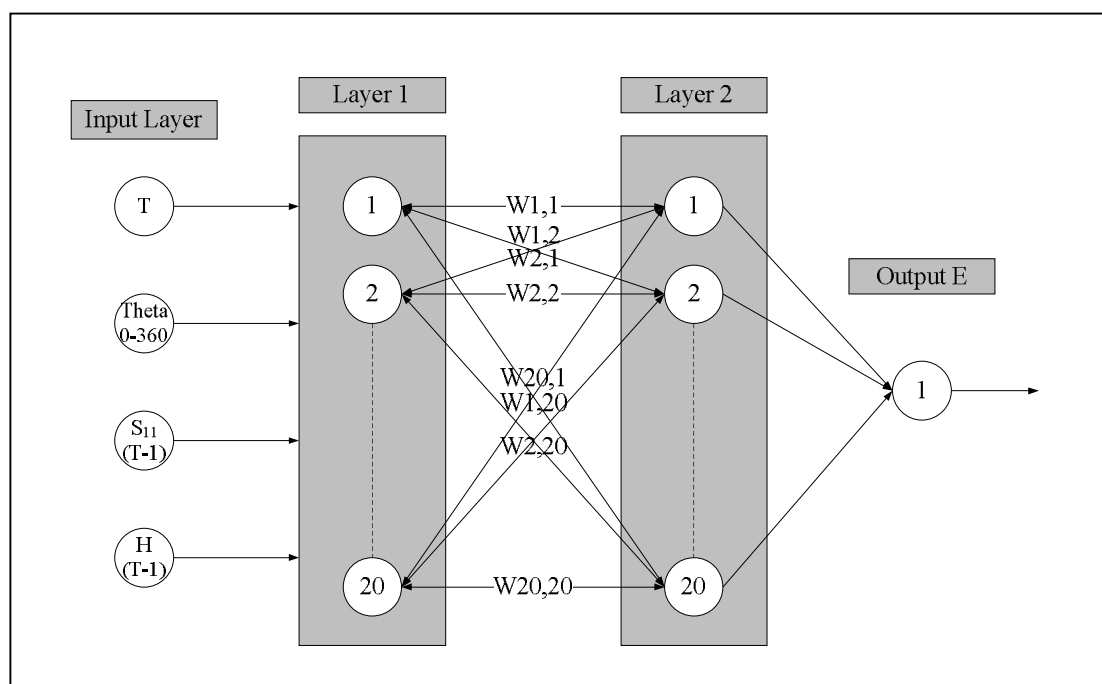


Figure 4.24 Training model of E-field.

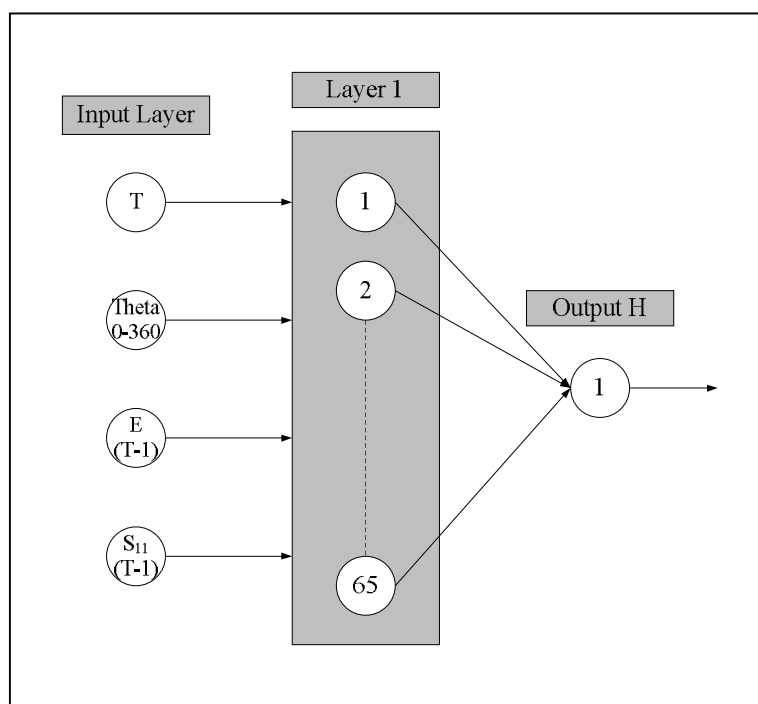


Figure 4.25 Training model of H-field.

The MATLAB, a high-level language and interactive environment for numerical computation, visualization, and programming which can analyze data, develop algorithms, and create models and applications, is applied to model and compute the training model of S_{11} , E-, and H-fields by using a programming languages, such as C++. Figure 4.26 and 4.27 show the feature of the program and while the program is running on MATLAB, respectively. From the results of this program, the S_{11} of the proposed antenna covered 1.920 to 2.170 GHz as shown in Figure 4.28. Figure 4.29 shows the normalized radiation patterns at 2.1 GHz. Also, the HPBW, the SLL, and the gain are shown in Table 5.3 in the next chapter.

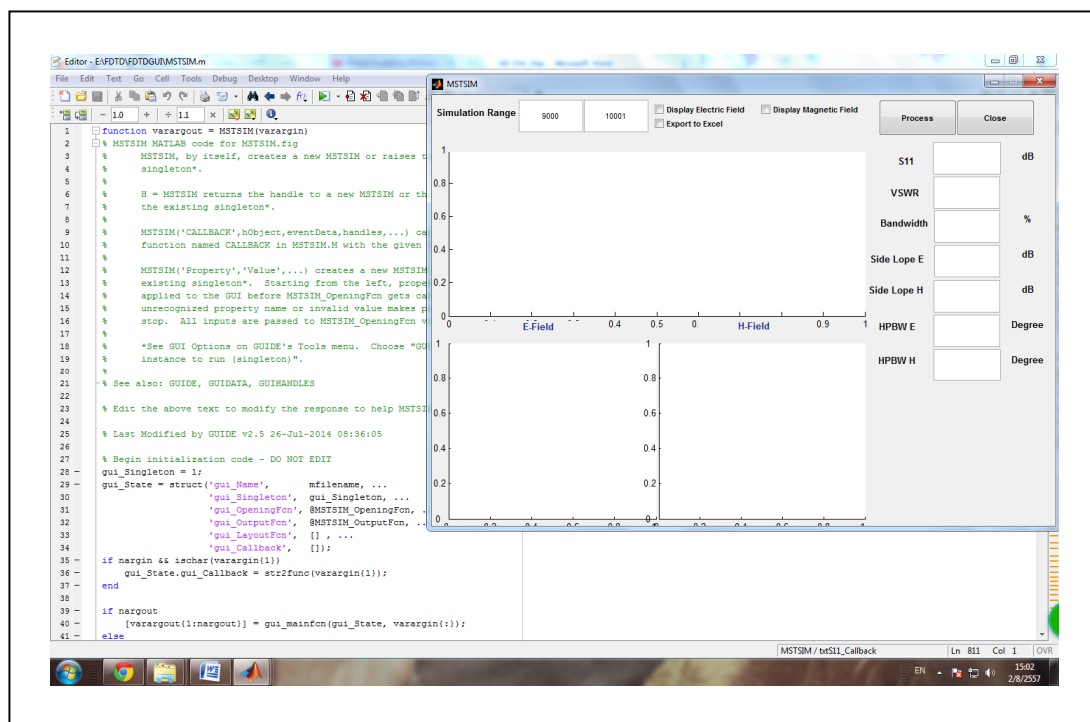
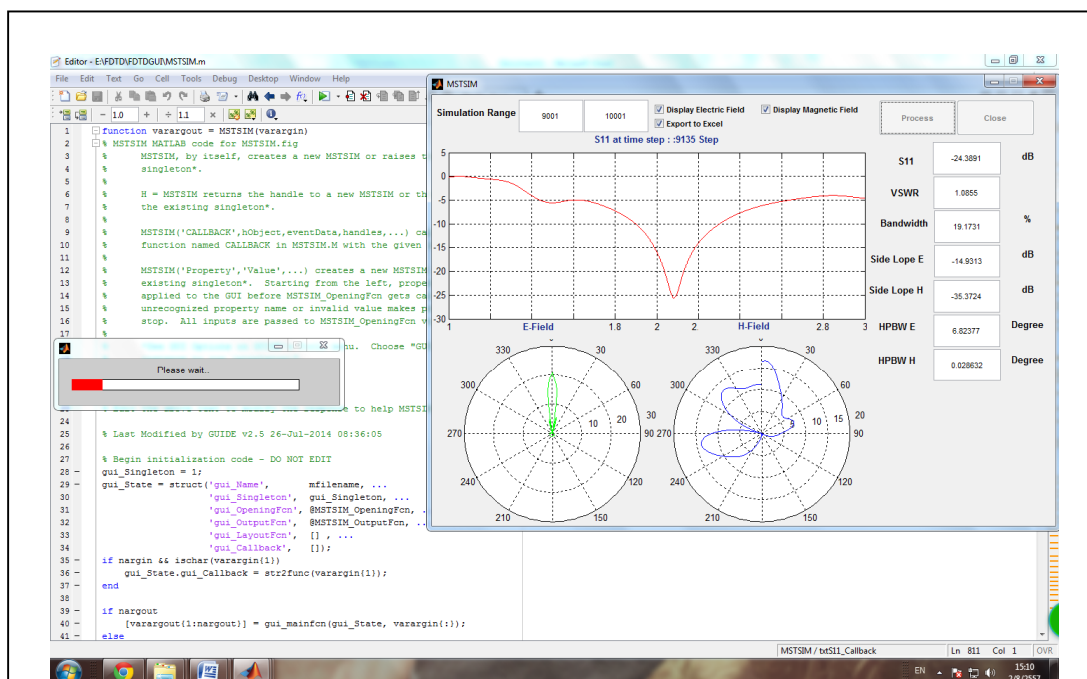
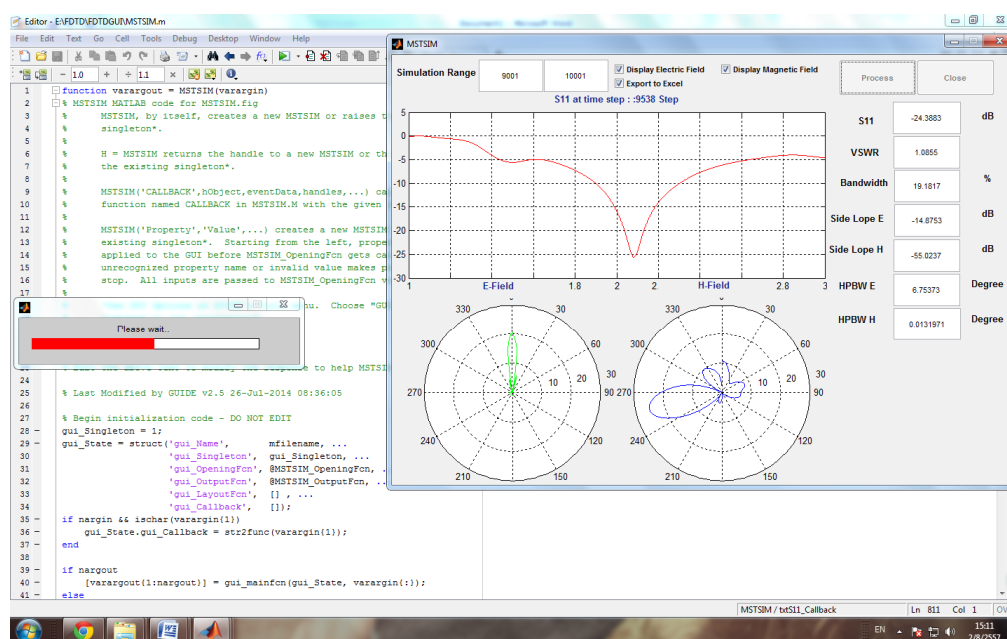


Figure 4.26 The feature of the program on MATLAB.

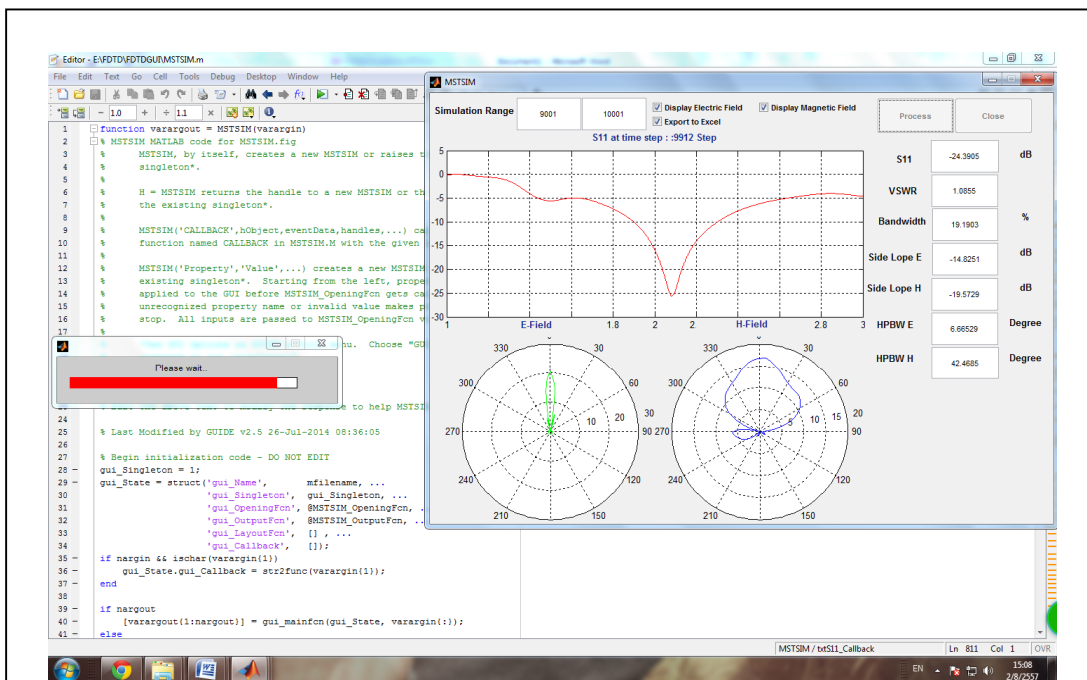


(a) At 9135 time Steps.

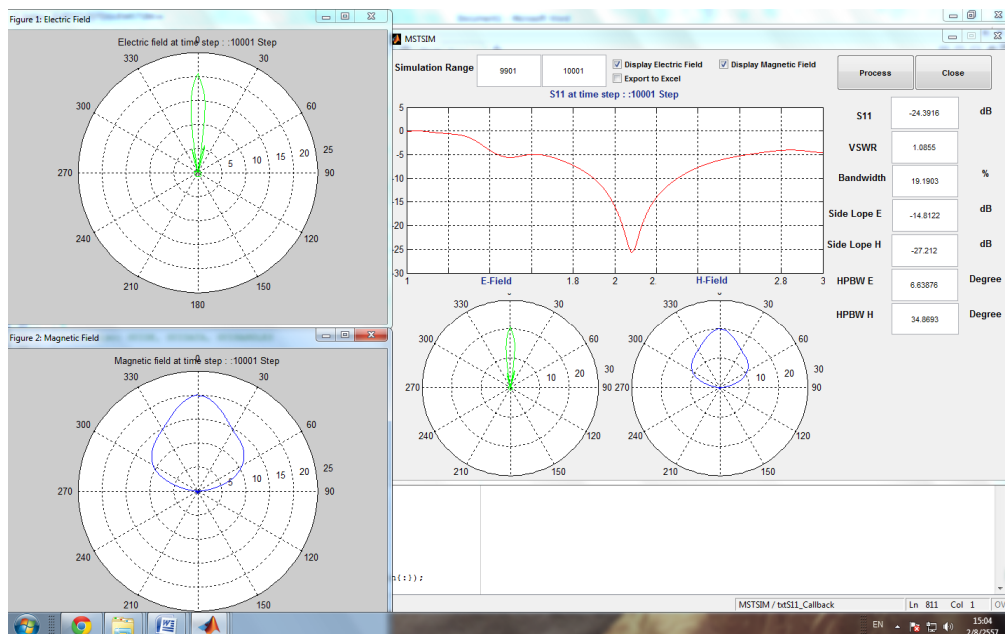


(b) At 9538 time Steps.

Figure 4.27 The running program on MATLAB.



(c) At 9912 time Steps.



(d) At 10001 time Steps (Finished).

Figure 4.27 The running program on MATLAB (Continued).

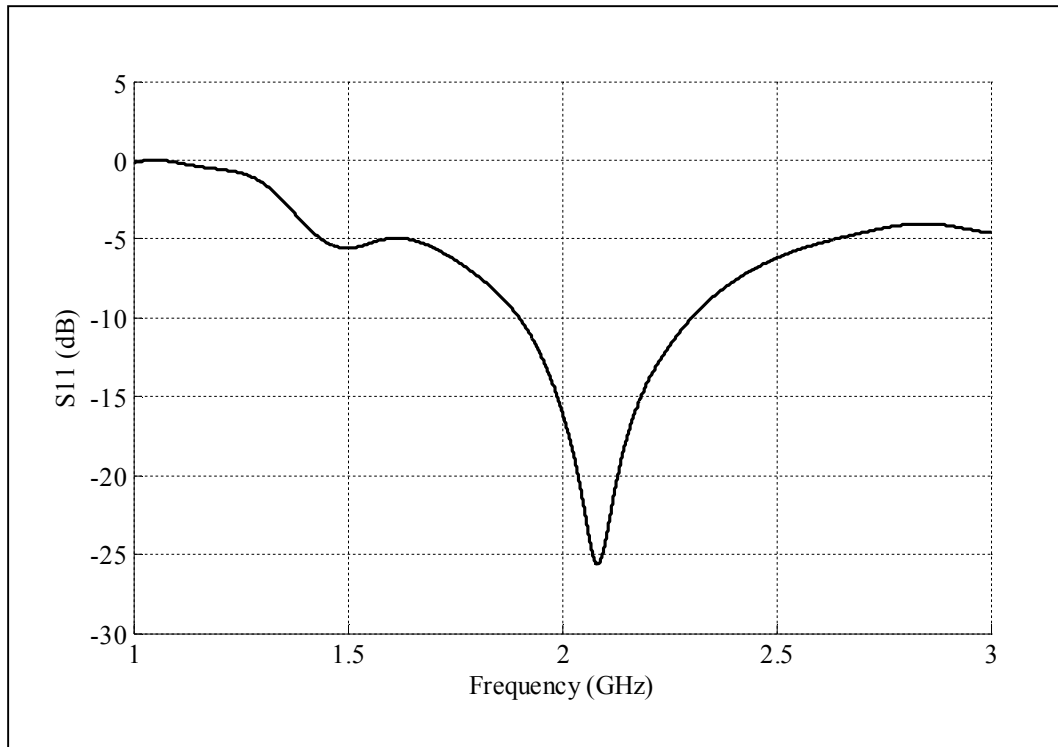


Figure 4.28 Computed reflected power.

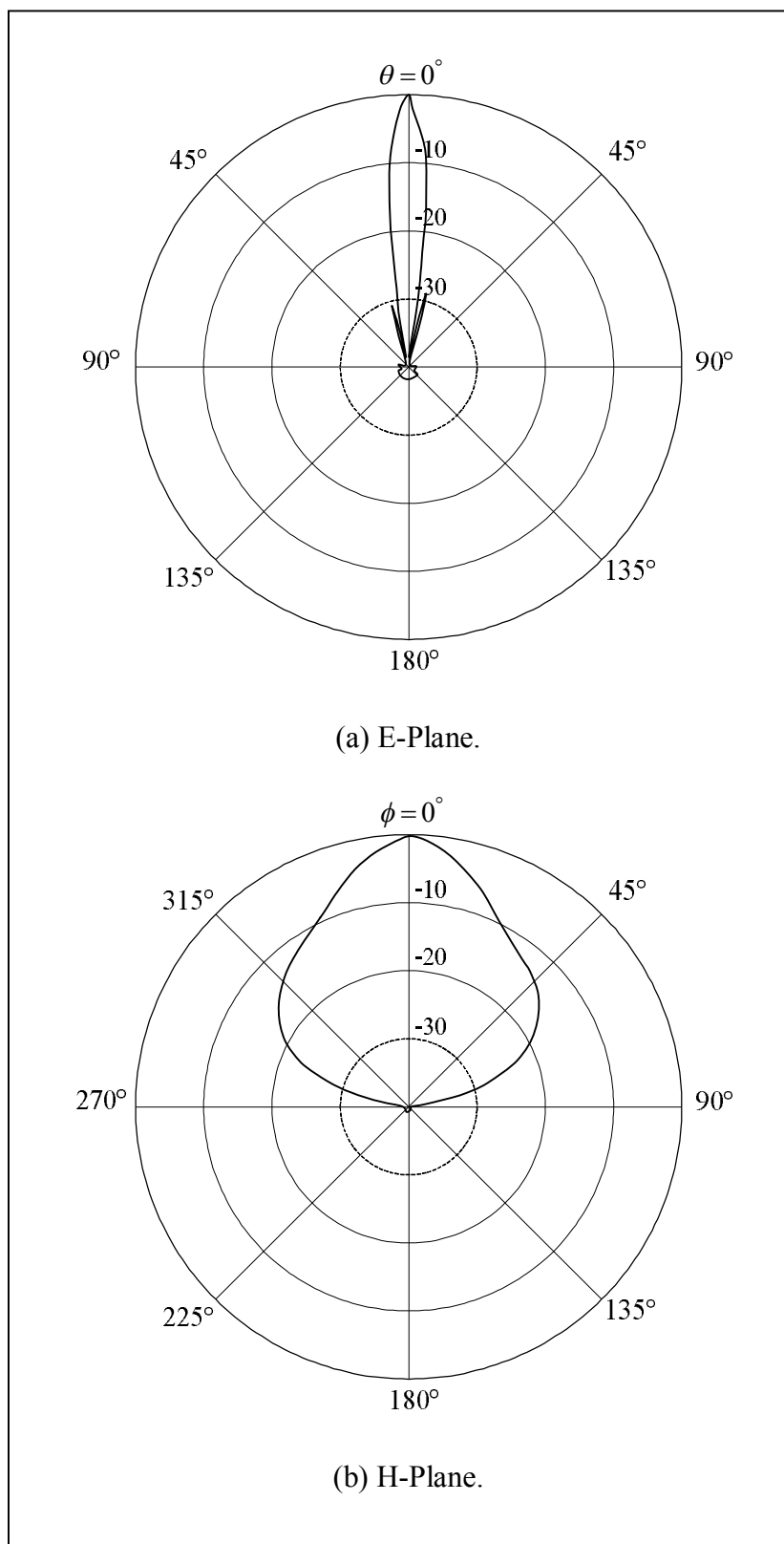


Figure 4.29 Computed normalized radiation patterns.

4.6 Chapter Summary

In this chapter presented analysis and design of a sector antenna for mobile base station. The first, the design and modification of the bidirectional microstrip slot antennas array to be the directional antenna by adding U-shaped reflector were simulated with CST software. The second, the increasing its gain with new technique, additional curved woodpile EBG structures was presented. We found that the directive gain of the proposed antenna was increased around 3 dB when such EBG structures were added, while its length of array was not enlarged. The most important technique for this accomplishment that is the EBG structures must be appropriately designed and calculated, especially the radius of the sectorial cylinder of woodpile EBG structures. The most proper radius of 3.34λ , the distance between a 1×8 array of microstrip slot antennas and curved woodpile EBG structures of 0λ , and the height of curved woodpile EBG of 3.91λ (18 curved filaments/ring) can provide the moderately highest gain of 20.84 dB at the operating frequency of 2.1 GHz. Finally, the FDTD and ANN methods are conducted to compute and carry out the S_{11} , E-, and H-fields.

CHAPTER V

MEASUREMENT AND DISCUSSION

5.1 Introduction

In order to understand the general background and the theory behind a sector antenna for mobile base station, the antenna measurements for the final verification of this proposed antenna operation will be presented in this chapter. It was fabricated and its performance was measured and discussed. To verify the theory calculation, the radiation patterns were measured in the outdoors by using vector network analyzer HP 8722D and compared with the simulated and computational results from CST software and FDTD and ANN methods, respectively. The effects of the support structures on the radiation patterns of the proposed antenna have been investigated experimentally.

5.2 The Antenna Prototype

5.2.1 A 1×8 Array of Microstrip Slot Antennas and U-shaped Reflector

In this research, we have chosen the microstrip slot antenna (Chawanonphithak and Phongcharoenpanich, 2007) to design for working in the UMTS band is utilized by the prototype for this proposed antenna. As describe in chapter 4, a 1×8 array of microstrip slot antennas and U-shaped reflector, antenna type *B*, was designed and analyzed at frequency of 2.1 GHz. It was designed by using CST software of input parameters as summarized in Table 5.1. To verify the performance of the antenna system, a 1×8 array of microstrip slot antennas is printed

on FR4 substrate with the size of each element of $60 \text{ mm} \times 60 \text{ mm}$ and the thickness of 1.6 mm and the U-shaped reflector has been fabricated with the PEC, the size of $400 \text{ mm} \times 1,000 \text{ mm}$, as shown in Figure 5.1.

Table 5.1 Dimensions of the microstrip slot antenna.

Description	Dimension (λ)	Dimension (mm)
The circular patch of the radius (a)	0.034	4.86
The gap distance (t)	0.007	1
The width of ground plane (W)	0.42	60
The length of ground plane (L)	0.42	60
The width of wide-slot ground plane (W_1)	0.287	41
The length of wide-slot ground plane (L_1)	0.166	23.72
The microstrip line length (L_2)	0.07	10

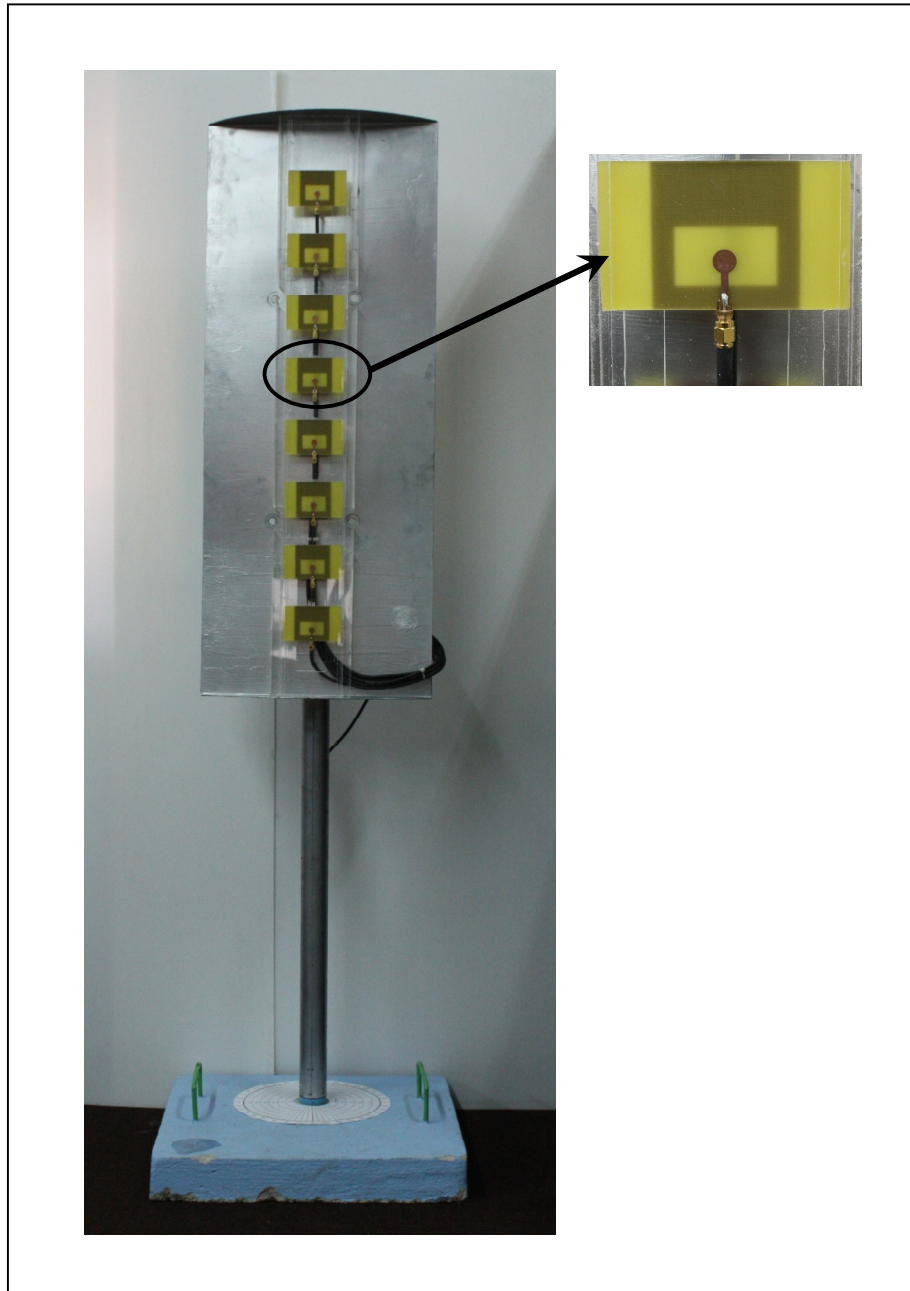


Figure 5.1 The prototype of a 1×8 array of microstrip slot antennas and U-shaped reflector (antenna type *B*).

5.2.2 The Curved Woodpile EBG Structures

This research applies the similar geometry of the planar (Weily et al., 2005; Lee et al., 2009) and the cylindrical woodpile EBG structures (Lee et al., 2010) to be the sector of curved woodpile EBG structures. Figure 5.2 shows the prototype of the curved woodpile EBG structures with two layers. The parameters for these structures are summarized in Table 5.2.

Table 5.2 Dimensions of the curved woodpile EBG structures.

Description	Dimension (λ)	Dimension (mm)
The filament thickness or diameter (w)	0.053	7.53
The outer radius (R_1)	3.45	493.11
The inner radius (R_2)	3.34	477.14
The height (h)	3.91	558.73
The number of curved filaments/ring (N_c)	18	
The number of radial filaments (N_{rad})	3	
The number of rings of the curved (N_{ring})	2	



Figure 5.2 The prototype of the curved woodpile EBG structures.

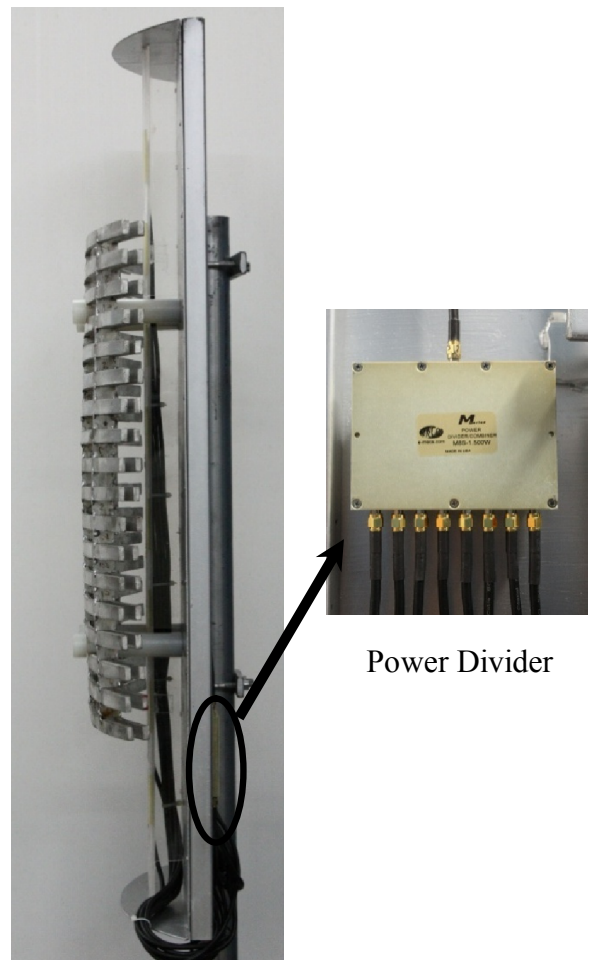
5.3 Antenna Measurement

A 1×8 array of microstrip slot antennas and U-shaped reflector with curved woodpile EBG structures, antenna type *C*, was constructed as shown in Figure 5.3. The antenna measurements are needed for the final verification of the antenna operation. Modern the CST simulation and analysis FDTD and ANN methods predicted often quite accurately the antenna characteristics, but for some complicated structures only measurements can give the accurate information on the antenna properties. In the all cases, it is beneficial to verify the computed results with measurements to ensure that antenna was correctly modeled in the simulations and correctly assembled. In this section, the measured results of radiation patterns, gain, bandwidth, input impedance, Standing Wave Ratio (SWR) and S_{11} of this proposed antenna are discussed.

The reciprocity theorem is applied to most antennas and, therefore, properties of antenna used to receive electromagnetic waves are the same as the properties for the same antenna when it is used to transmit electromagnetic waves. The space surrounding an antenna is commonly divided into three regions based on the behavior of the antenna radiation (Balanis, 2005): a reactive near-field region, a radiating near-field (Fresnel) region, and a far-field (Fraunhofer) regions. Figure 5.4 shows the three type field regions of antenna and R_1 and R_2 are defined as $\lambda/2\pi$ and $2D^2/\lambda$, respectively, where λ is the wavelength and D is the largest dimension of the antenna.



(a) Front View.



(b) Side View.

Figure 5.3 The prototype of the antenna system.

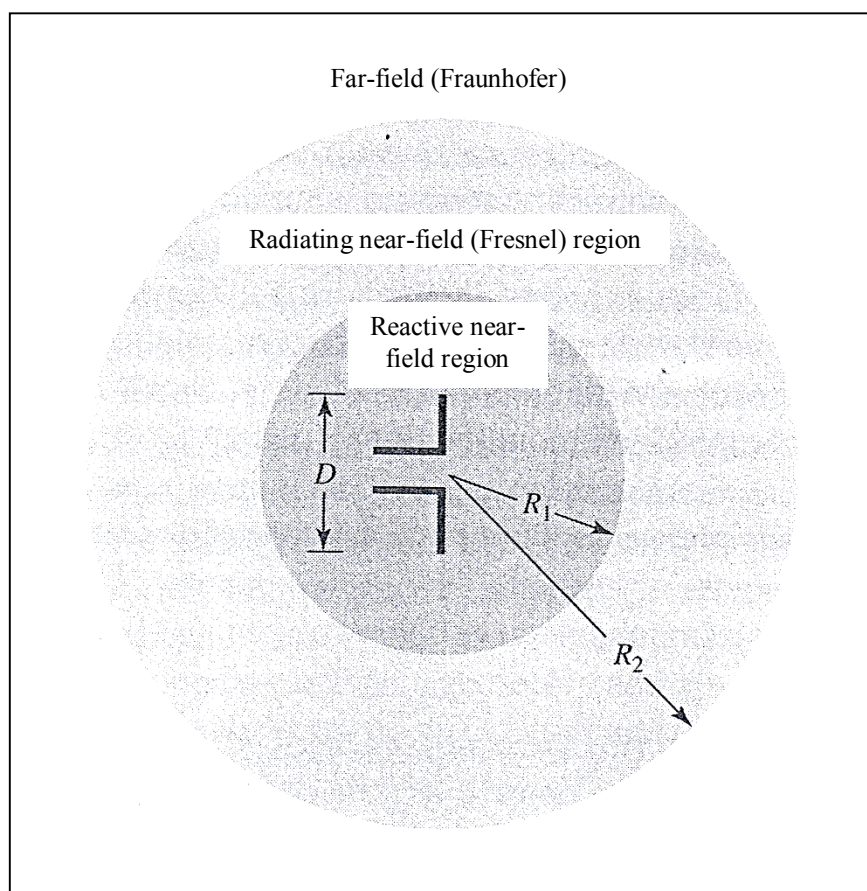


Figure 5.4 The three regions of an antenna (Balanis, 2005).

In the reactive near-field, the reactive field dominates and power is not propagating. The outer boundary of the reactive near-field is usually defined as $R < R_1$ from the antenna surface. The radiating near-field, or Fresnel region is a transition region between the reactive near-field region and the far-field region. In this region, the radiation fields predominate while the angular field distribution is dependent on the distance from the antenna. The inner boundary is taken to be the distance $R \geq R_1$ and the outer boundary the distance $R < R_2$. The far-field region is defined to begin at $R > R_2$. In the far-field region, the angular field distribution is independent of the distance from the antenna.

5.3.1 Radiation Patterns

Radiation patterns or antenna patterns are the mathematical function or the graphical representation of a quantity that characterizes the electromagnetic field generated by an antenna as a function of space coordinates. The antenna radiation patterns are displayed in the far-field region of the antenna in spherical coordinates at a constant radial distance and frequency. The field and power patterns are normalized with respect to their maximum value, yielding normalized field and power patterns (Balanis, 2005).

In the far-field antenna test, the prototype of this proposed antenna was measured in the outdoors. A single microstrip slot antenna is used to be transmitting antenna, while the antenna type *C* is in the receiving mode. The receiving antenna is installed on a turntable with the distance $R > R_2$ far from transmitting antenna as shown in Figure 5.5 and 5.6 for E- and H-planes, respectively. During the measurements, the receiving antenna was illuminated with a uniform plane wave and their receiving characteristics were measured.

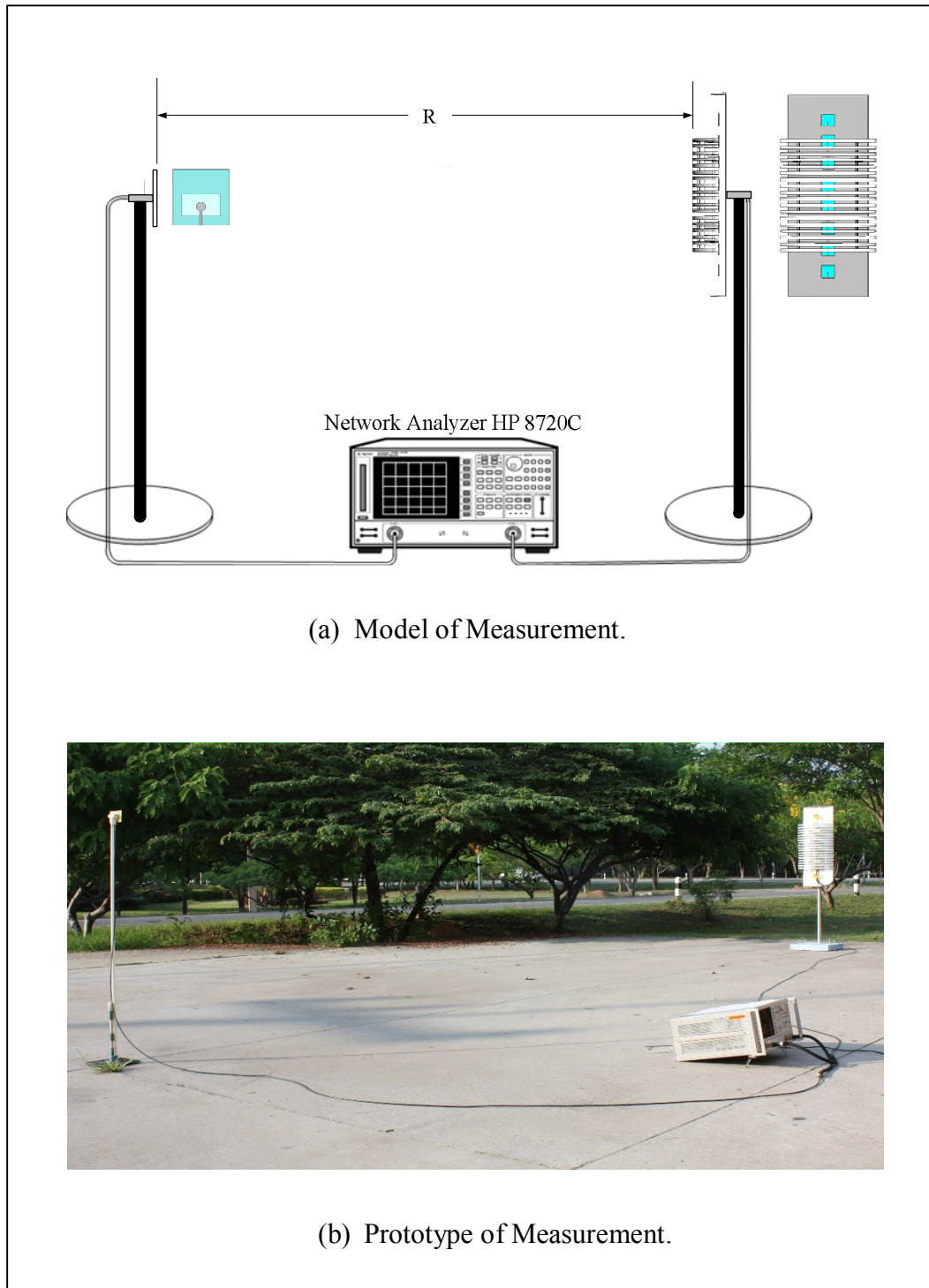


Figure 5.5 Measurement set up for the E-plane radiation pattern.

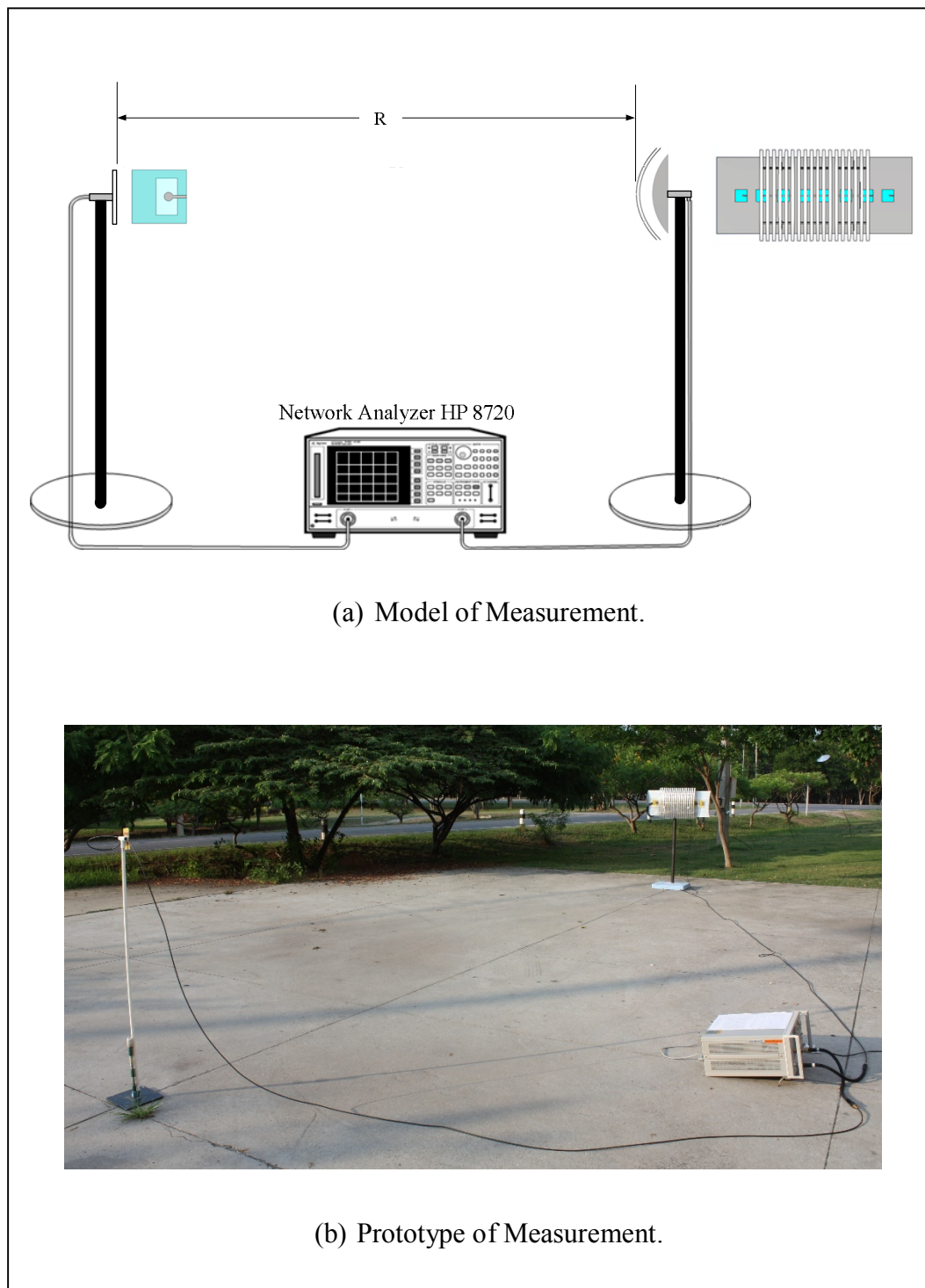


Figure 5.6 Measurement set up for the H-plane radiation pattern.

5.3.2 Gain

The gain of an antenna is the ratio of the radiation intensity, in a given direction, to the radiation intensity that would be obtained if the power accepted by the antenna is radiated isotropically (Balanis, 2005). From the absolute gain method, the theory is based on the Friis transmission formula as expressed in (5.1), which can be applied when two polarizations matched antennas aligned for the maximum directional radiation, and separated by a distance R that meets the far-field criteria, are used for the measurements,

$$G_{r,dB} + G_{t,dB} = P_{r,dB} - P_{t,dB} + 20 \log \left(\frac{4\pi R}{\lambda} \right), \quad (5.1)$$

where P_r is the received power,

P_t is the transmitted power,

G_r is the gain of the receiving antenna,

G_t is the gain of the transmitting antenna.

The absolute gain method requires no a knowledge of the transmitting or receiving antenna gain. If the receiving and transmitting antennas are identical antennas thus only one measurement is required and (5.1) can be simplified as

$$G_{r,dB} = G_{t,dB} = \frac{1}{2} \left[P_{r,dB} - P_{t,dB} + 20 \log \left(\frac{4\pi R}{\lambda} \right) \right]. \quad (5.2)$$

In this research, we consider the transmission line loss or L_t (21.13 dB) and the insertion loss of the power divider or L_i (9.03 dB). Therefore, the gain of this proposed antenna can be determine by

$$G_{r,dB} = P_{r,dB} - P_{i,dB} + 20 \log \left(\frac{4\pi R}{\lambda} \right) - G_{t,dB} - L_{t,dB} - L_{i,dB}. \quad (5.3)$$

5.3.3 Bandwidth

The bandwidth of an antenna is defined as the range of frequencies with in which the performance of the antenna, with respect to some characteristics, conforms to a specified standard. The bandwidth can be considered to be the range of frequencies, on either side of a center frequency, where the antenna characteristics such as input impedance, pattern, beamwidth, polarization, side lobe level, gain, beam direction or radiation efficiency, are within an acceptable value of those at the center frequency (Balanis, 2005).

For this research, the narrowband antenna is presented, the bandwidth is expressed as a percentage of the frequency difference (upper minus lower) over the center frequency of the bandwidth. Equation (5.4) is the fundamental formula to calculate the bandwidth of this proposed antenna from the return loss versus the frequency plot.

$$\text{Bandwidth (\%)} = \left[\frac{(f_{upper} - f_{lower})}{f_0} \right] \times 100\% \quad (5.4)$$

5.3.4 Input Impedance, Standing Wave Ratio and Reflected Power

The input impedance, SWR, and S_{11} are parameters which can be used to indicate the degree of mismatch between transmission line and its load (usually a radio antenna), or evaluate the effectiveness of impedance matching efforts. The input impedance, the impedance presented by an antenna at its terminals at the point, is in the range of 40 - 60 Ω can be accepted for impedance matching between transmission line and the antenna. The SWR, a function of the S_{11} which describes the power reflected from the antenna, is less than 2 can be also accepted for impedance matching which correspond to the S_{11} less than -10 dB.

5.4 Experimental Results

In this research, the operating frequency of this proposed antenna is 2.1 GHz. The measured results of S_{11} , bandwidth, SWR and input impedance are shown in Figure 5.7 to 5.10, respectively. It is found that the measured S_{11} at the operating frequency is -23.075 dB. Impedance matching which is referred to $S_{11} \leq -10$ dB is achieved. The measured impedance bandwidth is 0.407 GHz (1.92 – 2.327 GHz) or about 19.2%. The SWR at the operating frequency is 1.1533 ($SWR \leq 2$). The measured of input impedance of this proposed antenna is 53.082 Ω . The impedance is accepted because it is in the range of 40 - 60 Ω . From Figure 5.11, the measured far-field patterns, shows that this proposed antenna can provide the HPBW in E- and H-planes of 8.7° and 36.8°, respectively. It is correspond to the gain around 20.3 dB. As shown in Figure 5.12 and 5.13, the measured of S_{11} and far-field patterns in E- and H-planes are plotted together with the simulated results which are calculated by using CST software and FDTD and ANN methods. It is observed that the simulation results

of this proposed antenna are in good agreement with those of the measured results.

The measured results of this proposed antenna are summarized in Table 5.3.

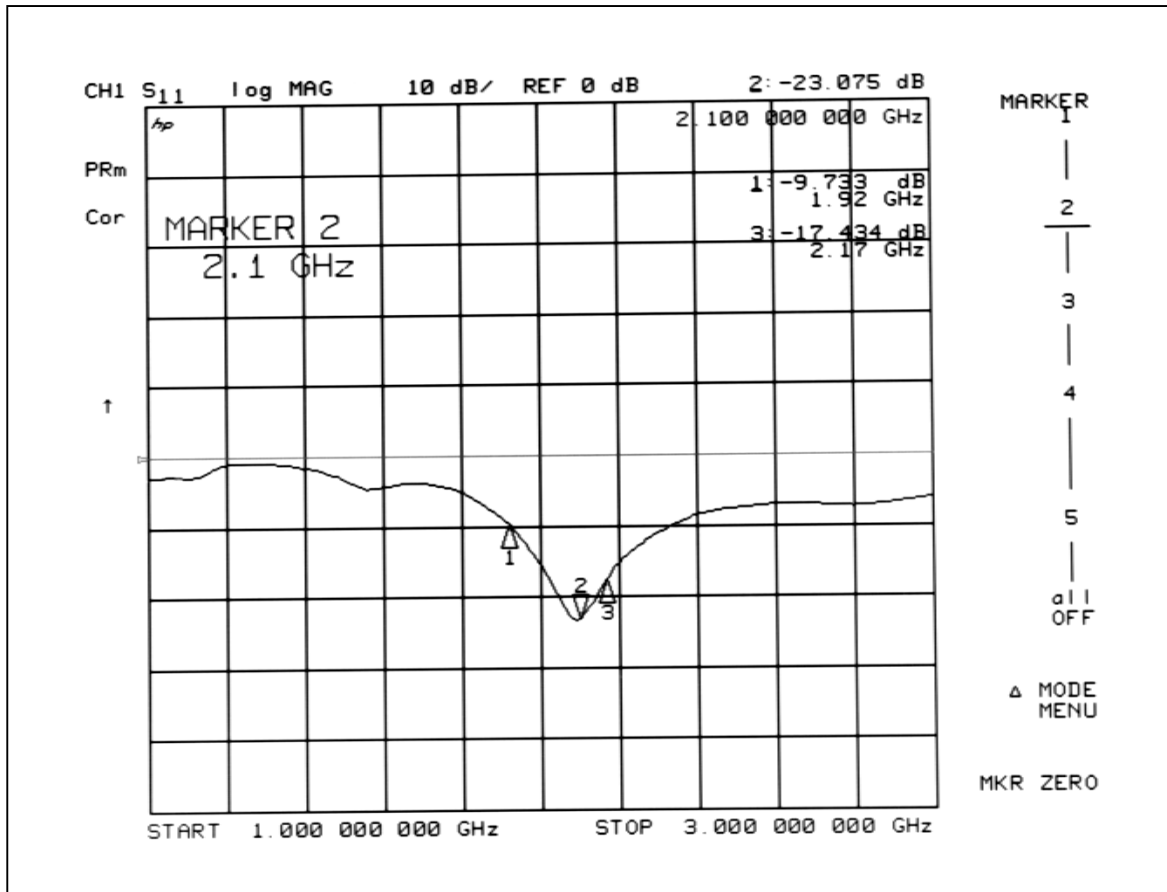


Figure 5.7 Measured reflected power.

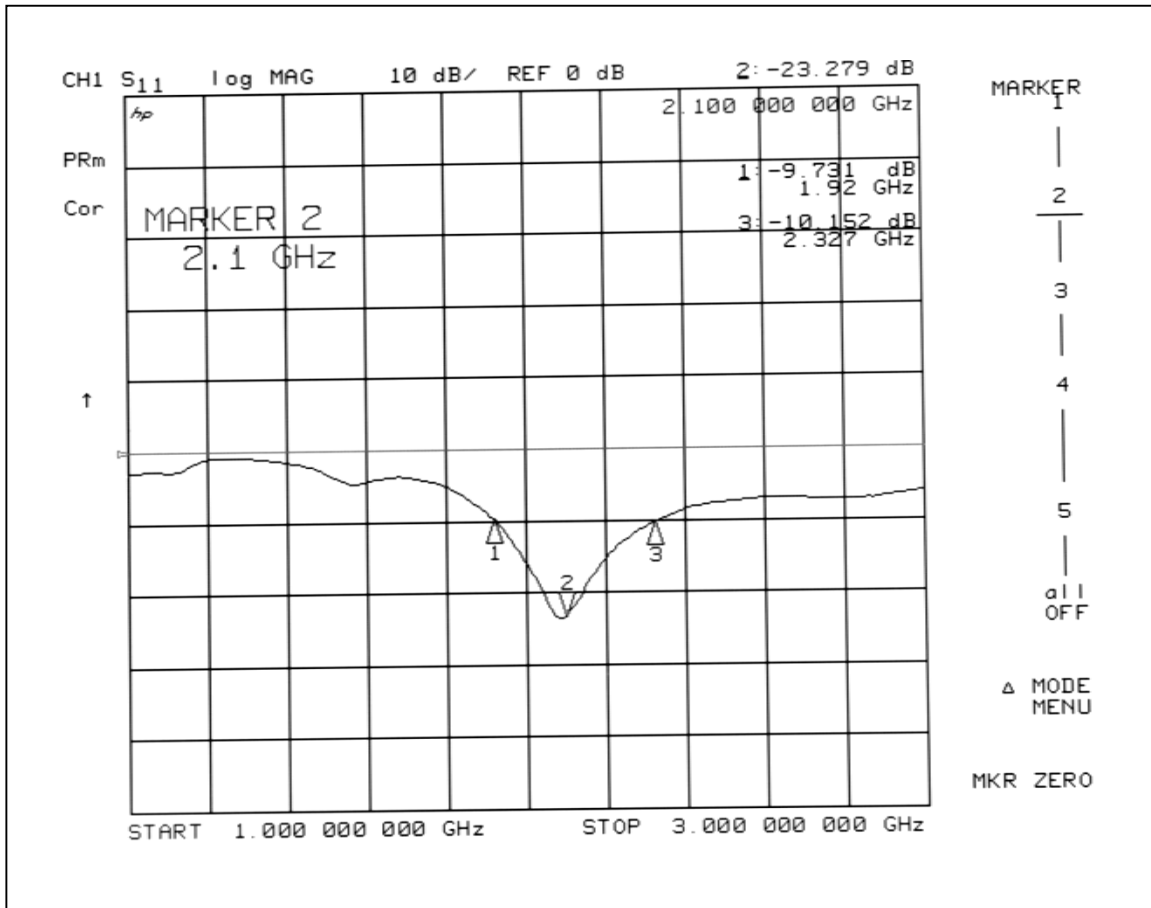


Figure 5.8 Measured bandwidth.

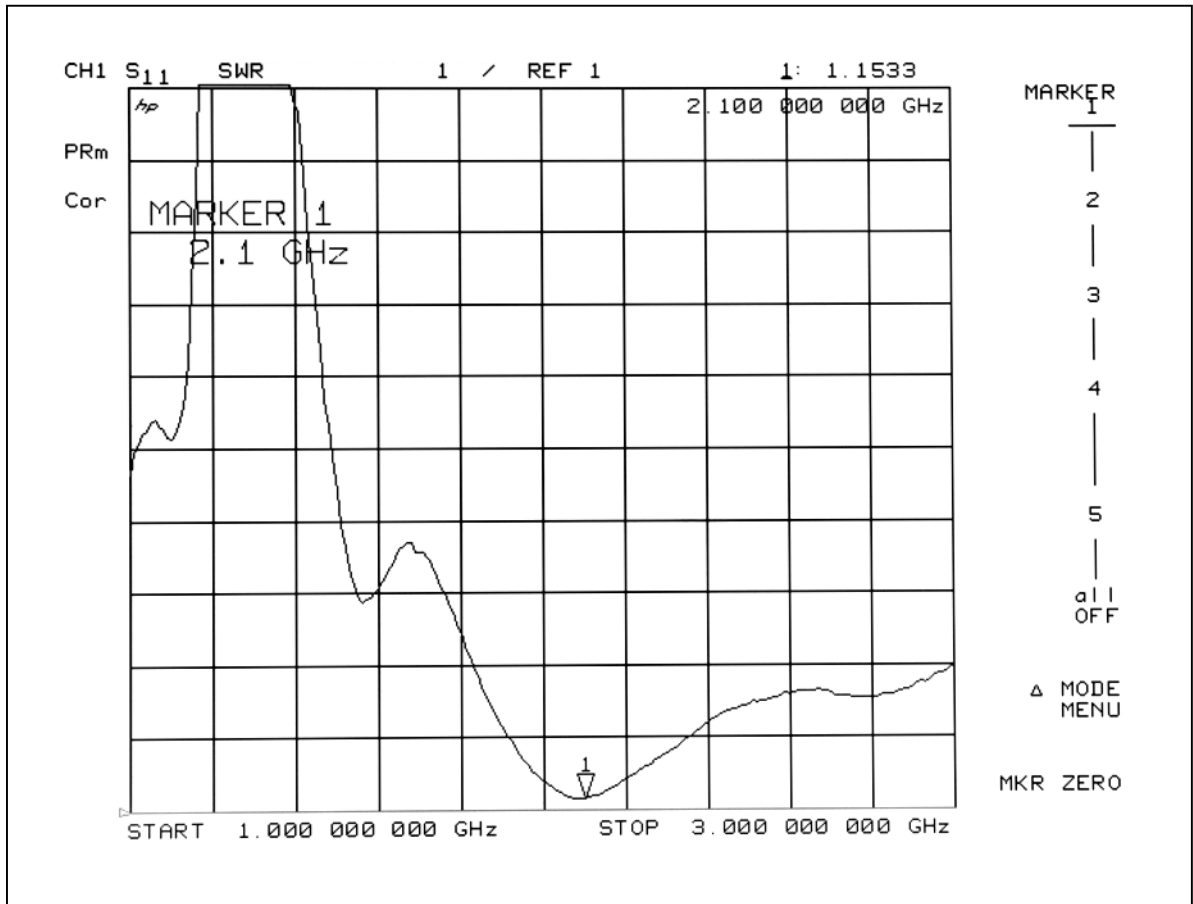


Figure 5.9 Measured standing wave ratio.

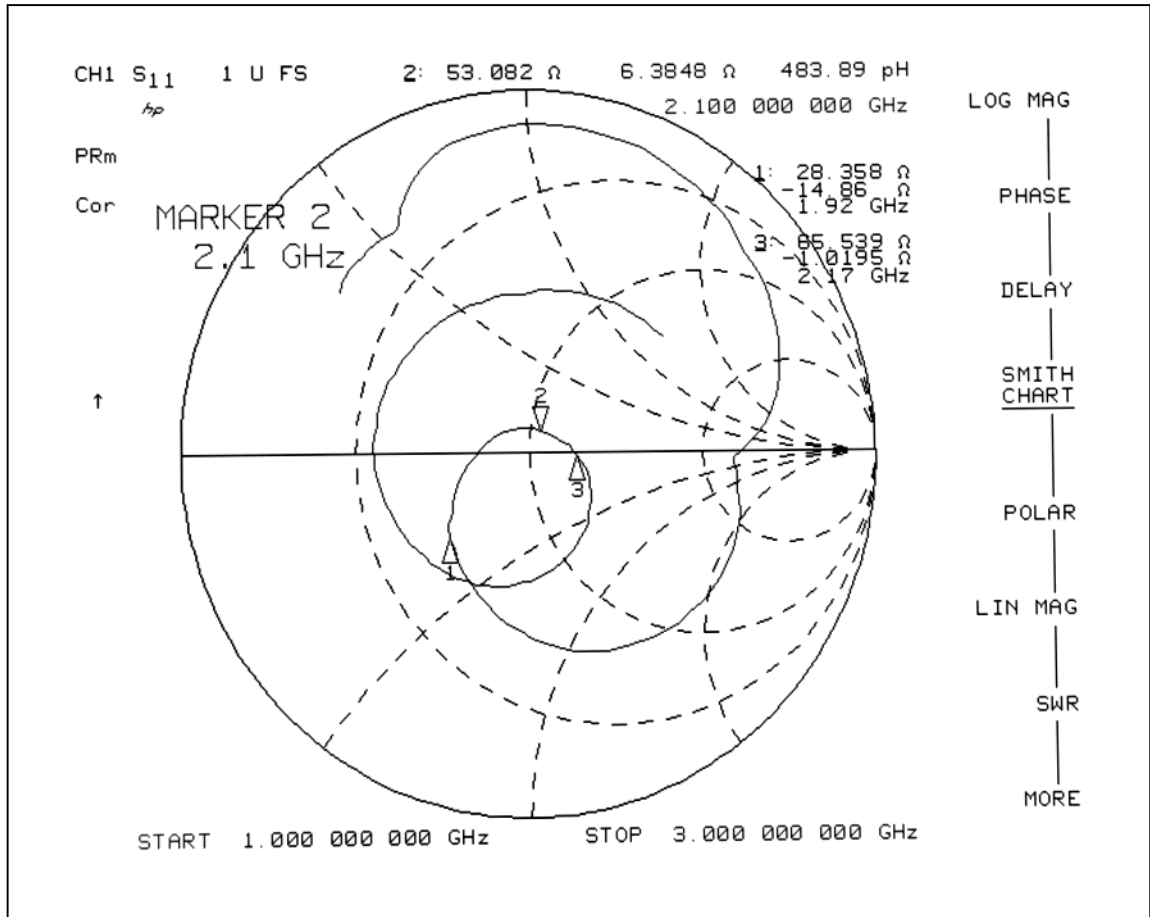


Figure 5.10 Measured impedance.

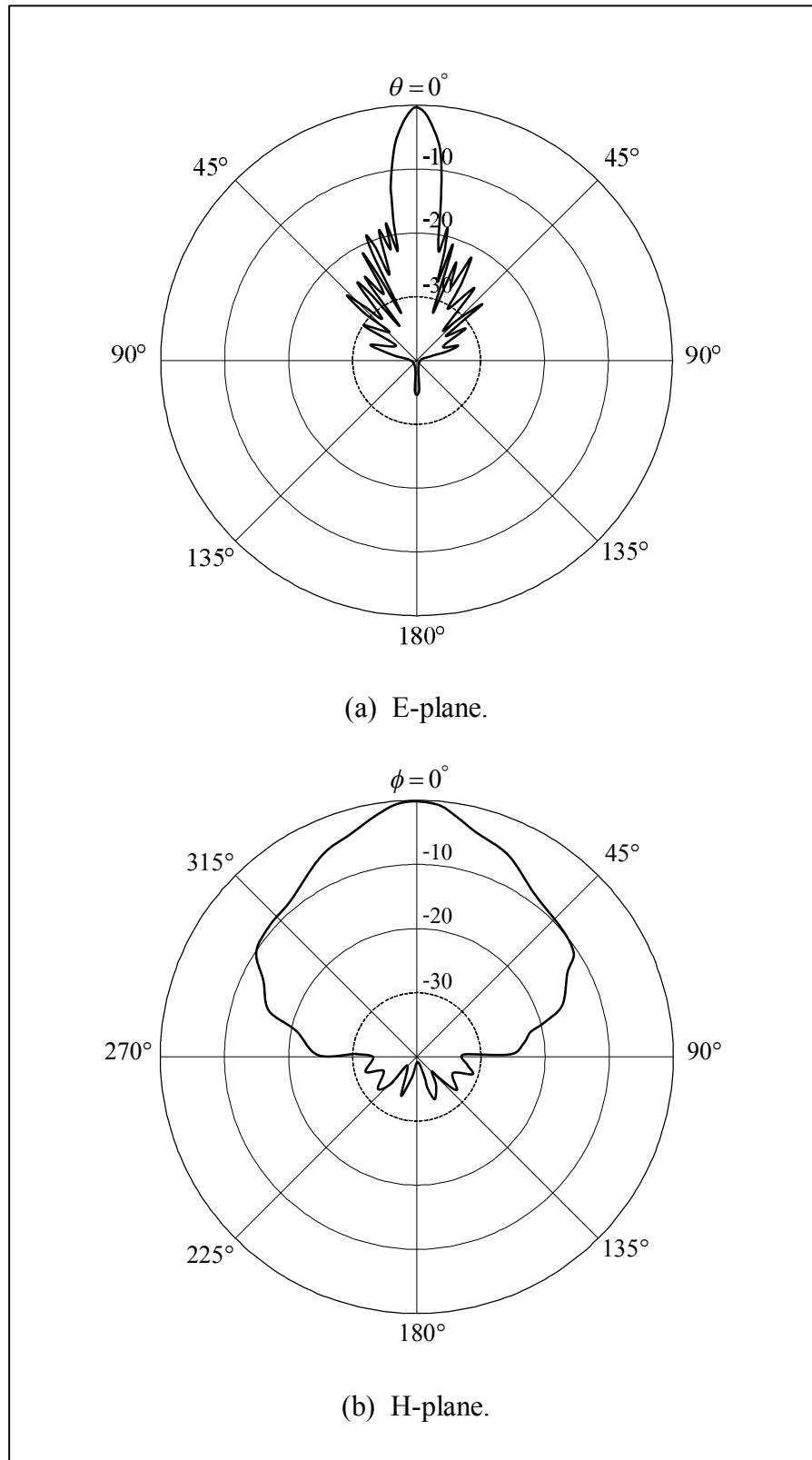


Figure 5.11 Measured radiation patterns.

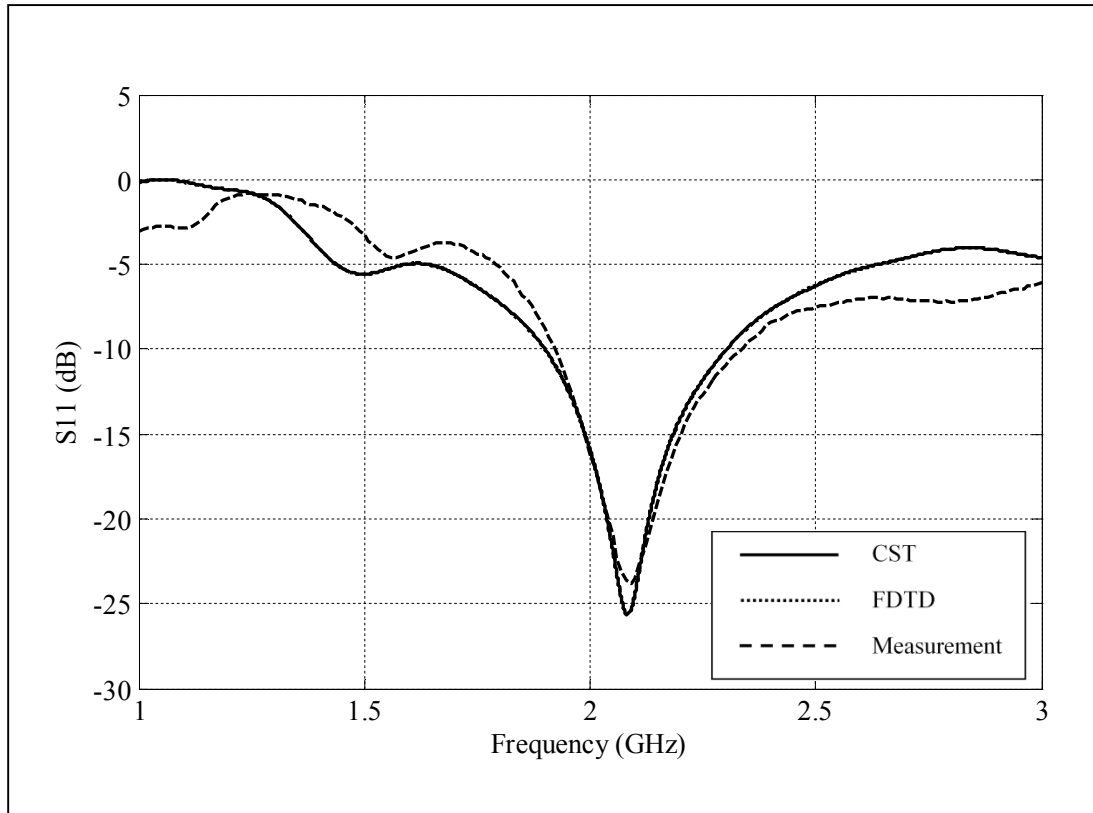


Figure 5.12 The reflected power.

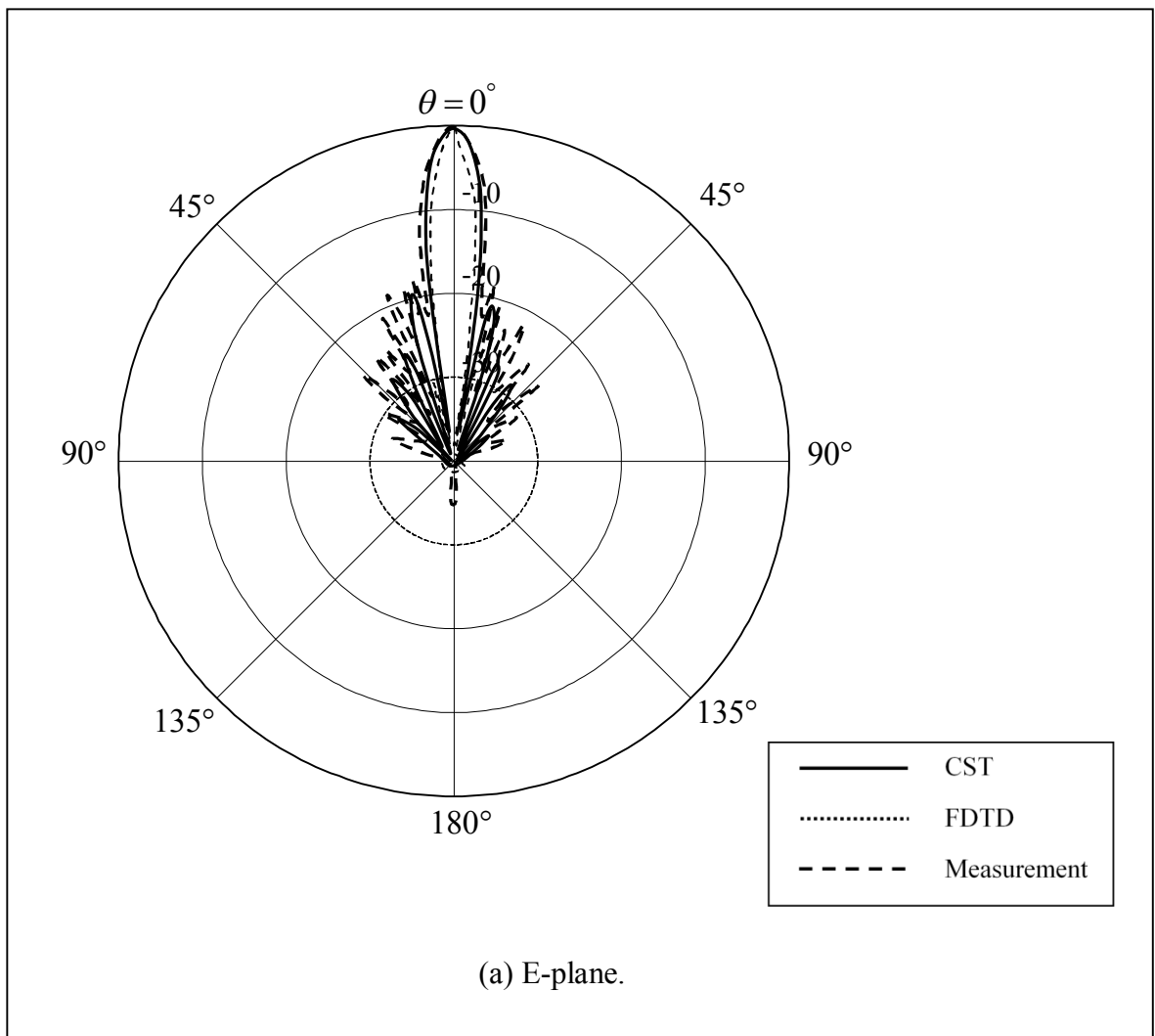


Figure 5.13 The radiation patterns.

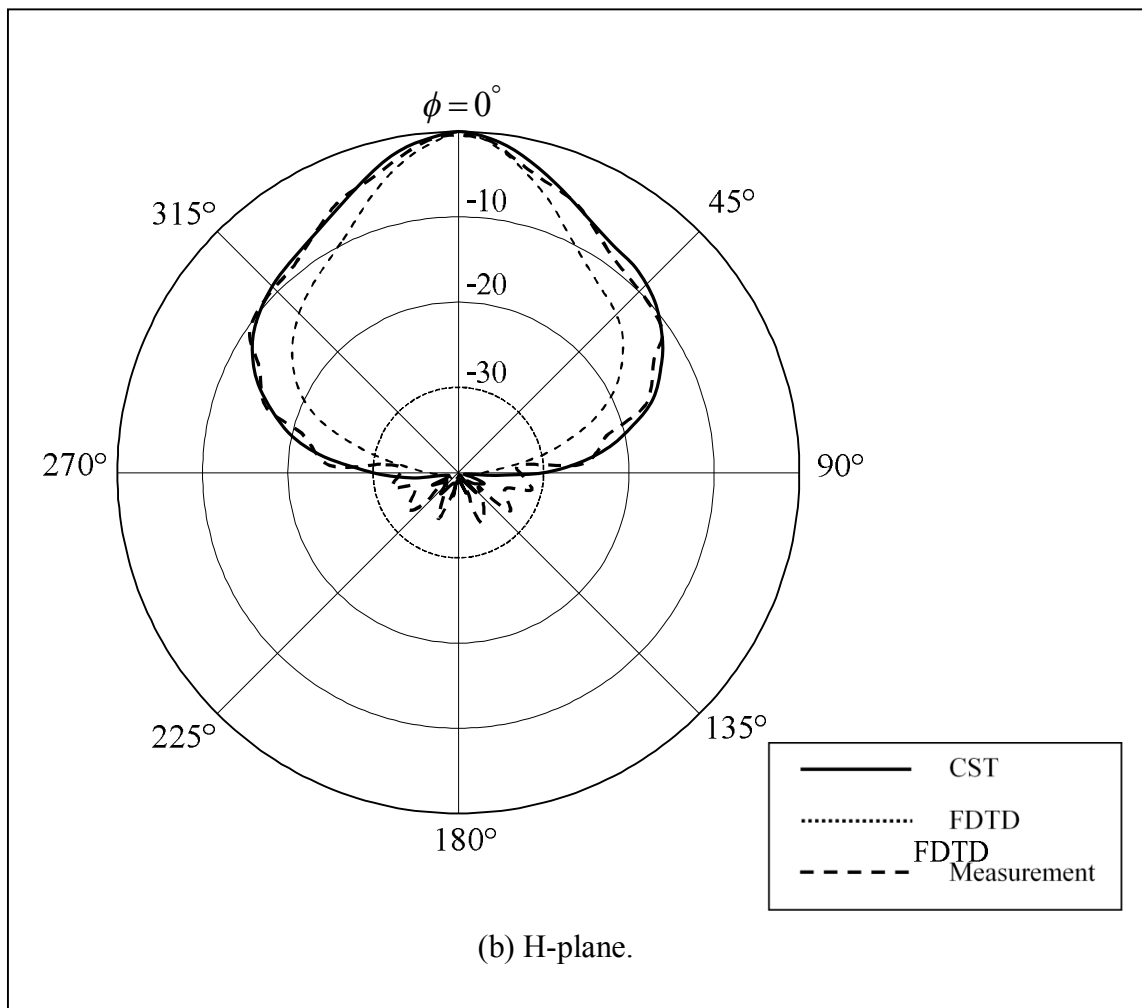


Figure 5.13 The radiation patterns (Continued).

Table 5.3 Comparison of simulated, calculated, and measured results.

Antenna characteristics	Simulated results from CST	Calculated results from FDTD and ANN Methods	Measured results
The reflection coefficient (S_{11})	-24.367 dB	-24.392 dB	-23.075 dB
The bandwidth	19%	19.19%	19.2%
The standing wave ratio (SWR)	1.1496	1.0855	1.1533
The gain	20.84 dB	20.6 dB	20.3 dB
The half power beamwidth (HPBW)(AZ:EL)	37.2:8.7 4.3:1	34.9:6.6 5.3:1	36.8:8.7 4.23:1

5.5 Chapter Summary

This chapter presents the antenna measurements in order to verify the computed results with measurements to ensure that antenna was correctly modeled in the simulations and correctly assembled. A sector antenna prototype for mobile base station was fabricated, by using FR4 (a 1×8 array of microstrip slot antennas), PEC (U-shaped reflector), and alumina rods (curved woodpile EBG structures), and measured radiation patterns in the outdoors. The measured maximum gain at $\theta = 0^\circ$ is around 20.3 dB. Good agreement between computed and measured results is obtained.

CHAPTER VI

CONCLUSIONS

6.1 Thesis Concluding Remarks

In this thesis, analysis of a sector antenna for base station of mobile phone service has been presented. We modified the bidirectional microstrip slot antennas array to be the directional antenna by adding the PEC U-shaped reflector and increasing its gain with new technique, additional curved woodpile EBG structures. The antenna geometry consists of a 1×8 array antenna by using microstrip slot antennas, a U-shaped reflector behind the panel of microstrip slot antennas array, a curved woodpile EBG, and a feed system.

The conventional method for gain increment, a lot of elements will be added in the array, which causes the dimension of antenna too long and its weight too heavy. Moreover, the great number of electromagnetic energy will be lost inside the phasing line. In our study, we found that the proper structure of EBG is capable to enhance the gain of antenna as the additional resonant circuit, exhibit bandgap characteristics at 2.1 GHz, installed at front of the array panel. Furthermore, the EBG structures can be appropriately shaped for reducing the side and back lobes of the directional antenna too. From investigation, the sector of cylindrical woodpile EBG structures is more suitable for the panel of microstrip slot antennas array.

From the results, explicitly, the directive gain of the proposed antenna was increased around 3 dB when such EBG structures were added, while its length of array was not enlarged. The most important technique for this accomplishment that is

the EBG structures must be appropriately designed and calculated, especially the radius of the sectorial cylinder of woodpile EBG structures. The most proper radius of 3.34λ , the distance between a 1×8 array of microstrip slot antennas and curved woodpile EBG structures of 0λ , and the height of curved woodpile EBG of 3.91λ (18 curved filaments/ring) can provide the moderately highest gain of 20.3 dB at the operating frequency of 2.1 GHz.

6.2 Remark for Future Studies

Based on the knowledge learned and acquired over this research, some recommendations for future EBG structures should be presented. In this thesis, the design examples of the curved woodpile EBG structures have applied the similar geometry of the planar and the cylindrical to be the sector of curved woodpile EBG structures. It was found that when we have changed woodpile EBG structures shapes, the antenna characteristics are also changed. In the future study, we can change woodpile EBG structures for variety shapes in order to provide variety of antenna characteristics. In applying the techniques of FDTD method to be conducted to carry out some parameters of antenna, the 2D FDTD in TE mode and the ANN methods are utilized for analyzing of a 1×8 array of microstrip slot antennas with U-shaped reflector and the curved woodpile EBG structures and training model, respectively. From this training model, we obtain the simulation program developed from the FDTD and ANN methods which can be applied to use with the realized problem of microstrip slot antennas array covered with EBG structures.

REFERENCE

- Aberle, J. T. and Pozar, D. M. (1990). Analysis of Infinite Arrays of One- and Two-Probe-Fed Circular Patches. **IEEE Transactions on Antennas and Propagation**. 38(4): 421-432.
- Aberle, J. T. and Zavosh, F. (1994). Analysis of Probe-Fed Circular Microstrip Patches Backed by Circular Cavities. **Electromagnetics**. 14(2): 239-258.
- Agrawal, P. K., and Bailey, M. C. (1977). An Analysis Technique for Microstrip Antenna. **IEEE Transactions on Antennas and Propagation**. 25(6): 756-759.
- Ahmed, I., Chua, E. K., Li, E. P., and Chen, Z. (2008). Development of the Three-Dimensional Unconditionally Stable LOD-FDTD Method. **IEEE Transactions on Antennas and Propagation**. 56(11): 3596-3600.
- Aminian, A. and Rahmat-Samii, Y. (2006). Spectral FDTD: A Novel Technique for the Analysis of Oblique Incident Plane Wave on Periodic Structures. **IEEE Transactions on Antennas and Propagation**. 54(6): 1818-1825.
- Axelrod, A., Kisliuk, M., and Maoz, J. (1989). Broadband Microstrip-Fed Slot Radiator. **Microwave Journal**. 32: 81-94.
- Balanis, C. A. (1989). **Advanced Engineering Electromagnetics**. John Wiley & Sons. New York.
- Balanis, C. A. (1997). **Antenna Theory Analysis and Design**. John Wiley & Sons. New York.

- Balanis, C. A. (2005). **Advanced Engineering Electromagnetic (Third edition)**. John Wiley & Sons. New York.
- Barlevy, A. S. and Rahmat-Samii, Y. (2001). Characterization of Electromagnetic Band-Gap Composed of Multiple Periodic Tripods with Interconnecting Vias: Concept Analysis, and Design. **IEEE Transactions on Antennas and Propagation**. 49(3): 242-353.
- Becache, E., Fauqueux, S., and Joly, P. (2003). Stability of Perfectly Matched Layers, Group Velocities and Anisotropic Waves. **Journal of Computational Physics**. 188(2): 399-433.
- Berenger, J. (1994). A Perfectly Matched Layer for the Absorption of Electromagnetic Waves. **Journal of Computational Physics**. 114(2): 185-200.
- Caloz, C., and Itoh, T. (2005). **Electromagnetic Metamaterials: Transmission Line Theory and Microwave Applications**. Wiley-IEEE Press, New Jersey.
- Chawanonphithak, Y. and Phongcharoenpanich, C. (2007). An Ultra-wideband Circular Microstrip Antenna Fed by Microstrip Line above Wide-Slot Ground Plane. **Proceedings of the 2007 Asia-Pacific Conference on Communications (APCC 2007)**. 99-102.
- Chen, I. F., Peng, C. M. and Liang, S. C. (2005). Single Layer Printed Monopole Antenna for Dual ISM-Band Operation. **IEEE Transactions on Antennas and Propagation**. 53(2): 1270-1273.
- Chew, W. C. and Weedon, W. H. (1994). A 3D Perfectly Matched Medium from Modified Maxwell's Equations with Stretched Coordinates. **Microwave and Optical Technology Letters**. 7(13): 599-604.

- De Assis Fonseca, S. B. and Giarola, A. J. (1984). Microstrip Dish Antennas, Part I: Efficiency of Space Wave Launching. **IEEE Transactions on Antennas and Propagation**. 32(6): 561-567.
- De Assis Fonseca, S. B. and Giarola, A. J. (1984). Microstrip Dish Antennas, Part II: The Problem of Surface Wave Radiation by Dielectric Truncation. **IEEE Transactions on Antennas and Propagation**. 32(6): 568-573.
- Deinega, A. and Valuev, I. (2011). Long-Time Behavior of PML Absorbing Boundaries for Layered Periodic Structures. **Computer Physics Communications**. 182(1): 149-151.
- Elayachi, M., Brachat, P., and Ratajczak, P. (2006). EBG Identification by the Reflection Phase Method (RPM) Design for Application WiFi Antenna. **Proceedings of the first European Conference on Antennas and Propagation (EuCAP 2006)**. 1-5.
- Fan, M. Y., Hu, R., Feng, Z. H., Zhang, X. X., and Hao, Q. (2003). Advance in 2D-EBG Research. **Journal of Infrared and Millimeter Waves**. 22(2).
- Fujimoto, K. and James, J. R. (1994). **Mobile Antenna Systems Handbook**. Artech House Publishers.
- Garg, R., Bhartia, P., Bahl, I., and Ittipipoon, A. (2001). **Mircostrip Antennas Design Handbook**. Artech House Publishers.
- Gedney, S.D. (1996). An Anisotropic Perfectly Matched Layer Absorbing Media for the Truncation of FDTD Lattices. **IEEE Transactions on Antennas and Propagation**. 44(12): 1630-1639.
- Gonzalo, R., de Maagt, P., and Sorolla, M. (1999). Enhanced Path-Antenna Performance by Suppressing Surface Waves using Photonic-Bandgap

- Substrates. **IEEE Transactions on Microwave Theory and Techniques**. 47(11): 2131-2138.
- Hao, Y. (2011). Advanced learning algorithms of neural networks. **Doctoral Dissertation of Auburn University Auburn**. Alabama, USA.
- Hao, Y. and Mittra, R. (2009). **FDTD Modeling of Metamaterials: Theory and Applications**. Artech House Publishers.
- Howell, J. W. (1975). Microstrip Antenna. **IEEE Transactions on Antennas and Propagation**. 23(1): 90-93.
- Huynh, T. and Lee, K. F. (1995). Single-Layer Single-Patch Wide Band Microstrip Antenna. **Electronics Letters**. 31(16): 1310-1312.
- Illuz, Z., Shavit, R., and Bauer, R. (2004). Micro-strip Antenna Phased Array with Electromagnetic Band-Gap Substrate. **IEEE Transactions on Antennas and Propagation**. 52(6):1446-1453.
- James, J. R. and Hall, P. S (1989). **Handbook of Microstrip Antenna**. Peter Peregrinus, London, UK.
- James, J. R., Hall, P. S., and Wood, C. (1981). **Microstrip Antenna Theory and Design**. Peter Peregrinus, London, UK.
- Jensen, M. A. (1994). **Time-Domain Finite-Difference Method in Electromagnetics: Application to Personal Communication**. Ph.D. Dissertation at University of California, Los Angeles.
- Joannopoulos, J. D., Meade, R. D., and Winn, J. N. (1995). **Photonic Crystals: Molding the Flow of Light**. Princeton University Press, New Jersey.
- Katsibas, K. D. (1996). Analysis and Design of Mobile Antennas for Handheld Unit. **Master's Thesis, Arizona State University**. Tempe, Arizona.

- Katsibas, K. D., Balanis, C. A., Tirkas, P. A., and Birtcher, C. R. (1998). Folded Loop Antenna for Mobile Handheld Units. **IEEE Transactions on Antennas and Propagation**. 46(2): 260-266.
- Kumar, G. and Gupta, K. C. (1985). Directly Coupled Multiple Resonator Wide-Band Microstrip Antenna. **IEEE Transactions on Antennas and Propagation**. 33(6): 588-593.
- Lee, Y., Lu, X., Hao, Y., Yang, S., Evans, J. R. G., and Parini, C. G. (2009). Low Profile Directive Millimeter-Wave Antennas using Free Formed Three-Dimensional (3D) Electromagnetic Band Gap Structures. **IEEE Transactions on Antennas and Propagation**. 57(10): 2893-2903.
- Lee, Y., Lu, X., Hao, Y., Yang, S., Evans, J. R. G., and Parini, C. G. (2010). Narrow-Beam Azimuthally Omni-Directional Millimetre-Wave Antenna using Free Formed Cylindrical Woodpile Cavity. **IET Microwaves, Antennas and Propagation**. 4(10): 1491-1499.
- Levenberg, K. (1944). A method for the solution of certain problems in least squares. **Quarterly of Applied Mathematics**. 5: 164–168.
- Llombart, N., Neto, A., Gerini, G., and de Maagt, P. (2005). Planar Circularly Symmetric EBG Structures for Reducing Surface Waves in Printed Antennas. **IEEE Transactions on Antennas and Propagation**. 53(10): 3210-3218.
- Lo, T. K., Ho, C.-O., Hwang, Y., Lam, E. K. W., and Lee, B. (1997). Miniature Aperture Coupled Microstrip Antenna of Very High Permittivity. **Electronics Letters**. 33(1): 9-10.
- Marquardt, D. (1963). An algorithm for least-squares estimation of nonlinear parameters. **SIAM Journal on Applied Mathematics**. 11(2):431–441.

- Ozbay, E., Abeyta, A., Tuttle, G., Tringides, M., Biswas, R., Chan, T., Soukoulis, C.M., and Ho, K. M. (1994). Measurement of a Three-Dimensional Photonic Band Gap in A Crystal Structure Made of Dielectric Rods. **Physical Review B: Condensed Matter and Materials Physics**. 50(3): 1945-1948.
- Phongcharoenpanich, C. and Chawanonphithak, Y. (2007). An Ultra-Wideband Circular Microstrip Antenna with Tuning Stub Fed by Microstrip Line above Wide-Slot Ground Plane. **Proceedings of the 2007 International Symposium on Antennas and Propagation (ISAP 2007)**. 33-36.
- Pozar, D. M. (1985). Microstrip Antenna Aperture-Coupled to a Microstrip line. **Electronics Letters**. 21(2): 49-50.
- Pozar, D. M. and Kaufman, B. (1987). Increasing the Bandwidth of a Microstrip Antenna by Proximity Coupling. **Electronics Letters**. 23(8): 368-369.
- Qu, D., Shafai, L., and Foroozesh, A. (2006). Improving Microstrip Patch Antenna Performance using EBG Substrates. **IEE Proceedings Microwaves, Antennas and Propagation**. 153(6): 558-563.
- Radisic, V., Qian, Y., Coccioli, R., and Itoh, T. (1998). Novel 2-D Photonic Bandgap Structure for Microstrip Lines. **IEEE Microwave and Guided Wave Letters**. 8(2): 69-71.
- Rahman, M. and Stuchly, M. A. (2001). Transmission Line – Periodic Circuit Representation of Planar Microwave Photonic Bandgap Structures. **Microwave and Optical Technology Letters**. 30(1): 15-19.
- Ramahi, O. M. (1997). The Complementary Operators Method in FDTD Simulations. **IEEE Antennas and Propagation Magazine**. 39(6): 33-45.

- Richards, W. F. and Lo, Y. T. (1983). Theoretical and Experimental Investigation of a Microstrip Radiator with Multiple Lumped Linear Loads. **Electromagnetics**. 3(3-4): 371-385.
- Richards, W. F. and Long, S. A. (1986). Adaptive Pattern Control of a Reactively Loads, Dual-Mode Microstrip Antenna. **Proceedings International Telemetry Conference**. 291-296.
- Richards, W. F., Lo, Y. T., and Harrison, D. D. (1981). An Improved Theory of Microstrip Antennas with Applications. **IEEE Transactions on Antennas and Propagation**. 29(1): 38-46.
- Rumelhart, D. E., McClelland, J. L. (1986). **Parallel distributed processing: Explorations in the microstructure of cognition. Volume I**. Cambridge. MA, MIT Press.
- Sievenpiper, D. (1999). **High-Impedance Electromagnetic Surfaces**. Ph.D. Dissertation at University of California, Los Angeles.
- Sievenpiper, D., Zhang, L., Broas, R. F. J., Alexopolus, N. G., and Yablonovitch, E. (1999). High-Impedance Electromagnetic Surfaces with a Forbidden Frequency Band. **IEEE Transactions on Microwave Theory and Techniques**. 47(11): 2059-2074.
- Taflove, A. and Hagness, S. C. (2005). **Computational Electrodynamics: The Finite-Difference Time-Domain Method**. Artech House Publishers.
- Taguchi, M., Egashira, S., and Tanaka, K. (1991). Sleeve Antenna with Ground Wires. **IEEE Transactions on Antennas and Propagation**. 39(1): 1-7.
- Tan, M. N. Md., Rahman, T. A., Rahim, S. K. A., Ali, M. T., and Jamlos, M. F. (2010). Antenna Array Enhancement using Mushroom-Like Electromagnetic

- Band Gap (EBG). **Proceedings of the fourth European Conference on Antennas and Propagation (EuCAP 2010)**. 1-5.
- Teixeira, F. L. and Chew, W. C. (1998). General Closed-Form PML Constitutive Tensors to Match Arbitrary Bianisotropic and Dispersive Linear Media. **IEEE Microwave and Guided Wave Letters**. 8(6): 223-225.
- Weily, A. R., Horvath, L., Esselle, K. P., Sanders, B. C., and Bird, T. S. (2005). A Planar Resonator Antenna Base on a Woodpile EBG Material. **IEEE Transactions on Antennas and Propagation**. 53(1): 216-223.
- Yang, F. and Rahmat-Samii, Y. (2001). Mutual Coupling Reduction of Microstrip Antennas using Electromagnetic Band-Gap Structure. **Proceedings IEEE AP-S International Symposium**. 2: 478-481.
- Yang, F. and Rahmat-Samii, Y. (2001). Step-Like Structure and EBG Structure to Improve the Performance of Patch Antennas on High Dielectric Substrate. **Proceedings IEEE AP-S International Symposium**. 2: 482-485.
- Yang, F. and Rahmat-Samii, Y. (2003). Microstrip Antennas Integrated with Electromagnetic Band-Gap (EBG) Structures: A Low Mutual Coupling Design for Array Applications. **IEEE Transactions on Antennas and Propagation**. 51(10): 2936-2946.
- Yang, F. and Rahmat-Samii, Y. (2009). **Electromagnetic Band Gap Structure in Antenna Engineering**. Cambridge University Press, New York.
- Yang, F., Ma, K., Qian, Y., and Itoh, T. (1999). A Uniplanar Compact Photonic-Bandgap (UC-PBG) Structure and Its Applications for Microwave Circuit. **IEEE Transactions on Microwave Theory and Techniques**. 47(8): 1509-1514.

- Yang, F., Zhang, X., Ye, X., and Rahmat-Samii, Y. (2001). Wide Band E-shaped Patch Antennas for Wireless Communications. **IEEE Transactions on Antennas and Propagation**. 49(7): 1094-1100.
- Yee, K. (1966). Numerical Solution of Initial Boundary Value Problems Involving Maxwell's Equations in Isotropic Media. **IEEE Transactions on Antennas and Propagation**. 14(3): 302-307.
- Yoshimura, Y. (1972). A Microstrip Line Slot Antenna. **IEEE Transactions on Microwave Theory and Techniques**. 20(11): 760-762.
- Zhen, F., Chen, Z., and Zhang, J. (2000). Toward the Development of a Three-Dimensional Unconditionally Stable Finite-Difference Time-Domain Method. **IEEE Transactions on Microwave Theory and Techniques**. 48(9): 1550-1558.

APPENDIX A

THE FDTD CODE

```

function varargout = MSTSIM(varargin)
% MSTSIM MATLAB code for MSTSIM.fig
%     MSTSIM, by itself, creates a new MSTSIM or raises the existing
%     singleton*.
%
%     H = MSTSIM returns the handle to a new MSTSIM or the handle to
%     the existing singleton*.
%
%     MSTSIM('CALLBACK',hObject,eventData,handles,...) calls the local
%     function named CALLBACK in MSTSIM.M with the given input arguments.
%
%     MSTSIM('Property','Value',...) creates a new MSTSIM or raises the
%     existing singleton*. Starting from the left, property value pairs
are
%     applied to the GUI before MSTSIM_OpeningFcn gets called. An
%     unrecognized property name or invalid value makes property
application
%     stop. All inputs are passed to MSTSIM_OpeningFcn via varargin.
%
%     *See GUI Options on GUIDE's Tools menu. Choose "GUI allows only one
%     instance to run (singleton)".
%
% See also: GUIDE, GUIDATA, GUIHANDLES

% Edit the above text to modify the response to help MSTSIM

% Last Modified by GUIDE v2.5 26-Jul-2014 08:36:05

% Begin initialization code - DO NOT EDIT
gui_Singleton = 1;
gui_State = struct('gui_Name',       mfilename, ...
                  'gui_Singleton',   gui_Singleton, ...
                  'gui_OpeningFcn', @MSTSIM_OpeningFcn, ...
                  'gui_OutputFcn',  @MSTSIM_OutputFcn, ...
                  'gui_LayoutFcn',   [] , ...
                  'gui_Callback',    []);
if nargin && ischar(varargin{1})
    gui_State.gui_Callback = str2func(varargin{1});
end

if nargout
    [varargout{1:nargout}] = gui_mainfcn(gui_State, varargin{:});
else
    gui_mainfcn(gui_State, varargin{:});
end
% End initialization code - DO NOT EDIT

% --- Executes just before MSTSIM is made visible.
function MSTSIM_OpeningFcn(hObject, eventdata, handles, varargin)
% This function has no output args, see OutputFcn.
% hObject    handle to figure
% eventdata  reserved - to be defined in a future version of MATLAB
% handles    structure with handles and user data (see GUIDATA)
% varargin   command line arguments to MSTSIM (see VARARGIN)

% Choose default command line output for MSTSIM
handles.output = hObject;

```

```

% Update handles structure
guidata(hObject, handles);

% UIWAIT makes MSTSIM wait for user response (see UIRESUME)
% uiwait(handles.figure1);

% --- Outputs from this function are returned to the command line.
function varargout = MSTSIM_OutputFcn(hObject, eventdata, handles)
% varargout cell array for returning output args (see VARARGOUT);
% hObject handle to figure
% eventdata reserved - to be defined in a future version of MATLAB
% handles structure with handles and user data (see GUIDATA)

% Get default command line output from handles structure
varargout{1} = handles.output;

function txtInit_Callback(hObject, eventdata, handles)
% hObject handle to txtInit (see GCBO)
% eventdata reserved - to be defined in a future version of MATLAB
% handles structure with handles and user data (see GUIDATA)

% Hints: get(hObject,'String') returns contents of txtInit as text
% str2double(get(hObject,'String')) returns contents of txtInit as a
double

% --- Executes during object creation, after setting all properties.
function txtInit_CreateFcn(hObject, eventdata, handles)
% hObject handle to txtInit (see GCBO)
% eventdata reserved - to be defined in a future version of MATLAB
% handles empty - handles not created until after all CreateFcns called

% Hint: edit controls usually have a white background on Windows.
% See ISPC and COMPUTER.
if ispc && isequal(get(hObject,'BackgroundColor'),
get(0,'defaultUiControlBackgroundColor'))
set(hObject,'BackgroundColor','white');
end

function txtFinish_Callback(hObject, eventdata, handles)
% hObject handle to txtFinish (see GCBO)
% eventdata reserved - to be defined in a future version of MATLAB
% handles structure with handles and user data (see GUIDATA)

% Hints: get(hObject,'String') returns contents of txtFinish as text
% str2double(get(hObject,'String')) returns contents of txtFinish as
a double

% --- Executes during object creation, after setting all properties.
function txtFinish_CreateFcn(hObject, eventdata, handles)
% hObject handle to txtFinish (see GCBO)
% eventdata reserved - to be defined in a future version of MATLAB
% handles empty - handles not created until after all CreateFcns called

% Hint: edit controls usually have a white background on Windows.
% See ISPC and COMPUTER.
if ispc && isequal(get(hObject,'BackgroundColor'),
get(0,'defaultUiControlBackgroundColor'))

```



```

        set(hObject,'BackgroundColor','white');
    end

%function S11=simS11(Init,Finish,handles)

%function BW=simBandWidth()

% --- Executes on button press in btnProcess.
function btnProcess_Callback(hObject, eventdata, handles)
% hObject    handle to btnProcess (see GCBO)
% eventdata  reserved - to be defined in a future version of MATLAB
% handles    structure with handles and user data (see GUIDATA)

clc;
%clear all;
tic;
disp ('Simulation Microstrip Array!');
%axes(handles.progress);
h=waitbar(0,'Please wait..');
set(h, 'Position', [10,300,300,50]);

A=zeros(3601,2);
A(:,2)=0:0.1:360;

HCPs=3.21;

M=zeros(10001,3);
x=1:0.0002:3;
M(:,1)=1000;
M(:,2)=x';

Init = get(handles.txtInit,'String');
Finish = get(handles.txtFinish,'String');

p=str2num(Init);
n=str2num(Finish);

axes(handles.axesS11);
diffR=n-p+1;

step=0;

set(handles.btnProcess,'Enable','off')
set(handles.btnClose,'Enable','off') ;

for i = p:1:n
    %*****Start of S11*****
    M(:,1)=i;
    load('MODEL_S11.mat');
    out=sim(net,M(:,1:2)');
    gamma=out(5501);
    vswr=abs((1+abs(gamma))/(1-abs(gamma)));
    axes(handles.axesS11);
    plot(M(:,2),out,'r');
    grid on;

```

```

t=strcat('S11 at time step :',' : ',int2str(i),' Step');

set(handles.lblS11,'String',t);
%title(t);
%ylabel('db');
%xlabel('frequency');
set(handles.txtVSWR,'String',num2str(vswr));
set(handles.txtS11,'String',gamma);

flag=false;
initB=0;
fnsB=0;

for j=1:1:10001
    if (flag==false)
        if(out(j)<=-10)
            initB=M(j,2);
            flag=true;
        end
    end

    if (flag==true)
        if(out(j)>=-10)
            fnsB=M(j,2);
            flag=false;
            break;
        end
    end
end
fmid=(initB+fnsB)/2;
bw=(abs(initB-fnsB)/fmid)*100;

set(handles.txtBandwidth,'String',bw);
%*****End*****
%*****Start E Field*****
A(:,1)=i;
load('MODEL_E.mat');
outE=sim(net,A(:,1:2)');
%theta=A(:,2)*pi/180;

axes(handles.axesE);
polar(A(:,2)*pi/180,abs(outE),'g');
view([90 -90]);

%*****Lope left*****
try
    dyE=diff(outE);
    flag=false;

    indexE=0;
    for j=1:500
        if flag==false
            if dyE(j)>0
                flag=true;
            end
        else
            if dyE(j)<0
                indexE=j;
                break;
            end
        end
    end
end

```

```

        end
    end
    sidelopeE=outE(indexE-1)-max(outE);
    set(handles.txtSSLE,'String',sidelopeE);
    catch

end

%*****Start Electric HBW*****
%%%%%%%%%%%%%%%%%%%%%%%%%%%%%%%%%%%%%%%%%%%%%%%%%%%%%%%%%%%%%%%%%%%%%%%%Left Angle%%%%%%%%%%%%%%%%%%%%%%%%%%%%%%%%%%%%%%%%%%%%%%%%%%%%%%%%%%%%%%%%%%%%%%%%
try
    maxOutE=max(outE);
    dbHBWE=maxOutE-3;
    db1=maxOutE;
    db2=0;
    theta=A(:,2)';
    theta1=theta(1);
    theta2=0;
    thetaHBWE1=0;

    outE1=abs(outE');

    for j=2:500

        if(outE1(j)<dbHBWE)
            theta2=theta(j);
            db2=outE1(j);
            m=(theta2-theta1)/(db2-db1);
            thetaHBWE1=(m*(dbHBWE-db1)+theta1);
            break;
        else
            theta1=theta(j);
            db1=outE1(j);
        end

    end

end
catch

end

%set(handles.txtHBWE,'String',thetaHBWE1);

%%%%%%%%%%%%%%%%%%%%%%%%%%%%%%%%%%%%%%%%%%%%%%%%%%%%%%%%%%%%%%%%%%%%%%%%Right Angle%%%%%%%%%%%%%%%%%%%%%%%%%%%%%%%%%%%%%%%%%%%%%%%%%%%%%%%%%%%%%%%%%%%%%%%%
try
    outE1=outE(3101:1:3601);
    outE1=fliplr(outE1);
    maxOutE=max(outE);
    dbHBWE=maxOutE-3;
    db1=maxOutE;
    db2=0;

    theta=A(:,2)';
    theta=theta(3101:1:3601);
    theta=fliplr(theta);

    %theta=A(:,2)';
    theta1=theta(1);
    theta2=0;

```

```

thetaHBWE2=0;

outE1=abs(outE');

for j=2:500

    if(outE1(j)<dbHBWE)
        theta2=theta(j);
        db2=outE1(j);
        m=(theta2-theta1)/(db2-dbl);
        thetaHBWE2=360-(m*(dbHBWE-dbl)+theta1);
        break;
    else
        theta1=theta(j);
        dbl=outE1(j);
    end

end

set(handles.txtHBWE,'String',thetaHBWE2+thetaHBWE1);
%set(handles.txtHBWE,'String',thetaHBWE1);
catch

end;

%*****End E Field*****

%*****Start Magnetic Field*****
load('MODEL_H.mat');
%load('MODEL_HV2.mat');
outH=sim(net,A(:,1:2));

axes(handles.axesH);
polar(A(:,2)*pi/180,abs(outH),'b');
view([90 -90]);

for k=1:1:3601
    if((k/10)>90&&(k/10)<270)

        outH(k)=outH(k)*10-HCPs;
    end
end

    % polar(A(:,2)*pi/180,abs(outH),'b');

%*****Side Lope HPlane*****
%try
dyH=diff(outH);
flag=false;

indexH=2;
for j=50:1500
    if flag==false
        if dyH(j)>0

            flag=true;

```

```

        end
    else
        if dyH(j)<0
            indexH=j;
            if (abs((outH(indexH)-outH(indexH-1)))>=5)
                break;
            end
        end

        end
    end
    end
    sidelopeH=outH(indexH-1)-max(outH);
    set(handles.txtSSLH,'String',sidelopeH);
% catch

%end;

%*****Start Magnetic HBW*****
%*****Left Angle*****
try
    maxOutH=max(outH);
    dbHBWH=maxOutH-3;
    db1=maxOutH;
    db2=0;
    theta=A(:,2)';
    theta1=theta(1);
    theta2=0;
    thetaHBWH1=0;

    outH1=abs(outH');

    for j=2:1000

        if(outH1(j)<dbHBWH)
            theta2=theta(j);
            db2=outE1(j);
            m=(theta2-theta1)/(db2-db1);
            thetaHBWH1=(m*(dbHBWH-db1)+theta1);
            break;
        else
            theta1=theta(j);
            db1=outH1(j);
        end

    end

    end
catch

end;
%set(handles.txtHBWH,'String',thetaHBWH1);
%*****Right Angle*****
try
    outH1=outH(3101:1:3601);
    outH1=fliplr(outH1);
    maxOutH=max(outH);
    dbHBWH=maxOutH-3;
    db1=maxOutH;
    db2=0;

```

```

theta=A(:,2)';
theta=theta(3101:1:3601);
theta=fliplr(theta);

%theta=A(:,2)';
theta1=theta(1);
theta2=0;
thetaHBWH2=0;

outH1=abs(outH');

for j=2:500

    if(outH1(j)<dbHBWH)
        theta2=theta(j);
        db2=outH1(j);
        m=(theta2-theta1)/(db2-dbl);
        thetaHBWH2=360-(m*(dbHBWH-dbl)+theta1);
        break;
    else
        theta1=theta(j);
        db1=outH1(j);
    end

end

set(handles.txtHBWH,'String',thetaHBWH2+thetaHBWH1);
catch

end;

%*****End Magnetic HBW*****

%*****End Magnetic Field*****

pause(0.0005);
step=step+1;
waitbar(step/diffR);
% pause(0.001);

end
close(h);
toc;

set(handles.btnProcess,'Enable','on')
set(handles.btnClose,'Enable','on') ;

vchkE = get(handles.chkDisplayE, 'Value');
vchkH = get(handles.chkDisplayH, 'Value');
vchkExport = get(handles.chkExport, 'Value');
%chkExport
if(vchkE==1)
    Finish = get(handles.txtFinish,'String');
    n=str2num(Finish);
    A(:,1)=n;
    load('MODEL_E.mat');
    outE=sim(net,A(:,1:2)');

```



```

maxTargetE=28.7376152; %Parameter EMax before normalize using for
convert to origin data
ME=zeros(3601,2);
ME(:,1)=0:0.1:360;
A(:,1)=n;
load('MODEL_E.mat');
outE=sim(net,A(:,1:2)');

ME(:,2)=outE';

%cla;

%polar(A(:,2)*pi/180,abs(outE'),'r');
%hold on;
%theta=E(:,2)*pi/180;
%polar(theta,abs(TE),'g');
%view([90 -90]);

%%%%%%%%%%%%%%%%%%%%%%%%%%%%%%%%%%%%%%%%%%%%%%%%%%%%%%%%%%%%%%%%%%%%%%%%%Start H Value%%%%%%%%%%%%%%%%%%%%%%%%%%%%%%%%%%%%%%%%%%%%%%%%%%%%%%%%%%%%%%%%%%%%%%%%%
maxTargetH=45.841833472000005;%Parameter HMax before normalize using
for convert to origin data
MH=zeros(3601,2);
MH(:,1)=0:0.1:360;
A(:,1)=n;
load('MODEL_H.mat');
outH=sim(net,A(:,1:2)');

for k=1:1:3601
    if((k/10)>90&&(k/10)<270)
        outH(k)=outH(k)*maxTargetH;
    end
end
MH(:,2)=outH';

%%%%%%%%%%%%%%%%%%%%%%%%%%%%%%%%%%%%%%%%%%%%%%%%%%%%%%%%%%%%%%%%%%%%%%%%%Start Export to excel %%%%%%%%%%%%%%%%%%%%%%%%%%%%%%%%%%%%%%%%%%%%%%%%%%%%%%%%%%%%%%%%%%%%%%%%%%
filename = 'S11Data.xlsx';
xlswrite(filename,M(:,2:3),1);

filename = 'Electric.xlsx';
xlswrite(filename,ME,1);

filename = 'Magnetic.xlsx';
xlswrite(filename,MH,1);
end

function txtVSWR_Callback(hObject, eventdata, handles)
% hObject    handle to txtVSWR (see GCBO)
% eventdata  reserved - to be defined in a future version of MATLAB
% handles    structure with handles and user data (see GUIDATA)

% Hints: get(hObject,'String') returns contents of txtVSWR as text
%        str2double(get(hObject,'String')) returns contents of txtVSWR as a
double

% --- Executes during object creation, after setting all properties.

```



```

function txtVSWR_CreateFcn(hObject, eventdata, handles)
% hObject    handle to txtVSWR (see GCBO)
% eventdata  reserved - to be defined in a future version of MATLAB
% handles    empty - handles not created until after all CreateFcns called

% Hint: edit controls usually have a white background on Windows.
%         See ISPC and COMPUTER.
if ispc && isequal(get(hObject,'BackgroundColor'),
get(0,'defaultUicontrolBackgroundColor'))
    set(hObject,'BackgroundColor','white');
end

function txtBandwidth_Callback(hObject, eventdata, handles)
% hObject    handle to txtBandwidth (see GCBO)
% eventdata  reserved - to be defined in a future version of MATLAB
% handles    structure with handles and user data (see GUIDATA)

% Hints: get(hObject,'String') returns contents of txtBandwidth as text
%         str2double(get(hObject,'String')) returns contents of txtBandwidth
as a double

% --- Executes during object creation, after setting all properties.
function txtBandwidth_CreateFcn(hObject, eventdata, handles)
% hObject    handle to txtBandwidth (see GCBO)
% eventdata  reserved - to be defined in a future version of MATLAB
% handles    empty - handles not created until after all CreateFcns called

% Hint: edit controls usually have a white background on Windows.
%         See ISPC and COMPUTER.
if ispc && isequal(get(hObject,'BackgroundColor'),
get(0,'defaultUicontrolBackgroundColor'))
    set(hObject,'BackgroundColor','white');
end

function txtSSLE_Callback(hObject, eventdata, handles)
% hObject    handle to txtSSLE (see GCBO)
% eventdata  reserved - to be defined in a future version of MATLAB
% handles    structure with handles and user data (see GUIDATA)

% Hints: get(hObject,'String') returns contents of txtSSLE as text
%         str2double(get(hObject,'String')) returns contents of txtSSLE as a
double

% --- Executes during object creation, after setting all properties.
function txtSSLE_CreateFcn(hObject, eventdata, handles)
% hObject    handle to txtSSLE (see GCBO)
% eventdata  reserved - to be defined in a future version of MATLAB
% handles    empty - handles not created until after all CreateFcns called

% Hint: edit controls usually have a white background on Windows.
%         See ISPC and COMPUTER.
if ispc && isequal(get(hObject,'BackgroundColor'),
get(0,'defaultUicontrolBackgroundColor'))
    set(hObject,'BackgroundColor','white');
end

```

end

```
function txtSSLH_Callback(hObject, eventdata, handles)
% hObject    handle to txtSSLH (see GCBO)
% eventdata  reserved - to be defined in a future version of MATLAB
% handles    structure with handles and user data (see GUIDATA)

% Hints: get(hObject,'String') returns contents of txtSSLH as text
%        str2double(get(hObject,'String')) returns contents of txtSSLH as a
double
```

% --- Executes during object creation, after setting all properties.

```
function txtSSLH_CreateFcn(hObject, eventdata, handles)
% hObject    handle to txtSSLH (see GCBO)
% eventdata  reserved - to be defined in a future version of MATLAB
% handles    empty - handles not created until after all CreateFcns called
```

% Hint: edit controls usually have a white background on Windows.

```
%        See ISPC and COMPUTER.
if      ispc      &&      isequal(get(hObject,'BackgroundColor'),
get(0,'defaultUicontrolBackgroundColor'))
    set(hObject,'BackgroundColor','white');
end
```

```
function txtHBWE_Callback(hObject, eventdata, handles)
```

```
% hObject    handle to txtHBWE (see GCBO)
% eventdata  reserved - to be defined in a future version of MATLAB
% handles    structure with handles and user data (see GUIDATA)
```

% Hints: get(hObject,'String') returns contents of txtHBWE as text

```
%        str2double(get(hObject,'String')) returns contents of txtHBWE as a
double
```

% --- Executes during object creation, after setting all properties.

```
function txtHBWE_CreateFcn(hObject, eventdata, handles)
% hObject    handle to txtHBWE (see GCBO)
% eventdata  reserved - to be defined in a future version of MATLAB
% handles    empty - handles not created until after all CreateFcns called
```

% Hint: edit controls usually have a white background on Windows.

```
%        See ISPC and COMPUTER.
if      ispc      &&      isequal(get(hObject,'BackgroundColor'),
get(0,'defaultUicontrolBackgroundColor'))
    set(hObject,'BackgroundColor','white');
end
```

```
function txtHBWH_Callback(hObject, eventdata, handles)
```

```
% hObject    handle to txtHBWH (see GCBO)
% eventdata  reserved - to be defined in a future version of MATLAB
% handles    structure with handles and user data (see GUIDATA)
```

% Hints: get(hObject,'String') returns contents of txtHBWH as text

```
%        str2double(get(hObject,'String')) returns contents of txtHBWH as a
double
```

```

% --- Executes during object creation, after setting all properties.
function txtHBWH_CreateFcn(hObject, eventdata, handles)
% hObject    handle to txtHBWH (see GCBO)
% eventdata  reserved - to be defined in a future version of MATLAB
% handles    empty - handles not created until after all CreateFcns called

% Hint: edit controls usually have a white background on Windows.
%         See ISPC and COMPUTER.
if ispc && isequal(get(hObject,'BackgroundColor'),
get(0,'defaultUicontrolBackgroundColor'))
    set(hObject,'BackgroundColor','white');
end

% --- Executes on button press in chkDisplayE.
function chkDisplayE_Callback(hObject, eventdata, handles)
% hObject    handle to chkDisplayE (see GCBO)
% eventdata  reserved - to be defined in a future version of MATLAB
% handles    structure with handles and user data (see GUIDATA)

% Hint: get(hObject,'Value') returns toggle state of chkDisplayE

% --- Executes on button press in chkDisplayH.
function chkDisplayH_Callback(hObject, eventdata, handles)
% hObject    handle to chkDisplayH (see GCBO)
% eventdata  reserved - to be defined in a future version of MATLAB
% handles    structure with handles and user data (see GUIDATA)

% Hint: get(hObject,'Value') returns toggle state of chkDisplayH

% --- Executes during object creation, after setting all properties.
function figure1_CreateFcn(hObject, eventdata, handles)
% hObject    handle to figure1 (see GCBO)
% eventdata  reserved - to be defined in a future version of MATLAB
% handles    empty - handles not created until after all CreateFcns called
%h.chkDisplayE = uicontrol(current_f,'Style','checkbox', 'Value',1);

% --- Executes during object creation, after setting all properties.
function chkDisplayE_CreateFcn(hObject, eventdata, handles)
% hObject    handle to chkDisplayE (see GCBO)
% eventdata  reserved - to be defined in a future version of MATLAB
% handles    empty - handles not created until after all CreateFcns called

% --- Executes on mouse press over figure background, over a disabled or
% --- inactive control, or over an axes background.
function figure1_WindowButtonDownFcn(hObject, eventdata, handles)
% hObject    handle to figure1 (see GCBO)
% eventdata  reserved - to be defined in a future version of MATLAB
% handles    structure with handles and user data (see GUIDATA)

% --- Executes on mouse motion over figure - except title and menu.
function figure1_WindowButtonMotionFcn(hObject, eventdata, handles)
% hObject    handle to figure1 (see GCBO)

```

```

% eventdata reserved - to be defined in a future version of MATLAB
% handles structure with handles and user data (see GUIDATA)
% --- Executes on mouse press over figure background, over a disabled or
% --- inactive control, or over an axes background.
function figure1_WindowButtonUpFcn(hObject, eventdata, handles)
% hObject handle to figure1 (see GCBO)
% eventdata reserved - to be defined in a future version of MATLAB
% handles structure with handles and user data (see GUIDATA)

% --- Executes on button press in btnClose.
function btnClose_Callback(hObject, eventdata, handles)
% hObject handle to btnClose (see GCBO)
% eventdata reserved - to be defined in a future version of MATLAB
% handles structure with handles and user data (see GUIDATA)
close all;
%close(handles.f);

function txtS11_Callback(hObject, eventdata, handles)
% hObject handle to txtS11 (see GCBO)
% eventdata reserved - to be defined in a future version of MATLAB
% handles structure with handles and user data (see GUIDATA)

% Hints: get(hObject,'String') returns contents of txtS11 as text
% str2double(get(hObject,'String')) returns contents of txtS11 as a
double

% --- Executes during object creation, after setting all properties.
function txtS11_CreateFcn(hObject, eventdata, handles)
% hObject handle to txtS11 (see GCBO)
% eventdata reserved - to be defined in a future version of MATLAB
% handles empty - handles not created until after all CreateFcns called

% Hint: edit controls usually have a white background on Windows.
% See ISPC and COMPUTER.
if ispc && isequal(get(hObject,'BackgroundColor'),
get(0,'defaultUicontrolBackgroundColor'))
set(hObject,'BackgroundColor','white');
end

% --- Executes on button press in chkExport.
function chkExport_Callback(hObject, eventdata, handles)
% hObject handle to chkExport (see GCBO)
% eventdata reserved - to be defined in a future version of MATLAB
% handles structure with handles and user data (see GUIDATA)

% Hint: get(hObject,'Value') returns toggle state of chkExport

```

APPENDIX B

LIST OF PUBLICATIONS

International Journal Paper

Wongsan, R., Krachodnok, P., and Kamphikul, P. (2014). **A Sector Antenna for Mobile Base Station using MSA Array with Curved Woodpile EBG.** Open Journal of Antennas and Propagation (OJAPr). 2(1): 1-8. (Scientific Research, ISSN: 2329-8413).

Kamphikul, P., Krachodnok, P., and Wongsan, R. (2014). **High Gain Mobile Base Station Antenna Using Curved Woodpile EBG Technique.** World Academy of Science, Engineering and Technology (WASET), International Journal of Electrical, Robotics, Electronics and Communications Engineering. 8(7): 910-916. (International Science Index, ISSN: 1307-6892).

International Conference Papers

Kamphikul, P., Krachodnok, P., and Wongsan, R. (2012). **High-gain Antenna for Base Station Using MSA and Triangular EBG Cavity.** The 2012 Progress in Electromagnetics Research Symposium (PIERS 2012). 534-537.

Kamphikul, P., Krachodnok, P., and Wongsan, R. (2012). **Gain Improvement of MSA Array for Base Station using Covered EBG.** The 2012 IEEE Asia-Pacific Conference on Antennas and Propagation (APCAP 2012). 193-194.

Kamphikul, P., Krachodnok, P., and Wongsan, R. (2012). **Beamwidth Improvement of MSA Array for Base Station Using Covered with Curved Woodpile EBG.** The 2012 Thailand-Japan MicroWave (TJMW 2012).

Kamphikul, P., Krachodnok, P., and Wongsan, R. (2014). **Gain Improvement of MSAs Array by Using Curved Woodpile EBG and U-shaped Reflector.**

The 2014 International Electrical Engineering Congress (iEECON 2014).

Kumsalee, P., Kamphikul, P., Krachodnok, P., and Wongsan, R. (2014).

Omnidirectional High-Gain Slot Array Antenna. The 2014 International Conference on Electrical Engineering/Electronics, Computer, Telecommunications and Information Technology (ECTI-CON 2014).

A Sector Antenna for Mobile Base Station Using MSA Array with Curved Woodpile EBG

Rangsan Wongsan, Piyaporn Krachodnok, Paowphattra Kamphikul*

School of Telecommunication Engineering, Institute of Engineering, Suranaree University of Technology, Nakhon Ratchasima, Thailand

Email: rangsan@sut.ac.th, priam@sut.ac.th, D5240395@g.sut.ac.th

Received 8 January 2014; revised 17 February 2014; accepted 10 March 2014

Copyright © 2014 by authors and Scientific Research Publishing Inc.

This work is licensed under the Creative Commons Attribution International License (CC BY).

<http://creativecommons.org/licenses/by/4.0/>



Abstract

This paper presents a sector antenna for base station of mobile phone using microstrip antenna (MSA) array with curved woodpile Electromagnetic Band Gap (EBG). The advantages of this proposed antenna are easy fabrication and installation, high gain, and light weight. Moreover, it provides a fan-shaped radiation pattern, a main beam having a narrow beam width in the vertical direction and a wider beamwidth in the horizontal direction, which are appropriate for mobile phone base station. The half-power beamwidths in the H-plane and E-plane are 37.4 and 8.7 degrees, respectively. The paper also presents the design procedures of a 1×8 array antenna using MSAs associated with U-shaped reflector for decreasing their back and side lobes. A Computer Simulation Technology (CST) software has been used to compute the reflection coefficient (S_{11}), radiation patterns, and gain of this antenna. The bandwidth, at S_{11} (-10 dB), is enough, which can be well utilized for 3G base station, with a gain 20.84 dB.

Keywords

Microstrip Antenna; Electromagnetic Band Gap; Base Station

1. Introduction

Recently, the development of antennas with new performances becomes currently imperatively essential for the new services and network of telecommunication. Microstrip antennas (MSA) are an attractive choice for many modern communication systems due to their light weight, low profile with conformability, and low cost [1] [2]. In principle, the MSA is a resonant-type antenna, where the antenna size is determined by the operating wavelength while the bandwidth is determined by the Q factor of the resonance. Two of the major disadvantages are

*Corresponding author.

the low gain and very narrow impedance bandwidth due to the resonant nature of the conventional MSA. Parasitic patches are used to form a multi-resonant circuit so that the operating bandwidth can be improved [3]. In [4], a multi-layer MSA is investigated with parasitic patches stacked on the top of the main patch. The multi-resonant behavior can also be realized by incorporating slots into the metal patch. Furthermore, several single-layer single-patch MSA have been reported, such as the U-slot MSA [5] and the E-shaped patch antenna [6]. Another important topic in MSA designs is to miniaturize the patch antenna size. Increasing the dielectric constant of the substrate is also a simple and effective way for reducing the antenna size [7]. However, there are several drawbacks with the use of high dielectric constant substrate, narrow bandwidth, low radiation efficiency, and poor radiation patterns, which result from strong surface waves excited in the substrate. The narrow bandwidth can be expanded by increasing the substrate thickness, which, however, will launch stronger surface waves. As a result, the radiation efficiency and patterns of the antenna will be further degraded.

Many new technologies have emerged in the modern antenna design arena and one exciting breakthrough is the development of Electromagnetic Band Gap (EBG) structures. The applications of EBG structures in antenna designs have become a thrilling topic for antenna engineering [8]. It's a matter of the technology of EBG structure, a new technology for the improvement of the performances of antenna, applicable on a frequential spectrum extremely wide covered from the acoustic until to the optical frequencies [9]. Besides that, EBG structures, also known as photonic crystals [10], are also used to improve the antenna performance [11]-[13]. These structures have the ability to open a bandgap, which is a frequency range for which the propagation of electromagnetic waves is forbidden. By employing, EBG structures are capable to enhance the performance of MSA in terms of gain, side lobe, back lobe level and also mutual coupling. This is due to EBG exhibits frequency band-pass and band-stop that can block the surface wave excitation in the operational frequency range of antennas [14]. The objectives in using EBG were basically either to increase the gain, to reduce the side lobe and back lobe level, to reduce the mutual coupling (S_{21}) or to produce dual band to operate at different frequencies [15]. From such advantages of EBG structures, this paper presents a 1×8 array antenna using MSAs covered with curved woodpile EBG structures providing the high gain and beam width suitable for mobile phone base station. The simulated results of the reflection coefficient (S_{11}), radiation patterns, and gain of the antenna are conducted with Computer Simulation Technology (CST) software.

At first, the general approach will be presented which are including the configurations of MSA and EBG structures as shown in Sections 2 and 3, respectively. In Section 4, we apply this approach into the results and discussions. Finally, the conclusions are given in Section 5.

2. MSA Configuration

2.1. A Circular MSA

The circular MSA [16] designed for working in the Universal Mobile Telecommunications System (UMTS) band of 2.1 GHz frequency is utilized by the prototype for this proposed antenna. The antenna is printed on FR4 substrate with the size of $60 \text{ mm} \times 60 \text{ mm}$ and the thickness of 1.6 mm. A circular MSA structure consists of the circular patch of the radius (a). This gap of distance (t) between the microstrip line length (L_2) is used for adjusting the impedance matching. These structures mounted on the dielectric substrate with the dielectric constant of ϵ_r and the height (h). The substrate is located on the ground plane of the width (W) and the length (L). This ground plane is cut to form the wide-slot ground plane (Size $W_1 \times L_1$). The design of a MSA is based on the conventional transmission line model at 2.1 GHz. The desired bandwidth is 1.920 - 2.170 GHz. The tuning stub is used to improve the level of reflection coefficient, while the microstrip line is designed to provide 50 Ohm at the operating frequency of 2.1 GHz. The dimension of the wide-slot ground plane is varied to enhance the bandwidth as illustrated in [16]. The simulated result shows that the gain at 2.1 GHz is 5 dB.

2.2. A 1×8 Array MSAs

To enhance gain characteristic, a circular MSA will be arrayed with element spacing of $3\lambda/4$ (antenna type *A*) as shown in **Figure 1**. Furthermore, the proposed antenna in this paper has added a U-shaped reflector with the size of $400 \text{ mm} \times 1000 \text{ mm}$ behind the panel of MSAs array to control the radiation pattern to be the directional pattern. **Figure 2** shows a 1×8 array of circular MSAs and U-shaped reflector (antenna type *B*). The simulated results show that the radiation patterns of the antenna type *A* and *B* at 2.1 GHz with the gain of 14 dB and 17.83 dB, respectively. The Half-Power Beam Width (HPBW) in the H-Plane and E-Plane, which shown as the ratio of

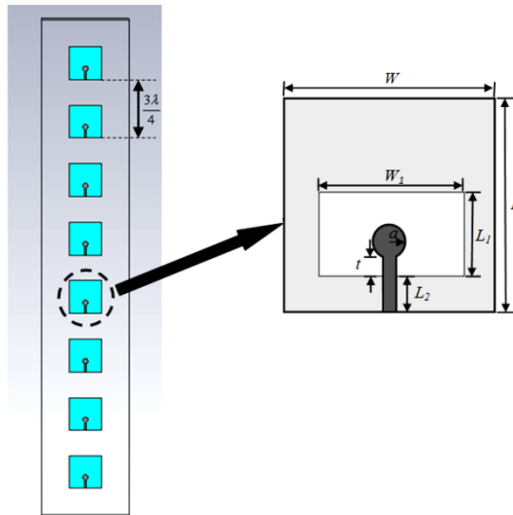


Figure 1. A 1×8 array of circular MSAs (antenna type *A*).

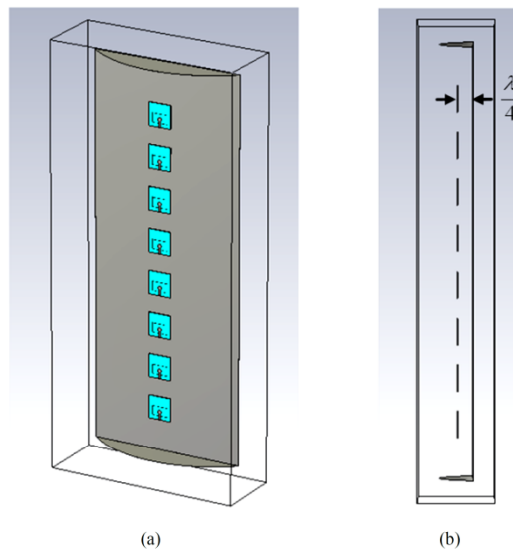


Figure 2. A 1×8 array of circular MSAs and U-shaped reflector (antenna type *B*). (a) Perspective view; (b) Side view.

azimuth pattern to evaluation pattern (AZ:EL), of the array antenna type *A* and *B* are $97.4^\circ:8.4^\circ$ and $89.4^\circ:8.3^\circ$, respectively.

3. EBG Configuration

In this section, the modified array antenna type *B* has been increased the gain by using new technique of EBG structures instead. The conventional method for gain increment, a lot of elements will be added in the array, which causes the dimension of antenna is too long and its weight is too heavy. Moreover, the great number of

electromagnetic energy will be lost inside the phasing line. From our study, we found that the proper structure of EBG is capable to enhance the gain of antenna as the additional resonant circuit which installed at front of the array panel. Furthermore, the EBG structures can be appropriately shaped for reducing the side and back lobes of the directional antenna too [17] [18]. From investigation, the sector of cylindrical woodpile EBG structures [19] are more suitable for the antenna type B. **Figure 3** shows the geometry of the curved woodpile EBG structures with two layers of the different diameters. The parameters for these structures are the filament thickness or diameter (w), the radius (R), the height (h), the number of radial filaments (N_{rad}), and the number of rings (N_{ring}) of the curved. To implement the curved woodpile EBG, we have used alumina rods (rectangular cross section) with parameters $\epsilon_r = 8.4$ and $\tan \delta = 0.002$. The parameters are given as follow [20] with $w = 0.05\lambda$, $R = 3.05\lambda$, $h = 1.23\lambda$, $N_{rad} = 3$, and $N_{ring} = 2$.

4. Results and Discussions

The gain improvement of 1×8 array of circular MSAs and U-shaped reflector with curved woodpile EBG structures (antenna type C) was simulated by CST software as shown in **Figure 4**.

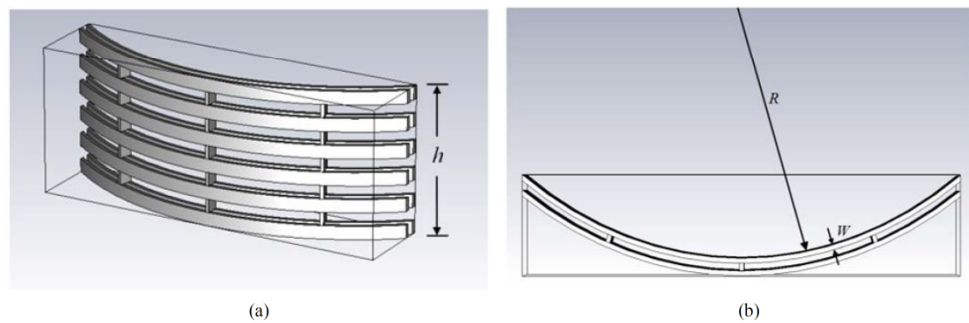


Figure 3. The geometry of the sector of curved woodpile EBG structures. (a) Perspective view; (b) Top view.

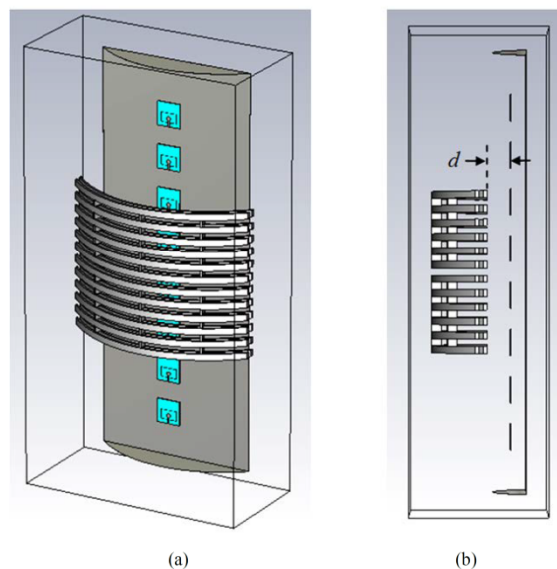


Figure 4. A 1×8 array of circular MSAs and U-shaped reflector improved gain with curved woodpile EBG structures (antenna type C). (a) Perspective view; (b) Side view.

The design parameters of the gain improvement for an antenna type *C* are the radius (R), the distance between a 1×8 array of circular MSAs and curved woodpile EBG structures (d), and the height of curved woodpile EBG (h). Firstly, we look at the effect of the variation of R , d and h are fixed at 0λ and 1.23λ , respectively. **Figure 5** shows the gain against the R at operating frequency of 2.1 GHz. The highest gain of 18.72 dB is provided at R is around at 3.34λ . Also, the appropriate HPBW in the H-plane appears at same radius of R of curved woodpile EBG, while its HPBW will be enlarged when the dimension of R increased. Secondly, we have investigated the effect of the distance d , while R and h are fixed at 3.34λ and 1.23λ , respectively. We note that the highest gain of 18.72 dB is achieved when $d = 0\lambda$ as shown in **Figure 6**. Next, we have studied the effect of the h variation versus the gain, R and d are fixed at 3.34λ and 0λ , respectively, thus its result is improved as shown in **Figure 7**. We found that the gain is increased from 18.72 dB to 20.84 dB at h equals to 3.91λ approximately. Although the gain increases when h also increases, while h is higher than 5.25λ , it will be mismatched and operating frequency of bandwidth will be shifted to the undesired frequency.

Finally, the highest gain of an antenna type *C* is optimized with $R = 3.34\lambda$, $d = 0\lambda$, and $h = 3.91\lambda$. The S_{11} (-10 dB) of the antenna type *A*, *B*, and *C*, covered 1.920 to 2.170 GHz, which are wide enough and can be well utilized for 3G base station as shown in **Figure 8**. **Figure 9** shows the normalized radiation patterns at 2.1 GHz of the antenna type *A*, *B*, and *C*. Although its HPBW of the antenna type *C* will narrow, but it can cover the desired service area of base station for mobile phone and still provides the high gain. Also, the HPBW, the Side Lobe Level (SLL), and the gain of the antenna type *A*, *B*, and *C* are shown in **Table 1**.

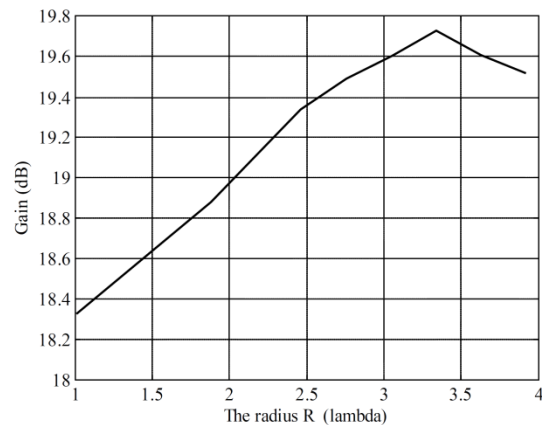


Figure 5. Simulated the gain against R .

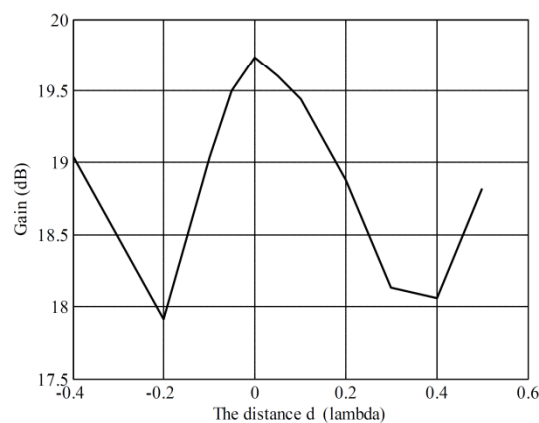


Figure 6. Simulated the gain against d .

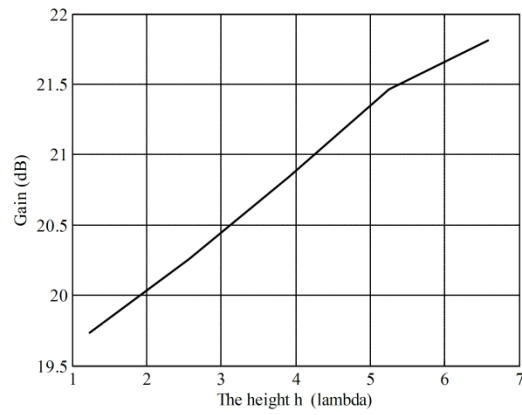


Figure 7. Simulated the gain against d .

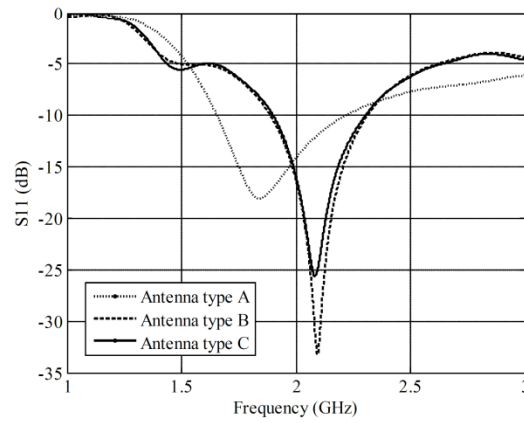


Figure 8. Simulated the reflection coefficient.

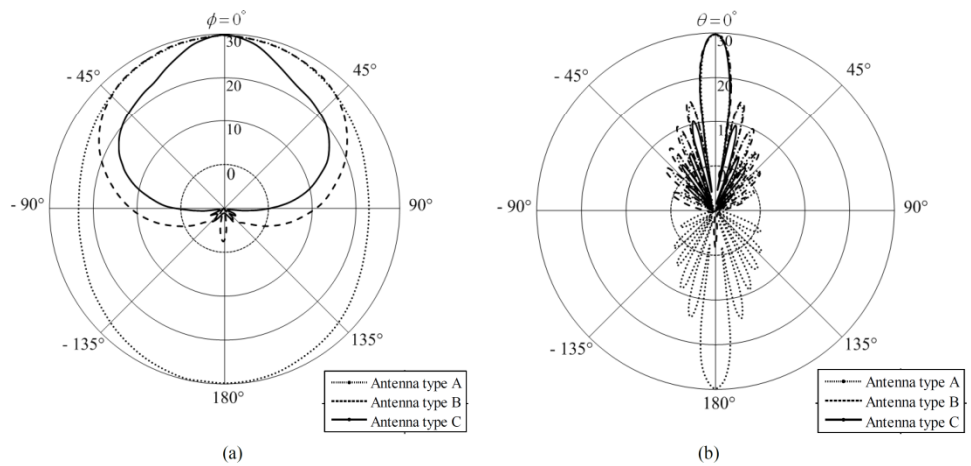


Figure 9. Simulated the normalized radiation patterns. (a) H-Plane; (b) E-Plane.

Table 1. Results of simulation.

Parameters	Antenna type A	Antenna type B	Antenna type C
The HPBW (AZ:EL)	97.4°:8.4° 11.6:1	89.4°:8.3° 10.8:1	37.2°:8.7° 4.3:1
The H-plane SLL	-	-30.6 dB	-27.3 dB
The E-plane SLL	-12.9 dB	-13.2 dB	-14.4 dB
The gain	14 dB	17.83 dB	20.84 dB

5. Conclusion

This paper presented a sector antenna for mobile base station by modifying the omnidirectional MSAs array to be the directional antenna by adding U-shaped reflector and increasing its gain with new technique, additional curved woodpile EBG structures. From the results, explicitly, the directive gain of the proposed antenna was increased around 3 dB when such EBG structures were added, while its length of array was not enlarged. The most important technique for this accomplishment is the EBG structures that must be appropriately designed and calculated, especially the radius of the sectorial cylinder of woodpile EBG structures. The most proper radius of 3.34λ , the distance between a 1×8 array of circular MSAs and curved woodpile EBG structures of 0λ , and the height of curved woodpile EBG of 3.91λ can provide the moderately highest gain of 20.84 dB at the operating frequency of 2.1 GHz. Therefore, this proposed antenna accords to the requirements and is appropriated for a sector antenna of mobile base station.

Acknowledgements

This work was supported by the Research Department Institute of Engineering, Suranaree University of Technology, Nakhon Ratchasima, Thailand.

References

- [1] Bahl, J.J. and Bhartia, P. (1980) *Microstrip Antennas*. Artech House, London.
- [2] Bhartia, P., Bahl, I., Garg, R. and Ittipipoon, A. (2000) *Microstrip Antennas Design Handbook*. Artech House, London.
- [3] Kumar, G. and Gupta, K.C. (1985) Directly Coupled Multiple Resonator Wide-Band Microstrip Antenna. *IEEE Transactions on Antennas and Propagation*, **33**, 588-593. <http://dx.doi.org/10.1109/TAP.1985.1143639>
- [4] Pozar, D.M. (1985) Microstrip Antenna Aperture-Coupled to a Microstripline. *Electronics Letters*, **21**, 49-50. <http://dx.doi.org/10.1049/el:19850034>
- [5] Huynh, T. and Lee, K.F. (1995) Single-Layer Single-Patch Wide Band Microstrip Antenna. *Electronics Letters*, **31**, 1310-1312. <http://dx.doi.org/10.1049/el:19950950>
- [6] Yang, F., Zhang, X., Ye, X. and Rahmat-Samii, Y. (2001) Wide Band E-Shaped Patch Antennas for Wireless Communications. *IEEE Transactions on Antennas and Propagation*, **49**, 1094-1100. <http://dx.doi.org/10.1109/8.933489>
- [7] Lo, T.K., Ho, C.-O., Hwang, Y., Lam, E.K.W. and Lee, B. (1997) Miniature Aperture Coupled Microstrip Antenna of Very High Permittivity. *Electronics Letters*, **33**, 9-10. <http://dx.doi.org/10.1049/el:19970053>
- [8] Yang, F. and Rahmat-Samii, Y. (2009) *Electromagnetic Band Gap Structures in Antenna Engineering*. Cambridge University Press, Cambridge.
- [9] Elayachi, M., Brachat, P. and Ratajczak, P. (2006) EBG Identification by the Reflection Phase Method (RPM) Design for Application WiFi Antenna. *Proceedings of the 1st European Conference on Antennas and Propagation*, Nice, 6-10 November 2006, 1-5.
- [10] Joannopoulos, J., Meade, R.D. and Winn, J.N. (1995) *Photonic Crystals: Molding the Flow of Light*. Princeton University Press, Princeton.
- [11] Gonzalo, R., de Maagt, P. and Sorolla, M. (1999) Enhanced Path-Antenna Performance by Suppressing Surface Waves Using Photonic-Bandgap Substrates. *IEEE Transactions on Microwave Theory and Techniques*, **47**, 2131-2138. <http://dx.doi.org/10.1109/22.798009>
- [12] Yang, F. and Rahmat-Samii, Y. (2003) Microstrip Antennas Integrated with Electromagnetic Bandgap (EBG) Structures: A Low Mutual Coupling Design for Array Applications. *IEEE Transactions on Antennas and Propagation*, **51**, 2936-2946. <http://dx.doi.org/10.1109/TAP.2003.817983>

- [13] Llombart, N., Neto, A., Gerini, G. and de Maagt, P. (2005) Planar Circularly Symmetric EBG Structures for Reducing Surface Waves in Printed Antennas. *IEEE Transactions on Antennas and Propagation*, **53**, 3210-3218. <http://dx.doi.org/10.1109/TAP.2005.856365>
- [14] Illuz, Z., Shavit, R. and Bauer, R. (2004) Micro-Strip Antenna Phased Array with Electromagnetic Band-Gap Substrate. *IEEE Transactions on Antennas and Propagation*, **52**, 1446-1453. <http://dx.doi.org/10.1109/TAP.2004.830252>
- [15] Md Tan, M.N., Rahman, T.A., Rahim, S.K.A., Ali, M.T. and Jamlos, M.F. (2010) Antenna Array Enhancement Using Mushroom-Like Electromagnetic Band Gap (EBG). 2010 *Proceedings of the 4th European Conference on Antennas and Propagation (EuCAP)*, Barcelona, 12-16 April 2010, 1-5.
- [16] Chawanonphithak, Y. and Phongcharoenpanich, C. (2007) An Ultra-Wideband Circular Microstrip Antenna Fed by Microstrip Line above Wide-Slot Ground Plane. *Asia-Pacific Conference on Communications*, Bangkok, 18-20 October 2007, 99-102.
- [17] Weily, A.R., Horvath, L., Esselle, K.P., Sanders, B. and Bird, T. (2005) A Planar Resonator Antenna Based on Woodpile EBG Material. *IEEE Transactions on Antennas and Propagation*, **53**, 216-223. <http://dx.doi.org/10.1109/TAP.2004.840531>
- [18] Lee, Y., Lu, X., Hao, Y., Yang, S., Evans, J.R.G. and Parini, C.G. (2009) Low Profile Directive Millimeter-Wave Antennas Using Free Formed Three-Dimensional (3D) Electromagnetic Band Gap Structures. *Transactions on Antennas and Propagation*, **57**, 2893-2903. <http://dx.doi.org/10.1109/TAP.2009.2029299>
- [19] Lee, Y., Lu, X., Hao, Y., Yang, S., Evans, J.R.G. and Parini, C.G. (2010) Narrow-Beam Azimuthally Omni-Directional Millimetre-Wave Antenna Using Free Formed Cylindrical Woodpile Cavity. *IET Microwaves, Antennas and Propagation*, **4**, 1491-1499. <http://dx.doi.org/10.1049/iet-map.2009.0224>
- [20] Kamphikul, P., Krachodnok, P. and Wongsan, R. (2012) Beamwidth Improvement of MSA Array for Base Station Using Covered with Curved Woodpile EBG. *Thailand-Japan MicroWave 2012*, Bangkok, 8-10 August 2012.

High Gain Mobile Base Station Antenna Using Curved Woodpile EBG Technique

P. Kamphikul, P. Krachodnok, R. Wongsan

Abstract—This paper presents the gain improvement of a sector antenna for mobile phone base station by using the new technique to enhance its gain for microstrip antenna (MSA) array without construction enlargement. The curved woodpile Electromagnetic Band Gap (EBG) has been utilized to improve the gain instead. The advantages of this proposed antenna are reducing the length of MSAs array but providing the higher gain and easy fabrication and installation. Moreover, it provides a fan-shaped radiation pattern, wide in the horizontal direction and relatively narrow in the vertical direction, which appropriate for mobile phone base station. The paper also presents the design procedures of a 1x8 MSAs array associated with U-shaped reflector for decreasing their back and side lobes. The fabricated curved woodpile EBG exhibits bandgap characteristics at 2.1 GHz and is utilized for realizing a resonant cavity of MSAs array. This idea has been verified by both the Computer Simulation Technology (CST) software and experimental results. As the results, the fabricated proposed antenna achieves a high gain of 20.3 dB and the half-power beam widths in the E- and H-plane of 36.8 and 8.7 degrees, respectively. Good qualitative agreement between measured and simulated results of the proposed antenna was obtained.

Keywords—Gain Improvement, Microstrip Antenna Array, Electromagnetic Band Gap, Base Station.

I. INTRODUCTION

NOWADAYS, wireless communication is used increasingly because users can connect to the network system from any area within the signal coverage range, so the users can conveniently connect to the system. From the development of wireless communication system, the antennas were improved with new performances becomes currently imperatively essential for the new services and network of telecommunication. Microstrip antennas (MSA) are an attractive choice for many modern communication systems due to their light weight, low profile, conformable to planar and nonplanar surfaces, inexpensive to manufacture using modern printed-circuit technology, and versatile in terms of resonant frequency, polarization, pattern, and impedance [1]-[2]. However, two of the important disadvantages of MSA are the low gain and very narrow impedance bandwidth due to the resonant nature of the conventional MSA. Parasitic patches are used to form a multi-resonant circuit so that the operating bandwidth can be improved [3]. A multi-layer MSA is examined with parasitic patches stacked on the top of the main patch [4]. The multi-resonant conducts to be realized by

incorporating slots into the metal patch. In addition, several single-layer single-patch MSA have been presented, such as the U-slot MSA [5] and the E-shaped patch antenna [6]. Another major topic in MSA designs is to miniaturize the patch antenna size such as increasing the dielectric constant of the substrate is also a simple and effective ways for reducing the antenna size [7]. Nevertheless, there are significant drawbacks with the use of high dielectric constant substrate such as narrow bandwidth, low radiation efficiency, and poor radiation patterns, which result from strong surface waves excited in the substrate. The narrow bandwidth can be expanded by increasing the substrate thickness, which, however, will launch stronger surface waves. As a result, the radiation efficiency and patterns of the antenna will be further degraded.

Numerous new technologies have emerged in the modern MSA design arena and one exciting breakthrough is the development of Electromagnetic Band Gap (EBG) structures. The applications of EBG structures in antenna designs have become a thrilling topic for antenna engineering. Besides that, EBG structures, also known as photonic crystals [8], have attracted increasing interests because of their desirable electromagnetic properties that cannot be observed in natural material (metamaterials). Many researches on EBG structures are on the initiate in the electromagnetic and antenna community such as low profile antennas, active phased array, TEM waveguides, and microwave filters [9]. The unique electromagnetic properties of EBG structures have led to a wide range of applications in MSA engineering because the EBG structures can be integrated into MSA designs and their surface wave band gap property helps to increase the antenna gain, minimize the side and back lobes, and reduce mutual coupling in array elements [10]-[12]. These structures have the ability to open a bandgap, which is a frequency range for which the propagation of electromagnetic waves is forbidden. This is due to EBG exhibits frequency band-pass and band-stop that can block the surface wave excitation in the operational frequency range of antennas [13]. From such advantages of EBG structures, this paper presents a 1x8 MSAs array with U-shaped reflector and curved woodpile EBG structures providing the high gain and beamwidth suitable for mobile phone base station. The simulated from CST software and measured results of the reflection coefficient (S_{11}), radiation patterns, and gain of the proposed antenna show good agreement which are presented.

This paper is organized as follows. In Section II, the configuration and design of the circular MSA is introduced. In addition, a curved woodpile EBG structure with its

P. Kamphikul, P. Krachodnok, and R. Wongsan are with the School of Telecommunication Engineering, Institute of Engineering, Suranaree University of Technology, Nakhon Ratchasima, CO 30000 Thailand (phone: +668 1955 2414; fax: +66 4422 4603 e-mail: D5240395@g.sut.ac.th, priam@sut.ac.th, and rangsan@sut.ac.th).

corresponding bandgap features is presented in Section III. In Section IV, we apply this approach into the simulated results and discussions. Next, the fabricated and experimented results of the prototype antenna are discussed in the Section V, followed by conclusions in Section VI.

II. MSA CONFIGURATION

A. A Circular MSA

The circular MSA [14], the most common radiating patch because of ease of analysis and fabrication, and low cross-polarization radiation, designed for working in the Universal Mobile Telecommunications System (UMTS) band of 2.1 GHz frequency is utilized by the prototype for this proposed antenna. The antenna is printed on FR4 ($\epsilon_r = 4.5, \tan\delta = 0.02$) substrate with the size of 60 mm x 60 mm and the thickness of 1.6 mm. A circular MSA structure consists of the circular patch of the radius (a). This gap of distance (t) between the microstrip line length (L_2) is used for adjusting the impedance matching. These structures mounted on the dielectric substrate with the dielectric constant of ϵ_r and the height (h). The substrate is located on the ground plane of the width (W) and the length (L). This ground plane is cut to form the wide-slot ground plane (Size $W_1 \times L_1$). The design of a MSA is based on the conventional transmission line model at 2.1 GHz. The desired bandwidth is 1.920 – 2.170 GHz. The tuning stub is used to improve the level of reflection coefficient, while the microstrip line is designed to provide 50 Ohm at the operating frequency of 2.1 GHz. The dimension of the wide-slot ground plane is varied to enhance the bandwidth as illustrated in [14]. The simulated result shows that the gain at 2.1 GHz is 5 dB.

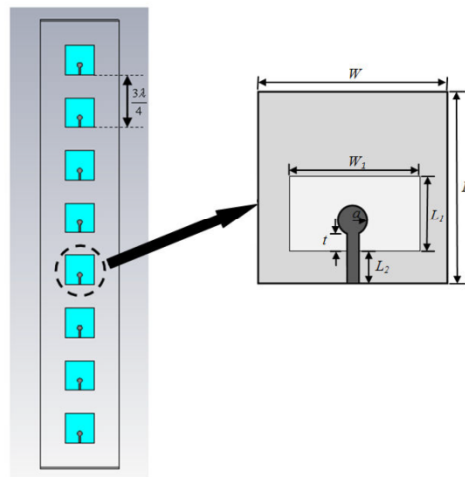


Fig. 1 A 1x8 array of circular MSAs (antenna type A)

B. A 1x8 MSAs Array

To improve gain characteristic, a circular MSA will be arrayed with element spacing of $3\lambda/4$ (antenna type A) as

shown in Fig. 1. In addition, the proposed antenna in this paper has added a U-shaped reflector with the size of 400 mm x 1,000 mm behind the panel of MSAs array to control the radiation pattern to be the directional pattern. Fig. 2 shows a 1x8 array of circular MSAs and U-shaped reflector (antenna type B). The simulated results show that the radiation patterns of the antenna type A and B at 2.1 GHz with the gain of 14 and 17.83 dB, respectively. The Half-Power Beamwidth (HPBW) in the H- and E-Plane, which shown as the ratio of azimuth pattern to evaluation pattern (AZ:EL), of the array antenna type A and B are $97.4^\circ:8.4^\circ$ and $89.4^\circ:8.3^\circ$, respectively.

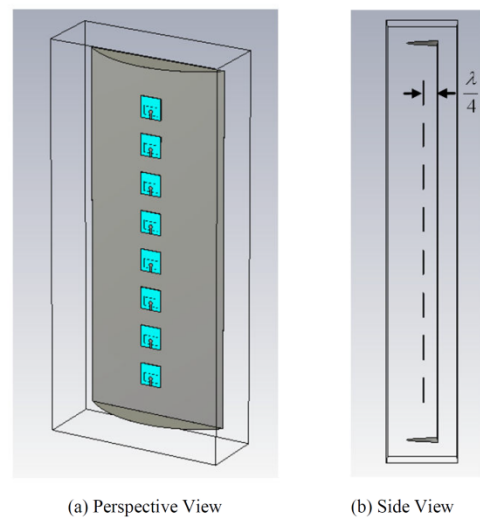


Fig. 2 A 1x8 array of circular MSAs and U-shaped reflector (antenna type B)

III. EBG CONFIGURATION

In this section, the modified array antenna type B has been increased the gain by using new technique of woodpile EBG structures instead. In the past, the conventional method for gain increment, a lot of elements will be added in the array, which causes the dimension of antenna is too long and its weight is too heavy. Furthermore, the great number of electromagnetic energy will be lost inside the phasing line. From our study [15]-[18], we found that the proper structure of EBG is capable to enhance the gain of MSAs array as the additional resonant circuit which installed at front of the array panel. Moreover, the EBG structures can be appropriately shaped such as planar woodpile EBG structures for reducing the side and back lobes of the directional antenna too [19]-[20]. From investigation, the sector of cylindrical woodpile EBG structures [21] are more suitable for the antenna type B. Fig. 3 shows the geometry of the curved woodpile EBG structures with two layers of the different diameters. The parameters for these structures are the filament thickness or diameter (w), the radius (R), the height (h), the number of

International Science Index Vol:8, No:7, 2014 waset.org/Publication/9998640

radial filaments (N_{rad}), and the number of rings (N_{ring}) of the curved. To implement the curved woodpile EBG, we have used alumina rods (rectangular cross section) with parameters $\epsilon_r = 8.4$ and $\tan\delta = 0.002$. The parameters are given as follow [18] with $w = 0.05\lambda$, $R = 3.05\lambda$, $h = 1.23\lambda$, $N_{rad} = 3$, and $N_{ring} = 2$.

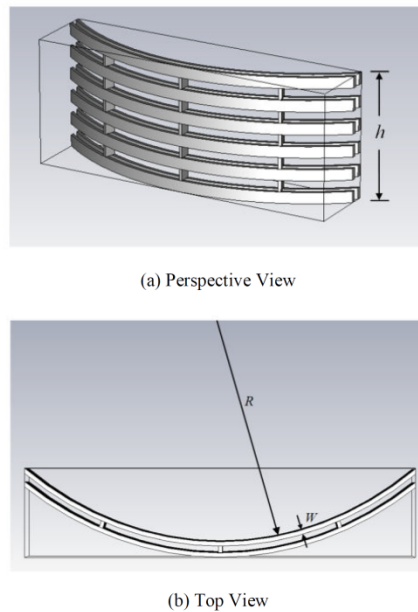


Fig. 3 The geometry of the sector of curved woodpile EBG structures

IV. SIMULATED RESULTS AND DISCUSSIONS

The gain improvement of a 1×8 array of circular MSAs and U-shaped reflector with curved woodpile EBG structures (antenna type C) was simulated by CST software as shown in Fig. 4.

The design parameters of the gain improvement for an antenna type C are the radius of curved woodpile EBG structures (R), the distance between a 1×8 circular MSAs array and curved woodpile EBG structures (d), and the height of curved woodpile EBG structures (h) [22]. Firstly, we look at the effect of the variation of R , d and h are fixed at 0λ and 1.23λ , respectively. Fig. 5 shows the gain against the R at operating frequency of 2.1 GHz. The highest gain of 18.72 dB is provided at R is around at 3.34λ . Also, the appropriate HPBW in the H-plane appears at same radius of R of curved woodpile EBG, while its HPBW will be enlarged when the dimension of R increased. Secondly, we have investigated the effect of the distance d , while R and h are fixed at 3.34λ and 1.23λ , respectively. We note that the highest gain of 18.72 dB is achieved when $d = 0\lambda$ as shown in Fig. 6. This property can be used to control the resonant frequency of curved woodpile EBG structures because its resonant frequency will change

when d is changed, while the bandwidth is constant. Next, we have studied the effect of the h variation versus the gain, R and d are fixed at 3.34λ and 0λ , respectively, thus its result is improved as shown in Fig. 7. We found that the gain is increased from 18.72 dB to 20.84 dB at h equals to 3.91λ approximately. Although the gain increases when h also increases, while h is higher than 5.25λ , it will be mismatched and operating frequency of bandwidth will be shifted to the undesired frequency.

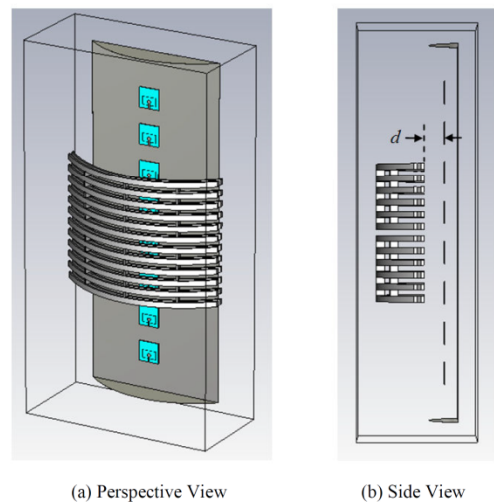


Fig. 4 A 1×8 MSAs array with U-shaped reflector and curved woodpile EBG structures (antenna type C)

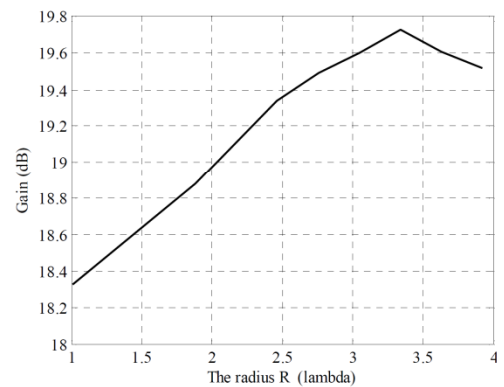


Fig. 5 Simulated gain against R of the antenna type C

International Science Index Vol:8, No:7, 2014 waset.org/Publication/9998640

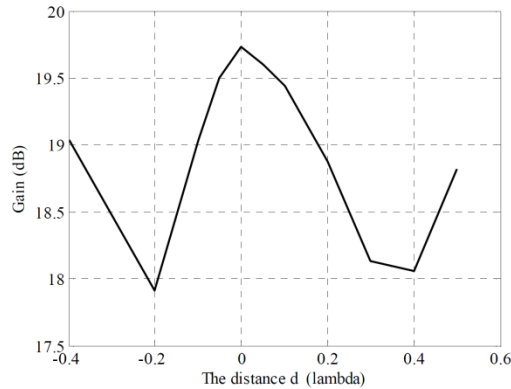


Fig. 6 Simulated gain against d of the antenna type C

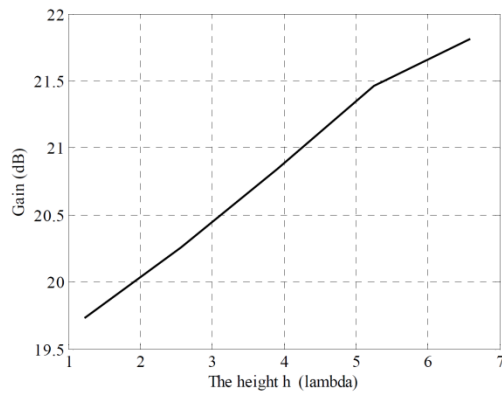


Fig. 7 Simulated gain against h of the antenna type C

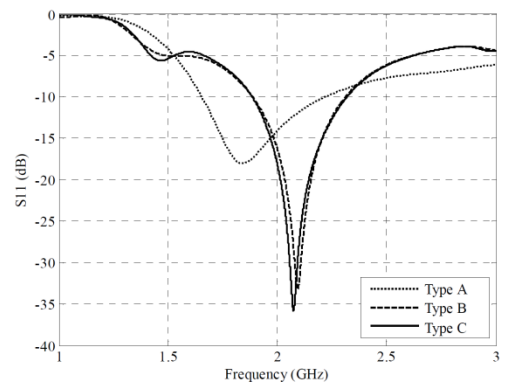
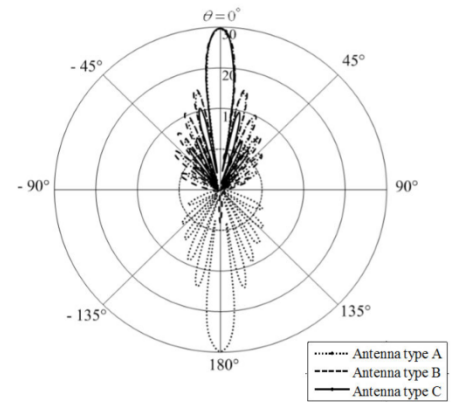


Fig. 8 Simulated reflection coefficient of the three type antennas

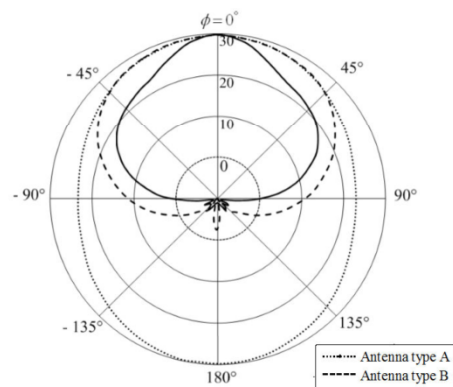
Finally, the highest gain of an antenna type C is optimized with $R = 3.34\lambda$, $d = 0\lambda$, and $h = 3.91\lambda$. The S_{11} (-10 dB) of the antenna type A, B, and C, covered 1.920 to 2.170 GHz, which are wide enough and can be well utilized for 3G mobile phone base station as shown in Fig. 8. Fig. 9 shows the normalized radiation patterns at 2.1 GHz of the antenna type A, B, and C. Although its HPBW of the antenna type C will narrow, but it can cover the desired service area of mobile phone base station and still provides the higher gain. Also, the HPBW, the Side Lobe Level (SLL), and the gain of the antenna type A, B, and C are shown in Table I.

TABLE I
RESULTS OF SIMULATION

Parameters	Antenna type A	Antenna type B	Antenna type C
The HPBW (AZ:EL)	97.4°:8.4°	89.4°:8.3°	37.2°:8.7°
The E-plane SLL	-12.9 dB	-13.2 dB	-14.4 dB
The H-plane SLL	-	-30.6 dB	-27.3 dB
The Gain	14 dB	17.83 dB	20.84 dB



(a) E-Plane



(b) H-Plane

Fig. 9 Simulated radiation patterns of the three type antennas

International Science Index Vol:8, No:7, 2014 wassef.org/Publication/9998640

V. EXPERIMENTAL RESULTS AND DISCUSSIONS

An antenna type C prototype has been simulated with the CST software and fabricated to validate the proposed concept. The geometry of an antenna type C prototype as shown in Fig. 4 is used. It consists of a 1x8 circular MSAs array, with element spacing of $3\lambda/4$, associated with U-shaped reflector, as a PEC reflector to decrease their back and side lobes and control the radiation pattern to be the directional pattern, and the curved woodpile EBG structures which exhibit bandgap characteristics at 2.1 GHz and are utilized for realizing a resonant cavity of MSAs array. Figs. 10 shows photograph of the fabricated the proposed antenna. The simulated and measured S_{11} of the antenna are shown in Fig. 11. A good agreement is obtained between calculated and measured results. From the measured curve, a bandwidth from 1.54 to 3 GHz (a fractional bandwidth of 64.32%) is achieved, which is enough to cover the 3G mobile phone base station, UMTS band of 2.1 GHz (1.920 to 2.170 GHz). A further study of the proposed antenna has focused on its radiation performance. The radiation patterns of the proposed antenna were measured in an outdoor. For comparison, numerical simulations for radiation patterns were also carried out using the CST software. The measured and simulated patterns are shown in Fig. 12. With reference to these curves, a good agreement between predictions and measured data can be observed. The HPBW in the H- and E-Plane, which shown as the ratio of azimuth pattern to evaluation pattern (AZ:EL), of the proposed antenna is $36.8^\circ:8.7^\circ(4.23:1)$. Note that the radiation patterns provide a fan-shaped pattern, a main beam having a narrow beamwidth in the vertical direction and a wider beamwidth in the horizontal direction, which appropriate for mobile phone base station. The measured gain of the proposed antenna is 20.3 dB at operating frequency of 2.1 GHz. In additional, the measured and simulated results of the HPBWs, the SLLs, and the gains of the proposed antenna are summarized in Table II. These measurements of the proposed antenna are unique and very positives. With such features, this antenna is suitable for a mobile phone base station.

International Science Index Vol:8, No:7, 2014 waset.org/Publication/9998640



Fig. 10 The prototype of the proposed antenna

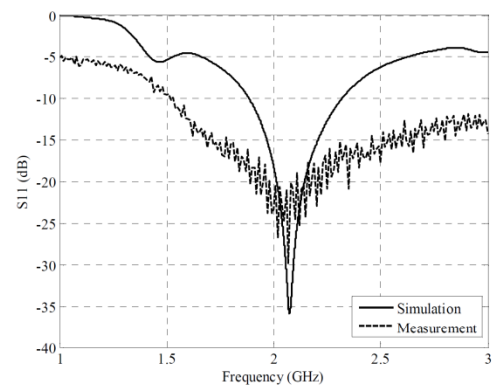


Fig. 11 The reflection coefficient of the proposed antenna

TABLE II
RESULTS OF MEASUREMENT

Parameters	Simulated Results	Measured Results
The HPBW (AZ:EL)	$37.2^\circ:8.7^\circ$	$36.8^\circ:8.7^\circ$
The E-plane SLL	-14.4 dB	-14 dB
The H-plane SLL	-27.3 dB	-25.3 dB
The Gain	20.84 dB	20.3 dB

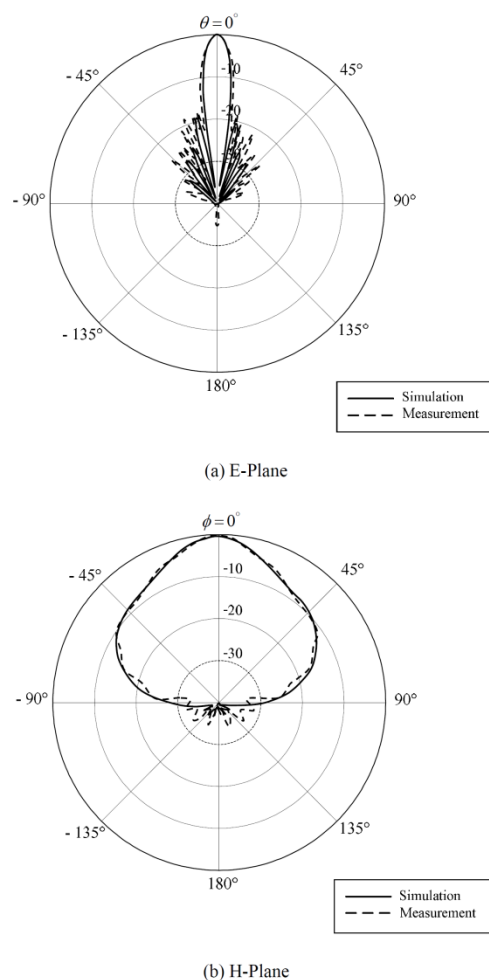


Fig. 12 The normalized radiation patterns of the proposed antenna

VI. CONCLUSIONS

This paper presented a sector antenna of a 1×8 MSAs array for mobile phone base station by modifying the bidirectional circular MSAs array to be the directional antenna by adding U-shaped reflector and increasing its gain with new technique, additional curved woodpile EBG structures. From the results, obviously, the proposed antenna provided the directive gain increasing around 3 dB when such EBG structures were added, while its length of array was not enlarged. Moreover, a fan-shaped radiation pattern in the horizontal direction according to our requirement was obtained. The most important technique for this accomplishment that is the EBG structures must be appropriately designed and calculated, especially the radius of the sectorial cylinder of woodpile EBG structures. The most proper radius of 3.34λ , the distance

between a 1×8 MSAs array and curved woodpile EBG structures of 0λ , and the height of curved woodpile EBG of 3.91λ can provide the moderately highest gain of 20.3 dB at the operating frequency of 2.1 GHz. A good agreement is obtained between simulated with CST software and experimental results. Therefore, this proposed antenna accords to the requirements and is appropriated for a sector antenna of 3G mobile phone base station, UMTS band of 2.1 GHz.

ACKNOWLEDGMENT

This work was supported by the National Research Council of Thailand (NRCT) and the Research Department Institute of Engineering, Suranaree University of Technology, Nakhon Ratchasima, Thailand.

REFERENCES

- [1] J.J. Bahl and P. Bhartia, "Microstrip Antennas," Artech House, 1980.
- [2] P. Bhartia, InderBahl, R. Garg, and A. Ittipipoon, "Microstrip Antennas Design Handbook," Artech House, 2000.
- [3] G. Kumar and K. C. Gupta, "Directly coupled multiple resonator wide-band microstrip antenna," *IEEE Transactions on Antennas and Propagation*, Vol. 33, No. 6, 1985, pp. 588-593.
- [4] D. M. Pozar, "Microstrip antenna aperture-coupled to a microstripline," *Electronics Letters*, Vol. 21, No. 2, 1985, pp. 49-50.
- [5] T. Huynh and K. F. Lee, "Single-layer single-patch wide band microstrip antenna," *Electronics Letters*, Vol. 31, No. 16, 1995, pp. 1310-1312.
- [6] F. Yang, X. Zhang, X. Ye, and Y. Rahmat-Samii, "Wide band E-shaped patch antennas for wireless communications," *IEEE Transactions on Antennas and Propagation*, Vol. 49, No. 7, 2001, pp. 1094-1100.
- [7] T. K. Lo, C.-O. Ho, Y. Hwang, E. K. W. Lam, and B. Lee, "Miniature aperture coupled microstrip antenna of very high permittivity," *Electronics Letters*, Vol. 33, No. 1, 1997, pp. 9-10.
- [8] J. D. Joannopoulos, R. D. Meade and J. N. Winn, "Photonic Crystals: Molding the Flow of Light," Princeton University Press, New Jersey, 1995.
- [9] F. Yang and Y. Rahmat-Samii, "Electromagnetic Band Gap Structures in Antenna Engineering," Cambridge University Press, Cambridge, 2009.
- [10] R. Gonzalo, P. de Maagt, and M. Sorolla, "Enhanced path-antenna performance by suppressing surface waves using photonic-bandgap substrates," *IEEE Transactions on Microwave Theory and Techniques*, Vol. 47, No. 11, 1999, pp. 2131-2138.
- [11] N. Llobert, A. Neto, G. Gerini, and P. de Maagt, "Planar circularly symmetric EBG structures for reducing surface waves in printed antennas," *IEEE Transactions on Antennas and Propagation*, Vol. 53, No. 10, 2005, pp. 3210-3218.
- [12] Illuz, Z., R. Shavit and R. Bauer, "Micro-strip Antenna Phased Array with Electromagnetic Band-Gap Substrate," *IEEE Transactions on Antennas and Propagation*, Vol. 52, No. 6, 2004, pp. 1446-1453.
- [13] F. Yang and Y. Rahmat-Samii, "Microstrip antennas integrated with electromagnetic bandgap (EBG) structures: A low mutual coupling design for array applications," *IEEE Transactions on Antennas and Propagation*, Vol. 51, No. 10, 2003, pp. 2936-2946.
- [14] Y. Chawanonphithak and C. Phongcharoenpanich, "An Ultra-wideband Circular Microstrip Antenna fed by Microstrip Line above Wide-Slot Ground Plane," in *Communications, (APCC) 2007. Asia-Pacific Conference on Communications*, Bangkok, Thailand, October 2007.
- [15] P. Kamphikul, P. Krachodnok, and R. Wongsan, "High-Gain Antenna for Base Station Using MSA and Triangular EBG Cavity," in *The 2012 Progress in Electromagnetics Research Symposium (PIERS 2012)*, Kuala Lumpur, Malaysia, March 2012, pp. 534-537.
- [16] P. Kamphikul, P. Krachodnok, and R. Wongsan, "Gain Improvement of MSA Array for Base Station using Covered EBG," in *The 2012 Asia-Pacific Conference on Antennas and Propagation (APCAP 2012)*, Singapore, August 2012, pp. 193-194.

- [17] P. Kamphikul, P. Krachodnok, and R. Wongsan, "Beamwidth Improvement of MSA Array for Base Station Using Covered with Curved Woodpile EBG," in *Thailand-Japan MicroWave 2012 (TJMW 2012)*, Bangkok, Thailand, August 2012.
- [18] P. Kamphikul, P. Krachodnok, and R. Wongsan, "Gain Improvement of MSAs Array by Using Curved Woodpile EBG and U-shaped Reflector," in *The 2014 International Electrical Engineering Congress (IEECON 2014)*, Pattaya City, Thailand, March 2014.
- [19] A.R. Weily, L. Horvath, K.P. Esselle, B. Sanders, and T. Bird, "A planar resonator antenna based on woodpile EBG material," *IEEE Transactions on Antennas and Propagation*, Vol. 53, No. 1, 2005, pp. 216–223.
- [20] Y. Lee, X. Lu, Y. Hao, S. Yang, J.R.G. Evans, and C.G. Parini, "Low profile directive millimeter-wave antennas using free formed three-dimensional (3D) electromagnetic band gap structures," *IEEE Transactions on Antennas and Propagation*, Vol. 57, No. 10, 2009, pp. 2893–2903.
- [21] Y. Lee, X. Lu, Y. Hao, S. Yang, J.R.G. Evans, and C.G. Parini, "Narrow-beam azimuthally omni-directional millimetre-wave antenna using free formed cylindrical woodpile cavity," *IET Microwaves, Antennas and Propagation*, Vol. 4, No. 10, 2010, pp. 1491–1499.
- [22] R. Wongsan, P. Krachodnok, and P. Kamphikul, "A Sector Antenna for Mobile Base Station using MSA Array with Curved Woodpile EBG," *Open Journal of Antennas and Propagation (OJAPr)*, Vol.2, No.1, 2014, pp. 1-8.



P.Kamphikul was born in Nakhon Ratchasima, Thailand, in 1984. She received the B.Eng. degree, the first class honors, and the M. Eng. degree in telecommunication engineering from Suranaree University of Technology, Thailand, in 2007 and 2009, respectively. She is currently working toward the Ph.D. degree in telecommunication engineering at Suranaree University of Technology.

Her research interests include electromagnetic theory, antenna engineering and Electromagnetic Band Gap.



P.Krachodnok was born in KhonKaen, Thailand, in 1974. She received the B.Eng. degree in telecommunication engineering from Suranaree University of Technology, Thailand, in 1997, M. Eng. degree in Electrical Engineering from Chulalongkorn University, Thailand, in 2001, and D.Eng. degree in telecommunication engineering from Suranaree University of Technology, Thailand, in 2008.

She received the APCC2007 Best paper award, IEEE Asia-Pacific Conference on Communications, Bangkok, Thailand. She is the reviewer of IEEE Conference. Her research interests are Electromagnetic Theory, Microwave Engineering, Antenna Engineering, and Electromagnetic Band Gap.

Assist Prof. Dr. Krachodnok is the member of the Electrical Engineering/Electronics, Computer, Telecommunications and Information Technology Association (ECTI) and The Institute of Electronics, Information and Communication Engineers (IEICE).



R.Wongsan was born in Rayong, Thailand, in 1964. He received his B.Eng. degree in Electronics Engineering at Rajamangala Institute of Technology in 1989, Thewes campus, M.Eng. degree in Electrical Engineering at King Mongkut's Institute of Technology, North Bangkok (KMITNB) in 1994, and D.Eng. degree in Electrical Engineering at King Mongkut's Institute of Technology Ladkrabang (KMITL) in 2003.

At present, he is the reviewer of many journals related to the electromagnetic applications society. His almost researches are in the antenna theory and electromagnetic applications. Currently, his research interests are the utilization of the Electromagnetic Band Gap for the efficiency improvement of conventional antennas and microwave devices.

Assoc. Prof. Dr. Wongsan is the member of the Electrical Engineering/Electronics, Computer, Telecommunications and Information Technology Association (ECTI) and The Institute of Electronics, Information and Communication Engineers (IEICE).

High-gain Antenna for Base Station Using MSA and Triangular EBG Cavity

P. Kamphikul, P. Krachodnok, and R. Wongsan

School of Telecommunication Engineering, Institute of Engineering
Suranaree University of Technology, Nakhon Ratchasima, Thailand

Abstract— This paper presents a high-gain antenna using microstrip antenna (MSA) with triangular Electromagnetic Band Gap (EBG) cavity for mobile base station. The advantages of this proposed antenna are light weight, easy fabrication and installation. Moreover, it provides the moderately high gain compare to the other antennas in the cellular phone system at present. The paper also presents the procedures of the 3-element MSA and triangular EBG cavity design. A Computer Simulation Technology (CST) software has been used to compute the return loss, VSWR, radiation pattern, and gain of the antenna. The azimuth patterns of the proposed antenna can cover 360 degree of user's areas according to our requirement. The bandwidth, at S_{11} (-10 dB), is between 1920 to 2170 MHz with a gain more than 10 dB of each element.

1. INTRODUCTION

Recently, the development of the antennas with new performances becomes currently imperatively essential for the new services and network of telecommunication. It's a matter of the technology of EBG structure, a new technology for the improvement of the performances of antenna, applicable on a frequential spectrum extremely wide covered from the acoustic until the optical frequencies [1] Microstrip antennas (MSA) are an attractive choice for many modern communication systems due to their light weight, low profile with conformability, easy to be integrated with carriers of missile and satellite [2]. Two of the major disadvantages are the low gain and very narrow impedance bandwidth due to the resonant nature of the conventional MSA. By employing, EBG structures are capable to enhance the performance of MSA in terms of gain, side lobe, back lobe level and also mutual coupling. This is due to EBG exhibits frequency band-pass and band-stop that can block surface wave excitation in the operational frequency range of the antennas [3]. The objectives in using EBG were basically either to increase the gain, to reduce the side lobe and back lobe level, to reduce the mutual coupling (S_{21}) or to produce dual band to operate at different frequencies [4]. From such advantages, this paper presents the 3-element MSA with triangular EBG cavity providing the moderately high gain suitable for mobile base station. The simulated results of the return loss, VSWR, radiation patterns, and gain of the antenna are conducted with CST software.

At first, the general approach will be presented which is including the configurations of MSA and EBG structures as shown in Section 2. In Section 3, we apply this approach into the results and discussion. Finally, the conclusions are given in Section 4.

2. MICROSTRIP ANTENNA AND EBG CONFIGURATIONS

The objective of this part is a dual band MSA design that can work in UMTS band of 2100 MHz frequency. The antenna is printed on FR4 substrate with the size of 50 mm \times 50 mm and the thickness of 1.6 mm as shown in Fig. 1 [5]. The design of a MSA is initiated by determining its patch dimension and adds stubs on original antenna as illustrated in [5]. The simulated result shows that the gain at 2.1 GHz is 2.48 dB.

The woodpile EBG material is a dielectric structure that is periodic in all three dimensions. The unit cell of this material is shown in Fig. 2 [6]. The woodpile EBG material is defined by the lattice constant or repeat distance in the horizontal plane (a), the rod width (w), the rod height (h), and the total height of the unit cell (b). Notice in Fig. 2 that consecutive layers are orthogonal to each other, and the parallel rods are offset from the rods two layers below by half a lattice constant, to obtain a four layer stacking sequence. To implement the woodpile we have used alumina rods ($\epsilon_r = 8.4$, $\tan \delta = 0.002$) that have a rectangular cross section. The lattice parameters are given as follow [6] with $a = 15.48$ mm, $w = h = 4.42$ mm, and $b = 17.70$ mm.

3. RESULTS AND DISCUSSION

The 3-element MSA, triangular EBG cavity, and PEC reflector were simulated by CST software, which uses the Finite Difference Time Domain Method (FDTD) approach in their modeling equations with the final model as shown in Fig. 3.

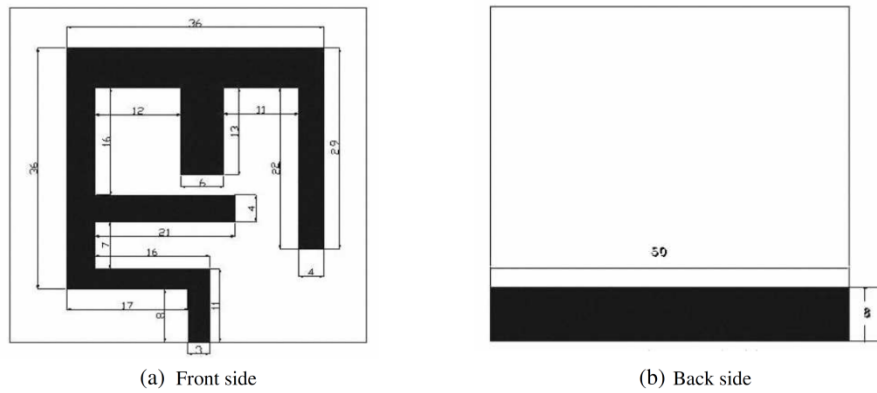


Figure 1: The geometry of the dual band MSA.

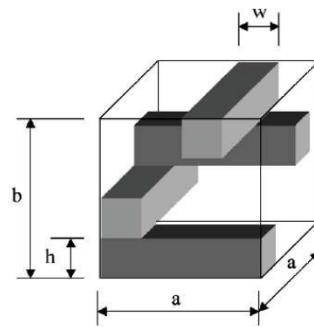


Figure 2: The unit cell for the woodpile EBG material.

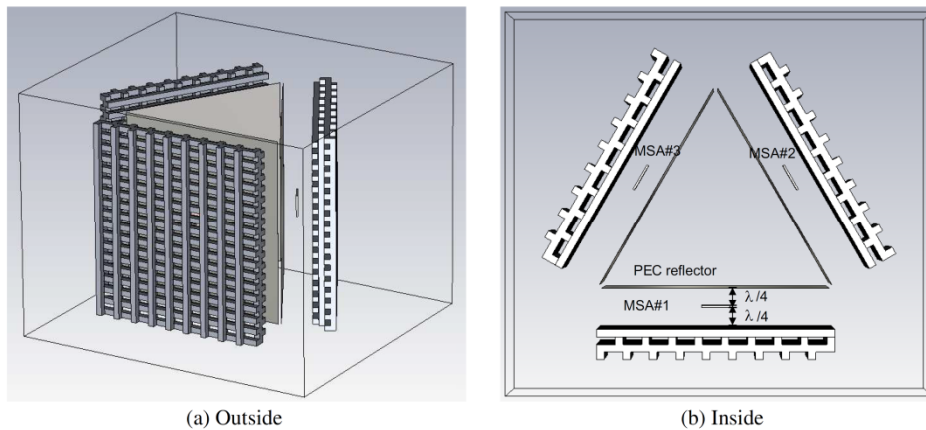


Figure 3: The 3-element MSA and triangular EBG cavity model.

The return losses of the antennas are obtained about -15 dB at the frequency of 2.1 GHz as shown in Fig. 4. Moreover as shown in Fig. 5, The VSWRs at 2.1 GHz are lower than 1.5 which are well matched antennas to the cable impedance. Also, the radiation patterns of the antennas are obtained as shown in Fig. 6 which is the azimuth patterns at 2.1 GHz. They can be observed from these radiations that the design antennas have stable radiation patterns throughout the whole operating band. The simulated results show that the gains at 2.1 GHz are 14.50 dB, 13.48 dB, and 13.43 dB of MSA#1, MSA#2, and MSA#3, respectively.

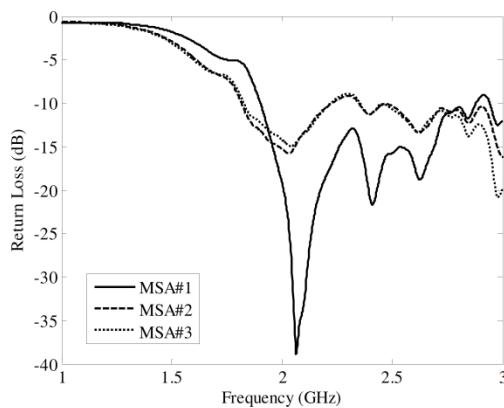


Figure 4: The return loss.

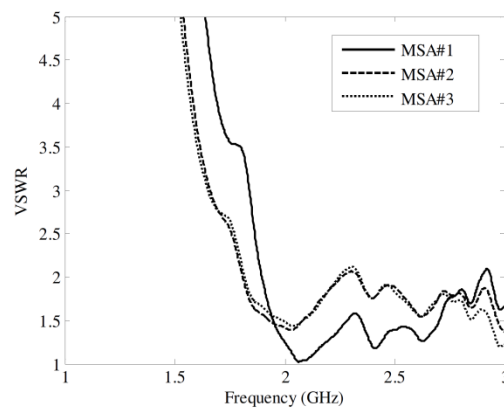


Figure 5: The VSWR.

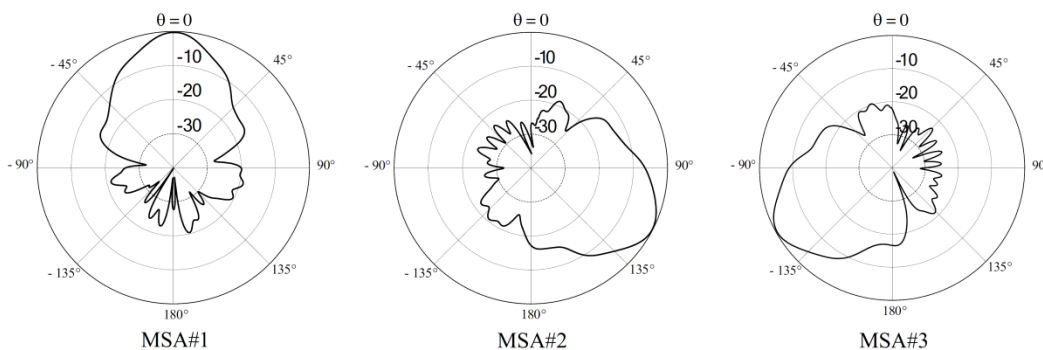


Figure 6: The azimuth pattern.

4. CONCLUSION

This paper has presented a high-gain antenna using the 3-element MSA with triangular EBG cavity. It provides the azimuth patterns that can cover user's areas according to our requirement and a high gain of 10 dB of each element. Therefore, this proposed antenna accords to the requirements and is appropriated for mobile base station. In the future, we will research to change MSA to other antennas that give the good results of gain and bandwidth.

REFERENCES

1. Elayachi, M., P. Brachat, and P. Ratajczak, "EBG identification by the reflection phase method (RPM) design for application WiFi antenna," *Proceedings EuCAP 2006*, Nice, France, Nov. 2006.
2. Zhu, L., G. Wang, X. Gao, and J. Liang, "Design of a new circular polarization broadband microstrip antenna," *Journal of Microwaves in China*, Vol. 24, 21–24, 2008.
3. Illuz, Z., R. Shavit, and R. Bauer, "Micro-strip antenna phased array with electromagnetic band-gap substrate," *IEEE Transactions on Antenna and Propagation*, Vol. 52, No. 6, 1064–1076, 1986.
4. Tan, M. N. M., T. A. Rahman, S. K. A. Rahim, M. T. Ali, and M. F. Jamlos, "Antenna array enhancement using mushroom-like electromagnetic band gap (EBG)," *Antennas and Propagation (EuCAP)*, 2010.
5. Tuan, T. M., "Design dual band microstrip antenna for next generation mobile communication," *The 2010 International Conference on Advanced Technologies for Communication*, 331–335, 2010.

Progress In Electromagnetics Research Symposium Proceedings, KL, MALAYSIA, March 27–30, 2012 537

6. Weily, A. R., L. Horvath, K. P. Esselle, B. C. Sanders, and T. S. Bird, "A planar resonator antenna based on a woodpile EBG material," *IEEE Transactions on Antennas and Propagation*, Vol. 53, No. 1, 216–223, 2005.

Gain Improvement of MSA Array for Base Station using Covered EBG

P. Kamphikul, P. Krachodnok, and R. Wongsan
 School of Telecommunication Engineering, Institute of Engineering,
 Suranaree University of Technology, Nakhon Ratchasima, Thailand
 E-mail: D5240395@g.sut.ac.th, priam@sut.ac.th, and rangsan@sut.ac.th

Abstract—This paper presents a sector antenna for mobile base station using microstrip antenna (MSA) array covered with Electromagnetic Band Gap (EBG). The advantages of this proposed antenna are light weight, easy fabrication and installation, and moderately high gain compare to the other antennas in the cellular phone system at present. Moreover, it provides a fan-shaped radiation pattern and wider in the horizontal direction. The paper also presents the procedures of a 1x4 array antenna using MSAs covered with the EBG structures design. A Computer Simulation Technology (CST) software has been used to compute the reflection coefficient (S_{11}), radiation pattern, and gain of the antenna system. The bandwidth, at S_{11} (-10 dB), is between 1920 to 2170 MHz with a gain 17.6 dB of the antenna system.

Keywords—microstrip antenna array; Electromagnetic Band Gap; base station

I. INTRODUCTION

Nowadays, the development of the antennas with new performances becomes currently imperatively essential for the new services and network of telecommunication. It's a matter of the technology of EBG structure, a new technology for the improvement of the performances of antenna, applicable on a frequential spectrum extremely wide covered from the acoustic until the optical frequencies [1]. Microstrip antennas (MSAs) are an attractive choice for many modern communication systems due to their light weight, low profile with conformability, easy to be integrated with carriers of missile and satellite [2]. Two of the major disadvantages are the low gain and very narrow impedance bandwidth due to the resonant nature of the conventional MSA. By employing, EBG structures are capable to enhance the performance of MSA in terms of gain, side lobe, back lobe level and also mutual coupling. This is due to EBG exhibits frequency band-pass and band-stop that can block surface wave excitation in the operational frequency range of the antennas [3]. The objectives in using EBG were basically either to increase the gain, to reduce the side lobe and back lobe level, to reduce the mutual coupling (S_{21}) or to produce dual band to operate at different frequencies [4]. From such advantages, this paper presents a 1x4 array antenna using MSAs covered with EBG structures providing the moderately high gain suitable for mobile base station. The simulated results of the

reflection coefficient (S_{11}), radiation pattern, and gain of the antenna are conducted with CST software.

At first, the general approach will be presented which is including the configurations of MSAs and EBG structures as shown in section 2. In section 3, we apply this approach into the results and discussion. Finally, the conclusions are given in section 4.

II. MICROSTRIP ANTENNA AND EBG CONFIGURATIONS

A. Microstrip Antenna

The objective of this part is a dual band MSA design that works in UMTS band of 2100 MHz frequency. The antenna is printed on FR4 substrate with the size of 50 mm x 50 mm and the thickness of 1.6 mm. The design of a MSA is initiated by determining its patch dimension and adding stubs on original antenna as illustrated in [5]. The simulated result shows that the gain at 2.1 GHz is 2.48 dB [6].

To improve gain characteristics, a dual band MSA will be arrayed with element spacing of $3\lambda/4$ to increase the gain as shown in Figure 1. This work proposes the design of 1x4 array of a dual band MSA. The simulated result shows that the azimuth pattern of the array antenna at 2.1 GHz with the gain of 10.28 dB is shown in Figure 5.

B. EBG Structures

The woodpile EBG material is a dielectric structure that is periodic in all three dimensions. The unit cell of this material is shown in Figure 2 [7]. Dimension the woodpile EBG material is specified by the distance in the horizontal plane (a), the rod width (w), the rod height (h), and the total height of the unit cell (b). To implement the woodpile, we have used alumina rods ($\epsilon_r = 8.4$, $\tan\delta = 0.002$) that have a rectangular cross section. The lattice parameters are given as follow [7] with $a = 0.108\lambda$, $w = h = 0.031\lambda$, and $b = 0.124\lambda$.

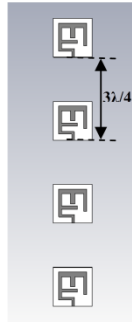


Figure 1. A 1x4 array antenna using dual band MSAs.

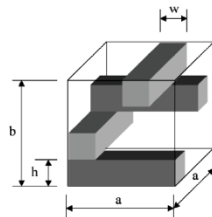
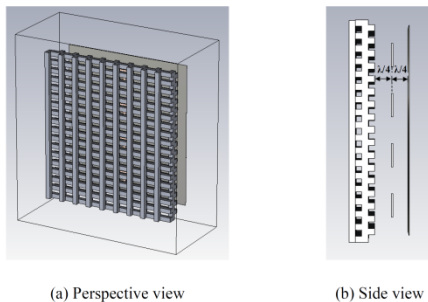


Figure 2. The unit cell for the woodpile EBG material.

III. RESULTS AND DISCUSSION

A 1x4 array antenna using MSAs, EBG structures and PEC reflector were simulated by CST software, which uses the Finite Difference Time Domain Method (FDTD) approach in their modeling equations with the final model as shown in Figure 3.



Figures 3. A 1x4 array antenna covered with EBG structures model.

The S_{11} of the antenna system is obtained about -15 dB at the frequency of 2.1 GHz which are good matching to the cable impedance as shown in Figure 4. Also, the radiation pattern of the antenna system is obtained as shown in Figure 5, which is the azimuth pattern at 2.1 GHz. It can be observed from this radiation that is a fan-shaped radiation pattern and wider in the horizontal direction. The simulated result shows that the gain at 2.1 GHz is 17.6 dB.

IV. CONCLUSION

This paper has presented a sector antenna of a 1x4 array antenna using MSAs covered with EBG structures. It provides a fan-shaped radiation pattern according to our requirement and a high gain of 17.6 dB. Therefore, this

proposed antenna accords to the requirements and is appropriated for a sector antenna of mobile base station.

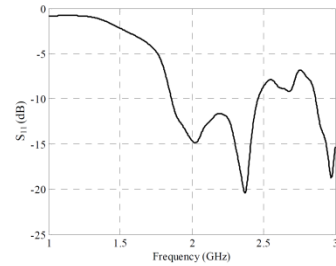


Figure 4. The S_{11} of MSA array with EBG.

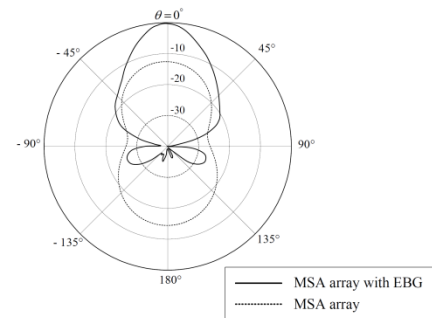


Figure 5. The radiation patterns of MSA array with and without EBG (azimuth pattern) at 2.1 GHz.

REFERENCES

- [1] M. Elayachi, P. Brachet, and P. Ratajczak, "EBG Identification by the Reflection Phase Method (RPM) Design for Application WiFi Antenna," in Proceedings EuCAP 2006, Nice, France, 2006.
- [2] L. ZHU, G. WANG, X. GAO, and J. LIANG, "Design of a New Circular Polarization Broadband Microstrip Antenna," Journal of Microwaves in China, vol. 24, pp. 21-24, 2008.
- [3] Z. Illuz, R. Shavit and R. Bauer, "Micro-strip Antenna Phased Array with Electromagnetic Band-Gap Substrate," IEEE Transactions on Antenna and Propagation, Vol. 52, No 6, pp. 1064-1076, 1986.
- [4] M.N.Md. Tan, T.A. Rahman, S.K.A. Rahim, M.T. Ali and M.F. Jamlos, "Antenna Array Enhancement using Mushroom-Like Electromagnetic Band Gap (EBG)," in Antennas and Propagation (EuCAP), 2010.
- [5] T.M. Tuan, "Design Dual Band Microstrip Antenna For Next Generation Mobile Communication," in The 2010 International Conference on Advanced Technologies for communication, pp. 331-335, 2010.
- [6] P. Kamphikul, P. Krachodnok, and R. Wongsan, "High-Gain Antenna for Base Station Using MSA and Triangular EBG Cavity," in Progress In Electromagnetics Research Symposium (PIERS), Kuala Lumpur, Malaysia, 2012.
- [7] A. R. Weily, L. Horvath, K. P. Esselle, B. C. Sanders, and T. S. Bird, "A Planar Resonator Antenna Based on a Woodpile EBG Material," IEEE Transactions on Antennas and Propagation, Vol. 53, No. 1, pp. 216 - 223, 2005.

Beamwidth Improvement of MSA Array for Base Station Using Covered with Curved Woodpile EBG

Paowphattra KAMPHIKUL, Piyaporn KRACHODNOK and Rangsan WONGSAN

School of Telecommunication Engineering, Institute of Engineering,

Suranaree University of Technology, Nakhon Ratchasima, Thailand

E-mail: D5240395@g.sut.ac.th, priam@sut.ac.th, and rangsan@sut.ac.th

Abstract This paper presents a sector antenna for mobile base station using microstrip antenna (MSA) array covered with curved woodpile Electromagnetic Band Gap (EBG). The advantages of this proposed antenna are light weight, easy fabrication and installation, and high gain. Moreover, it provides a fan-shaped radiation pattern and wider in the H-Plane. The half-power beamwidth (HPBW) in the H-Plane and E-Plane are 62 and 18 degree, respectively. The paper also presents the procedures of a 1x4 array antenna using MSAs covered with curved woodpile EBG structures design. A Computer Simulation Technology (CST) software has been used to compute the reflection coefficient (S_{11}), radiation patterns, and gain of the antenna system. The bandwidth, at S_{11} (-10 dB), is between 1.920 to 2.170 GHz with a gain 15 dB of the antenna system.

Keyword Microstrip Antenna Array, Electromagnetic Band Gap, Base Station

1. INTRODUCTION

Nowadays, the development of the antennas with new performances becomes currently imperatively essential for the new services and network of telecommunication. It's a matter of the technology of Electromagnetic Band Gap (EBG) structure, a new technology for the improvement of the performances of antenna, applicable on a frequential spectrum extremely wide covered from the acoustic until the optical frequencies. Microstrip antennas (MSAs) are an attractive choice for many modern communication systems due to their light weight, low profile with conformability, easy to be integrated with carriers of missile and satellite [1]. Two of the major disadvantages are the low gain and very narrow impedance bandwidth due to the resonant nature of the conventional MSA. By employing, EBG structures are capable to enhance the performance of MSA in terms of gain, side lobe, back lobe level and also mutual coupling. This is due to EBG exhibits frequency band-pass and band-stop that can block surface wave excitation in the operational frequency range of the antennas [2]. From such advantages, this paper presents a 1x4 array antenna using MSAs covered with curved woodpile EBG structures providing the high gain and beamwidth suitable for mobile base station. The simulated results of the reflection coefficient (S_{11}), radiation patterns, and gain of the antenna are conducted with CST software.

2. MICROSTRIP ANTENNA AND CURVED WOODPILE EBG CONFIGURATIONS

2.1. MICROSTRIP ANTENNA

The objective of this part is a dual band MSA design that works in UMTS band of 2100 MHz frequency. The antenna is printed on FR4 substrate with the size of 50 mm x 50 mm and the thickness of 1.6 mm. The design of a MSA is initiated by determining its patch dimension and adding stubs on original antenna as illustrated in [3]. The simulated result shows that the gain at 2.1 GHz is 2.48 dB [4].

To improve gain characteristics, a dual band MSA will be arrayed with element spacing of $3\lambda/4$ to increase the gain as shown in Fig.1. This work proposes the design of 1x4 array of a dual band MSA. The simulated result shows that the radiations pattern of the array antenna at 2.1 GHz with the gain of 10.28 dB is shown in Fig.5. The main lobe of each plane is 180 degree, although the half-power beamwidth (HPBW) in the H-Plane and E-Plane are 108 and 17 degree, respectively.

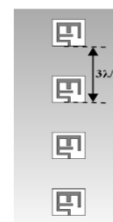


Fig.1. A 1x4 array antenna using dual band MSAs.

2.2. CURVED WOODPILE EBG STRUCTURES

This paper applies a similar geometry as in the planar woodpile EBG structures to design the curved woodpile EBG structures as shown Fig.2 [5]. The

parameters for the curved woodpile EBG are the filament thickness (w), the inner (R_1) and outer (R_2) radii, the height (h), the number of radial filaments (N_{rad}), and the number of rings (N_{ring}) of the curved. To implement the curved woodpile EBG, we have used alumina rods ($\epsilon_r = 8.4$, $\tan\delta = 0.002$) that have a rectangular cross section. The parameters are given as follow [5] with $w = 0.133\lambda$, $R_1 = 12\lambda$, $R_2 = 12.27\lambda$, $h = 3.36\lambda$, $N_{rad} = 5$, and $N_{ring} = 2$.

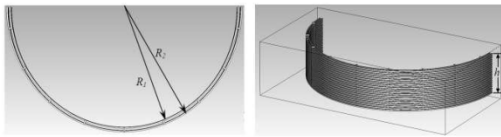


Fig.2. The geometry of the curved woodpile EBG structures.

3. RESULTS AND DISCUSSION

A 1×4 array antenna using MSAs, curved woodpile EBG structures and PEC reflector were simulated by CST software as shown in Fig.3.

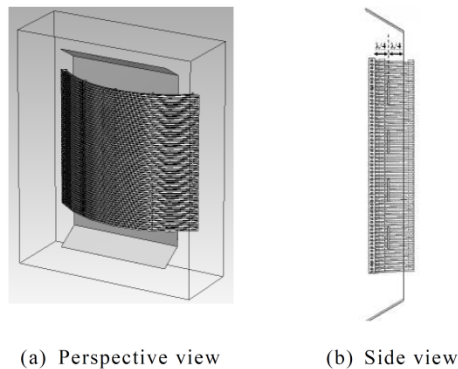


Fig.3. A 1×4 array antenna covered with curved woodpile EBG structures model.

The S_{11} of the antenna system is lower than -10 dB which is between 1.9 to 2.4 GHz. as shown in Fig.4. Fig.5. shows the radiation patterns at 2.1 GHz. of the antenna system. It can be observed from this radiation pattern in the horizontal direction that is a fan-shaped radiation pattern and wider. Also, the HPBW in the H-Plane and E-Plane are 62 and 18 degree, respectively. The simulated result shows that the gain at 2.1 GHz is 15 dB.

4. CONCLUSION

This paper has presented a sector antenna of a 1×4 array antenna using MSAs covered with curved

woodpile EBG structures. It provides a fan-shaped radiation pattern in the horizontal direction according to our requirement and a high gain of 15 dB. Therefore, this proposed antenna accords to the requirements and is appropriated for a sector antenna of mobile base station.

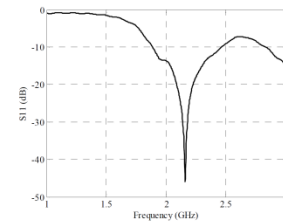


Fig.4. The S_{11} of MSA array with EBG structures.

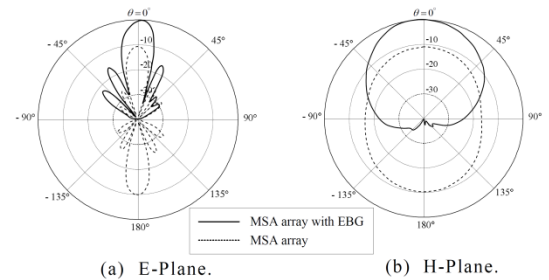


Fig.5. The radiation patterns of MSA array with and without EBG structures at 2.1 GHz.

5. References

- [1] L. ZHU, G. WANG, X. GAO, and J. LIANG, "Design of a New Circular Polarization Broadband Microstrip Antenna," *Journal of Microwaves in China*, vol. 24, pp. 21-24, 2008.
- [2] Z. Illuz, R. Shavit and R. Bauer, "Micro-strip Antenna Phased Array with Electromagnetic Band-Gap Substrate," *IEEE Transactions on Antenna and Propagation*, Vol. 52, No 6, pp. 1064-1076, 1986.
- [3] T.M. Tuan, "Design Dual Band Microstrip Antenna For Next Generation Mobile Communication," The 2010 International Conference on Advanced Technologies for communication, pp. 331-335, 2010.
- [4] P. Kamphikul, P. Krachodnok, and R. Wongsan, "High-Gain Antenna for Base Station Using MSA and Triangular EBG Cavity," The 31st PIERS, Kuala Lumpur, Malaysia, 2012.
- [5] S. Kampeephat, P. Krachodnok, and R. Wongsan, "High-Gain and Light-Weight Antenna for Radar System Using a Horn Covered with Curved Woodpile EBG," The 31st PIERS, Kuala Lumpur, Malaysia, 2012.

Gain Improvement of MSAs Array by Using Curved Woodpile EBG and U-shaped Reflector

Rangsan Wongsan, Piyaporn Krachodnok, and Paowphattra Kamphikul
 School of Telecommunication Engineering, Institute of Engineering,
 Suranaree University of Technology, Nakhon Ratchasima, Thailand
 rangsan@sut.ac.th, priam@sut.ac.th, andD5240395@g.sut.ac.th

Abstract— Gain improvement of a sector antenna of base station for mobile phone using microstrip antenna (MSA) array with curved woodpile Electromagnetic Band Gap (EBG) is presented. The advantages of this proposed antenna are easy fabrication and installation, high gain, and light weight. Moreover, it provides a fan-shaped radiation pattern and wider in the horizontal direction, which appropriate for mobile phone base station. The half-power beam widths in the H-plane and E-plane are 40 and 8 degrees, respectively. The paper also presents the design procedures of a 1x8 array antenna using MSAs associated with U-shaped reflector for decreasing their back and side lobes. A Computer Simulation Technology (CST) software has been used to compute the reflection coefficient (S_{11}), radiation patterns, and gain of this antenna. The bandwidth, at S_{11} (-10 dB), is enough which can be well utilized for 3G base station, with a gain 20 dB.

Index Terms— Microstrip antenna, Electromagnetic Band Gap, Base station.

I. INTRODUCTION

Nowadays, the development of the antennas with new performances becomes currently essential for the new services and networks of telecommunication. Microstrip antennas (MSA) are an attractive choice for many modern communication systems due to their light weight, low profile with conformability, and low cost [1-2]. In principle, the MSA is a resonant type of antenna, where the antenna size is determined by the operating wavelength and the bandwidth is determined by the Q factor of the resonance. Two of the major disadvantages are the low gain and very narrow impedance bandwidth due to the resonant nature of the conventional MSA.

Many new technologies have emerged in the modern antenna design arena and one exciting breakthrough is the development of Electromagnetic Band Gap (EBG) structures. The applications of EBG structures in antenna designs have become a thrilling topic for antenna engineering [3]. It's a matter of the technology of EBG structure, a new technology for the improvement of the performances of antenna, applicable on a frequential spectrum extremely wide covered from the acoustic until the optical frequencies [4]. By employing, EBG structures are capable to enhance the performance of MSA in terms of gain, side lobe level, back lobe level and also mutual coupling. This is due to EBG exhibits frequency band-pass and band-stop that can block

surface wave excitation in the operational frequency range of the antennas [5]. From such advantages, this paper presents a 1x8 array antenna using MSAs covered with curved woodpile EBG structures providing the moderately high gain suitable for mobile base station. The simulated results of the reflection coefficient (S_{11}), radiation pattern, and gain of the antenna are conducted with CST software.

At first, the general approach will be presented which is including the configurations of MSAs and EBG structures as shown in section II. In section III, we apply this approach into the results and discussion. Finally, the conclusions are given in section IV.

II. MSAs AND EBG CONFIGURATIONS

A. MSAs Configurations

The circular MSA [6] designed for working in the Universal Mobile Telecommunications System (UMTS) band of 2.1 GHz frequency is used for the prototype for this proposed antenna. The antenna is printed on FR4 substrate with the size of 60 mm x 60 mm and the thickness of 1.6 mm. A circular MSA structure consists of the circular patch of the radius a . This gap of distance t between the microstrip line length L_2 is used for adjusting the impedance matching. These structures mounted on the dielectric substrate with the dielectric constant of ϵ_r and the height h . The substrate is located on the ground plane of the width W and the length L . This ground plane is cut to form the wide-slot ground plane (Size $W_1 \times L_1$). The design of a MSA is based on the conventional transmission line model at 2.1 GHz. The desired bandwidth is 1.920 – 2.170 GHz. The microstrip line is designed to provide 50 Ohm at the operating frequency of 2.1 GHz.

To enhance gain characteristic, a circular MSA will be arrayed with element spacing of $3\lambda/4$ (antenna type A) as shown in Fig. 1. Moreover, this paper adds a U-shaped reflector with the size of 400 mm x 1,000 mm at back side of MSAs array to control the radiation pattern to be the directional pattern. Figure 2 shows a 1x8 array of circular MSAs and U-shaped reflector (antenna type B). The simulated results show that the radiation patterns of the antenna type A and type B at 2.1 GHz with the gain of 14 and 17.83 dB, respectively. The Half-Power Beamwidth (HPBW) in the H-Plane and E-Plane, the azimuth pattern: the evaluation

pattern (AZ:EL), of the array antenna *type A* and *type B* are $97^\circ:8^\circ$ and $89^\circ:8^\circ$, respectively.

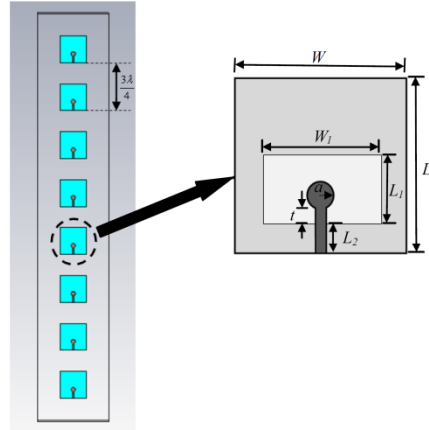


Fig. 1. A 1×8 array of circular MSAs (antenna *type A*).

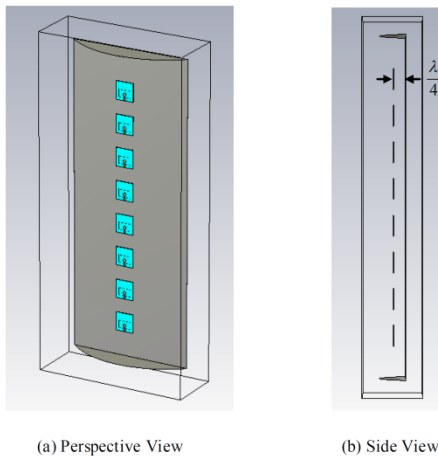


Fig. 2. A 1×8 array of circular MSAs and U-shaped reflector (antenna *type B*).

B. EBG Configurations

This paper applies the similar geometry of the planar [7–8] and the cylindrical woodpile EBG structures [9] to be the sector of curved woodpile EBG structures. Figure 3 shows the geometry of the curved woodpile EBG structures with two layers of the different diameters. The parameters for these structures are the filament thickness or diameter (w), the inner (R_1) and outer (R_2) radii, the height (h), the number of radial filaments (N_{rad}), and the number of rings (N_{ring}) of the curved. To implement the curved woodpile EBG, we have used

alumina rods ($\epsilon_r = 8.4$, $\tan\delta = 0.002$) that have a rectangular cross section. The parameters are given as follow [10] with $w = 0.13\lambda$, $R_1 = 14.4\lambda$, $R_2 = 14.7\lambda$, $h = 13.4\lambda$, $N_{rad} = 3$, and $N_{ring} = 2$.

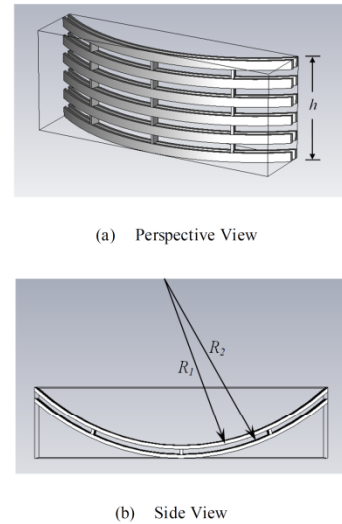


Fig. 3. The geometry of the curved woodpile EBG structures.

III. RESULTS AND DISCUSSION

A 1×8 array of circular MSAs and U-shaped reflector improved gain with curved woodpile EBG structures (antenna *type C*) was simulated by CST software as shown in Fig. 4.

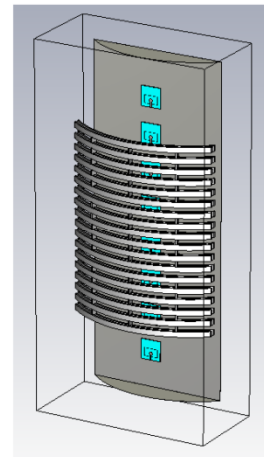


Fig. 4. A 1×8 array of circular MSAs and U-shaped reflector improved gain with curved woodpile EBG structures (antenna *type C*).

The S_{11} (-10 dB) of the antenna *type A*, *type B*, and *type C*, covered 1.920 to 2.170 GHz, are enough which can be well utilized for 3G base station as shown in Fig. 5. Figure 6 shows the radiation patterns at 2.1 GHz of the antenna *type A*, *type B*, and *type C*. From this radiation patterns in the H-plane, we found that the radiation patterns of the antenna *type B* and *type C* that are a fan-shaped radiation pattern. Although its HPBW of the antenna *type C* will narrow, but it can cover the desire area of base station for mobile phone and provide a high gain. Also, the HPBW, the Side Lobe Level (SLL), and the gain of the antenna *type A*, *type B*, and *type C* as shown in Table I.

TABLE I. RESULTS OF SIMULATION.

Parameters	Antenna <i>type A</i>	Antenna <i>type B</i>	Antenna <i>type C</i>
The HPBW (AZ:EL)	97°:8°	89°:8°	40°:8°
The H-plane SLL	-	-30.6 dB	-26.2 dB
The E-plane SLL	-12.9 dB	-13.2 dB	-14.4 dB
The Gain	14 dB	17.83 dB	20 dB

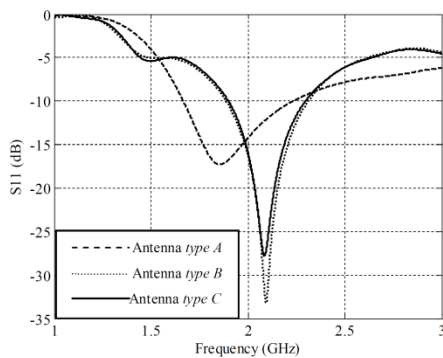
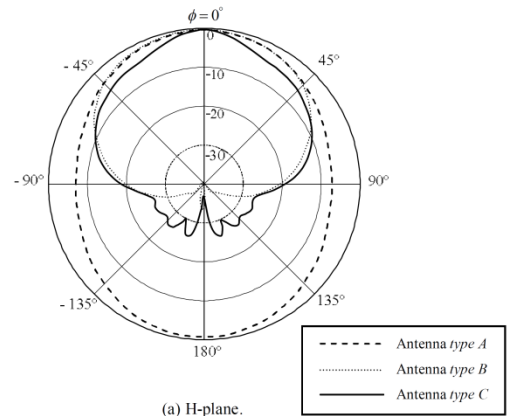


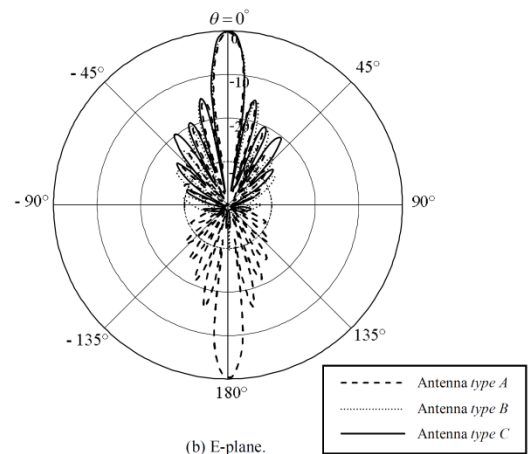
Fig.5. The S_{11} of the antenna *type A*, *type B*, and *type C*.

IV. CONCLUSION

This paper has presented a sector antenna of a 1×8 array of circular MSAs and U-shaped reflector improved gain with curved woodpile EBG structures. It provides a fan-shaped radiation pattern in the horizontal direction according to our requirement and a high gain of 20 dB. Therefore, this proposed antenna accords to the requirements and is appropriated for a sector antenna of mobile base station.



(a) H-plane.



(b) E-plane.

Fig.6. The radiation patterns at 2.1 GHz of the antenna *type A*, *type B*, and *type C*.

ACKNOWLEDGMENT

This work was supported by the Research Department Institute of Engineering, Suranaree University of Technology, Nakhonratchasima, Thailand.

REFERENCES

- [1] J.J. Bahl and P. Bhartia, *Microstrip Antennas*. Artech House, 1980.
- [2] P. Bhartia, Inder Bahl, R. Garg, and A. Ittipipoon, *Microstrip Antennas Design Handbook*. Artech House, 2000.
- [3] F. Yang and Y. Rahmat-Samii, *Electromagnetic Band Gap Structures in Antenna Engineering*. New York, Cambridge University Press, 2009.
- [4] M. Elayachi, P. Brachat, and P. Ratajczak, "EBG Identification by the Reflection Phase Method (RPM) Design for Application WiFi Antenna," in *Antenna and Propagation, EuCAP 2006*, Nice, France, November 2006.
- [5] Z. Illuz, R. Shavit and R. Bauer, "Micro-strip Antenna Phased Array with Electromagnetic Band-Gap Substrate," *IEEE Trans. Antennas Propagat.*, Vol. 52, No 6, pp. 1064–1076, 1986.
- [6] Y. Chawanonphithak and C. Phongcharoenpanich, "An Ultra-wideband Circular Microstrip Antenna fed by Microstrip Line above Wide-Slot Ground Plane," in *The Asia-Pacific Conference on Communications*, 2007.
- [7] A.R. Weily, L. Horvath, K.P. Esselle, B. Sanders, and T. Bird, "A planar resonator antenna based on woodpile EBG material," *IEEE Trans. Antennas Propagat.*, Vol. 53, No. 1, pp. 216–223, 2005.
- [8] Y. Lee, X. Lu, Y. Hao, S. Yang, J.R.G. Evans, and C.G. Parini, "Low profile directive millimeter-wave antennas using free formed three-dimensional (3D) electromagnetic bandgap structures," *IEEE Trans. Antennas Propagat.*, Vol. 57, pp. 2893–2903, 2009.
- [9] Y. Lee, X. Lu, Y. Hao, S. Yang, J.R.G. Evans, and C.G. Parini, "Narrow-beam azimuthally omni-directional millimetre-wave antenna using freeformed cylindrical woodpile cavity," *IET Microw. Antennas Propagat.*, Vol. 4, Iss. 10, pp. 1491–1499, 2010.
- [10] P. Kamphikul, P. Krachodnok, and R. Wongsan, "Beamwidth Improvement of MSA Array for Base Station Using Covered with Curved Woodpile EBG," in *Thailand-Japan MicroWave 2012*, Bangkok, Thailand, August, 2012.

Omnidirectional High-Gain Wide Slot Antenna Array for Mobile Phone Base Station

Peerasan Kumsalee, Paowphattra Kamphikul, Piyaporn Krachodnok, and Rangsan Wongsan
School of Telecommunication Engineering, Institute of Engineering,
Suranaree University of Technology, Nakhon Ratchasima, Thailand
mpeerasan.k@gmail.com, D5240395@g.sut.ac.th, priam@sut.ac.th, and rangsan@sut.ac.th

Abstract—This paper proposes an omnidirectional high-gain slot array antenna for mobile phone base station. The advantages of this proposed antenna are low profile, light weight, and easy fabrication and installation. Moreover, it provides not only the moderately high gain but also the omnidirectional pattern, which more appropriate for mobile phone base station. The half-power beamwidths in E-plane is around 24 degrees, while its radiation pattern is similar to the circle or omnidirection. The paper also presents the design procedures of a 1×4 array antenna using slot antennas associated with two side-wings for increasing its gain. A Computer Simulation Technology (CST) software has been used to compute the reflection coefficient (S_{11}), radiation patterns, and gain of this antenna. The bandwidth, at S_{11} (-10 dB), is which can be well utilized for 3G base station, with a gain around 9 dB.

Keywords—slot antenna; omnidirectional pattern; base station

I. INTRODUCTION

In many areas of wireless communications are not only required sector antennas but also can be used omnidirectional antennas such as monopole antenna. The monopole antenna [1]-[2], its broadband characteristics and simple construction, is perhaps to most common antenna element for portable equipment such as cellular telephone, cordless telephones, and automobiles. However, if the monopole antenna is designed correctly, it will provide excellent performance. While its significant disadvantages such as: susceptibility to damage, additional manufacturing cost, and potential performance degradation due to the user's interaction with the exposed antenna still be concerned. In this paper the slot antenna has been selected to modify for yielding the omnidirectional pattern for wireless communications due to light weight, low profile with conformability and low cost [3]-[9]. From such advantages, this paper presents a broadside array of a 1x4 array antenna using slot antennas associated with providing omnidirectional radiation pattern and moderately high gain suitable for mobile base station. The simulated results of the reflection coefficient (S_{11}), radiation patterns, and gain of the antenna are conducted with CST software.

Many applications, they are desirable to have the maximum radiation of an array directed normal to axis of

the array broadside; $\theta_0 = 90^\circ$. To optimize the design, the maximum of the single element and of the array factor should both be directed toward $\theta_0 = 90^\circ$. The requirements of the single element can be accomplished by the judicious choice of the radiator and those of the array factor by the proper separation and excitation of the individual radiators. Thus for a uniform array with $\beta = 0$ and $d = n\lambda$, in addition to have the maxima of the array factor directed broadside ($\theta_0 = 90^\circ$) to the axis of the array [10].

At first, the general approach will be presented which including the configurations of slot antennas as shown in section II. In section III, we apply this approach into the results and discussion. Finally, the conclusions are given in section IV.

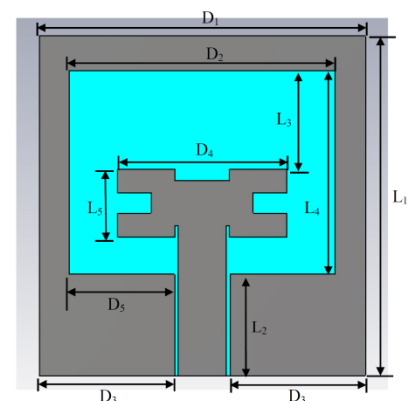


Fig.1. The configuration of single slot antenna.

II. SLOT ANTENNAS CONFIGURATIONS

In this paper, we used an antenna prototype in [11] as shown in Fig.1 for developing to be array. This prototype antenna was designed for working in the Universal Mobile Telecommunications System (UMTS) band of 2.1 GHz frequency. Such antenna was printed on FR4 substrate ($\epsilon_r = 4.5$, $\tan\delta = 0.02$) with the size of 50 mm x 48 mm and

the thickness of 1.6 mm. The coplanar waveguide fed line was designed to provide 50 Ohm connected to SMA connector and the distance gap of 6 mm and 0.48 mm, respectively. The dimensions of this antenna are shown in Table I. The simulated results in [11] show the radiation patterns of single slot antenna at 2.1 GHz yielded the gain of 3.3 dB and provided the radiation pattern (at frequency band 1.92-2.17 GHz) in H-plane similar to omnidirection as shown in Fig.8, 9, and 10, although some directions have lower radiation. This is the main reason that we brought this antenna model to be the elements of our array.

TABLE I. THE DIMENSIONS OF SLOT ANTENNA.

Parameters	Sizes	Parameters	Sizes
D ₁	48 mm	L ₁	50 mm
D ₂	43 mm	L ₂	12 mm
D ₃	7.42 mm	L ₃	7.72 mm
D ₄	15 mm	L ₄	30 mm
D ₅	15.84 mm	L ₅	10 mm
D _{TR}	6 mm	h	1.6 mm
W	5 mm	L	50 mm
A	8 mm	B	4.5 mm
C ₁	3.5 mm	C ₂	3 mm
C ₃	1.7 mm		

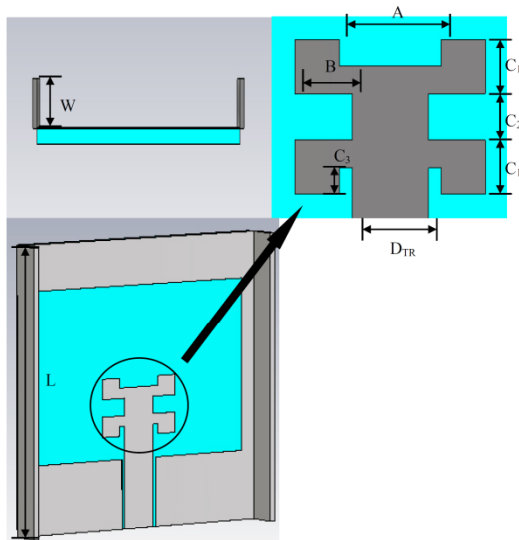


Fig.2. The single slot antenna with two side-wings.

III. RESULTS AND DISCUSSION

To improve gain and radiation pattern characteristics, at first, a wide slot antenna will be added with two small wings made from metal, which are located on the left and right sides of antenna as shown in Fig.2. The proper dimension for each wing is optimized at $3 \times 5 \times 50 \text{ mm}^3$. The design of main slot antenna is based on the conventional transmission line model at the operating frequency at 2.1 GHz [11]. The simulated results of a slot antenna with two side-wings show its gain is around 4 dB and still provide the radiation pattern in H-plane similar to the circle as shown in Figure as shown in Fig.8, 9, and 10.

Finally, to enhance the gain characteristic, four wide slot antennas with two side-wings have been arrayed with element spacing of 0.52λ as shown in Fig.3. The simulated results of the array of 1×4 slot antennas with two side-wings show the gain around 9 dB and still provide the radiation pattern in H-plane similar to the circle as well, as shown in Fig.8, 9, and 10. Furthermore, the values of S_{11} (-10 dB) of three types of antennas are compared each other in Fig.4. We found that the frequency bandwidth of the proposed antenna array still cover the required frequency from 1.92-2.17 GHz, which are enough for utilizing for 3G mobile phone base station.

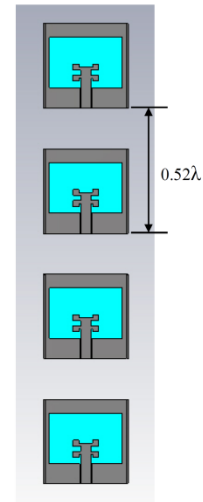


Fig.3. A 1×4 array of slot antennas with two side-wings.

The fabricated prototype is shown in Fig.5. All the measurements have been performed in shielded anechoic chamber, using a Hewlett Packard Network Analyzer (HP8772D) vector network analyzer. The S_{11} (-10 dB) of a 1×4 array of slot antennas with two side-wings are enough which can be well utilized for 3G base station as shown in Fig.6. It has been observed that the antenna resonates

at 2.1 GHz; at this frequency, the measured magnitude of the reflection parameter is -13.432 dB.

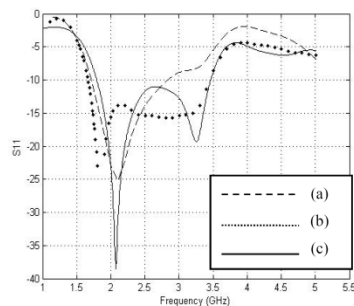


Fig.4. The S_{11} of (a) a single slot antenna, (b) a single slot antenna with two side-wings, and (c) a 1×4 array of slot antennas with two side-wings.

Fig.7 shows the radiation patterns at 2.1 GHz of 1×4 array of slot antennas with two side-wings. From this radiation patterns in the H-plane, we found that the radiation patterns are similar to the circle or omnidirection. The measured gains of a single slot antenna with two side-wings and a 1×4 array of slot antennas with two side-wings are 3.9 dB and 8.39 dB, respectively.

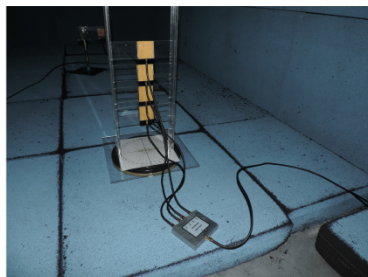


Fig.5. The fabricated prototype of 1×4 array of slot antennas with two side-wings.

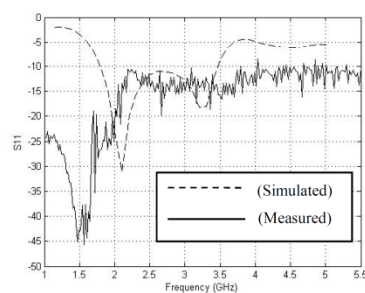


Fig.6. Measured and simulated S_{11} of 1×4 array of slot antennas with two side-wings.

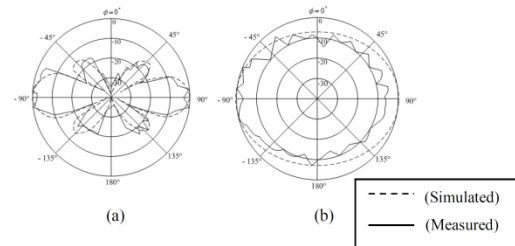


Fig.7. Measured and simulated radiation patterns at 2.1 GHz in (a) E-plane and (b) H-plane.

IV. CONCLUSION

This paper presented the omnidirectional high-gain slot array antenna for 3G mobile phone base station. The slot antenna invested with the initial gain 3.3 dB from single slot antenna and has been modified by adding two side-wings on the left and right sides of slot antenna. After that four slot antennas has been arrayed to be the broadside radiation of 1×4 elements with such side-wings for increasing gain from 3.3 dB to be around 9 dB, approximately and provide the omnidirectional pattern which is appropriated for the mobile phone base station.

ACKNOWLEDGMENT

This research work was supported by the Research Department Institute of Engineering, Suranaree University of Technology, Nakhon Ratchasima, Thailand.

REFERENCES

- [1] Kin-Lu Wong, Gwo-Yun Lee, Tzung-Wern Chiou, "A Low-Profile Planar Monopole Antenna for Multiband Operation of Mobile Handsets," *IEEE Trans. Antennas Propagat.*, Vol.51, No 1, pp. 121-125, January 2003.
- [2] Chen, I. F., Peng, C. M. and Liang, S. C., "Single Layer Printed Monopole Antenna for Dual ISM-Band Operation," *IEEE Trans. Antennas Propagat.* 53(2), pp. 1270-1273, 2005.
- [3] Marek Kitliński, Tomasz Borodo., "Single Layer Printed Monopole Antenna for Dual ISM-Band Operation," *Gdańsk University of Technology, Gdańsk*, 2006.
- [4] Jen-Fen Huang., "A Simple Model of Designing CPW-Fed Slot Antenna," *IEEE*, pp. 577-580, 2000.
- [5] Chen, I. F., Peng, C. M. and Liang, S. C., "Broadband cross-shaped microstrip-fed slot antenna," *Electron. Lett.* Vol.36, No 25, pp. 2056-2057, 7 December 2000.
- [6] Jyh-Ying Chiou, Jia-Yi Sze, Kin-Lu Wong., "A Broad-Band CPW-Fed Strip-Loaded Square Slot Antenna," *IEEE Trans. Antennas Propagat.*, Vol.51, No 4, pp. 719-721, April 2003.
- [7] Horng-Dean Chen., "Broadband CPW-Fed Square Slot Antennas With a Widened Tuning Stub," *IEEE Trans. Antennas Propagat.*, Vol.51, No 8, pp. 1982-1986, 8 August 2003.
- [8] Chien-Jen Wang, Jin-Jei Lee., "A Pattern-Frequency-Dependent Wide-Band Slot Antenna," *IEEE Antennas Wireless Propagat. Lett.*, No 8, pp. 65-68, 2006.

- [9] Aliakbar Dastranj, Habibollah Abiri, "Bandwidth Enhancement of Printed E-Shaped Slot Antennas Fed by CPW and Microstrip Line," IEEE Trans. Antennas Propagat., Vol.58, No 4, pp. 1402-1407, April 2010.
- [10] Constantine A. Balanis, Antenna Theory Analysis and Design, 3rd Edition.
- [11] Tanan Hongnara, Chatree Mahatthanajatuphat, Prayoot Akkaraekthalin., "Study of CPW-Fed Slot Antennas with Fractal Stubs," ECTI, pp. 188-191, Conference 2011.

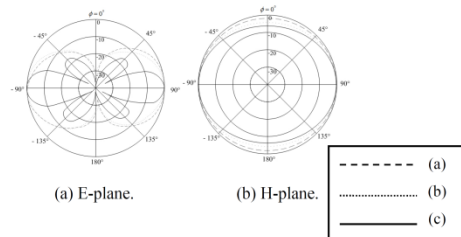


Fig.8. The radiation patterns at 1.92 GHz of (a) a single slot antenna, (b) a single slot antenna with two side-wings, and (c) a 1×4 array of slot antennas with two side-wings.

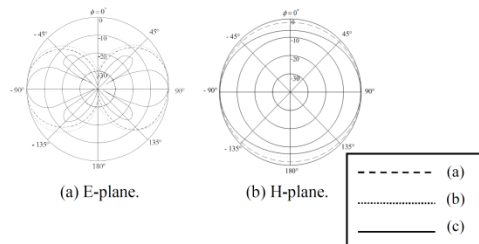


Fig.9. The radiation patterns at 2.1 GHz of (a) a single slot antenna, (b) a single slot antenna with two side-wings, and (c) a 1×4 array of slot antennas with two side-wings.

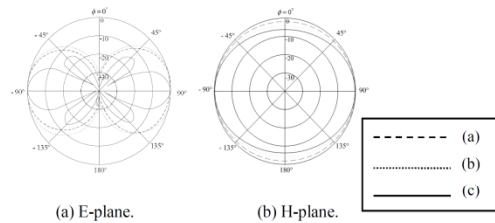


Fig.10. The radiation patterns at 2.17 GHz of (of) (a) a single slot antenna, (b) a single slot antenna with two side-wings, and (c) a 1×4 array of slot antennas with two side-wings.

APPENDIX C

COMPARISON OF 3G BASE STATION

DIRECTIONAL ANTENNAS

Comparison of 3G base station directional antennas

Parameters	Antenna type 1*	Antenna Type 2**	The proposed antenna
Frequency Range (GHz)	1.92 – 2.17	1.92 – 2.17	1.92 – 2.17
The Gain (dB)	21	17.83	20.3
The HPBW (AZ:EL)	31°:16° 1.9:1	64°:6.3° 10.2:1	36.8°:8.7° 4.23:1
The E-plane SLL (dB)	-15	-13.2 dB	-14.4 dB
The H-plane SLL (dB)	-15	-30.6 dB	-27.3 dB
Height/width/depth (mm)	1320×280×80	1360×160×80	1000×470×147
Weight (kg)	12.5	11	17

*Kenbotong Technology Co., LTD (KBT)

**Anderson Tec CO.,LTD

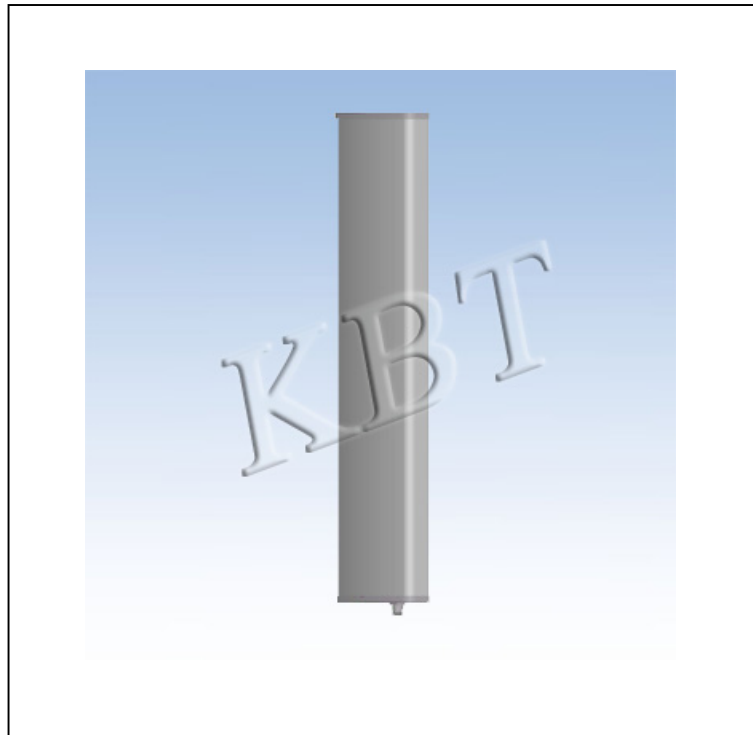


Figure 1 Antenna type 1 (Kenbotong Technology Co., LTD)



Figure 2 Antenna type 2 (Anderson Tec CO.,LTD)

BIOGRAPHY

Miss Paowphattra Kamphikul was born on February 17th, 1984 in Nakhon Ratchasima, Thailand. She received the Bachelor Degree of Engineering (First Class Honor) and the Master's Degree of Engineering in telecommunication engineering from Suranaree University of Technology, Nakhon Ratchasima, Thailand, in 2007 and 2009, respectively. After that she received scholarship from the National Research Council of Thailand (NRCT) for the Joint Ph.D program in telecommunication engineering, institute of engineering at Suranaree University of Technology. Her research interests include electromagnetic theory, antenna engineering and Electromagnetic Band Gap.